Combinatorics and Gauge-String Duality

David P. R. Garner

Submitted in partial fulfillment of the requirements
of the Degree of Doctor of Philosophy

Centre for Research in String Theory
School of Physics and Astronomy
Queen Mary University of London
327 Mile End Road, London E1 4NS

June 2015

Statement of Originality

I, David Garner, confirm that the research included within this thesis is my own work or that where it has been carried out in collaboration with, or supported by others, that this is duly acknowledged below and my contribution indicated. Previously published material is also acknowledged below.

I attest that I have exercised reasonable care to ensure that the work is original, and does not to the best of my knowledge break any UK law, infringe any third party's copyright or other Intellectual Property Right, or contain any confidential material.

I accept that the College has the right to use plagiarism detection software to check the electronic version of the thesis.

I confirm that this thesis has not been previously submitted for the award of a degree by this or any other university.

Signature:

The research in this thesis was undertaken by myself with various collaborators, and has been presented in three papers:

1. D. Garner and S. Ramgoolam, "Holographic Hierarchy in the Gaussian Matrix Model via the Fuzzy Sphere," Nucl. Phys. B **875** (2013) 244 [arXiv:1303.3246 [hep-th]].

2. D. Garner, S. Ramgoolam and C. Wen, "Thresholds of large N factorization in CFT_4: exploring bulk spacetime in AdS_5," JHEP **1411**, 076 (2014) [arXiv:1403.5281 [hep-th]].

3. L. Freidel, D. Garner and S. Ramgoolam, "On the permutation combinatorics of worldsheet moduli space," arXiv:1412.3979 [hep-th].

Abstract

This thesis exhibits a range of applications of combinatoric methods to string theory. The concepts and techniques used in the counting of ribbon graphs, the theory of finite groups, and the construction of cell complexes can give powerful methods and interesting insights into the nature of gauge-string duality, the limits of CFT factorisation, and the topology of worldsheet moduli space.

The first part presents a candidate space-time theory of the Belyi string with a holographic extension to three-dimensional Euclidean gravity. This is a model of gauge-string duality in which the correlators of the Gaussian Hermitian matrix model are identified with sums over worldsheet embeddings onto the 2-sphere target space. We show that the matrix model can be reformulated on the sphere by using $su(2)$ representation couplings, and that the analogues of Feynman diagrams in this model can be holographically extended to 3-manifolds within the Ponzano-Regge model.

The second part explores the limits of large N factorisation in conformal field theory and the dual interpretation in supergravity. By considering exact finite N correlators of single and multi-trace half-BPS operators in $\mathcal{N} = 4$ super Yang-Mills theory in four dimensions, we can explicitly find the exact threshold of the operator dimensions at which the correlators fail to factorise. In the dual supergravity, this is the energy regime at which quantum correlations between distinct gravitons become non-vanishing.

The third part develops a cell decomposition of the moduli space of punctured Riemann surfaces. The cells are specified by a particular family of ribbon graphs, and we show that these graphs correspond to equivalence classes of permutation tuples arising from branched coverings of the Riemann sphere. This description yields efficient computational approaches for understanding the topology of moduli space.

Acknowledgements

I gratefully acknowledge my collaborators Laurent Freidel, Congkao Wen, and my supervisor Sanjaye Ramgoolam, whose guidance and assistance was invaluable throughout the writing of this thesis.

I would like to thank all the CRST students, past and present, with whom I have had interesting mathematical and physical discussions. In particular, I'd like to thank Reza Doobary, Paolo Mattioli, James McGrane, Sam Playle, and Felix Rudolph for many interesting office discussions.

Part of the research in this thesis was undertaken while visiting the High Energy Physics theory group at the University of Southampton. I gratefully acknowledge SEPnet for the financial support, and would like to thank Ariana Christodoulou and Nick Evans for several interesting discussions.

I am exceptionally grateful for the strong support of my family. I thank my parents, my grandparents, and my godmother Nettie for their steadfast support. I thank my brother Andrew for the many engaging physical and mathematical discussions that have taken place over the years.

And, of course, I especially thank Becky for her continuous support.

Contents

0 Introduction **8**

1 The spacetime theories of the Belyi string **15**

1.1 Strings from Belyi maps 17

1.1.1 Tensor space notation and the Gaussian Hermitian matrix model 17

1.1.2 Ribbon graphs and dessins d'enfants 20

1.1.3 Branched coverings and Belyi maps 22

1.1.4 The Belyi string 25

1.2 The matrix model on the fuzzy sphere 27

1.2.1 Spherical harmonics on S^2 29

1.2.2 Fuzzy spherical harmonics 30

1.2.3 Scalar field theory on the fuzzy sphere 32

1.3 Ribbon graphs in the fuzzy sphere matrix model 38

1.3.1 Trivalent ribbon graphs 40

1.3.2 Evaluating spin network state sums 45

1.3.3 Examples of ribbon graph and spin network state sums 51

1.3.4 General multi-trace correlators 53

1.4 A three-dimensional interpretation: The Ponzano-Regge model 58

1.4.1 The Ponzano-Regge model 59

1.4.2 The Turaev-Viro model as a regulator 60

1.4.3 Belyi triangulations 64

1.5 Belyi 3-complexes of planar graphs 67

1.5.1 Constructing the inner Belyi 3-complex 68

1.5.2 Constructing the complete Belyi 3-complex 73

1.6 Complete Belyi 3-complexes of non-planar graphs 76

1.6.1 Triangulations of the solid torus 78

1.6.2 Trivalent graph moves on complete Belyi 3-complexes 82

1.6.3 Complete Belyi 3-complexes of general handlebodies 84
1.7 Discussion 88

2 Thresholds of factorisation in the AdS/CFT correspondence 91
2.1 Factorisation thresholds and bulk interpretations 93
2.1.1 Thresholds of factorisation in the gauge theory 93
2.1.2 The breakdown of bulk effective field theory at the threshold . . 96
2.1.3 Refined investigations of the factorisation thresholds 98
2.2 The extremal three-point correlator with $J_1 = J_2$ 101
2.2.1 Review of asymptotics and series 102
2.2.2 Asymptotics of the three-point correlator 103
2.2.3 Solving the factorisation threshold equation 107
2.2.4 Similarities to the running coupling of gauge theories 110
2.2.5 Expansion of the threshold as a transseries 112
2.3 The extremal three-point correlator with $J_1 \neq J_2$ 115
2.3.1 Scaling limits and the threshold equation 116
2.3.2 A change of variables 123
2.4 Non-extremal correlators 124
2.4.1 The 'near-extremal' correlator 126
2.4.2 $J_1 = J_2$ 129
2.4.3 $J_1 \neq J_2$ 130
2.5 Multi-gravitons and non-trivial backgrounds 132
2.5.1 The $(k+1)$-graviton correlator 132
2.5.2 Factorisation thresholds for large backgrounds 134
2.6 Discussion 136

3 The light-cone cell decomposition of moduli space 140
3.1 Nakamura graphs 142
3.1.1 Giddings-Wolpert differentials 142
3.1.2 Graphs and strip decompositions 144
3.1.3 Parameters of Nakamura graphs 147
3.1.4 Alternative definitions of moduli space 149
3.2 Equivalence classes of permutation tuples 152
3.2.1 Nakamura graphs from branched coverings 153
3.2.2 Slide-equivalence classes and reduced tuples 159
3.2.3 Split tuples 161
3.3 The cell decomposition of moduli space 164

3.3.1 Cells . . . 165
3.3.2 Boundaries . . . 169
3.3.3 Example: $\mathcal{M}_{0,4}$ and $\mathcal{M}_{0,1[3]}$ . . . 173
3.3.4 Example: $\mathcal{M}_{1,2}$ . . . 179
3.4 The cell decomposition of Teichmüller space . . . 183
3.5 Verifying the cell decomposition with orbifold Euler characteristics . . . 186
3.5.1 The orbifold Euler characteristic . . . 187
3.5.2 The Gaussian Hermitian matrix model . . . 190
3.5.3 The complex matrix model . . . 193
3.5.4 Counting graphs using GAP . . . 196
3.6 Discussion . . . 198

4 Conclusion **200**

A The coupling coefficients of $su(2)$ representations **203**
A.1 Clebsch-Gordan coefficients . . . 203
A.2 Wigner $3j$ symbols . . . 205
A.3 Wigner $6j$ symbols . . . 206
A.4 Quantum $6j$ symbols . . . 210

B Summary of the trivalent graph and Pachner moves **212**

C The Lambert W-function **214**

D Combinatoric calculations using character sums **216**
D.1 The non-extremal operator norm . . . 216
D.2 The $(k+1)$-graviton correlator character sum . . . 219

E Moduli space, the mapping class group, and Teichmüller space **221**

F Counting Nakamura graphs in the S_d picture using GAP **225**
F.1 I-structures . . . 227
F.2 An algorithm utilising I-structures . . . 230
F.3 Tables of Nakamura graphs with $|\chi| = 7$ . . . 236

Chapter 0

Introduction

The discovery of the AdS/CFT correspondence has strongly influenced the last eighteen years of research in high energy physics. Since then, many other related types of gauge-string dualities for critical string theories have been discovered, and AdS/CFT has been scrutinised and used prolifically as a tool for calculations in string theory and in gauge theory, but the origins and mechanisms of the duality are still mysterious. A deeper understanding of the gauge-string correspondence is of great importance, as it can provide more insight into non-perturbative string theory and bring us closer to a complete theory of quantum gravity.

The primary aim of this thesis is to investigate the nature of gauge-string duality by considering two tractable examples. In the first example, we consider a candidate for the simplest example of a gauge-string duality, and build on this theory by proposing and developing a spacetime theory which matches the worldsheet theory. In the second example, we consider the original $\mathrm{AdS}_5/\mathrm{CFT}_4$ correspondence and investigate the limits at which energetic CFT operators can be matched to local excitations within the bulk. For these investigations, we employ a wide range of discrete tools and mathematical frameworks including Hurwitz theory, matrix models, Belyi maps, dessins d'enfants, spin networks, simplicial complexes, Ponzano-Regge calculus, Pachner moves, and Schur polynomials.

The secondary aim of this thesis is to develop new ways of investigating the topology of the moduli space of Riemann surfaces. Moduli space is a fundamentally important object of study within worldsheet bosonic string theory and in many branches of mathematics, but is highly non-trivial to describe explicitly in all but the simplest cases. We develop a cell decomposition of moduli space specified via ribbon graphs which leads to powerful computational methods of finding topological invariants of moduli space. While these two aims of the thesis are quite different, the discrete methods used in both cases are very similar, and both contribute towards a greater

understanding of fundamental aspects of string theory.

This thesis is divided into three parts, with the first two parts concentrating on gauge-string duality and the third part focusing on moduli space. In the first chapter of this thesis we consider "the simplest gauge-string duality" and find an extension to a spacetime theory and a gravitational theory. The gauge theory considered is the Gaussian Hermitian matrix model, which is a zero-dimensional quantum field theory where the field is a single Hermitian matrix, the action is a Gaussian, and the observables of the theory are the correlators of products of traces of the matrix. The combinatorics of the Wick contractions of these correlators can be expressed in terms of conjugacy classes of finite permutation groups. These correlators are equal to sums over triples of permutations which multiply to the identity [1, 2].

Each triple of permutations corresponds to a holomorphic branched covering from a Riemann surface onto the Riemann sphere with three branch points, known as a *Belyi map*. The sum over permutation triples corresponds to a sum over Riemann surface embeddings onto the sphere, weighted by genus. In [3], the domain Riemann surfaces were interpreted as worldsheets, and the Riemann sphere as the target space, giving a stringy interpretation of the sum over Belyi maps which we call the *Belyi string*. This idea was developed in [4, 5, 6] by noting that the (planar) correlators of the topological A-model string on the 2-sphere match the matrix model correlators. This suggests that the topological string on S^2 is the *worldsheet* string theory dual of the Gaussian Hermitian matrix model, and equivalent to the Belyi string.

We develop another approach for arguing in favour of S^2 as the target space of the dual string theory of the Hermitian matrix model. The algebra of $N \times N$ matrices is generated by the representation matrices $\{J_1, J_2, J_3\}$ of the N-dimensional irreducible representation of $su(2)$. This algebra has a geometric interpretation via the *fuzzy sphere* [7], in which the representation matrices are viewed as noncommutative deformations of a set of continuous coordinate functions $\{x_1, x_2, x_3\}$. The quadratic Casimir equation $J_1^2 + J_2^2 + J_3^2 = j(j+1)$, with $N = (2j+1)$, is the matrix version of the equation $x_1^2 + x_2^2 + x_3^2 = R^2$ defining the 2-sphere via an embeddeding in $\mathbb{R}^3$. Standard continuous field theories on the sphere can be deformed into noncommutative theories by replacing the continuous coordinate functions with the fuzzy sphere generators in such a way that the commuting theories are recovered in the large N limit. Using the fuzzy sphere algebra, we show in the following that the Gaussian Hermitian matrix model is a cut-off version of a simple topological scalar field theory on the sphere. We interpret this scalar theory as the *spacetime* theory of the Belyi string.

The *fuzzy spherical harmonics* provide an alternate basis for the fuzzy sphere al-

gebra of $N \times N$ matrices, which share many of the properties of the conventional spherical harmonics on the 2-sphere. By reformulating the matrix model in terms of the fuzzy spherical harmonics, we can express the matrix model correlators in terms of Wigner $3j$ and $6j$ symbols, which are the coupling coefficients of $su(2)$ representations. We show that the correlators can be expressed exclusively in terms of sums over representations weighted by $6j$ symbols. This result is an adaptation of arguments from the spin networks literature [8, 9]. For convenience, we mainly restrict our attention to matrix model correlators of cubic traces, which are generated by matrix actions with a perturbative $\mathrm{tr}X^3$ term. In this case, the matrix model correlators evaluate to sums over trivalent ribbon graphs where every vertex has valency three. Each trivalent ribbon graph has an associated $6j$ sum, determined by the spin network evaluation of the graph, which evaluates to a power of N.

We find an interpretation of the trivalent ribbon graphs and their associated $6j$ sums within a three-dimensional theory of gravity. Gravity in three dimensions is a topological theory with no propagating degrees of freedom, and has been shown to be equivalent to Chern-Simons theory with gauge group depending on the signature of the spacetime and the sign of the cosmological constant [10]. Euclidean gravity with zero cosmological constant is equivalent to Chern-Simons with gauge group $ISO(3)$, the three-dimensional Euclidean group. This theory has been identified with the *the Ponzano-Regge model* [11, 12, 13], which assigns a partition function to any triangulated three-dimensional manifold with edges labelled by $su(2)$ representations and tetrahedra labelled by Wigner $6j$ symbols. The Ponzano-Regge partition function of a manifold depends on the topology of the manifold and the choice of labelled triangulation on the boundary, but is independent of the choice of triangulation of the manifold interior.

Each trivalent ribbon graph of the Hermitian matrix model is dual to a triangulation of a surface, and planar graphs are dual to triangulations of the sphere. For a general trivalent ribbon graph, we can generate a particular triangulation of a three-dimensional *handlebody* which contains a copy of the graph within the boundary triangulation. On assigning a particular choice of $su(2)$ representations to the boundary edges, the partition function of this manifold matches the evaluation of its associated ribbon graph. For planar graphs, we can find triangulations of the solid ball with partition functions matching the $6j$ sum exactly. This gives us an interpretation of the handlebody triangulations as providing the holographic extension to a gravitational theory of the spacetime field theory of the Belyi string.

In the second chapter of this thesis, we use exact results for gauge theory correlators

to uncover the threshold energies at which large N conformal field theory factorisation breaks down within gauge-string duality. In the seminal AdS/CFT correspondence of Maldacena, type IIB string theory on an $AdS_5 \times S^5$ background is matched with four-dimensional $\mathcal{N} = 4$ super Yang-Mills theory with $SU(N)$ gauge group in the large N limit [14, 15, 16]. An early successful verification of this correspondence was the explicit large N calculation and matching of the three-point correlators of gauge theory operators with their associated graviton correlators in supergravity [17]. On the gauge theory side, chiral primary operators are symmetric traceless combinations of the six adjoint scalar fields of super Yang-Mills, and their three-point correlators can be calculated at zero gauge coupling. On the supergravity side, the corresponding dual fields arise from the Kaluza-Klein reduction along the 5-sphere of excitations of the metric and the self-dual 5-form field strength. The agreement between the three-point correlators on both sides of the correspondence is possible because three-point functions of chiral primary operators are not renormalised [18, 19, 20, 21, 22, 23].

The half-BPS sector of chiral primary operators is described by a single holomorphic matrix $Z = \Phi_5 + i\Phi_6$, formed from the complex combination of two adjoint Hermitian scalars of SYM [24, 25, 26]. Single trace operators consisting of a small number of Z matrices can be matched to single particle bulk graviton states, and multi-trace operators can be matched to multi-graviton states. The number of matrices J in a single trace operator corresponds to the angular momentum of the dual Kaluza-Klein graviton in the S^5 directions. For a three-point extremal correlator of the form

$$\langle \mathrm{tr} Z^{J_1}(x_1) \mathrm{tr} Z^{J_2}(x_2) \mathrm{tr} Z^{\dagger J_1 + J_2}(y) \rangle, \tag{0.0.1}$$

the conformal symmetry of $\mathcal{N} = 4$ super Yang-Mills theory allows the spacetime dependence of the correlator to be factored out completely. The remaining factor is purely combinatoric, and can be calculated exactly at finite N by considering the combinatorics of the Wick contractions [27, 28]. This combinatoric factor is the conformal field theory inner product of $\mathcal{N} = 4$ SYM, which is also called the Zamolodchikov metric [29]. With an appropriate choice of normalisation, this free-field correlator goes to zero in the large N limit, when the operator dimensions J_i $(i = 1, 2)$ are kept fixed. This is an example of a general property of large N physics called *large N factorisation*.

Single-trace and multi-trace operators form a complete basis of the half-BPS sector of $\mathcal{N} = 4$ SYM, and this basis is orthogonal at large N. Orthogonality of these operators allows us to identify the single-traces and multi-traces as 1-graviton and

2-graviton states respectively, leading to a Fock space description of the dual bulk theory. The single trace operators can be matched with a set of graviton oscillators

$$\mathrm{tr}Z^J \leftrightarrow \alpha_J, \tag{0.0.2}$$

with the commutation relations $[\alpha_{J_1}, \alpha^\dagger_{J_2}] = \delta_{J_1,J_2}$, which annihilate the AdS vacuum state $\alpha_J|0\rangle = 0$. The excitations of the vacuum state form a Fock space, and correlators of states with different numbers of excitations are orthogonal [17],

$$\langle 0|\alpha_{J_1}\alpha_{J_2}\alpha^\dagger_{J_1+J_2}|0\rangle = 0, \tag{0.0.3}$$

which is in agreement with the CFT correlator at large N.

We undertake a careful investigation of the required growth of the operator dimensions J_i which leads to the failure of factorisation. If the J_i are constant, or grow slowly with N, then large N factorisation holds. If the J_i grow sufficiently rapidly with N, then the normalised correlator diverges in the large N limit. We study the *factorisation threshold*, defined to be the submanifold of the space of parameters (the dimensions of the operators J_i and the gauge group rank N) on which the normalized correlator is equal to a constant. By using the known exact evaluation of the correlator for finite N and some careful asymptotic analysis at large N, we find that the threshold occurs when the product of the holomorphic operator dimensions is of order $N \log N$. We also investigate some other free field correlators with known exact evaluations, and deduce a similar threshold behaviour in all cases. As the Fock space bulk picture is valid below the threshold and cannot be valid above the threshold, we interpret this factorisation threshold as the energy scale at which a new spacetime theory is emerging in the bulk.

In the third and final chapter of this thesis we find and develop a useful description of the *light-cone* cell decomposition of moduli space in terms of equivalence classes of permutation tuples. In bosonic light-cone string theory, the computation of string amplitudes uses *light-cone diagrams* parametrised by string lengths and twist parameters along with interaction times. The light-cone gauge in string theory involves only physical degrees of freedom and leads to a manifestly unitary S-matrix, while Lorentz invariance appears non-trivially [32, 33]. The covariant gauge has manifest Lorentz invariance, but unitarity is non-trivial. String amplitudes are calculated by integration over $\mathcal{M}_{g,n}$, the moduli space of inequivalent Riemann surfaces of genus g with n labelled punctures.

Giddings and Wolpert showed in [30] that each closed string light-cone diagram

corresponds to a punctured Riemann surface with a uniquely-determined meromorphic one-form, later called the *Giddings-Wolpert differential*. This correspondence was used to argue that the light-cone string diagrams lead to a single cover of moduli space, which is necessary for the light-cone and covariant formulations of string theory to be equivalent. However, this approach had some issues involving the overcounting of discrete factors, analogous to the symmetry factors appearing in Feynman diagram expansions. In addition, the higher order string interactions are tricky to describe in the light-cone picture.

These issues were addressed by Nakamura in [31] with the introduction of a particular type of ribbon graph on each punctured Riemann surface determined by the Giddings-Wolpert differential. Every Riemann surface has a uniquely-determined embedded graph of this type, which we call the *Nakamura graph* of the surface. Inequivalent Riemann surfaces can have the same Nakamura graph, and so the set of distinct Nakamura graphs partitions moduli space into disjoint subsets, with each subset corresponding to a graph. It was demonstrated in [31] that these graphs specify a cell decomposition of moduli space by counting the distinct graphs for low genus and few punctures, evaluating the orbifold Euler characteristic of the decomposition, and comparing this to known exact formulae from [34]. This is highly non-trivial evidence for the consistency of the light-cone cell decomposition, as a very large number of graphs were counted to confirm the orbifold Euler characteristic.

The use of graphs in the light-cone cell decomposition is analogous to the graphs in the Kontsevich-Penner cell decomposition of decorated moduli space [35, 36]. Indeed, the Kontsevich-Penner cell decomposition has been used to compute homology groups and intersection numbers of Mumford-Morita classes on moduli space. This cell decomposition is well studied in mathematics and has also been used recently in describing the link between string theory integrals and Feynman integrals [37]. The light-cone and Kontsevich-Penner cell decompositions both involve ribbon graphs embedded on surfaces. However, the Nakamura graphs are much more restricted because of certain causality relations controlling the connectivity of the vertices. As a result the light-cone cell decomposition requires fewer cells, and so is the more economical of the cell decompositions.

We initiate a systematic study of the light-cone cell decomposition via Nakamura graphs. The graphs can be described in terms of equivalence classes of permutation tuples in a similar way to Grothendieck's dessins d'enfants [38], which are also considered in this thesis in the description of the Belyi string. Such a permutation tuple is enough to reconstruct the Nakamura graph, and so the counting and classification

of light-cone cells in moduli space can be reduced to a problem of counting Hurwitz classes satisfying certain criteria.

The description of Nakamura graphs in terms of permutation tuples has several advantages. The basic structure of the cell associated to a graph can be read off from the tuple, including the boundaries of the cell and its orbifold quotienting group. We can also use the tuples description to build links between the correlators of Hermitian and complex matrix models and the counting of the higher-dimensional cells in moduli space. In addition, the tuples description allows for efficient computational methods of counting the graphs, which we use to confirm the orbifold Euler characteristic of more elaborate moduli spaces. This suggests that Nakamura graphs, described by permutation tuples, provide a powerful calculational tool for understanding the topology of moduli space.

Chapter 1

The spacetime theories of the Belyi string

A convincing candidate for the simplest version of a gauge-string duality is the matrix model/Belyi maps correspondence [3, 4, 5]. On the gauge side, the quantum field theory is a zero-dimensional matrix model with a Gaussian action, in which the observables of the theory are correlators of traces of a single Hermitian matrix. On the string theory side, the worldsheets are Riemann surfaces, the target space is a 2-sphere, and the worldsheets cover the target space with *Belyi maps*, which are holomorphic maps branched at three points. Planar correlators of the matrix model can be matched to the topological A-model string theory on the sphere [40, 41], which suggests that the topological A-string is the *worldsheet* theory of the Belyi maps string theory.

In this chapter, we expand upon this simple exact model of gauge-string duality, with a view to providing insight into the fundamental nature of gauge-string duality to future researchers. The main results of this chapter are the construction of two related spacetime theories that match the Belyi maps string theory. We use the fuzzy sphere construction [7] to derive a topological field theory on the 2-sphere target which reproduces the correlators of the matrix model. By taking the ribbon graphs of this matrix model and extending them to triangulations of 3-manifolds, we find a three-dimensional theory of gravity which matches the terms in the matrix model correlators. These 3-manifolds contain the data of the two-dimensional theory on their boundaries, which suggests that the gravitational theory is a holographic lift of the target space theory into three dimensions.

This chapter is organised as follows. Section 1.1 reviews the construction of the Belyi string model from the Hermitian matrix model correlators and permutation triples. Tensor space notation is introduced as a tool for describing the Wick contractions and multi-trace operators in the Hermitian matrix model, and the equivalent cyclically-ordered graphs associated to these terms are discussed. The link between branched coverings of the sphere and tuples of permutations is established, and used to give a

stringy interpretation of the matrix model.

The fuzzy sphere is reviewed in Section 1.2, paying particular attention to the fuzzy spherical harmonic basis and its relation to the continuous spherical harmonics on the 2-sphere. We show that switching from the conventional Hermitian matrix model measure to the fuzzy spherical harmonic modes measure gives a trivial Jacobian, allowing the identification of the topological fuzzy sphere theory as a matrix model. We conclude the section by discussing how to interpret the fuzzy sphere matrix model as the spacetime theory of the Belyi string. The fuzzy sphere can be viewed as the means of truncating the momentum modes of the spacetime theory on the 2-sphere, and as an actual noncommutative deformation of the target space. The size N of the matrix is the genus-counting parameter for the Belyi string theory with a classical sphere target, and also measures the non-commutativity of the fuzzy sphere in the spacetime field theory.

In Section 1.3 we consider the ribbon graphs of the Hermitian matrix model expressed in terms of the fuzzy sphere variables. The graphs evaluate to sums involving Wigner $3j$ and $6j$ symbols, which contain the *spin network* evaluation of the graph. We show that the $3j$s can be summed out to give expressions in terms of $6j$ symbols only. An extension to non-trivalent ribbon graphs is also discussed.

In Section 1.4 we introduce the Ponzano-Regge model and its quantum deformation, the Turaev-Viro model, which serves as a regulator. These models assign partition functions to triangulations of 3-manifolds with edges labelled by $su(2)$ representations and tetrahedra labelled by $6j$ symbols. We look for triangulations of three-dimensional manifolds which encode the data of the ribbon graph, with the aim of matching their partition functions with the ribbon graph $6j$ sums. We introduce two types of triangulations of surfaces generated from the Belyi maps associated to ribbon graphs called *Belyi triangulations*. The *inner Belyi triangulation* is the dual of the trivalent ribbon graph. The *outer Belyi triangulation* contains the ribbon graph itself, in addition to extra vertices and edges added according to specified rules.

In Section 1.5, we give a prescription for generating a labelled triangulation of the 3-ball for a planar ribbon graph. Labelled triangulations of the ball can be constructed with inner Belyi triangulations on their boundary, which we call *inner Belyi 3-complexes*. This was shown to have a Ponzano-Regge partition function equal to its spin network evaluation in [8], and we present another proof of this result. By appending tetrahedra to the exterior of the inner Belyi 3-complex, we can construct a labelled triangulation of the ball with an outer Belyi triangulation on its boundary, which we call a *complete Belyi 3-complex*. The Ponzano-Regge partition function of

this complex matches the $6j$ sum of its associated ribbon graph.

In Section 1.6 we extend our construction of complete Belyi 3-complexes to non-planar ribbon graphs. Trivalent non-planar ribbon graphs are dual to triangulations of higher genus surfaces, which can be extended to three-dimensional triangulations of *handlebodies* with outer Belyi triangulations on their boundary. We prove that the evaluation of a ribbon graph of any genus matches the Ponzano-Regge partition function of the complex constructed from the graph. We conclude this chapter with some discussion in Section 1.7 of the links between the two spacetime theories, the differences between the planar and non-planar cases, and possible embeddings of this three-dimensional manifold within more conventional constructs in string theory.

1.1 Strings from Belyi maps

In this section we review the construction, originally from [3], of an exact analogue of gauge-string duality using Belyi maps. We introduce tensor space notation as a means to understand the Feynman graphs of the Hermitian matrix model correlators, which can be described by permutation sums. We outline the relation between branched holomorphic coverings of the Riemann sphere and their associated combinatoric descriptions in terms of equivalence classes of permutation triples, and then summarise the evidence that this leads to a basic form of gauge-string duality between the topological A-string and the Hermitian matrix model.

1.1.1 Tensor space notation and the Gaussian Hermitian matrix model

We start by reviewing some techniques and methods of tensor spaces. Let V be an N-dimensional vector space with a basis $|e_i\rangle$. The linear operator X associated to a matrix $X^i{}_j$ is

$$X|e_j\rangle = X^i{}_j|e_i\rangle. \tag{1.1.1}$$

The space $V^{\otimes 2n}$, formed from taking the tensor product of $2n$ copies of V, has a basis

$$|e_{j_1}e_{j_2}\dots e_{j_{2n}}\rangle := |e_{j_1}\rangle \otimes |e_{j_2}\rangle \otimes \dots |e_{j_{2n}}\rangle. \tag{1.1.2}$$

The multilinear action of X on vectors in $V^{\otimes 2n}$ is

$$X \otimes X \otimes \ldots \otimes X |e_{j_1} e_{j_2} \ldots e_{j_{2n}}\rangle = X^{i_1}_{\ j_1} X^{i_2}_{\ j_2} \ldots X^{i_{2n}}_{\ j_{2n}} |e_{i_1} e_{i_2} \ldots e_{i_{2n}}\rangle, \tag{1.1.3}$$

and by introducing the dual vectors in $V^{*\otimes 2n}$, we can write

$$X^{i_1}_{\ j_1} X^{i_2}_{\ j_2} \ldots X^{i_{2n}}_{\ j_{2n}} = \langle e^{i_1} e^{i_2} \ldots e^{i_{2n}} |\mathbf{X}| e_{j_1} e_{j_2} \ldots e_{j_{2n}}\rangle, \tag{1.1.4}$$

where we have introduced the notation $\mathbf{X} = X \otimes X \otimes \ldots \otimes X$ for the operator on $V^{\otimes 2n}$ formed from the tensor product of $2n$ copies of X. Contracting all the indices of a matrix product (1.1.4) gives a product of traces of X. For example, we could write $\mathrm{tr} X \mathrm{tr}(X^3)$ as

$$\mathrm{tr} X \mathrm{tr}(X^3) = X^{i_1}_{\ i_1} X^{i_2}_{\ i_3} X^{i_3}_{\ i_4} X^{i_4}_{\ i_2} = \langle e^{i_1} e^{i_2} e^{i_3} e^{i_4} |\mathbf{X}| e_{i_1} e_{i_3} e_{i_4} e_{i_2}\rangle. \tag{1.1.5}$$

Any product of traces of a single matrix can be written in terms of a permutation acting on the tensor space $V^{\otimes 2n}$ and the multilinear operator $\mathbf{X}$. Defining the linear action of a permutation $\sigma \in S_{2n}$ on $V^{\otimes 2n}$ by the action on the basis vectors

$$\sigma |e_{j_1} e_{j_2} \ldots e_{j_{2n}}\rangle = |e_{j_{\sigma(1)}} e_{j_{\sigma(2)}} \ldots e_{j_{\sigma(2n)}}\rangle, \tag{1.1.6}$$

then the trace product corresponding to a permutation σ is

$$\begin{aligned} \mathrm{tr}_{2n}(\mathbf{X}\sigma) &:= \langle e^{i_1} e^{i_2} \ldots e^{i_{2n}} |\mathbf{X}\sigma| e_{i_1} e_{i_2} \ldots e_{i_{2n}}\rangle \\ &= \langle e^{i_1} e^{i_2} \ldots e^{i_{2n}} |\mathbf{X}| e_{i_{\sigma(1)}} e_{i_{\sigma(2)}} \ldots e_{i_{\sigma(2n)}}\rangle. \end{aligned} \tag{1.1.7}$$

For example, the permutation $\sigma = (1)(234)$ specifies the trace product

$$\begin{aligned} \mathrm{tr}_4(\mathbf{X}(1)(234)) &= \langle e^{i_1} e^{i_2} e^{i_3} e^{i_4} |\mathbf{X}(1)(234)| e_{i_1} e_{i_2} e_{i_3} e_{i_4}\rangle \\ &= \langle e^{i_1} e^{i_2} e^{i_3} e^{i_4} |\mathbf{X}| e_{i_1} e_{i_3} e_{i_4} e_{i_2}\rangle \\ &= \mathrm{tr} X \mathrm{tr}(X^3). \end{aligned} \tag{1.1.8}$$

Each permutation $\sigma \in S_{2n}$ determines a trace product with $2n$ matrices, but there can be many permutations corresponding to the same trace product. Two permutations $\sigma,\ \tilde{\sigma} \in S_{2n}$ give the same multi-trace correlator if and only if they are *conjugate*, i.e. $\tilde{\sigma} = \gamma\sigma\gamma^{-1}$ for some $\gamma \in S_{2n}$. The conjugacy classes of S_{2n} are in one-to-one correspondence with the trace products, or *multi-trace operators*, of $2n$ copies of a single matrix.

The Gaussian Hermitian matrix is a zero-dimensional quantum field theory where the field is a single Hermitian matrix, the action is a Gaussian, and the observables of the theory are the correlators of products of traces of the matrix. The path-integral expression for a normalised correlator is

$$\langle \cdots \rangle = \frac{\int DX e^{-\frac{1}{2}\mathrm{tr}X^2}(\cdots)}{\int DX e^{-\frac{1}{2}\mathrm{tr}X^2}} \tag{1.1.9}$$

with the integration measure

$$DX = \prod_{k=1}^{N} dX^k_{\ k} \prod_{1\leq i<j\leq N} d(\mathrm{Re}X^i_{\ j}) d(\mathrm{Im}X^i_{\ j}). \tag{1.1.10}$$

This integral is performed over a finite number of variables weighted by an exponentially-decaying factor, and so the correlators are well-defined and convergent. The propagator of the Hermitian matrix model is

$$\langle X^{i_1}_{\ j_1} X^{i_2}_{\ j_2} \rangle = \delta^{i_1}_{j_2} \delta^{i_2}_{j_1} \tag{1.1.11}$$

which gives, via Wick's theorem, the general correlator of $2n$ matrices

$$\langle X^{i_1}_{\ j_1} X^{i_2}_{\ j_2} \dots X^{i_{2n}}_{\ j_{2n}} \rangle = \sum_{\tau\in[2^n]} \delta^{i_1}_{j_{\tau(1)}} \delta^{i_2}_{j_{\tau(2)}} \dots \delta^{i_{2n}}_{j_{\tau(2n)}}. \tag{1.1.12}$$

This sum is performed over $[2^n]$, the S_{2n} conjugacy class consisting of all the permutations which are products of n disjoint 2-cycles. This sum can be written in tensor space notation as

$$\langle X^{i_1}_{\ j_1} X^{i_2}_{\ j_2} \dots X^{i_{2n}}_{\ j_{2n}} \rangle = \sum_{\tau\in[2^n]} \langle e^{i_1} e^{i_2} \dots e^{i_{2n}} | \tau | e_{j_1} e_{j_2} \dots e_{j_{2n}} \rangle \tag{1.1.13}$$

or, more fundamentally, as the operator equation

$$\langle \mathbf{X} \rangle = \sum_{\tau\in[2^n]} \tau. \tag{1.1.14}$$

This gives a general expression for a multi-trace correlator as a sum over Wick con-

tractions,

$$\begin{aligned}\langle \mathrm{tr}_{2n}(\mathbf{X}\sigma)\rangle &= \sum_{\tau\in[2^n]} \mathrm{tr}_{2n}(\tau\sigma) = \mathrm{tr}_{2n}(\sigma\tau) \\ &= \sum_{\tau\in[2^n]} N^{C_{\sigma\tau}}, \end{aligned} \tag{1.1.15}$$

where we have used the conjugacy-invariance of σ in the trace to commute σ and τ, and where $C_{\sigma\tau}$ is the number of disjoint cycles in the product permutation $\sigma\tau$. The delta function on a permutation group is defined to be non-zero only for the identity permutation:

$$\delta(\sigma) = \begin{cases} 1 & \sigma = (1)(2)\dots(2n) \\ 0 & \sigma \neq (1)(2)\dots(2n). \end{cases} \tag{1.1.16}$$

Since $C_\gamma = C_{\gamma^{-1}}$, this allows us to express the multi-trace correlator as

$$\langle \mathrm{tr}_{2n}(\mathbf{X}\sigma)\rangle = \sum_{\gamma\in S_{2n}} \sum_{\tau\in[2^n]} \delta(\sigma\tau\gamma) N^{C_\gamma}. \tag{1.1.17}$$

Finally, by the conjugacy-invariance of a multi-trace under $\sigma \mapsto \alpha\sigma\alpha^{-1}$ for any $\alpha \in S_{2n}$, we can replace σ in the delta function with any σ' in the conjugacy class of σ (denoted $[\sigma]$) and perform the sum over the conjugacy class weighted by its size $|[\sigma]|$,

$$\langle \mathrm{tr}_{2n}(\mathbf{X}\sigma)\rangle = \frac{1}{|[\sigma]|} \sum_{\sigma'\in[\sigma]} \sum_{\gamma\in S_{2n}} \sum_{\tau\in[2^n]} \delta(\sigma'\tau\gamma) N^{C_\gamma}. \tag{1.1.18}$$

In summary, the observables in the (free Gaussian) Hermitian matrix model have a purely group-theoretic description as sums over triples of permutations that multiply to the identity. We remark that these observables are invariant under the adjoint action $X \mapsto UXU^\dagger$ for unitary U, as traces and the integration measure (1.1.10) are both preserved under this action [42].

1.1.2 Ribbon graphs and dessins d'enfants

The Feynman graphs of the matrix model correlators can be formulated in several equivalent ways. The traditional physics way is to use double-line diagrams [43] and the closely related ribbon graphs and Grothendieck's dessins d'enfants [38]. Each Wick contraction of a correlator $\langle \mathrm{tr}_{2n}(\mathbf{X}\sigma)\rangle$ can be described by a permutation $\tau \in [2^n]$, and

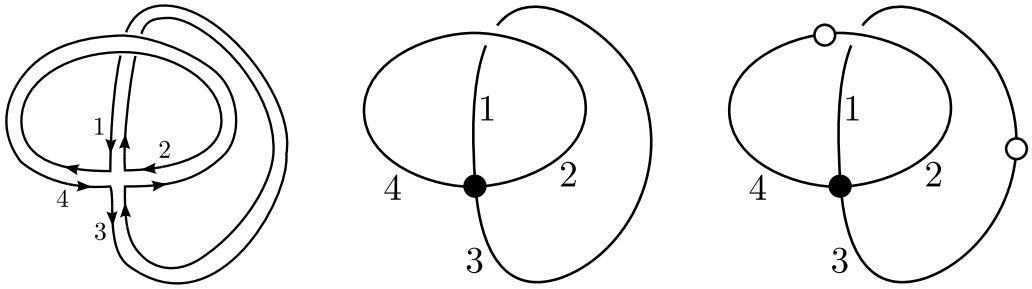

a b c

Figure 1.1: The double-line graph, ribbon graph, and dessin d'enfant associated with a non-planar Wick contraction of $\mathrm{tr}(X^4)$.

contributes a factor of

$$\mathrm{tr}_{2n}(\sigma\tau) = \langle e^{i_1} e^{i_2} \dots e^{i_n} | e_{i_{\sigma\tau(1)}} e_{i_{\sigma\tau(2)}} \dots e_{i_{\sigma\tau(n)}} \rangle = N^{C_{\sigma\tau}} \tag{1.1.19}$$

to the correlator sum. To construct the **double-line graph** for this correlator contribution (Wick contraction), we can associate to each disjoint k-cycle in σ a double-line vertex of valency k, with each connecting half-edge labelled by the numbers in the cycle. We then connect these vertices together with the edges corresponding to the disjoint 2-cycles in τ. The closed loops formed by the double line graph now correspond to the permutation γ such that $\sigma\tau\gamma = 1$. The correlator contribution associated to this graph is N to the power of the number of closed loops in the graph. The same information of a double-line diagram can be represented by a **ribbon graph**, which is constructed by shrinking the double-lines to single-lines and keeping track of the cyclic orientation at each vertex. The faces of a ribbon graph correspond to the loops of the double-line graph.

A **dessin d'enfant** is a bipartite ribbon graph in which there are two types of vertices, coloured black and white, with the edges linking only black vertices to white vertices and vice versa. If all the vertices of one colour have valency two, then the dessin is called **clean**. Any ribbon graph can be made into a dessin by colouring the original vertices of the ribbon graph in black and introducing a white vertex of valency two into each edge of the ribbon graph. For a correlator contribution corresponding to (σ, τ), the associated dessin has edges labelled from 1 to $2n$, with the cycles of σ corresponding to the cyclic ordering of the edges about the black vertices and τ corresponding to the cyclic ordering of the edges about the white vertices.

An example of such a double-line graph is given in Figure 1.1a, arising from the permutations $\sigma = (1234)$ and $\tau = (13)(24)$. The permutation $\gamma = \tau^{-1}\sigma^{-1} = (1234)$

corresponds to the single loop of the double-line. The equivalent ribbon graph is given in Figure 1.1b with the half-edges labelled, and the associated dessin d'enfant is given in Figure 1.1c with the labelled edges.

Each connected ribbon graph and dessin d'enfant has a well-defined genus, which is the lowest possible genus of a surface into which it is possible to embed the graph without self-intersection. A connected ribbon graph embedded into a surface partitions the surface into contractible faces. The faces of a dessin d'enfant with vertices determined by σ and τ correspond to cycles in the permutation γ such that $\sigma\tau\gamma = 1$.

Each triple of permutations (σ, τ, γ) multiplying to the identity determines a ribbon graph. There will in general be many triples of permutations $(\tilde{\sigma}, \tilde{\tau}, \tilde{\gamma})$ which determine the same ribbon graph, up to relabellings of the edges. Two triples of permutations describe the same ribbon graph if and only if they are *conjugate*: that is, there exists some $\alpha \in S_{2n}$ such that

$$(\tilde{\sigma}, \tilde{\tau}, \tilde{\gamma}) = (\alpha^{-1}\sigma\alpha, \alpha^{-1}\tau\alpha, \alpha^{-1}\gamma\alpha). \tag{1.1.20}$$

The conjugacy equivalence classes of permutation triples (σ, τ, γ) satisfying $\sigma\tau\gamma = 1$ are called **Hurwitz classes**. There is a unique Hurwitz class associated to each dessin d'enfant.

Dessins can also be used to describe Belyi maps, which are holomorphic maps from Riemann surfaces onto the sphere branched at three points. The counting of Belyi maps is equivalent to the counting of Hurwitz classes of permutation triples. In the following section, we review this construction and its interpretation as a string theory.

1.1.3 Branched coverings and Belyi maps

We recall some facts about holomorphic branched coverings of the Riemann sphere, and their relation to symmetric groups. A continuous holomorphic surjective map $f : \Sigma \to S^2$ from a Riemann surface Σ onto the sphere S^2 is a **branched cover** if every point Q on S^2 has some open neighbourhood U_Q such that $f^{-1}(U_Q)$ is a collection of disjoint open sets, and there exist local complex coordinates w on U_Q and z_i on each preimage of U_Q such that f maps $z_i \mapsto w = z_i^{r_i}$ for some positive integer r_i. For most points on the sphere, there are d preimages on the surface Σ, where d is the degree of the map. About these points, there exist complex coordinate patches z and w such that such that f maps $z \mapsto w = z$. There is a finite set of m points on the target space S^2 which each have fewer than d preimages. These are the **branch points** of the map f. For a given branch point Q with local coordinates w, each preimage P_i of

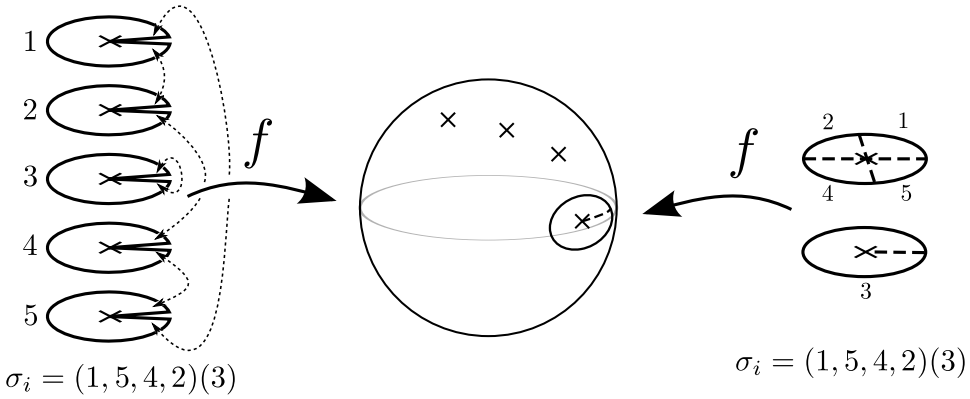

Figure 1.2: The preimages of a cut disc on S^2 are a set of cut discs, whose gluing is specified by a permutation σ_i.

the branch point with local coordinates z_i has an associated unique positive integer r_i such that f maps $z \mapsto w = z^{r_i}$ about that point. If $r_i \geq 2$, then this preimage P_i is a **ramification point** of the map f.

The neighbourhoods of ramification points can be described in terms of a gluing construction. Take a disc with coordinates $|w| < 1$ around a branch point Q located at $w = 0$, and cut the disc along the real interval $w \in [0, 1)$. The preimages of the cut disc on the surface Σ are d identical copies of the cut disc. The cuts along the intervals can be identified to recover the neighbourhoods on Σ around the ramification points. If we choose a labelling of the cut discs with the integers $\{1, 2, \ldots, d\}$, then the gluing of the cut discs corresponds to a mapping from the set $\{1, 2, \ldots, d\}$ to itself, which is a permutation $\sigma \in S_d$. The lower edge of the cut on disc i is glued to the upper edge of the cut on disc $\sigma(i)$, as shown by example on the left of Figure 1.2. Each cut disc is holomorphic to a 'wedge' of a disc subtending an angle $2\pi/r$ for some r, as can be seen on the right of Figure 1.2.

There is another way of arriving at the permutation description of branch points by considering the preimages of loops on the target space S^2. Choose an unbranched base point on the sphere, and label its preimages with integers from 1 to d. For each of the m branch points on the sphere, draw a directed closed path starting and ending on the base point, which can be contracted to a neighbourhood of the branch point without passing through a branch point. The preimages of each of the m directed loops on the sphere are directed closed paths on the Riemann surface Σ which connect the d distinct labelled preimages of the base point. Each branch point gives a bijective mapping from the set $\{1, \ldots d\}$ to itself which we obtain by following the paths of

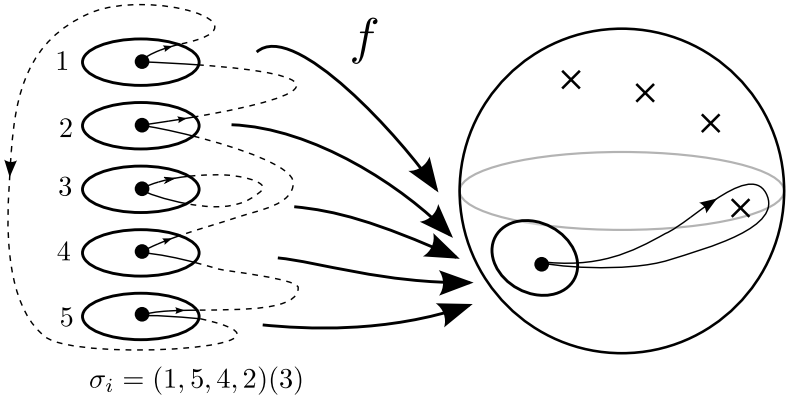

Figure 1.3: The target space S^2 is drawn on the right and the d preimages on the surface Σ of a disc about a marked unbranched point on the sphere are drawn on the left. The preimages of a loop drawn around one of the branch points on the sphere are a set of trajectories connecting the d labelled preimages of the marked point on Σ, specifying a permutation in S_d.

the preimages of the loops. We associate a permutation $\sigma_i \in S_d$, $i = 1, \dots m$ to each branch point of the map f. On the sphere, the path constructed by following all m loops around is contractible. Hence, the permutations $\sigma_1, \dots, \sigma_m$ multiply together to give the identity,

$$\sigma_1 \sigma_2 \dots \sigma_m = 1. \tag{1.1.21}$$

The permutation tuple $(\sigma_1, \sigma_2, \dots \sigma_m)$ describes the branching of a cover f from a Riemann surface Σ on to the sphere S^2. The ramification points correspond to the disjoint cycles of the permutations σ_i. This loop construction is demonstrated in Figure 1.3.

There is an arbitrariness in the way we label the preimages of the marked point from 1 to d: any relabelling of these points yields the same branching profile. We consider two permutation tuples to be equivalent if there is a permutation $\gamma \in S_d$ which conjugates one sequence to the other, i.e. the tuples $(\sigma_1, \dots, \sigma_m)$ and $(\sigma'_1, \dots, \sigma'_m)$ are equivalent if

$$(\sigma'_1, \dots, \sigma'_m) = (\gamma \sigma_1 \gamma^{-1}, \dots, \gamma \sigma_m \gamma^{-1}). \tag{1.1.22}$$

The equivalence classes of these tuples are Hurwitz classes. Each branched cover of the sphere determines a Hurwitz class.

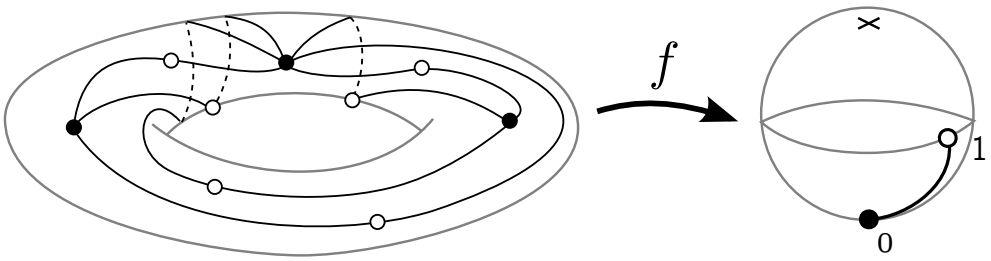

Figure 1.4: Any dessin d'enfant on a Riemann surface can be realised as the preimage of $[0, 1]$ on some branched covering of the sphere.

There is also a notion of equivalence of branched coverings in terms of bijective holomorphic maps (or **biholomorphisms**). Two branched covers of the sphere f and f' are equivalent if there exists some biholomorphism $\phi : \Sigma \to \Sigma$ such that $f' = f \circ \phi$. Equivalent branched covers of a Riemann surface have the same Hurwitz class. The converse is also true by the *Riemann existence theorem* [44, 45]: if we have a Hurwitz class of m permutations in S_d, and choose m labelled points on the sphere, then there exists a Riemann surface Σ and a mapping $f : \Sigma \to S^2$, with branching at the m labelled points corresponding to the Hurwitz class. The surface Σ and mapping f is unique up to biholomorphism equivalence. The notions of biholomorphism equivalence of branched covers and S_d conjugation equivalence of Hurwitz classes coincide.

Dessins d'enfants can be realised as branched coverings of the sphere. We specialise to the case when there are three branch points on the sphere, which we can choose to be located at $w = 0, 1, \infty$. Consider the real interval $[0, 1]$ on the target sphere. The preimage of this interval is an embedded ribbon graph on Σ. By colouring the preimages of the point $w = 0$ in black and the preimages of $w = 1$ in white, this embedded ribbon graph becomes a dessin d'enfant embedded on Σ. If we choose a labelling of the d preimages of the real interval, then we can read off the Hurwitz class defining the dessin d'enfant, which coincides with the defining equivalence class of the branched covering. A branched covering f of the sphere with three branch points is called a **Belyi map**, and a representative triple (σ, τ, γ) of its associated Hurwitz class, which satisfies $\sigma\tau\gamma = 1$, is a **Belyi triple**. The pair (Σ, f) consisting of a Riemann surface and a branched covering is a **Belyi pair**.

1.1.4 The Belyi string

The Riemann-Hurwitz relation gives us a means to interpret sums over triples of permutations as sums over holomorphic maps from worldsheets onto a target space. If

Σ is a surface containing several connected components with respective genera g_j, then the Riemann-Hurwitz relation states that a Belyi pair (Σ, f) with branching given by (σ, τ, γ) satisfies

$$\sum_j (2 - 2g_j) = 2d - (d - C_\sigma) - (d - C_\tau) - (d - C_\gamma). \tag{1.1.23}$$

Considering the case when the degree of the map is $d = 2n$ for some n, and τ is a product of n 2-cycles, this formula becomes

$$\sum_j (2 - 2g_j) = C_\sigma + C_\gamma - n. \tag{1.1.24}$$

With a judicious choice of normalisation, the matrix model correlator (1.1.18) can be written as

$$\frac{|[\sigma]|}{(2n)!} N^{C_\sigma - n} \langle \mathrm{tr}_{2n}(\mathbf{X}\sigma) \rangle = \frac{1}{2n!} \sum_{\sigma' \in [\sigma]} \sum_{\gamma \in S_{2n}} \sum_{\tau \in [2^n]} \delta(\sigma' \tau \gamma) N^{C_\gamma + C_\sigma - n}, \tag{1.1.25}$$

Splitting the sum over triples into a sum over Hurwitz classes, and using the the orbit-stabiliser theorem and the fact that C_γ and C_σ are invariant under conjugation, we have

$$\frac{1}{(2n)!} \sum_{\sigma' \in [\sigma]} \sum_{\gamma \in S_{2n}} \sum_{\tau \in [2^n]} \delta(\sigma' \tau \gamma) N^{C_\gamma + C_\sigma - n} = \sum_{\substack{\text{Hurwitz} \\ \text{classes}}} \frac{1}{|\mathrm{Aut}(\sigma, \tau, \gamma)|} N^{C_\gamma + C_\sigma - n}, \tag{1.1.26}$$

where the sum is taken over all Hurwitz classes $[(\sigma', \tau, \gamma)]$ with $\sigma' \in [\sigma]$ and $\tau \in [2^n]$, and where $\mathrm{Aut}(\sigma, \tau, \gamma)$ is the automorphism group of permutations which preserve each of σ, τ, and γ separately under conjugation.

By the Riemann existence theorem, this sum over triples of permutations corresponds to a sum over Riemann surfaces and branched coverings of the sphere. The automorphism group of branched coverings corresponds to the automorphism group of a Hurwitz class (which is well-defined up to isomorphism). The Hermitian matrix model correlator can be expressed as a sum over Belyi pairs (Σ, f) with branching $[\sigma]$ and $[2^n]$ at two points on the target S^2, and arbitrary branching at the third point:

$$\boxed{\frac{|[\sigma]|}{(2n)!} N^{C_\sigma - n} \langle \mathrm{tr}_{2n}(\mathbf{X}\sigma) \rangle = \sum_{(\Sigma, f)} \frac{1}{|\mathrm{Aut}(f)|} \prod_i N^{2-2g_i}.} \tag{1.1.27}$$

We can give a stringy interpretation to this sum over Belyi maps by thinking of the Riemann surfaces Σ as worldsheets, and the target space S^2 as the background space. With this interpretation, the identification of Hermitian matrix model correlators with sums over worldsheet mappings gives an exact realisation of the gauge-string correspondence for a simple, combinatoric theory. The only free parameter of the theory is N, the order of the matrix field X, which appears in the sum over Belyi maps along with the Euler characteristic of the worldsheet. This suggests an interpretation of the parameter as the string coupling constant $g_s^{-1} \leftrightarrow N$, as in conventional string perturbation theory. Unlike in the more conventional examples of gauge-string duality, this correspondence is exact and does not require a large N limit for explicit comparison.

It was conjectured in [4] that the worldsheet theory of the Belyi string is the topological A-model with an S^2 target. Evidence for this conjecture was given in [4, 5, 6] by comparing the planar connected correlators of the topological A-string to the Hermitian matrix model via the Eguchi-Yang matrix model [46]. In this thesis, instead of exploring the worldsheet theory, we work on a candidate *spacetime* theory of the Belyi string, which exactly matches the matrix model correlators and so also matches the planar topological A-string correlators. From the two-dimensional spacetime theory, we are able to find a three-dimensional gravitational theory that reproduces the correlator terms of the spacetime theory. This lifting to a three-dimensional theory can be interpreted as an analogue of a membrane for the Belyi string which holographically reduces down to the two-dimensional spacetime theory.

1.2 The matrix model on the fuzzy sphere

In the previous section we have introduced a discrete analogue of a string theory. Each observable in the matrix model determines a sum over equivalence classes of triples of permutations (Hurwitz classes), which is equivalent to a sum over equivalence classes of Belyi maps. The only parameter of the free theory is N, the size of the matrix X, which appears as the inverse string coupling g_s^{-1} in the sum over Belyi maps. This string/QFT duality is an exact duality, as the string theory interpretation is defined directly in terms of the quantum field theory. The target space of the Belyi string theory is S^2, and the matrix model is a zero-dimensional field theory.

We seek a way of linking the two-dimensional geometry of the target space to the matrix model. Our approach to creating this link is to use the matrix algebra of the *fuzzy sphere*. This is the canonical example of a noncommutative geometry, which is a deformation of a smooth space with the fundamental object of study being a

noncommuting algebra approximating the algebra of functions on the smooth space. The fuzzy sphere is formulated by deforming the algebra of smooth square-integrable functions on the sphere to be noncommuting in such a way that the $SO(3)$ symmetry of the sphere is preserved. The algebra depends on some discrete parameter N, which can be interpreted as either a short distance cutoff or as the quantum mechnical parameter $\hbar = 1/N$, depending on the formalism. The commutative algebra of functions on the sphere is recovered in the limit $N \to \infty$.

The algebra of functions of the fuzzy sphere with parameter N is isomorphic to the matrix algebra of $N \times N$ matrices. This allows us to reformulate the Gaussian Hermitian matrix model in terms of the degrees of freedom of the fuzzy sphere, which are the spherical harmonic modes cut off by the parameter N. Rephrasing the degrees of freedom of the matrix model in terms of the fuzzy sphere, which is manifestly $SO(3)$ covariant, leads to a formulation of the matrix model in terms of the representation theory of $SO(3)$. The combinatorics of equivalence classes of permutations in the conventional matrix model is essentially replaced by the combinatorics of the couplings of irreducible representations of $su(2)$.

Writing the Gaussian Hermitian matrix model as a theory on the fuzzy sphere gives us a way to reproduce the string theory correlators on the (cutoff) target space. One possible interpretation of this approach is that reformulating the field theory from the worldsheet theory to the target space theory is equivalent to creating a *spacetime action* for the string theory, in analogy to the low energy effective actions that can be constructed on the spacetimes of ten-dimensional string theories. The parameter N is analogous to the high-energy cutoff of the spacetime theory; a local divergent spacetime action is recovered as the cutoff is taken to infinity. (An alternative earlier interpretation of the fuzzy sphere matrix model was as an extension of the Belyi string theory to a *string field theory*, as string field theory is a field theory on the target space.) Regardless of its spacetime interpretation, the fuzzy sphere formulation of the matrix model leads to an equivalent matrix model determined by the combinatorics of $su(2)$ representation couplings, which can be extended to a three-dimensional model with gravity.

In this section, we first review some facts about the spherical harmonics on the smooth sphere, which form a basis for the commutative algebra of functions on S^2. We then discuss how to generalise this algebra to the noncommutative algebra of *fuzzy spherical harmonics*, which form a basis of the fuzzy sphere algebra of $N \times N$ matrices. Each spherical harmonic is labelled by a pair of quantum numbers (j, m), where j is a half-integer corresponding to an irreducible representation of $su(2)$, and

m determines a state in this representation. We refer to the labels j and m as a **spin label** and a **state label** respectively. In the following, we adopt the convention of using j and j_i to refer to spin labels taking half-integer values, and l_i for labels which are constrained to be integers. We reformulate the matrix model on the fuzzy sphere, and show by matching the observables of the matrix model in the two pictures that the Jacobian of the change of basis is trivial. We conclude this section by discussing how the fuzzy sphere matrix model can be thought of as a cutoff scalar field theory on the S^2 spacetime.

1.2.1 Spherical harmonics on S^2

We review some facts about the conventional algebra of functions on the smooth sphere S^2, before abstracting to the noncommutative algebra. The **spherical harmonics** $\tilde{Y}_{l,m}(\theta,\phi)$ are the eigenfunctions of the operators $\mathbf{L}^2 = L_i L_i$ and L_3, where $\mathbf{L} = -i\mathbf{r}\times\nabla$ is the orbital angular momentum operator on the sphere. They satisfy

$$\mathbf{L}^2\tilde{Y}_{l,m}(\theta,\phi) = l(l+1)\tilde{Y}_{l,m}(\theta,\phi), \tag{1.2.1}$$

$$L_3\tilde{Y}_{l,m}(\theta,\phi) = m\tilde{Y}_{l,m}(\theta,\phi), \tag{1.2.2}$$

where $l \in \{0,1,2,\ldots\}$ and $m \in \{-l,-l+1,\ldots,l\}$. With respect to the inner product

$$(\tilde{f},\tilde{g}) = \frac{1}{4\pi}\int d\Omega\ \tilde{f}(\theta,\phi)^*\tilde{g}(\theta,\phi), \tag{1.2.3}$$

the spherical harmonics are orthonormal: $(\tilde{Y}_{l,m},\tilde{Y}_{l',m'}) = \delta_{l,l'}\delta_{m,m'}$. The complex conjugate of a spherical harmonic is

$$\tilde{Y}_{l,m}(\theta,\phi)^* = (-)^m\tilde{Y}_{l,-m}(\theta,\phi). \tag{1.2.4}$$

The space of square-integrable functions on the sphere is a Hilbert space, and the set of spherical harmonics forms a complete orthonormal basis of this space. In particular, the product of two spherical harmonics can be expanded in terms of spherical harmonics:

$$\tilde{Y}_{l_1,m_1}(\theta,\phi)\tilde{Y}_{l_2,m_2}(\theta,\phi) = \sum_{l_3=0}^{\infty}\sum_{m_3=-l_3}^{l_3}\sqrt{(2l_1+1)(2l_2+1)(2l_3+1)} \times \begin{pmatrix} l_1 & l_2 & l_3 \\ 0 & 0 & 0 \end{pmatrix}\begin{pmatrix} l_1 & l_2 & l_3 \\ m_1 & m_2 & -m_3 \end{pmatrix}(-)^{m_3}\tilde{Y}_{l_3,m_3}(\theta,\phi). \tag{1.2.5}$$

The symbols in the brackets are the **Wigner** $3j$ **symbols**, which are essentially more symmetric versions of the Clebsch-Gordan coefficients of $su(2)$. Some properties and relations of $3j$ symbols are given in Appendix A. The symmetry properties of the $3j$ symbols ensure that this coefficient is invariant under the interchanging of the pair of variables (l_1, m_1) and (l_2, m_2).

1.2.2 Fuzzy spherical harmonics

All of the properties of spherical harmonics in the previous subsection can be generalised to the fuzzy sphere algebra. In the commutative sphere, the orbital angular momentum operators L_i form a representation of the Lie algebra $su(2)$, acting on the infinite-dimensional space of functions on the sphere. Consider the N-dimensional irreducible representation V of the Lie algebra $su(2)$, which has the $N \times N$ Hermitian matrix generators J_i. The N-dimensional irreducible representation of $su(2)$ is conventionally labelled by the half-integer j, where

$$j = \frac{1}{2}(N-1), \qquad N = 2j+1. \tag{1.2.6}$$

In the following we will freely interchange between describing $su(2)$ representations with the spin label j and their dimension N. The **fuzzy spherical harmonics** $Y_{l,m}$ are a set of $N \times N$ matrices which are the eigenvectors of the Lie algebra operators under the adjoint action of the matrix generators J_3 and $\mathbf{J}^2$. They satisfy

$$\begin{aligned} [J_i, [J_i, Y_{l,m}]] = \ & \mathrm{ad}_{J_i}(\mathrm{ad}_{J_i}(Y_{l,m})) && = l(l+1)Y_{l,m}, \\ [J_3, Y_{l,m}] = \ & \mathrm{ad}_{J_3}(Y_{l,m}) && = mY_{l,m}. \end{aligned} \tag{1.2.7}$$

where $l \in \{0, 1, \ldots, 2j\}$, $m \in \{-l, -l+1, \ldots, l\}$. The inner product on the fuzzy spherical harmonics is the matrix trace

$$(f, g) = \frac{1}{N}\mathrm{tr}(f^\dagger g), \tag{1.2.8}$$

in which the fuzzy spherical harmonics are orthonormal: $(Y_{l_1,m_1}, Y_{l_2,m_2}) = \delta_{l_1,l_2}\delta_{m_1,m_2}$. The Hermitian conjugate of a fuzzy spherical harmonic is

$$Y_{l,m}^\dagger = (-)^m Y_{l,-m}. \tag{1.2.9}$$

Unlike the continuous spherical harmonics, there are only finitely many fuzzy spherical harmonics within the algebra of $N \times N$ matrices for any given N. The parameter

N acts like a cutoff: all the fuzzy spherical harmonics have $l \leq 2j = N-1$. Within the algebra $\mathcal{A}_N$ of $N \times N$ matrices, the fuzzy spherical harmonics form a complete orthonormal basis. In particular, we can expand the product of two fuzzy spherical harmonics:

$$Y_{l_1,m_1} Y_{l_2,m_2} = \sum_{l_3=0}^{2j} \sum_{m_3=-l_3}^{l_3} \sqrt{(2l_1+1)(2l_2+1)(2l_3+1)} \times (-)^{3j} \sqrt{2j+1} \left| \begin{array}{ccc} l_1 & l_2 & l_3 \\ j & j & j \end{array} \right| \left(\begin{array}{ccc} l_1 & l_2 & l_3 \\ m_1 & m_2 & -m_3 \end{array} \right) (-)^{m_3} Y_{l_3,m_3}. \quad (1.2.10)$$

The symbol in the straight brackets is the **Wigner** $6j$ **symbol**, which corresponds to the coupling of six irreducible representations of $su(2)$ into a singlet. The definition and some properties of $6j$ symbols are given in Appendix A. This expression shows that the fuzzy spherical harmonics do not commute, as a phase is introduced on interchanging the pairs (l_1, m_1) and (l_2, m_2) in (1.2.10). In the limit as $N = 2j+1$ tends to infinity, the $6j$ symbol asymptotes to

$$\lim_{j\to\infty} (-)^{3j} \sqrt{2j+1} \left| \begin{array}{ccc} l_1 & l_2 & l_3 \\ j & j & j \end{array} \right| = \left(\begin{array}{ccc} l_1 & l_2 & l_3 \\ 0 & 0 & 0 \end{array} \right), \quad (1.2.11)$$

which shows that the fuzzy spherical harmonics algebra reproduces the spherical harmonics algebra (1.2.5) in the large N limit. A more symmetric coefficient of the $N \times N$ fuzzy spherical harmonics algebra is

$$\begin{aligned} A_{l_1,m_1,l_2,m_2,l_3,m_3} &= N^{-1} \mathrm{tr}(Y_{l_1,m_1} Y_{l_2,m_2} Y_{l_3,m_3}) \\ &= \sqrt{(2l_1+1)(2l_2+1)(2l_3+1)} (-)^{3j} \sqrt{2j+1} \left| \begin{array}{ccc} l_1 & l_2 & l_3 \\ j & j & j \end{array} \right| \left(\begin{array}{ccc} l_1 & l_2 & l_3 \\ m_1 & m_2 & m_3 \end{array} \right), \end{aligned} \quad (1.2.12)$$

which allows us to write a product of fuzzy spherical harmonics as

$$Y_{l_1,m_1} Y_{l_2,m_2} = \sum_{l_3,m_3} A_{l_1,m_1,l_2,m_2,l_3,m_3} Y^\dagger_{l_3,m_3} \quad (1.2.13)$$

where the factor of N has been introduced in this definition for later convenience. This coefficient is invariant under the cyclic interchange of the pairs (l_i, m_i), but changes by a phase under the transposition of any two pairs. The parameter j (or equivalently N) is the noncommutativity parameter of the fuzzy sphere. An exact expression for

fuzzy spherical harmonics is given in [47]:

$$Y_{l,m} = \sqrt{(2l+1)(2j+1)} \sum_{\mu,\nu} (-)^{j-l+\mu} \begin{pmatrix} j & j & l \\ -\mu & \nu & m \end{pmatrix} |j,\mu\rangle\langle j,\nu|. \tag{1.2.14}$$

The state vectors $|j,\mu\rangle$, where $\mu \in \{-j, -j+1, \ldots, j\}$, are an orthonormal basis of the N-dimensional $su(2)$ representation V.

1.2.3 Scalar field theory on the fuzzy sphere

Scalar field theories can be constructed on the fuzzy sphere by analogy with those on the commutative sphere [48, 49, 50]. On the commutative sphere, any function can be expanded in terms of the spherical harmonics, and the degrees of freedom of the function are a discrete set of expansion coefficients. The path integral of a field on the sphere is performed by integrating over these modes.

The noncommutative version of a field on the fuzzy sphere is an $N \times N$ matrix in the fuzzy sphere algebra $\mathcal{A}_N$. Any $N \times N$ matrix can be expanded in terms of the fuzzy spherical harmonics

$$X = \frac{1}{\sqrt{N}} \sum_{l=0}^{N-1} \sum_{m=-l}^{l} a_{l,m} Y_{l,m}, \tag{1.2.15}$$

where the N^2 coefficients $a_{l,m}$ are the coefficients of the fuzzy spherical harmonic expansion. As the fuzzy spherical harmonics satisfy $Y_{l,m}^\dagger = (-)^m Y_{l,-m}$, we can set the matrix X to be Hermitian by demanding that the complex conjugate of each mode $a_{l,m}$ satisfies

$$a_{l,m}^* = (-)^m a_{l,-m}. \tag{1.2.16}$$

For a one-field theory with an action $S[X]$, the partition function is

$$Z = \int Da\ e^{-S[X]}, \tag{1.2.17}$$

where the path integral is performed over the N^2 real degrees of freedom with the measure

$$Da = \prod_{l=0}^{N-1} \left[da_{l,0} \prod_{m=1}^{l} da_{l,m} da_{l,m}^* \right]. \tag{1.2.18}$$

In [48, 49, 50], the scalar field theories considered on the fuzzy sphere have the action

$$S[X] = \mathrm{tr}\left(\frac{1}{2}X[J_i,[J_i,X]] + \frac{1}{2}\mu^2 X^2 + V(X)\right), \tag{1.2.19}$$

which includes a Laplacian, a mass term, and a general potential term. The propagator of this theory is

$$\langle a^*_{l,m} a_{l',m'}\rangle := \frac{\int Da\ e^{-S} a^*_{l,m} a_{l',m'}}{\int Da\ e^{-S}} = \frac{\delta_{l,l'}\delta_{m,m'}}{l(l+1)+\mu^2}. \tag{1.2.20}$$

In this thesis, we will constrain our attention to *topological* theories on the fuzzy sphere with vanishing Laplacian. We drop the Laplacian from the action and for now we set the potential term to zero, leaving just a mass term. Setting $\mu^2 = 1$ and using the fact that the trace of two matrices can be expanded into fuzzy spherical harmonic modes as

$$\begin{aligned}\mathrm{tr}(X^2) &= \frac{1}{N}\sum_{l,l'=0}^{N-1}\sum_{m=-l}^{l}\sum_{m'=-l'}^{l'} a_{l,m}a_{l',m'}\mathrm{tr}(Y_{l,m}Y_{l',m'}) \\ &= \sum_{l=0}^{N-1}\sum_{m=-l}^{l} a^*_{l,m}a_{l,m},\end{aligned} \tag{1.2.21}$$

we arrive at the partition function for the topological scalar theory on the fuzzy sphere

$$Z = \int Da\ e^{-\frac{1}{2}\mathrm{tr}X^2} = \int Da\ \exp\left(-\frac{1}{2}\sum_{l=0}^{N-1}\sum_{m=-l}^{l} a^*_{l,m}a_{l,m}\right). \tag{1.2.22}$$

This is a Gaussian Hermitian matrix model like the one discussed in Section 1.1, but with the N^2 real degrees of freedom rewritten in the $su(2)$-covariant form $a_{l,m}$ instead of the $U(N)$-covariant form $X^i{}_j$. We will prove in this subsection that the matrix models are equivalent by comparing the correlators of arbitrary products of traces in the two pictures. This will implicitly show that the Jacobian generated from changing the measure $DX \to Da$ is trivial. The propagator in the topological theory is

$$\langle a^*_{l,m} a_{l',m'}\rangle := \frac{\int Da\ e^{-\frac{1}{2}\left(\sum_{l,m} a^*_{l,m}a_{l,m}\right)} a^*_{l,m}a_{l',m'}}{\int Da\ e^{-\frac{1}{2}\left(\sum_{l,m} a^*_{l,m}a_{l,m}\right)}} = \delta_{l,l'}\delta_{m,m'}. \tag{1.2.23}$$

By Wick's theorem, the correlator of a set of $2n$ Fourier modes is

$$\langle a_{l_1,m_1} \dots a_{l_{2n},m_{2n}} \rangle = \sum_{\tau \in [2^n]} \prod_{\substack{\text{disjoint cycles} \\ (ik) \text{ in } \tau}} \langle a_{l_i,m_i} a_{l_k,m_k} \rangle \tag{1.2.24}$$

$$= \sum_{\tau \in [2^n]} \prod_{(ik) \in \tau} (-)^{m_i} \delta_{l_i,l_k} \delta_{m_i,-m_k}. \tag{1.2.25}$$

As in the conventional Gaussian Hermitian matrix model, the traces and products of traces of a matrix are invariant under the adjoint action of $U(N)$. The observables of this topological fuzzy sphere theory can also be taken to be the correlators of multi-traces. The correlator of a trace $\mathrm{tr}X^{2n}$ separates out into the modes and the trace of the fuzzy spherical harmonics:

$$\langle \mathrm{tr}X^{2n} \rangle = \frac{1}{N^n} \langle a_{l_1,m_1} \dots a_{l_{2n},m_{2n}} \rangle \mathrm{tr}(Y_{l_1,m_1} \dots Y_{l_{2n},m_{2n}}). \tag{1.2.26}$$

and similiarly a product of traces separates out in this manner into a Fourier modes correlator and a product traces of fuzzy spherical harmonics. The traces over fuzzy spherical harmonics can be expanded out by using the fuzzy spherical harmonics algebra

$$\mathrm{tr}(Y_{l_1,m_1} Y_{l_2,m_2} Y_{l_3,m_3}) = N A_{l_1,m_1,l_2,m_2,l_3,m_3}, \tag{1.2.27}$$

$$\mathrm{tr}(Y_{l_1,m_1} Y_{l_2,m_2}) = N(-)^{m_1} \delta_{l_1,l_2} \delta_{m_1,-m_2}. \tag{1.2.28}$$

This allows us to express any correlator in the fuzzy sphere theory as a sum over spin labels and the fuzzy sphere algebra coefficients $A_{l_1,m_1\dots}$, which becomes a sum over spin labels weighted by Wigner $3j$ and $6j$ symbols. Unsurprisingly, we will find that the evaluation of any product of traces of a matrix in the conventional matrix model picture agrees with its evaluation in the fuzzy sphere theory. The Jacobian associated to the transformation between the matrix model measure (1.1.10) and the fuzzy sphere measure (1.2.18) is trivial. We show this at the level of the observables by showing that the fuzzy sphere correlators satisfy the relation (1.1.15) of the conventionally-defined matrix model,

$$\langle \mathrm{tr}_{2n}(\mathbf{X}\sigma) \rangle = \sum_{\tau \in [2^n]} N^{C_{\sigma\tau}}. \tag{1.2.29}$$

Firstly, we recall that the fuzzy spherical harmonics act on an N-dimensional $su(2)$ representation $|j,\mu\rangle$, where $\mu \in \{-j, -j+1, \dots, j\}$ and $N = 2j+1$. We abbreviate

these state vectors to $|\mu\rangle$ in the following. In the tensor space notation, a general product of traces can be expressed by a permutation $\sigma \in S_{2n}$ acting on a product of states

$$\begin{aligned} \mathrm{tr}_{2n}(\mathbf{X}\sigma) &= \sum_{\mu_1,\ldots,\mu_{2n}} \langle \mu_1\mu_2\ldots\mu_{2n}|\mathbf{X}\sigma|\mu_1\mu_2\ldots\mu_{2n}\rangle \\ &:= \sum_{\mu_1,\ldots,\mu_{2n}} \langle \mu_1\mu_2\ldots\mu_{2n}|\mathbf{X}|\mu_{\sigma(1)}\mu_{\sigma(2)}\ldots\mu_{\sigma(2n)}\rangle \end{aligned} \tag{1.2.30}$$

where $\mathbf{X} = X \otimes \ldots \otimes X$ is the operator formed from $2n$ copies of X. This tensor product can be decomposed into the fuzzy spherical harmonic modes and a *tensor* product of fuzzy spherical harmonics,

$$\mathbf{X} = \frac{1}{N^n} \sum_{l_1\ldots l_{2n}} \sum_{m_1\ldots m_{2n}} a_{l_1,m_1} a_{l_2,m_2}\ldots a_{l_{2n},m_{2n}} Y_{l_1,m_1} \otimes Y_{l_2,m_2} \otimes \ldots \otimes Y_{l_{2n},m_{2n}}. \tag{1.2.31}$$

From (1.2.25), the fuzzy sphere correlator of this operator evaluates to a sum running over the conjugacy class of disjoint products of 2-cycles $[2^n]$. For a given $\tau \in [2^n]$, the weight associated to each 2-cycle $(ik) \in \tau$ is

$$(-)^{m_i} \delta_{l_i,l_k} \delta_{m_i,-m_k}. \tag{1.2.32}$$

A tensor product of fuzzy spherical harmonics $Y_{l_i,m_i} \otimes Y_{l_k,m_k}$ is an operator acting on the tensor product space $V \otimes V$. We can evaluate the operator formed from contracting the fuzzy spherical harmonics with (1.2.32) by using the explicit expression for the fuzzy spherical harmonics (1.2.14), and the orthogonality relations of the Wigner $3j$ symbols:

$$\sum_{\substack{l_i,m_i \\ l_k,m_k}} (-)^{m_i} \delta_{l_i,l_k} \delta_{m_i,-m_k} Y_{l_i,m_i} \otimes Y_{l_k,m_k} \tag{1.2.33}$$

$$= \sum_{\substack{l_i m_i \\ l_k, m_k}} \sum_{\substack{\mu_i, \nu_i \\ \mu_k, \nu_k}} (2j+1)\sqrt{(2l_i+1)(2l_k+1)}(-)^{m_i+2j-l_i+\mu_i-l_k+\mu_k}\delta_{l_i,l_k}\delta_{m_i,-m_k}$$
$$\times \begin{pmatrix} j & j & l_i \\ -\mu_i & \nu_i & m_i \end{pmatrix} \begin{pmatrix} j & j & l_k \\ -\mu_k & \nu_k & -m_k \end{pmatrix} |\mu_i\rangle\langle\nu_i| \otimes |\mu_k\rangle\langle\nu_k|$$

$$= N \sum_{l_i, m_i} \sum_{\substack{\mu_i, \nu_i \\ \mu_k, \nu_k}} (-)^{2j+\mu_i+\nu_k}(2l_i+1) \begin{pmatrix} j & j & l_i \\ -\mu_i & \nu_i & m_i \end{pmatrix} \begin{pmatrix} j & j & l_i \\ -\nu_k & \mu_k & m_i \end{pmatrix} |\mu_i\rangle\langle\nu_i| \otimes |\mu_k\rangle\langle\nu_k|$$

$$\begin{aligned} &= N \sum_{\substack{\mu_i, \nu_i \\ \mu_k, \nu_k}} (-)^{2j+\mu_i+\nu_k}\delta_{\mu_i,\nu_k}\delta_{\nu_i,\mu_k} m_i |\mu_i\rangle\langle\nu_i| \otimes |\mu_k\rangle\langle\nu_k| \\ &= N \sum_{\mu_i, \mu_k} |\mu_i\rangle\langle\mu_k| \otimes |\mu_k\rangle\langle\mu_i|. \end{aligned} \tag{1.2.34}$$

This operator acts on $V \otimes V$ by interchanging the basis elements $|\mu_i\rangle$ from the first copy of V with the basis elements $|\mu_k\rangle$ in the second copy of V. We see from the defining equation (1.1.6) for the action of permutations on tensor space that the contracted spherical harmonics pair acts on the basis vectors in the same way as a transposition. We can therefore write the following operator equation, valid when acting on tensor product space $V^{\otimes 2n}$,

$$\frac{1}{N} \sum_{\substack{l_i, m_i \\ l_k, m_k}} (-)^{m_i} \delta_{l_i,l_k}\delta_{m_i,-m_k} Y_{l_i,m_i} \otimes Y_{l_k,m_k} = (i,k). \tag{1.2.35}$$

By applying Wick's theorem (1.2.25), the fuzzy sphere correlator of a tensor product of $2n$ operators is

$$\begin{aligned} \langle \mathbf{X} \rangle &= \frac{1}{N^n} \sum_{\substack{l_1, l_2, \ldots \\ m_1, m_2, \ldots}} \langle a_{l_1,m_1} a_{l_2,m_2} \ldots a_{l_{2n},m_{2n}} \rangle Y_{l_1,m_1} \otimes Y_{l_2,m_2} \otimes \ldots \otimes Y_{l_{2n},m_{2n}} \\ &= \frac{1}{N^n} \sum_{\substack{l_1, l_2, \ldots \\ m_1, m_2, \ldots}} \left[\sum_{\tau \in [2^n]} \prod_{(ik) \in \tau} (-)^{m_i} \delta_{l_i,l_k}\delta_{m_i,-m_k} \right] Y_{l_1,m_1} \otimes Y_{l_2,m_2} \otimes \ldots \otimes Y_{l_{2n},m_{2n}} \\ &= \sum_{\tau \in [2^n]} \tau. \end{aligned} \tag{1.2.36}$$

The matrix model on the fuzzy sphere exactly reproduces the operator equation (1.1.14). The correlator in the fuzzy sphere matrix model of a general product of

traces specified by a permutation $\sigma \in S_{2n}$ is

$$\langle \mathrm{tr}_{2n}(\mathbf{X}\sigma)\rangle \;=\; \sum_{\tau\in[2^n]} \mathrm{tr}_{2n}(\sigma\tau). \tag{1.2.37}$$

We conclude by direct comparison of the observables of the two formulations of the matrix models the Jacobian of the path integral under the change of variables $X^i{}_j \to a_{l,m}$ is trivial.

While the topological fuzzy sphere can be thought of as a theory of matrices, the above partition functions can be rephrased into theories of continuous functions on the sphere with an angular momentum cutoff and a modified multiplication of the fields. The partition function of the matrix model on a fuzzy sphere with a trivalent potential is written

$$\begin{aligned} Z &= \int Da\ \exp\left(-\frac{1}{2}\mathrm{tr}X^2 + \lambda\sqrt{N}\mathrm{tr}X^3\right) \\ &= \int Da\ \exp\left(-\frac{1}{2}\sum_{l=0}^{N-1}\sum_{m=-l}^{l} a^*_{l,m}a_{l,m} + \lambda \sum_{\substack{l_1,l_2,l_3\\ m_1,m_2,m_3}} A_{l_1,m_1,l_2,m_2,l_3,m_3}a_{l_1,m_1}a_{l_2,m_2}a_{l_3,m_3}\right). \end{aligned} \tag{1.2.38}$$

For a given $N = 2j+1$, the **star product** on a pair of continuous spherical harmonics $\tilde{Y}_{l_1,m_1}, \tilde{Y}_{l_2,m_2}$ with angular momenta $l_1, l_2 < N$ reproduces the fuzzy spherical harmonics algebra (1.2.12),

$$\tilde{Y}_{l_1,m_1} \star \tilde{Y}_{l_2,m_2} = \sum_{l_3=0}^{N-1}\sum_{m_3=-l_3}^{l_3} A_{l_1,m_1,l_2,m_2,l_3,m_3}\tilde{Y}^\dagger_{l_3,m_3}. \tag{1.2.39}$$

A scalar field on the sphere consisting of only low-energy modes can be expanded as

$$\tilde{X} = \sum_{l=0}^{N-1}\sum_{m=-l}^{l} \tilde{a}_{l,m}\tilde{Y}_{l,m}, \tag{1.2.40}$$

which allows the matrix model partition function (1.2.38) to be equivalently written as

$$Z = \int D\tilde{a}|_{l<N} \exp\left(-\frac{1}{4\pi}\int d\Omega\left(\frac{1}{2}\tilde{X}^2 - \lambda\tilde{X}\star\tilde{X}\star\tilde{X}\right)\right). \tag{1.2.41}$$

Here, the partition function integration is performed only over the low-energy modes

$a_{l,m}$ with $l < N$. The large N limit of this partition function is the topological theory on the continuous sphere,

$$\tilde{Z} = \int D\tilde{a}\ \exp\left(-\frac{1}{4\pi}\int d\Omega\left(\frac{1}{2}\tilde{X}^2 - \lambda\tilde{X}^3\right)\right). \tag{1.2.42}$$

It seems natural to interpret (1.2.41) as the low energy cutoff version of this topological field theory on the continuous sphere. This makes manifest the fact that the fuzzy sphere matrix model is a theory on the S^2 target space, and so gives a convincing candidate for the spacetime theory of the Belyi string.

1.3 Ribbon graphs in the fuzzy sphere matrix model

In the previous section, we reformulated the matrix model on the fuzzy sphere, showed that it was equivalent to the conventionally-defined matrix model, and proposed that this is the spacetime theory of the Belyi string. In this section, we investigate the matrix model on the fuzzy sphere by studying the ribbon graphs of the correlators. For a product of traces determined by a permutation σ, the matrix model correlator of this trace product evaluates to a sum over the Wick contractions, ranging over the conjugacy class $\tau \in [2^n]$. Each pair (σ, τ) determines a ribbon graph $\mathcal{G}(\sigma, \tau)$ of the correlator. The contribution to the correlator coming from the Wick contraction τ is

$$\langle \mathrm{tr}_{2n}(\mathbf{X}\sigma)\rangle\big|_\tau \quad = \quad \mathrm{tr}_{2n}(\sigma\tau) = N^{C_{\sigma\tau}}, \tag{1.3.1}$$

where $\sigma\tau$ is the permutation describing the faces of the ribbon graph. The number of cycles in the product permutation $\sigma\tau$ is the number of faces of the ribbon graph $\mathcal{G}$. If we introduce the normalisation factor $N^{C_\sigma - n}$, then we can use the formula for the Euler characteristic of a graph embedded on a surface, and the fact that the cycles of σ correspond to the vertices of the ribbon graph, to state that

$$N^{C_\sigma - n}\langle \mathrm{tr}_{2n}(\mathbf{X}\sigma)\rangle\big|_\tau = \prod_i N^{2-2g_i} \tag{1.3.2}$$

where the product is performed over all the connected components of the graph, and g_i is the genus of each connected component of the ribbon graph.

For a pair of permutations (σ, τ) determining a connected ribbon graph $\mathcal{G}$ of genus g, we define the **ribbon graph evaluation** $\mathcal{R}$ of the graph to be the contribution to

the correlator associated with this graph:

$$\mathcal{R}(\mathcal{G}) := \langle \mathrm{tr}_{2n}(\mathbf{X}\sigma)\rangle|_\tau = N^{C_{\sigma\tau}} = N^{2-2g-C_\sigma+n}. \tag{1.3.3}$$

Fuzzy sphere correlator contributions can also be expanded as a sum over spin labels and spin states:

$$\mathcal{R}(\mathcal{G}) = N^{-n} \sum_{\substack{l_1,l_2,\ldots \\ m_1,m_2,\ldots}} \langle a_{l_1,m_1} a_{l_2,m_2} \ldots a_{l_{2n},m_{2n}}\rangle|_\tau \, \mathrm{tr}_{2n}(Y_{l_1,m_1} \otimes Y_{l_2,m_2} \otimes \ldots \otimes Y_{l_{2n},m_{2n}}\sigma). \tag{1.3.4}$$

The contribution from τ to the correlator of modes is proportional to a product of n Kronecker deltas relating the spin labels l_i, and n Kronecker deltas relating the spin states m_i. The trace of the product of fuzzy spherical harmonics is a product of factors including $3j$ symbols, $6j$ symbols, and dimensions of $su(2)$ representations. We will show in this section that the structure of both of these factors can be read off from the ribbon graph by deriving a set of Feynman rules. While it may seem superfluous to expand a ribbon graph in terms of quite an involved product of $su(2)$-covariant factors when the exact answer $\mathcal{R}(\mathcal{G})$ can be read off counting faces, this expanded spin state sum is crucial for deriving a three-dimensional interpretation of the Belyi string within the Ponzano-Regge spin foam model.

Each trivalent ribbon graph corresponds to a sum over spin labels l_p and spin states m_p, weighted by $3j$ and $6j$ symbols. The sum over spin states m_p with $3j$ weights corresponds to the evaluation of a *spin network* found in the literature [51, 52, 53, 9]. We show in this section that any spin network state sum can be evaluated explicitly to a product of $6j$ symbols and representation dimensions with a series of *trivalent graph moves*.

Initially, we only consider correlators of trace triples, which generate trivalent ribbon graphs with V vertices and E edges, where $3V = 2E$. These trace products correspond to conjugacy classes of the form $\sigma \in [3^V]$:

$$\langle \mathrm{tr}_{2E}(\mathbf{X}\sigma)\rangle = \langle (\mathrm{tr}X^3)^V\rangle = \sum_{\tau\in[2^E]} \mathrm{tr}_{2E}(\sigma\tau). \tag{1.3.5}$$

Such correlators can be generated by adding a potential term to the action of the

matrix model on the fuzzy sphere:

$$Z = \int Da\; e^{-\frac{1}{2}\mathrm{tr}X^2+\lambda\sqrt{N}\mathrm{tr}X^3} \;=\; \sum_{k\geq 0}\frac{\lambda^{2k}N^k}{(2k)!}\langle(\mathrm{tr}X^3)^{2k}\rangle. \tag{1.3.6}$$

In such cases, the structure of the representation sum is particularly simple: there is a spin label pair (l_p, m_p) for each of the $2E = 6k$ fuzzy spherical harmonic modes, a $3j$ and a $6j$ symbol generated by each trace, and a Kronecker delta for each of the E Wick contractions. Later in this section, we will show that any multi-trace correlator can be 'expanded' into a partially-contracted correlator of trace triples, which corresponds to a sum over trivalent ribbon graphs.

1.3.1 Trivalent ribbon graphs

In this section we adopt the short-hand notation of representing a spin label and spin state pair (l_p, m_p) by a generalised index L_p, and abbreviate $a_{l_p,m_p} \to a^{L_p}$, $Y_{l_p,m_p} \to Y_{L_p}$, and $A_{l_1,m_1,l_2,m_2,l_3,m_3} \to A_{L_1L_2L_3}$. We introduce the **eta symbol** to describe the trace of a pair of fuzzy spherical harmonics,

$$\eta^{L_pL_q} := (-)^{m_p}\delta_{l_p,l_q}\delta_{m_p,-m_q}. \tag{1.3.7}$$

Consider a trivalent ribbon graph $\mathcal{G}$ with V vertices described by the cycles of a permutation $\sigma \in [3^V]$ and with edges described by the cycles of $\tau \in [2^E]$, where $3V = 2E$. The contribution to the matrix model correlator from this ribbon graph is

$$\mathcal{R}(\mathcal{G}) = N^{-E}\sum_{\substack{l_1,l_2,\ldots\\ m_1,m_2,\ldots}}\langle a_{l_1,m_1}a_{l_2,m_2}\ldots a_{l_{2E},m_{2E}}\rangle|_\tau\,\mathrm{tr}_{2n}(Y_{l_1,m_1}\otimes Y_{l_2,m_2}\otimes\ldots\otimes Y_{l_{2E},m_{2E}}\sigma). \tag{1.3.8}$$

In this expression, we are only considering the Wick contraction corresponding to the permutation τ. For example, if $\tau = (1,2)(3,4)\ldots(2E-1,2E)$, then the Wick contraction is

$$\begin{aligned}\langle a_{l_1,m_1}a_{l_2,m_2}\ldots a_{l_{2E},m_{2E}}\rangle|_\tau &= \langle a_{l_1,m_1}a_{l_2,m_2}\rangle\langle a_{l_3,m_3}a_{l_4,m_4}\rangle\ldots\langle a_{l_{2E-1},m_{2E-1}}a_{l_{2E},m_{2E}}\rangle\\ &= (-)^{m_1+m_3+\ldots+m_{2E-1}}\delta_{l_1,l_2}\delta_{m_1,-m_2}\ldots\delta_{l_{2E-1},l_{2E}}\delta_{m_{2E-1},-m_{2E}}.\end{aligned} \tag{1.3.9}$$

In terms of the eta symbols and short-hand indices, this can be written

$$\langle a^{L_1} a^{L_2} \dots a^{L_{2E}} \rangle\big|_\tau = \eta^{L_1 L_2} \eta^{L_3 L_4} \dots \eta^{L_{2E-1} L_{2E}}. \tag{1.3.10}$$

The tensor product trace of fuzzy spherical harmonics becomes a product of triples of traces of fuzzy spherical harmonics determined by the permutation $\sigma \in [3^V]$. For example, if $\sigma = (1,2,3)(4,5,6)\dots$, then the tensor product trace becomes

$$\mathrm{tr}_{2E}(Y_{l_1,m_1} \otimes \dots \otimes Y_{l_{2E},m_{2E}} \sigma) = \mathrm{tr}(Y_{l_1,m_1} Y_{l_2,m_2} Y_{l_3,m_3}) \mathrm{tr}(Y_{l_4,m_4} Y_{l_5,m_5} Y_{l_6,m_6}) \dots . \tag{1.3.11}$$

In terms of the coupling coefficients (1.2.12) corresponding to the trace of a product of fuzzy spherical harmonics, this trace product can be written in the short-hand notation

$$\begin{aligned} \mathrm{tr}_{2E}(Y_{L_1} \otimes Y_{L_2} \otimes \dots \otimes Y_{L_{2E}} \sigma) &= \mathrm{tr}(Y_{L_1} Y_{L_2} Y_{L_3}) \mathrm{tr}(Y_{L_4} Y_{L_5} Y_{L_6}) \dots \\ &= N^V A_{L_1 L_2 L_3} A_{L_4 L_5 L_6} \dots . \end{aligned} \tag{1.3.12}$$

With the expression (1.3.10) for the Wick contractions, a general trivalent ribbon graph sum will be of the form

$$\mathcal{R}(\mathcal{G}) = N^{V-E} \sum_{L_1, L_2, \dots} \eta^{L_1 L_2} \eta^{L_3 L_4} \dots A_{L_1 L_2 L_3} A_{L_4 L_5 L_6} \dots , \tag{1.3.13}$$

where the sum runs over all spin label pairs. There is a spin label pair (l_p, m_p) assigned to each *half-edge* of the ribbon graph (denoted by L_p), a factor of $A_{L_p L_q L_r}$ associated to each of the V vertices of the graph, and a factor of $\eta^{L_p L_q}$ associated to each of the E edges of the graph.

In writing ribbon graph evaluations in terms of the traces $\eta^{L_p L_q}$ and $A_{L_p L_q L_r}$, we have essentially hidden away the representation-dependent factors from the sums, such as the Wigner $3j$ and $6j$ symbols, the representation dimensions, and various phases. We can bring these factors back to write down the evaluation of a graph directly in terms of the $3j$ and $6j$ symbols. There is a factor of

$$\eta^{L_p L_q} = (-)^{m_p} \delta_{l_p, l_q} \delta_{m_p, -m_q} \tag{1.3.14}$$

associated to each of the E edges of the graph, and a factor of

$$A_{L_pL_qL_r} = \sqrt{N}(-)^{3j}\sqrt{(2l_p+1)(2l_q+1)(2l_r+1)}\left(\begin{array}{ccc} l_p & l_q & l_r \\ m_p & m_q & m_r \end{array}\right)\left|\begin{array}{ccc} l_p & l_q & l_r \\ j & j & j \end{array}\right| \tag{1.3.15}$$

associated to each of the V vertices. Collating the powers of N arising from the normalisation and the V factors of $A_{L_pL_qL_r}$, we have an overall factor of $N^{3V/2-E}$. Since we are working with a trivalent graph, we know that $3V = 2E$, and so the overall factor of N vanishes. Also noting that $(-)^{3jV} = (-)^{2jE}$, we can arrive at an expression for $\mathcal{R}(\mathcal{G})$ by associating a factor of

$$\left(\begin{array}{ccc} l_p & l_q & l_r \\ m_p & m_q & m_r \end{array}\right)\left|\begin{array}{ccc} l_p & l_q & l_r \\ j & j & j \end{array}\right| \tag{1.3.16}$$

to each vertex connecting the half-edges labelled p, q, and r; a factor of

$$(2l_p+1)(-)^{2j+m_p}\delta_{l_p,l_q}\delta_{m_p,-m_q} \tag{1.3.17}$$

to each edge connecting the half-edges labelled p and q; and evaluating a sum over all the spin labels l_p and their associated spin states m_p. We find that the Wigner $3j$ and $6j$ sum associated to the graph is

$$\mathcal{R}(\mathcal{G}) = (-)^{2jE}\sum_{\substack{l_1,\ldots l_{2E} \\ m_1,\ldots,m_{2E}}}\left(\prod_{\text{edges}}(2l_p+1)(-)^{m_p}\delta_{l_p,l_q}\delta_{m_p,-m_q}\right) \times\left(\prod_{\text{vertices}}\left(\begin{array}{ccc} l_p & l_q & l_r \\ m_p & m_q & m_r \end{array}\right)\left|\begin{array}{ccc} l_p & l_q & l_r \\ j & j & j \end{array}\right|\right). \tag{1.3.18}$$

This sum is performed over the $2E$ spin labels l_p and the $2E$ state labels m_p. As each edge is associated to a pair of Kronecker deltas, we can immediately sum out half of the spin labels. This results in a sum over E pairs of spin labels, with a single label pair associated to each edge. Summing out the factors of $\delta_{m_p,-m_q}$ will result in each spin state label m_p appearing in two different Wigner $3j$ symbols with different signs.

The evaluation of a trivalent ribbon graph becomes

$$\mathcal{R}(\mathcal{G}) = (-)^{2jE} \sum_{\substack{l_1,\dots l_E \\ m_1,\dots m_E}} \prod_{\text{edges}} (-)^{m_p}(2l_p{+}1) \prod_{\text{vertices}} \left| \begin{matrix} l_p & l_q & l_r \\ j & j & j \end{matrix} \right| \left(\begin{matrix} l_p & l_q & l_r \\ \pm m_p & \pm m_q & \pm m_r \end{matrix} \right). \tag{1.3.19}$$

We can partition the sum (1.3.19) into two parts by considering just the m_p-dependent factors, which are the $3j$s and phase factors $(-)^{m_p}$, and performing the sums over the state labels m_p. For a trivalent ribbon graph $\mathcal{G}$ with the spin labels (l_p, m_p) assigned to each edge, we fix each spin label l_p and allow the spin state labels m_p to run over the ranges $\{-l_p, -l_p+1, \dots, l_p\}$ to get the $3j$ sum

$$\boxed{S(\mathcal{G}, \{l_p\}) := \sum_{m_1,\dots,m_E} \prod_{\text{edges}} (-)^{m_p} \prod_{\text{vertices}} \left(\begin{matrix} l_p & l_q & l_r \\ \pm m_p & \pm m_q & \pm m_r \end{matrix} \right).} \tag{1.3.20}$$

Expressions of this form appear frequently in the literature [51, 52, 53, 9]. This sum over $3j$ symbols corresponds to the evaluation of a *spin network*, which is a trivalent graph labelled by $su(2)$ representations with a particular set of weights assigned to the edges and vertices. Hence we call $S(\mathcal{G}, \{l_p\})$ the **spin network state sum**, or the $3j$ sum, associated to a trivalent ribbon graph $\mathcal{G}$ with labelled edges l_p. The ribbon graph evaluation can now be written as a sum over purely the spin labels l_p, weighted by $6j$s, dimensions, and the spin network state sum,

$$\boxed{\mathcal{R}(\mathcal{G}) = (-)^{2jE} \sum_{l_p} S(\mathcal{G}, \{l_p\}) \prod_{\text{edges}} (2l_p+1) \prod_{\text{vertices}} \left| \begin{matrix} l_p & l_q & l_r \\ j & j & j \end{matrix} \right|.} \tag{1.3.21}$$

This is the form of the ribbon graph sum that we will use in the next section to build a link between the matrix model on the fuzzy sphere and the three-dimensional Ponzano-Regge model.

We conclude this subsection with an example. The simplest non-trivial trivalent ribbon graph correlator is

$$\langle \mathrm{tr}_6(\mathbf{X}\sigma) \rangle = \langle (\mathrm{tr} X^3)^2 \rangle, \tag{1.3.22}$$

where $\sigma = (1,2,3)(4,5,6) \in [3^2]$ is a product of two 3-cycles. The Wick contractions

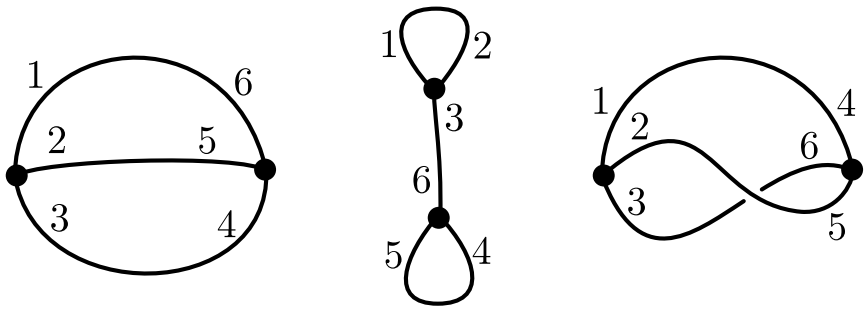

Figure 1.5: The two-vertex trivalent ribbon graphs with labelled half-edges.

of this correlator generate three distinct graphs, given in Figure 1.5. In this diagram, each half-edge label p corresponds to a spin label pair (l_p, m_p), abbreviated to the single index L_p. The first graph corresponds to the Wick contraction $\tau = (1,6)(2,5)(3,4)$, and has the associated ribbon graph sum

$$\mathcal{R}(\mathcal{G}) = \langle (\mathrm{tr} X^3)^2 \rangle \big|_\tau = N^{2-3} \eta^{L_1 L_6} \eta^{L_2 L_5} \eta^{L_3 L_4} A_{L_1 L_2 L_3} A_{L_4 L_5 L_6}. \tag{1.3.23}$$

The $\eta^{L_p L_q}$ symbols, which are proportional to deltas, can be summed out to give a sum over the three spin label pairs (l_1, m_1), (l_2, m_2), and (l_3, m_3). This corresponds to dropping half of the integer labels on the ribbon graph and assigning a single label to each edge, as in Figure 1.6. Using the formula (1.3.19), we find the ribbon graph sum

$$\begin{aligned}\mathcal{R}(\mathcal{G}) = (-)^{2j} \sum_{\substack{l_1,l_2,l_3 \\ m_1,m_2,m_3}} (-)^{m_1+m_2+m_3} (2l_1+1)(2l_2+1)(2l_3+1) \\ \times \begin{vmatrix} l_1 & l_2 & l_3 \\ j & j & j \end{vmatrix} \begin{pmatrix} l_1 & l_2 & l_3 \\ m_1 & m_2 & m_3 \end{pmatrix} \begin{vmatrix} l_1 & l_3 & l_2 \\ j & j & j \end{vmatrix} \begin{pmatrix} l_1 & l_3 & l_2 \\ -m_1 & -m_3 & -m_2 \end{pmatrix}. \end{aligned} \tag{1.3.24}$$

The spin network part of this sum is

$$\begin{aligned} S(\mathcal{G}, \{l_1, l_2, l_3\}) &= \sum_{m_1,m_2,m_3} (-)^{m_1+m_2+m_3} \begin{pmatrix} l_1 & l_3 & l_2 \\ m_1 & m_3 & m_2 \end{pmatrix} \begin{pmatrix} l_1 & l_2 & l_3 \\ -m_1 & -m_2 & -m_3 \end{pmatrix} \\ &= \sum_{m_1,m_2,m_3} \begin{pmatrix} l_1 & l_2 & l_3 \\ m_1 & m_2 & m_3 \end{pmatrix} \begin{pmatrix} l_1 & l_2 & l_3 \\ m_1 & m_2 & m_3 \end{pmatrix} \\ &= \Delta(l_1, l_2, l_3), \end{aligned} \tag{1.3.25}$$

where this Delta function is equal to one when the spin labels l_1, l_2, l_3 satisfy the **triangle constraint**, and zero otherwise. The triangle constraint on a triple of integers

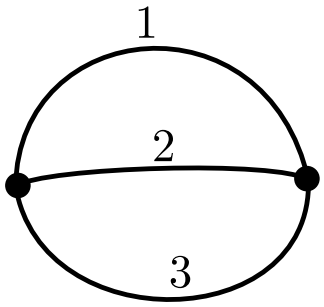

Figure 1.6: The 'theta' ribbon graph with one spin label pair on each edge.

l_1, l_2, l_3 is satisfied when $(l_1 + l_2 + l_3)$ is an integer and

$$|l_2 - l_3| \leq l_1 \leq l_2 + l_3, \qquad |l_3 - l_1| \leq l_2 \leq l_3 + l_1, \qquad |l_1 - l_2| \leq l_3 \leq l_1 + l_2. \quad (1.3.26)$$

These triangle constraints are imposed on the ribbon graph sums by the presence of the $6j$ symbols. In general, a spin network configuration evaluates to zero unless the spin labels assigned to the edges meeting at every vertex satisfy the triangle constraint. This leads us to the ribbon graph evaluation, or $6j$ sum, of the form given in (1.3.21)

$$\mathcal{R}(\mathcal{G}) = (-)^{2j} \sum_{l_1,l_2,l_3} (2l_1+1)(2l_2+1)(2l_3+1) \left| \begin{array}{ccc} l_1 & l_2 & l_3 \\ j & j & j \end{array} \right| \left| \begin{array}{ccc} l_1 & l_2 & l_3 \\ j & j & j \end{array} \right|. \quad (1.3.27)$$

1.3.2 Evaluating spin network state sums

In this section we describe how to evaluate the spin network sum (1.3.20) associated to any trivalent graph $\mathcal{G}$ with a set of assigned spin labels $\{l_p\}$. Spin network state sums can always be evaluated by using the various identities relating the $3j$ and $6j$ symbols. In the simplest cases, the spin network evaluation can be read off quite easily. For example, as was discussed in the previous subsection, the spin network sum corresponding to the 'theta' graph is

$$S\left(\begin{array}{c}\scriptstyle 1\\ \scriptstyle 2\\ \scriptstyle 3\end{array}\right) = \Delta(l_1, l_2, l_3). \quad (1.3.28)$$

Each integer $p \in \{1, 2, 3\}$ in the diagram in (1.3.28) represents a fixed spin label l_p and a summed state label m_p. Another simple example of a spin network is the tetrahedral graph, consisting of a graph with four vertices and six edges. The spin

network evaluation of this graph is a $6j$ symbol purely by its definition:

$$S\left(\quad\right) = \sum_{m_i} (-)^{m_1+m_2+m_3+m_4+m_5+m_6} \begin{pmatrix} l_1 & l_2 & l_3 \\ m_1 & m_2 & m_3 \end{pmatrix} \begin{pmatrix} l_1 & l_5 & l_6 \\ -m_1 & -m_5 & m_6 \end{pmatrix}$$
$$\times \begin{pmatrix} l_3 & l_4 & l_5 \\ -m_3 & m_4 & m_5 \end{pmatrix} \begin{pmatrix} l_2 & l_6 & l_4 \\ -m_2 & -m_6 & -m_4 \end{pmatrix} := \begin{vmatrix} l_1 & l_2 & l_3 \\ l_4 & l_5 & l_6 \end{vmatrix}. \qquad (1.3.29)$$

For more elaborate and non-planar trivalent graphs, we need to systematically employ a series of relations on the $3j$ symbols to pull out the various dimension factors and $6j$ symbols. Each of the relevant $3j$ identities has an interpretation as an operation on the trivalent graph. We call these operations the **trivalent graph moves**. Using some general properties of ribbon graphs, we can describe the series of moves that reduces any graph down to a theta or tetrahedral graph.

Before describing these moves, it is convenient in the following to extend the evaluation of a spin network to include graphs with external edges. As well as the spin label l_p assigned to each edge of the graph, we assign a spin label m_p to each external edge, which is not summed over in the spin network evaluation. We also do not assign a weight of $(-)^{m_p}$ to the external edges, and choose the sign in front of the m_p entry in the associated $3j$ symbol to be positive. A pair of external edges with the same spin label l and the respective spin labels m, $\tilde{m}$ can be contracted by summation and a delta function:

$$\sum_{m,\tilde{m}} (-)^m \delta_{m,-\tilde{m}} S\left(\quad\right) = S\left(\quad\right) \qquad (1.3.30)$$

We also define an edge with no vertices to be proportional to a delta function:

$$S\left(\quad\right) = (-)^m \delta_{m,-\tilde{m}}. \qquad (1.3.31)$$

In the following, we will only consider trivalent graphs labelled with integer spin labels, as the ribbon graph sums constrain the l_p to be integer. We will also denote spin label pairs (l_p, m_p) in diagrams by an integer p.

There are four trivalent graph moves, which we call the orthogonality relation, the '2-2' move, the '3-1' move, and the parity move.

1. **The orthogonality relation** between two $3j$s can be expressed as

$S\Big($ 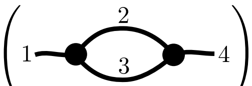 $\Big)$

$$= \sum_{m_2,m_3} (-)^{m_2+m_3} \begin{pmatrix} l_1 & l_2 & l_3 \\ m_1 & m_2 & m_3 \end{pmatrix} \begin{pmatrix} l_2 & l_4 & l_3 \\ -m_2 & m_4 & -m_3 \end{pmatrix}$$
$$= \frac{(-)^{m_1}}{(2l_1+1)} \delta_{l_1,l_4} \delta_{m_1,-m_4} \Delta(l_1,l_2,l_3). \quad (1.3.32)$$

By interpreting the product of delta functions and phase factor $(-)^{m_1}$ as the spin network evaluation of a straight line, we can write this orthogonality relation diagrammatically as

$S\Big($ 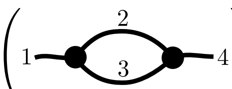 $\Big)$

$= \frac{1}{(2l_1+1)}\, S\Big($  $\Big)\, \delta_{l_1,l_4} \Delta(l_1,l_2,l_3).$ (1.3.33)

2. The $3j$ symbols also satisfy an identity corresponding to **the '2-2' move**

$$\sum_{m_3} (-)^{m_3} \begin{pmatrix} l_1 & l_2 & l_3 \\ m_1 & m_2 & -m_3 \end{pmatrix} \begin{pmatrix} l_4 & l_5 & l_3 \\ m_4 & m_5 & m_3 \end{pmatrix} =$$
$$= \sum_{l_6,m_6} (-)^{m_6} (2l_6+1) \begin{pmatrix} l_5 & l_1 & l_6 \\ m_5 & m_1 & m_6 \end{pmatrix} \begin{pmatrix} l_2 & l_4 & l_6 \\ m_2 & m_4 & -m_6 \end{pmatrix} \begin{vmatrix} l_1 & l_2 & l_3 \\ l_4 & l_5 & l_6 \end{vmatrix}. \quad (1.3.34)$$

This can be expressed diagrammatically as

$S\Big($ 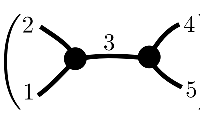 $\Big)$

$= \sum_{l_6} (2l_6+1) \begin{vmatrix} l_1 & l_2 & l_3 \\ l_4 & l_5 & l_6 \end{vmatrix}\, S\Big($ 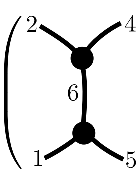 $\Big).$ (1.3.35)

3. The third $3j$ identity is associated to **the '3-1' move**, which reduces three $3j$ symbols to a single $3j$ and a $6j$,

$$\sum_{m_4,m_5,m_6} (-)^{m_4+m_5+m_6} \begin{pmatrix} l_5 & l_1 & l_6 \\ m_5 & m_1 & -m_6 \end{pmatrix} \begin{pmatrix} l_4 & l_3 & l_5 \\ m_4 & m_3 & -m_5 \end{pmatrix} \begin{pmatrix} l_6 & l_2 & l_4 \\ m_6 & m_2 & -m_4 \end{pmatrix}$$
$$= \begin{pmatrix} l_1 & l_2 & l_3 \\ m_1 & m_2 & m_3 \end{pmatrix} \begin{vmatrix} l_1 & l_2 & l_3 \\ l_4 & l_5 & l_6 \end{vmatrix}, \quad (1.3.36)$$

which is expressed diagrammatically as

$S\Big($ 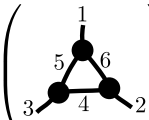

$\Big) = \begin{vmatrix} l_1 & l_2 & l_3 \\ l_4 & l_5 & l_6 \end{vmatrix} \; S\Big($ 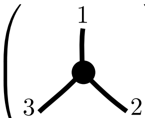

$\Big).$ (1.3.37)

The inverse of this move is called the '1-3' move.

We note that the 3-1, 2-2 and orthogonality moves are not independent, as the 3-1 move could be deduced by using the 2-2 move and the orthogonality relation. Alternatively, the orthogonality relation could be deduced from the 2-2 and 3-1 moves, provided the graph considered has more than two vertices.

4. The final trivalent graph move is **the 'parity' move**, which reverses the cyclic ordering of the edges connecting to a vertex. This corresponds to transposing a pair of spins (l_1, m_1) and (l_2, m_2) in a $3j$ symbol,

$$\begin{pmatrix} l_1 & l_2 & l_3 \\ m_1 & m_2 & m_3 \end{pmatrix} = (-)^{l_1+l_2+l_3} \begin{pmatrix} l_2 & l_1 & l_3 \\ m_2 & m_1 & m_3 \end{pmatrix}. \tag{1.3.38}$$

Diagramatically, we write

$S\Big($ 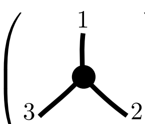

$\Big) = (-)^{l_1+l_2+l_3} \; S\Big($ 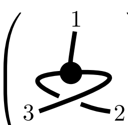

$\Big).$ (1.3.39)

Unlike the other moves, this trivalent graph move does not in general preserve the genus of a graph. This move is necessary to reduce down a non-planar spin network to a planar spin network.

The action of these moves on a labelled trivalent graph will generate in the spin network state sum evaluation $S(\mathcal{G})$ a string of factors of $(2l+1)$, $(-)^{l_1+l_2+l_3}$, and sums over new labels, as well as the $6j$ symbols, which are the evaluations of tetrahedral graph. The tetrahedral graph are irreducible under the trivalent graph moves, as any application of the moves on them will generate the same $6j$ or an expression which evaluates to the same $6j$. Therefore, the evaluation of a general graph by reduction must be a sum of a product of these factors. We show algorithmically that all trivalent graphs can be reduced down in this manner.

A trivalent ribbon graph partitions a surface into vertices, edges, and faces. Each vertex is incident to either one, two, or three faces, and each edge is incident to either

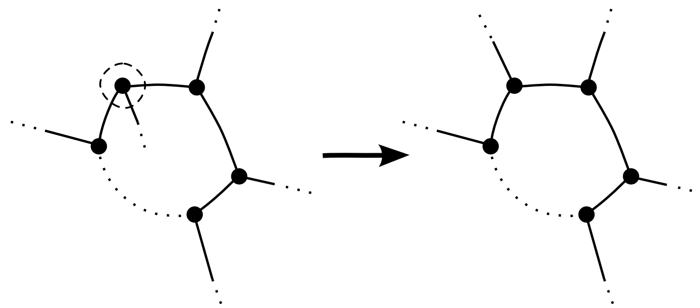

Figure 1.7: The parity move produces a polygon from a face of a non-planar ribbon graph.

one or two faces. We say that a face is a **polygon** if it is homeomorphic to a disc when considered with its bounding edges and vertices. A necessary and sufficient condition for a face to be a polygon is for each edge bounding the face to be incident to two distinct faces.

The first step in the algorithm is to isolate a polygon of the ribbon graph. Not all ribbon graphs possess a polygonal face, but it is always possible to generate such a face from any ribbon graph by applying a single parity move. To see this, follow the boundary of a face around until a vertex is visited twice, and apply the parity move at this vertex, as demonstrated in Figure 1.7. This will always produce a polygon from a non-polygonal face. A planar graph always has at least one polygonal face, so can be reduced without applying the parity move.

Once a polygon has been isolated, we can use a combination of the remaining trivalent moves to remove the polygon from the graph and reduce the number of vertices by two, as in Figure 1.8. If the polygon is bounded by a single edge and a single vertex, then it is a 'tadpole', and can be removed using the 2-2 move and orthogonality relation. Applying the '2-2' move on the edge that connects the vertex to a different vertex, and then the orthogonality move, we have

S 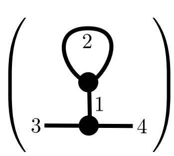 $= \sum_{l_5} \begin{vmatrix} l_1 & l_2 & l_2 \\ l_5 & l_4 & l_3 \end{vmatrix} (2l_5+1)\ S$ 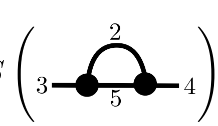

$= \sum_{l_5} \begin{vmatrix} l_1 & l_2 & l_2 \\ l_5 & l_4 & l_3 \end{vmatrix} \left(\frac{2l_5+1}{2l_3+1}\right) \delta_{l_3,l_4} S$ 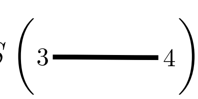 . (1.3.40)

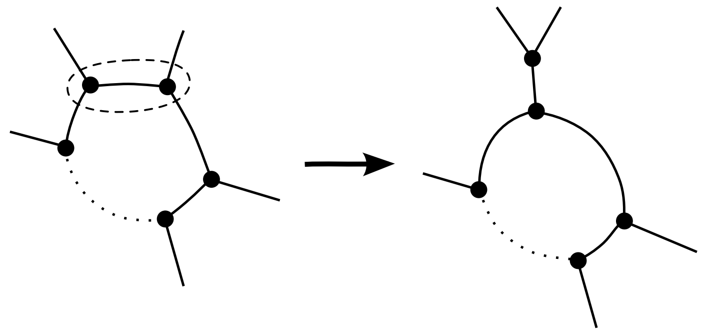

Figure 1.8: The '2-2' move on a polygon reduces the number of edges bounding the polygon by one.

The sum over the spin label l_5 can be removed by using the $6j$ identity

$$\sum_{l_5}\left(\frac{2l_5+1}{2l_3+1}\right)\begin{vmatrix} l_1 & l_2 & l_2 \\ l_5 & l_3 & l_3 \end{vmatrix} = (-)^{l_2+l_3}\delta_{l_1,0}\sqrt{\frac{2l_2+1}{2l_3+1}}, \tag{1.3.41}$$

and so we can replace the tadpole from the trivalent graph with a factor:

$S\Bigg($ 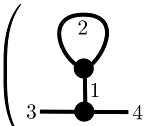 $\Bigg) = \delta_{l_3,l_4}\delta_{l_1,0}(-)^{l_2+l_3}\sqrt{\frac{2l_2+1}{2l_3+1}}\; S\Bigg($  $\Bigg).$ (1.3.42)

If the polygon is bounded by two edges, then it can be removed using the orthogonality move. If the polygon has three edges, then it can be reduced to a vertex using the 3-1 move. Otherwise, the polygon has four or more edges, and applying the 2-2 move on adjacent vertices of the face will reduce the number of edges (and vertices) bounding the face by one. Performing this move repeatedly will eventually result in a polygon with three edges, which can be reduced to a vertex using the 3-1 move. The generation and reduction of a polygon will always reduce the number of vertices of the graph by two. Therefore, this procedure will eventually reduce the graph down to a trivial loop, which evaluates to a dimension factor $(2l+1)$. The string of factors and sums that are produced in performing these moves gives the final evaluation of the spin network state sum $S(\mathcal{G})$ as a product of $6j$s, phases, and dimension factors. In summary, the algorithm is:

1. Choose a face that is homeomorphic to a disc. If no face is homeomorphic to a disc, then apply the parity move to construct such a face, as in Figure 1.7.

2. Apply the 3-1 and 2-2 moves and the orthogonality relation to remove the face,

as in Figure 1.8.

3. Repeat these steps until the graph is reduced to a theta graph.

1.3.3 Examples of ribbon graph and spin network state sums

In this subsection we give a few examples of the ribbon graph and spin network evaluations of some simple graphs. It can be shown directly from the orthogonality relations on $6j$ symbols that these ribbon graph sums evaluate to N^F.

The simplest graph that we can consider is the theta graph. For this graph, the $3j$ (spin network) sum is trivial, and so the total $6j$ sum is

$\mathcal{R}$ (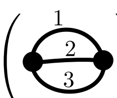)

$$= (-)^{2j} \sum_{l_1 l_2 l_3} (2l_1+1)(2l_2+1)(2l_3+1) \begin{vmatrix} l_1 & l_2 & l_3 \\ j & j & j \end{vmatrix} \begin{vmatrix} l_1 & l_2 & l_3 \\ j & j & j \end{vmatrix}. \quad (1.3.43)$$

Orthogonality of the $6j$s, and the contraint on the range of summation $0 \leq l_i \leq 2j$, give the expected final answer,

$$\mathcal{R}(\mathcal{G}) = \frac{1}{(2j+1)} \sum_{l_1 l_2} (2l_1+1)(2l_2+1) = N^3. \quad (1.3.44)$$

The tetrahedral network has the ribbon graph evaluation

$\mathcal{R}$ (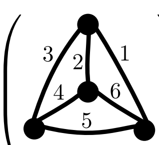)

$$= \sum_{l_1 \ldots l_6} (2l_1+1)(2l_2+1)(2l_3+1)(2l_4+1)(2l_5+1)(2l_6+1)$$

$$\times \begin{vmatrix} l_1 & l_2 & l_3 \\ l_4 & l_5 & l_6 \end{vmatrix} \begin{vmatrix} l_1 & l_2 & l_3 \\ j & j & j \end{vmatrix} \begin{vmatrix} l_2 & l_6 & l_4 \\ j & j & j \end{vmatrix} \begin{vmatrix} l_1 & l_5 & l_6 \\ j & j & j \end{vmatrix} \begin{vmatrix} l_3 & l_4 & l_5 \\ j & j & j \end{vmatrix}. \quad (1.3.45)$$

The $6j$ sum can be evaluated explicitly by using the Biedenharn-Elliot identity (A.3.9), given in the appendix, to elimate a spin label and a $6j$. The remaining sums can be performed by using the orthogonality relation, giving $\mathcal{R}(\mathcal{G}) = N^4$.

The following is an example of a more complicated non-planar ribbon graph,

$$\mathcal{R}\left(\quad\right) = N^{-2}\sum_{l_1\ldots l_6}(2l_1+1)(2l_2+1)(2l_3+1)(2l_4+1)(2l_5+1)(2l_6+1)$$
$$\times S\left(\quad\right)\left|\begin{matrix} l_1 & l_2 & l_3 \\ j & j & j\end{matrix}\right|\left|\begin{matrix} l_2 & l_3 & l_4 \\ j & j & j\end{matrix}\right|\left|\begin{matrix} l_4 & l_5 & l_6 \\ j & j & j\end{matrix}\right|\left|\begin{matrix} l_1 & l_5 & l_6 \\ j & j & j\end{matrix}\right|. \quad (1.3.46)$$

The spin network state sum of this labelled graph $\mathcal{G}$ is

$$S\left(\quad\right) = \sum_{m_1\ldots m_6}(-)^{m_1+m_2+m_3+m_4+m_5+m_6}\begin{pmatrix} l_1 & l_2 & l_3 \\ m_1 & m_2 & m_3\end{pmatrix}$$
$$\times\begin{pmatrix} l_2 & l_3 & l_4 \\ -m_2 & -m_3 & -m_4\end{pmatrix}\begin{pmatrix} l_4 & l_5 & l_6 \\ m_4 & m_5 & m_6\end{pmatrix}\begin{pmatrix} l_1 & l_5 & l_6 \\ -m_1 & -m_5 & -m_6\end{pmatrix}. \quad (1.3.47)$$

We can apply the algorithm to evaluate $S(\mathcal{G})$. This ribbon graph has no polygonal faces, so we apply a parity move to one of the vertices to get

$$S(\mathcal{G},\{l_i\}) = S\left(\quad\right). \quad (1.3.48)$$

We can now apply the orthogonality relation on the bubble,

$$S(\mathcal{G},\{l_i\}) = \frac{(-)^{l_4+l_5+l_6}}{(2l_4+1)}\delta_{l_1,l_4}\Delta(l_4,l_5,l_6)\ S\left(\quad\right), \quad (1.3.49)$$

and a second parity move on the graph will reduce the graph to a theta graph, which evaluates to a Delta. We deduce that

$$S\left(\quad\right) = \frac{(-)^{l_2+l_3+l_5+l_6}}{(2l_1+1)}\delta_{l_1,l_4}\Delta(l_1,l_2,l_3)\Delta(l_1,l_5,l_6), \quad (1.3.50)$$

and that the ribbon graph sum is

$$\mathcal{R}(\mathcal{G}) = \sum_{l_1 l_2 l_3 l_5 l_6} (-)^{l_2+l_3+l_5+l_6}(2l_1+1)(2l_2+1)(2l_3+1)(2l_5+1)(2l_6+1) \times \begin{vmatrix} l_1 & l_2 & l_3 \\ j & j & j \end{vmatrix} \begin{vmatrix} l_1 & l_2 & l_3 \\ j & j & j \end{vmatrix} \begin{vmatrix} l_1 & l_5 & l_6 \\ j & j & j \end{vmatrix} \begin{vmatrix} l_1 & l_5 & l_6 \\ j & j & j \end{vmatrix}. \quad (1.3.51)$$

This expression can be evaluated to $N^F = N^2$ by using the identity (A.3.15).

1.3.4 General multi-trace correlators

So far, we have only considered the correlators of triples of traces in the fuzzy sphere matrix model, which generate trivalent ribbon graphs. We can extend the above analysis to more general correlators of the form $\langle \mathrm{tr}_{2n}(\mathbf{X}\sigma)\rangle$. A general permutation $\sigma \in [1^{k_1}2^{k_2}\dots(2n)^{k_{2n}}]$ consists of k_p p-cycles for each $p \in \{1,2,\dots,2n\}$, where $\sum_p pk_p = 2n$. The multi-trace operator associated with this conjugacy class is

$$\mathrm{tr}_{2n}(\sigma\mathbf{X}) = \prod_{p=1}^{2n} (\mathrm{tr}X^p)^{k_p}. \quad (1.3.52)$$

There is a trace of p matrices in this product for each p-cycle of σ. In this subsection, we outline a way of converting each trace in the trace product into a product of Wick-contracted triples of traces. We do this by first writing any trace of fuzzy spherical harmonics in terms of the coupling coefficients $A_{L_pL_qL_r}$ and the Kronecker deltas $\eta^{L_pL_q}$ introduced earlier in this section, and then relating these expressions to Wick-contracted operators of the form $(\mathrm{tr}X^3)^V$. This allows the methods of trivalent ribbon graphs to be applied to any correlator in the fuzzy sphere matrix model.

Consider a trace of k matrices corresponding to a k-cycle of σ. This can be expanded into modes and fuzzy spherical harmonics,

$$\mathrm{tr}(X^k) = N^{-k/2} \sum_{L_1,\dots L_k} a^{L_1}\dots a^{L_k}\mathrm{tr}(Y_{L_1}Y_{L_2}\dots Y_{L_k}). \quad (1.3.53)$$

If $k = 2$ or $k = 3$, then we can immediately write the trace of the fuzzy spherical harmonics in terms of the symbol $\eta^{L_pL_q}$ or $A_{L_pL_qL_r}$,

$$\mathrm{tr}(Y_{L_1}Y_{L_2}) = N\eta^{L_1L_2}, \qquad \mathrm{tr}(Y_{L_1}Y_{L_2}Y_{L_3}) = NA_{L_1L_2L_3}. \quad (1.3.54)$$

The fuzzy sphere algebra (1.2.12) and the hermiticity property (1.2.9) allow us to

express any product of fuzzy spherical harmonics in terms of the coupling coefficients $A_{L_pL_qL_r}$ corresponding to the trace of a triple of fuzzy spherical harmonics:

$$Y_{L_p}Y_{L_q} = \sum_{L_r} A_{L_pL_qL_r}Y^{\dagger}_{L_r} \quad = \quad \sum_{L_r,L_s} A_{L_pL_qL_r}\eta^{L_rL_s}Y_{L_s}. \tag{1.3.55}$$

By repeatedly applying (1.3.55), we can decompose any trace of four or more fuzzy spherical harmonics into a sum over spin labels weighted by factors of $\eta^{L_pL_q}$ and $A_{L_pL_qL_r}$. For $k \geq 4$, the trace of k fuzzy spherical harmonics $\mathrm{tr}(Y_{L_1}\dots Y_{L_k})$ is

$$N \sum_{L_{k+1},L_{k+2}\dots} A_{L_1L_2L_{k+1}}\eta^{L_{k+1}L_{k+2}}A_{L_{k+2}L_3L_{k+3}}\dots\eta^{L_{3k-7}L_{3k-6}}A_{L_{3k-6}L_{k-1}L_k}. \tag{1.3.56}$$

The trace of k fuzzy spherical harmonics decomposes into $(k-2)$ symbols $A_{L_pL_qL_r}$ and $(k-3)$ contractions $\eta^{L_pL_q}$, with summations over $(2k-6)$ new spin label pairs $L_p \sim (l_p, m_p)$. For example, the trace of four fuzzy spherical harmonics is

$$\begin{aligned}\mathrm{tr}(Y_{L_1}Y_{L_2}Y_{L_3}Y_{L_4}) &= \sum_{L_5,L_6}\mathrm{tr}((A_{L_1L_2L_5}\eta^{L_5L_6}Y_{L_6})Y_{L_3}Y_{L_4})) \\ &= \sum_{L_5,L_6} A_{L_1L_2L_5}\eta^{L_5L_6}\mathrm{tr}(Y_{L_6}Y_{L_3}Y_{L_4}) \\ &= N\sum_{L_5,L_6} A_{L_1L_2L_5}\eta^{L_5L_6}A_{L_6L_3L_4}.\end{aligned} \tag{1.3.57}$$

We can also derive an expression in terms of $A_{L_pL_qL_r}$ and $\eta^{L_pL_q}$ for a trace of a single fuzzy spherical harmonic by using the identity derived in Section 1.2.3,

$$\frac{1}{N}\sum_{L_p,L_q}\eta^{L_pL_q}Y_{L_p}\otimes Y_{L_q} = \sum_{\mu_p,\mu_q}|j,\mu_p\rangle\langle j,\mu_q|\otimes|j,\mu_q\rangle\langle j,\mu_p|. \tag{1.3.58}$$

The integers μ_p, μ_q run over the range $-j, -j+1, \dots, j$. By considering the trace of three fuzzy spherical harmonics with two of the fuzzy spherical harmonics contracted, we have

$$\begin{aligned}\sum_{L_2,L_3}\eta^{L_2L_3}\mathrm{tr}(Y_{L_1}Y_{L_2}Y_{L_3}) &= \sum_{L_2L_3}\mathrm{tr}(Y_{L_1}N\sum_{\mu_2,\mu_3}|j,\mu_2\rangle\langle j,\mu_3|j,\mu_3\rangle\langle j,\mu_2|) \\ &= N^2\mathrm{tr}(Y_{L_1}),\end{aligned} \tag{1.3.59}$$

which we can rephrase as

$$\mathrm{tr}(Y_{L_1}) = \frac{1}{N}\sum_{L_2,L_3} A_{L_1L_2L_3}\eta^{L_2L_3}. \tag{1.3.60}$$

The above expressions allow us to write any trace $\mathrm{tr}X^k$ as a partially Wick-contracted operator $(\mathrm{tr}X^3)^V$. Recall that a Wick contraction in the fuzzy sphere is proportional to the η^{pq} symbol,

$$\langle a^{L_1}a^{L_2}\rangle = \eta^{L_1L_2}. \tag{1.3.61}$$

The expression (1.3.60) allows us to write the trace of a single matrix as

$$\begin{aligned}
\mathrm{tr}(X) &= \frac{1}{\sqrt{N}}\sum_{L_1} a^{L_1}\mathrm{tr}(Y_{L_1}) \\
&= \frac{1}{N^{3/2}}\sum_{L_1,L_2,L_3} a^{L_1}\eta^{L_2L_3}A_{L_1L_2L_3} \\
&= \frac{1}{N^{5/2}}\sum_{L_1,L_2,L_3} a^{L_1}\langle a^{L_2}a^{L_3}\rangle\mathrm{tr}(Y_{L_1}Y_{L_2}Y_{L_3}) \\
&= \frac{1}{N}\mathrm{tr}(X\overbrace{XX}).
\end{aligned} \tag{1.3.62}$$

The trace of two matrices can be written as a pair of contractions on a pair of trace triples. By contracting a pair of fuzzy spherical harmonics, we can write

$$\begin{aligned}
\frac{1}{N}\sum_{L_3,L_4}\eta^{L_3L_4}\mathrm{tr}(Y_{L_1}Y_{L_2}Y_{L_3})\mathrm{tr}(Y_{L_4}) &= \sum_{L_3,L_4}\mathrm{tr}(Y_{L_1}Y_{L_2}|j,\mu_3\rangle\langle j,\mu_4|)\mathrm{tr}(|j,\mu_4\rangle\langle j,\mu_3|) \\
&= \mathrm{tr}(Y_{L_1}Y_{L_2}),
\end{aligned} \tag{1.3.63}$$

which, from the above, leads us to

$$\begin{aligned}
\mathrm{tr}(X^2) &= \frac{1}{N}\sum_{L_1,L_2} a^{L_1}a^{L_2}\mathrm{tr}(Y_{L_1}Y_{L_2}) \\
&= \frac{1}{N^2}\sum_{L_1,\ldots L_4} a^{L_1}a^{L_2}\eta^{L_3L_4}\mathrm{tr}(Y_{L_1}Y_{L_2}Y_{L_3})\mathrm{tr}(Y_{L_4}) \\
&= \mathrm{tr}(XX\overbrace{X)\mathrm{tr}(X}) \\
&= \frac{1}{N}\mathrm{tr}(XX\overbrace{X)\mathrm{tr}(X}\overbrace{XX}).
\end{aligned} \tag{1.3.64}$$

We can use (1.3.56) to express a trace of $k \geq 4$ matrices as a sequence of contractions

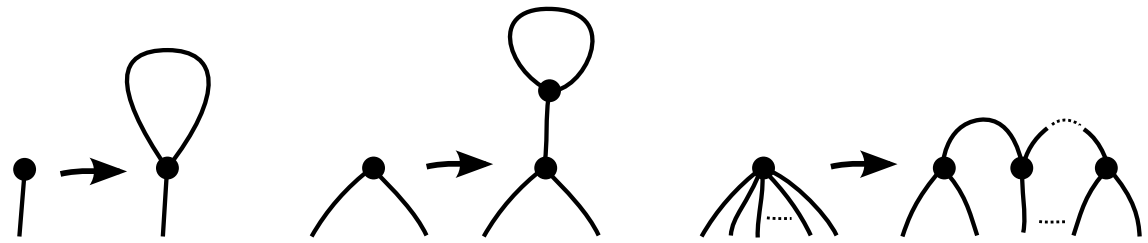

a b c

Figure 1.9: The expansion of vertices of valency 1, 2, and k into trivalent vertices.

on $(k-2)$ triples of traces,

$$\begin{aligned}
\mathrm{tr}(X^k) &= N^{-k/2} \sum_{L_1,\ldots L_k} a^{L_1} \ldots a^{L_k} \mathrm{tr}(Y_{L_1} Y_{L_2} \ldots Y_{L_k}) \\
&= N^{-k/2+1} \sum_{L_1,L_2,\ldots} a^{L_1} \ldots a^{L_k} A_{L_1 L_2 L_{k+1}} \eta^{L_{k+1} L_{k+2}} \ldots A_{L_{3k-6} L_{k-1} L_k} \\
&= N^{-3k/2+3} \sum_{L_1,L_2} a^{L_1} \ldots a^{L_k} \mathrm{tr}(Y_{L_1} Y_{L_2} Y_{L_{k+1}}) \langle a^{L_{k+1}} a^{L_{k+2}} \rangle \ldots \\
&= \mathrm{tr}(\overbrace{XXX}) \mathrm{tr}(\overbrace{XXX}) \ldots \overbrace{\mathrm{tr}(XXX)}. \qquad (1.3.65)
\end{aligned}$$

This shows that every product of traces can be 'expanded' into a product of triples of traces with some extra Wick contractions. We can interpret this expansion diagrammatically: each k-cycle in σ corresponds to a vertex of valency k. The edges of the graphs correspond to the Wick contractions of the correlator. A vertex of valency one corresponding to the trace of a single matrix is, via (1.3.62), equivalent to a contracted trace triple (up to a factor of N). Diagrammatically, this corresponds to adding a 'tadpole' to a valency one vertex, as in Figure 1.9a. From (1.3.64), a vertex of valency two corresponding to a trace of two matrices is equivalent to a pair of vertices with a 'tadpole', up to a factor of N, as demonstrated in Figure 1.9b. A vertex of valency $k \geq 4$ corresponds to $k-2$ trivalent vertices contracted together in a series, as in Figure 1.9c.

The correlator of an operator $\langle \mathrm{tr}_{2n}(\mathbf{X}\sigma) \rangle$ is a sum over Wick contractions $\tau \in [2^n]$. In expanding the correlator to a trace-triple correlator with $3V = 2E$ matrices, we introduce $(2E-2n)$ extra matrices, an inverse power of N for each 1-cycle and 2-cycle

in σ, and fix some of the Wick contractions in the sum:

$$\begin{aligned} \langle \mathrm{tr}_{2n}(\mathbf{X}\sigma)\rangle &= N^{-k_1-k_2}\, \langle \mathrm{tr}_{2E}(\mathbf{X}\hat{\sigma})\rangle|_{\mathrm{part-contracted}} \\ &= N^{-k_1-k_2} \sum_{\tau\in[2^n]\times\hat{\tau}} \mathrm{tr}_{2E}(\hat{\sigma}\tau). \end{aligned} \tag{1.3.66}$$

Here, the permutation $\hat{\sigma} \in [3^V]$ is a product of 3-cycles, the permutation $\hat{\tau} \in [2^{E-n}]$ encodes the Wick contractions generated in the expansion of the operator $\mathrm{tr}_{2n}(\mathbf{X}\sigma)$ into the product of trace triples $\mathrm{tr}_{2E}(\mathbf{X}\hat{\sigma})$, and the sum runs over all the permutations in $[2^E]$ which contain $\hat{\tau}$. Each pair of permutations $(\hat{\sigma}, \tau)$ corresponds to a trivalent ribbon graph with an associated $3j$ spin network sum and a $6j$ spin label sum, which evaluates to N^F, the number of faces of the ribbon graph.

1.4 A three-dimensional interpretation: The Ponzano-Regge model

We have argued that the Hermitian matrix model is the target space theory of the Belyi string. We can expand upon this idea by presenting a higher-dimensional theory of gravity which reproduces the data of the spacetime theory, giving a possible membrane interpretation to the Belyi string.

The *Ponzano-Regge model* assigns a partition function to any triangulated three-dimensional manifold with boundary with spin labels l_p assigned to the edges of the triangulation and $6j$ symbols assigned to the tetrahedra [11, 54, 9]. The partition function depends on the topology of the 3-manifold and the labelled triangulation on the boundary, but is independent of the choice of triangulation of the interior of the manifold. The model is known to correspond to Chern-Simons theory with $ISO(3)$ gauge group, which is equivalent to three-dimensional Euclidean quantum gravity [12, 13]. It is also the first example of a spin foam model in loop quantum gravity [52].

The Ponzano-Regge partition functions are sums over $su(2)$ representations weighted by $6j$ symbols and representation dimension factors. As the ribbon graphs generated by the Hermitian matrix model on the fuzzy sphere are also of this form, we can attempt to construct triangulated manifolds which reproduce the $6j$ sums generated by the fuzzy sphere matrix model. We find that every trivalent ribbon graph generates a triangulated 3-manifold whose Ponzano-Regge partition function corresponds to the ribbon graph $6j$ sum, and with the graph itself embedded on the triangulation of the boundary. A genus g ribbon graph corresponds to a triangulated handlebody of genus g with particular boundary data.

We begin this section by reviewing the Ponzano-Regge model on a triangulated manifold with boundary. The partition functions of this model diverge when the triangulation has vertices in the interior of the manifold, so we also review the *Turaev-Viro model* as a means to regularising the theory. This theory is formulated by replacing the representations of $su(2)$ and their $6j$ couplings in the Ponzano-Regge model with the representations and couplings of the quantum algebra $U_q(su(2))$, where q is some deformation parameter. For the manifolds with boundary that we consider in this thesis, there will always be a well-defined limit $q \to 1$, where the quantum algebra becomes the original $su(2)$ algebra, and so we use the $q \to 1$ limit of the Turaev-Viro model as our definition of the Ponzano-Regge model. We conclude this section by in-

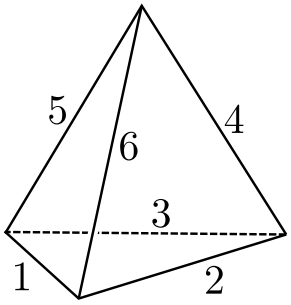

Figure 1.10: Each $6j$ symbol in the Ponzano-Regge state sum corresponds to a labelled tetrahedron.

troducing some triangulations of surfaces generated by trivalent ribbon graphs, which we will use in the next section to build the appropriate 3-complexes.

1.4.1 The Ponzano-Regge model

The **Ponzano-Regge model** is defined by assigning a partition function to any triangulation of a 3-manifold, possibly with boundary, with a spin label j_i assigned to each edge, and a sum performed over all possible values of the spin labels corresponding to internal edges. The sum is weighted by the function

$$W = \prod_{\text{interior edges}} (-)^{2j_p}(2j_p+1) \prod_{\text{tetrahedra}} \left| \begin{array}{ccc} j_1 & j_2 & j_3 \\ j_4 & j_5 & j_6 \end{array} \right|, \tag{1.4.1}$$

hence the **Ponzano-Regge partition function**

$$Z = \sum_{\text{interior edges}} W \tag{1.4.2}$$

is a function of the values of the spin labels on the boundary.

In the Hermitian matrix model, the range of summation of the spins is $0 \leq l_p \leq 2j$, where $l_p \in \mathbb{Z}$, but in the Ponzano-Regge state sum exhibited above, the spin labels in general range over all possible half-integer values up to infinity. However, there are constraints on the ranges that these labels can take, which are imposed by the $6j$ symbols. Recall that the $6j$ symbol

$$\left| \begin{array}{ccc} j_1 & j_2 & j_3 \\ j_4 & j_5 & j_6 \end{array} \right| \tag{1.4.3}$$

is zero unless the triples $\{j_1, j_2, j_3\}$, $\{j_1, j_5, j_6\}$, $\{j_2, j_4, j_6\}$, $\{j_3, j_4, j_5\}$ all satisfy the

triangle inequalities. These triples correspond to the four triangles in the cell complex that border each tetrahedron[1]. This means that if two out of three edges in a triangle are constrained to a finite range, then a triangle inequality constrains the third edge to a finite range. As the labels on the boundary edges are fixed, there is a set of edges in the complex whose labels span a finite range, which can be found iteratively. In particular, if all the edges in the complex span a finite range, then the state sum must converge, but if any labels are unconstrained then the state sum will in general diverge. It can be shown that any triangulation with a vertex in the interior must possess spin labels that diverge. The converse statement, that any triangulation with no internal vertices must converge, is not true in general, but does hold for all the triangulations that we consider in this thesis.

We wish to construct labelled tetrahedral complexes whose state sums reproduce the ribbon graph sums in a systematic manner. While it is possible to do this without introducing internal vertices, it is clearer and more systematic to use triangulations with a single internal vertex, and to introduce a method of regularising these sums. In the next section we introduce the *Turaev-Viro partition function*, which is a state sum model similar to the Ponzano-Regge model, that naturally constrains all the ranges of summation to be finite. We can use this model to recover the Ponzano-Regge state sums, and hence the ribbon graph sums, in the 'classical' limit.

1.4.2 The Turaev-Viro model as a regulator

The Ponzano-Regge model assigns partition functions to complexes labelled by the irreducible representations of $su(2)$. The **Turaev-Viro state sum** model is defined by replacing the representations of $su(2)$ in the state sum with representations of the quantum deformation of the universal enveloping algebra $U_q(su(2))$, where q is a deformation parameter. The classical Lie algebra is recovered when q is set to one. This deformed algebra has representations analagous to the irreducible representations of $su(2)$, labelled by half-integers j, and containing $(2j+1)$ states, which can be recoupled to generate quantum $3j$ and quantum $6j$ symbols [55]. Unlike $su(2)$, however, the number of representations of the quantum algebra is finite whenever q is a root of unity not equal to one. Taking q to be a root of unity and replacing all the representation-dependent expressions in the Ponzano-Regge state sums with their quantum analogues

[1]Note that the tetrahedron associated with a $6j$ in the Ponzano-Regge model is different from the tetrahedral network associated to a $6j$ in the previous section. The labels associated to edges meeting at a vertex of a trivalent graph satisfy a triangle constraint, while the labels associated to a face of a tetrahedron satisfy a triangle constraint in the Ponzano-Regge model. These two labelled tetrahedra are dual to each other.

gives us well-defined Turaev-Viro state sums over the representations of the quantum algebra. These state sums will diverge as q tends towards one (while still being a root of unity), but there is a natural way of regulating this divergence that coincides with the Ponzano-Regge model for the cases where both state sums are convergent. We can thus define the Ponzano-Regge model for divergent sums as the classical limit of the quantum state sum model, as in [13]. A more detailed treatment of the quantum state sum model is given in [56]. We present here the details of how the relevant quantities, such as summation ranges, representation dimensions, and the $6j$ symbols, are deformed after being taken to their quantum analogues.

We take an integer $r \geq 3$, and define q to be an r^{th} root of unity, $q := e^{2\pi i/r}$. The **quantum integer** $[n]$ is

$$[n] := \frac{q^{n/2} - q^{-n/2}}{q^{1/2} - q^{-1/2}}, \tag{1.4.4}$$

which has the property that $[n] \to n$ as $r \to \infty$ and $q \to 1$. The **quantum factorial** $[n]!$ is

$$[n]! := [n][n-1]\dots[2][1]. \tag{1.4.5}$$

We say that a triple of spin labels $\{j_1, j_2, j_3\}$ satisfy the **quantum triangle constraints** if they satisfy the classical triangle constraints with the extra conditions

$$j_i \leq (r-2)/2, \qquad j_1 + j_2 + j_3 \leq r - 2. \tag{1.4.6}$$

We define $\Delta_q(j_1, j_2, j_3)$ to be one when the the spin labels $\{j_1, j_2, j_3\}$ satisfy the quantum triangle constraints, and zero otherwise. By taking the explicit expression of a $6j$ symbol in terms of sums and products of factorials with triangle constraints given in [57, 58], we can replace the factorials in the definition of a $6j$ symbol with the quantum factorials, and upgrade the triangle constraints to quantum triangle constraints, to generate the quantum $6j$ symbol

$$\left| \begin{array}{ccc} j_1 & j_2 & j_3 \\ j_4 & j_5 & j_6 \end{array} \right|_q . \tag{1.4.7}$$

This definition coincides with the definition of a quantum $6j$ given in terms of the recouplings of representations of the quantum algebra [59]. The quantum $6j$ symbol converges to the classical $6j$ as $q \to 1$, but crucially is only non-zero for finitely many

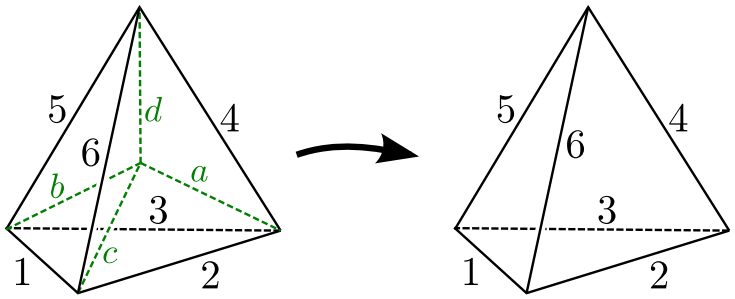

Figure 1.11: The '4-1' Pachner Move.

j_i for each value of r. This means that if we replace all the $6j$ symbols in the Ponzano-Regge state sum with quantum $6j$s, we arrive at an always-convergent state sum with weight

$$W_q = \prod_{\text{interior edges}} (-)^{2j_p}[2j_p+1] \prod_{\text{tetrahedra}} \left| \begin{array}{ccc} j_1 & j_2 & j_3 \\ j_4 & j_5 & j_6 \end{array} \right|_q . \tag{1.4.8}$$

Each term in this expression converges to the classical analogue as $q \to 1$, hence this partition function reproduces the original Ponzano-Regge state sum in the $q \to 1$ limit in the cases where the original Ponzano-Regge state sum converges. For complexes with interior vertices, we introduce the quantum normalisation factor

$$w^2 = -\frac{2r}{(q^{\frac{1}{2}} - q^{-\frac{1}{2}})^2} \tag{1.4.9}$$

and define the **Turaev-Viro partition function**

$$Z_q = w^{-2v} \sum_{\text{interior edges}} W_q, \tag{1.4.10}$$

where v is the number of internal vertices in the triangulation.

One of the most important properties of the Turaev-Viro is triangulation independence. Any two triangulations of a 3-manifold that are equal on the boundary can be deformed from one to the other by a series of operations on the complex called **Pachner moves** [60]. These moves are mergings and splittings of glued tetrahedra that will change the terms that appear in the $6j$ sums, but due to two identities relating sums of products of quantum $6j$ symbols, these operations will not change the overall value of the partition function.

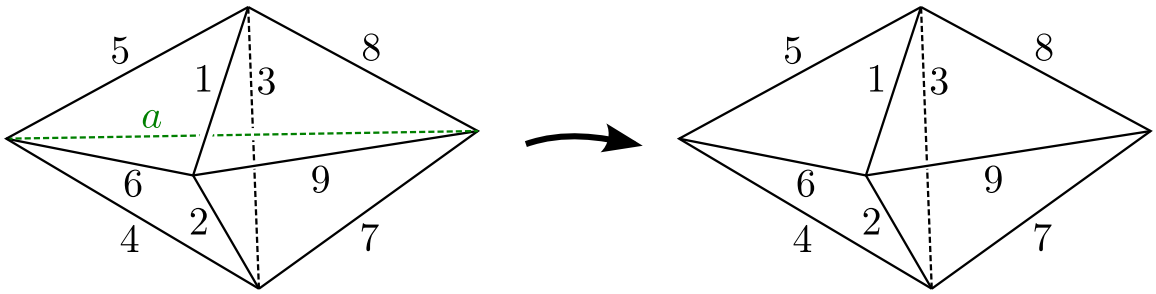

Figure 1.12: The '3-2' Pachner Move.

The identity corresponding to the **'4-1' move** (shown in Figure 1.11) is

$$w^{-2}\sum_{a,b,c,d}(-)^{2a+2b+2c+2d}[2a+1][2b+1][2c+1][2d+1]\times$$
$$\left|\begin{array}{ccc} j_1 & j_2 & j_3 \\ a & b & c \end{array}\right|_q \left|\begin{array}{ccc} j_1 & j_5 & j_6 \\ d & c & b \end{array}\right|_q \left|\begin{array}{ccc} j_2 & j_4 & j_6 \\ d & c & a \end{array}\right|_q \left|\begin{array}{ccc} j_3 & j_4 & j_5 \\ d & b & a \end{array}\right|_q = \left|\begin{array}{ccc} j_1 & j_2 & j_3 \\ j_4 & j_5 & j_6 \end{array}\right|_q, \quad (1.4.11)$$

and the identity corresponding to the **'3-2' move** (shown in Figure 1.12) is the Biedenharn-Elliot identity (which also holds in the $q \to 1$ limit),

$$\sum_a (-)^{2a}[2a+1]\left|\begin{array}{ccc} j_1 & j_5 & j_6 \\ a & j_9 & j_8 \end{array}\right|_q \left|\begin{array}{ccc} j_2 & j_4 & j_6 \\ a & j_9 & j_7 \end{array}\right|_q \left|\begin{array}{ccc} j_3 & j_4 & j_5 \\ a & j_8 & j_7 \end{array}\right|_q$$
$$= \left|\begin{array}{ccc} j_1 & j_2 & j_3 \\ j_4 & j_5 & j_6 \end{array}\right|_q \left|\begin{array}{ccc} j_1 & j_2 & j_3 \\ j_7 & j_8 & j_9 \end{array}\right|_q. \quad (1.4.12)$$

In addition to the identities corresponding to Pachner moves, the quantum integers satisfy the identity

$$\sum_{a,b}(-)^{2a+2b}[2a+1][2b+1]\Delta_q(a,b,c) = w^2(-)^{2c}[2c+1]. \quad (1.4.13)$$

and the orthogonality relation

$$\sum_f (-)^{2c+2f}[2c+1][2f+1]\left|\begin{array}{ccc} a & b & c \\ d & e & f \end{array}\right|_q \left|\begin{array}{ccc} a & b & c' \\ d & e & f \end{array}\right|_q = \Delta_q(d,e,c)\Delta_q(a,b,c)\delta_{c,c'}. \quad (1.4.14)$$

The latter relation also holds in the $q \to 1$ limit for the conventional $6j$ symbols.

By its construction the Turaev-Viro partition function is finite for any root of unity

q, and converges to the Ponzano-Regge partition function when the Ponzano-Regge partition function is finite. It is more difficult to prove that Z_q tends to a finite value for more general complexes, but it can be proved by showing that all interior vertices can be removed from a triangulated manifold with boundary by the Pachner moves. For the classes of manifolds with boundary that we will be constructing, the $q \to 1$ limit is well-defined, and so we take this as the definition of the regularised Ponzano-Regge partition function Z for complexes with interior vertices,

$$Z = \lim_{q \to 1} Z_q. \tag{1.4.15}$$

This approach was also used in [12, 13].

The partition functions of the Turaev-Viro model are multiplicative. If $\mathcal{M}_1$ and $\mathcal{M}_2$ are disjoint labelled complexes, then

$$Z_q[\mathcal{M}_1 \amalg \mathcal{M}_2] = Z_q[\mathcal{M}_1] Z_q[\mathcal{M}_2]. \tag{1.4.16}$$

This multiplicative rule is modified slightly when the subcomplexes $\mathcal{M}_1$ and $\mathcal{M}_2$ are not disjoint but share a boundary. If all the edges on the shared boundary remain on the boundary of the glued complex, then the above relation still holds. For a more general gluing, edges that are on the boundary of $\mathcal{M}_1$ may be in the interior of $\mathcal{M}_1 \cup \mathcal{M}_2$, so new weight factors and sums need to be introduced. The partition function of the glued complex Z_q is

$$Z_q[\mathcal{M}_1 \cup \mathcal{M}_2] = w^{-2v} \sum_{j_i \in \mathcal{B}} \left(\prod_{j_i \in \mathcal{B}} (-)^{2j_i} [2j_i + 1] \right) Z_q[\mathcal{M}_1] Z_q[\mathcal{M}_2], \tag{1.4.17}$$

where $\mathcal{B}$ is the subset of spin labels assigned to lines in $\partial\mathcal{M}_1 \cap \partial\mathcal{M}_2$ that are in the interior of $\mathcal{M}_1 \cup \mathcal{M}_2$, and v is the number of vertices that were on the boundary of $\mathcal{M}_1$ and $\mathcal{M}_2$ but are in the interior of the glued manifold $\mathcal{M}_1 \cup \mathcal{M}_2$. The multiplicative rule transfers across to the Ponzano-Regge model in the $q \to 1$ limit.

1.4.3 Belyi triangulations

We wish to construct labelled triangulations of 3-manifolds, or **3-complexes**, which can be generated from the ribbon graph and reproduce the ribbon graph evaluation in the fuzzy sphere matrix model. These 3-complexes can be constructed by using *Belyi triangulations*, which are triangulations of a two-dimensional surface generated from an embedded dessin d'enfant.

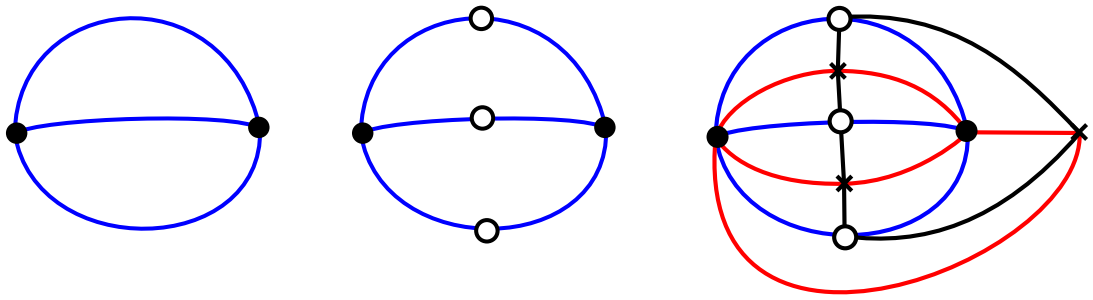

a b c

Figure 1.13: The ribbon graph, dessin, and Belyi triangulation associated to the 'theta' graph.

A connected ribbon graph of genus g can be embedded into a surface of genus g. Recall from Section 1.1.3 that a ribbon graph can be converted into a clean dessin d'enfant by colouring the vertices in black and introducing a new, bivalent white vertex on each edge of the ribbon graph. An embedded ribbon graph can be realised as the preimage of the interval $[0, 1]$ of a Belyi map, where 0 and 1 are branch points on the map; the preimage of 0 corresponds to the black vertices, and the preimages of 1 correspond to the white vertices.

Now consider the preimages of the third branch point at infinity under the Belyi map. There is a preimage of infinity for each face of the dessin d'enfant; we mark these points by crosses in the diagrams in this subsection. By also adding the preimages of the intervals $[1, \infty]$ on the positive real axis and $[\infty, 0]$ on the negative real axis, we construct a triangulation of the domain surface containing the dessin d'enfant. This is the **Belyi triangulation** of the surface associated to the Belyi map and the dessin d'enfant. Each triangle on the preimage surface maps onto one of the two triangles on the target sphere, which are the regions $\mathrm{Im}(z) > 0$ and $\mathrm{Im}(z) < 0$. On the triangulated domain surface, each preimage of infinity is connected to every vertex bounding the face of the original dessin. In the following diagrams, we draw the preimages of the interval $[0, 1]$ (corresponding to the dessin) in blue, the preimages of the interval $[1, \infty]$ in black, and the preimages of the negative real axis interval $[\infty, 0]$ in red. An example of a ribbon graph being converted into a clean dessin and a Belyi triangulation is given in Figure 1.13.

Now consider the Belyi triangulations associated to trivalent ribbon graphs. In this case, the Belyi triangulation can be split into two distinct triangulations. Consider first the blue and red edges embedded on the surface. Each white vertex connects to two blue edges; if we remove the white vertex and consider the connecting edges to be

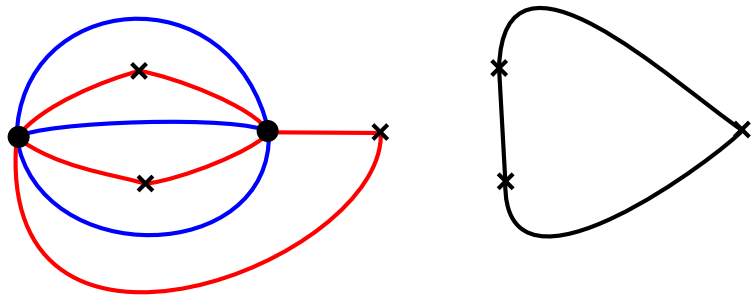

a b

Figure 1.14: The outer and inner triangulations of the 'theta' graph.

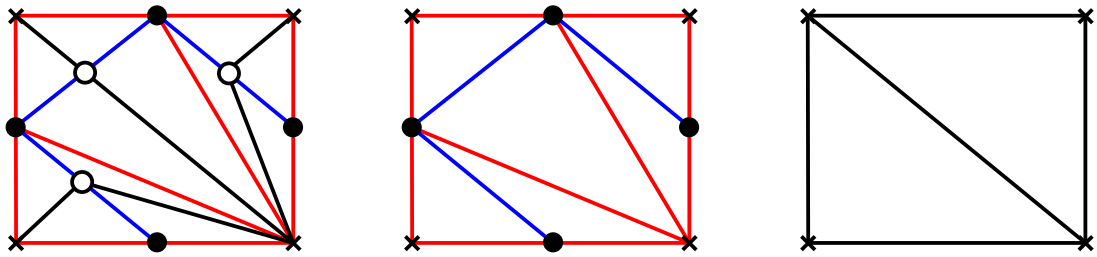

a b c

Figure 1.15: The Belyi triangulations of the two-vertex genus one ribbon graph.

a single edge, then the blue and red edges form a triangulation of the surface. Each triangle on the surface is bounded two red edges and a blue edge. We call this the **outer Belyi triangulation** of the graph.

Next, consider the black edges of the original Belyi triangulation. Each white vertex connects to exactly two black edges; we can similarly remove these vertices and consider the connected pair of edges to be a single edge. This generates a black edge for every edge of the original ribbon graph, and a vertex for every face of the original graph; this is the *dual* of the ribbon graph. As the ribbon graph is trivalent, each dual face is a triangle, and so the black edges form a triangulation of the surface. We call this the **inner Belyi triangulation** of the graph.

In Figure 1.14, we have given an example of the inner and outer Belyi triangulations associated to the 'theta' graph. In Figure 1.15, we have shown a Belyi triangulation of a torus and its associated outer and inner Belyi triangulations, drawn on a rectangle with opposite sides identified.

The Belyi triangulations of surfaces can be extended to triangulations of **handlebodies**, which are 3-manifolds formed by embedding a surface into $\mathbb{R}^3$ and taking the enclosed volume. Given a ribbon graph $\mathcal{G}$ of genus g, we can consider a

labelled triangulation of the genus g handlebody with a boundary triangulation matching the inner Belyi triangulation of the graph. On assigning integer spin labels l_p to the boundary edges, where $0 < l_p \leq 2j$, we create an **inner Belyi 3-complex** of the graph. We can also consider a labelled triangulation of the genus g handlebody that matches the outer Belyi triangulation of the graph on its boundary. To each red edge of the boundary triangulation, we assign the spin label $j = \frac{1}{2}(N-1)$. To each blue edge of the boundary triangulation, we assign the spin label zero, corresponding to the trivial representation of $su(2)$. We call a labelled triangulation of a handlebody with this boundary data a **complete Belyi 3-complex** of the graph. Since the Ponzano-Regge partition function of a complex is independent of the choice of the *interior* triangulation of the manifold, the partition function is a function purely of the boundary data of the complex and its topology, and so the partition function is determined by the ribbon graph. Any two complete Belyi 3-complexes of the same graph will have the same Ponzano-Regge partition function. In the following sections, we will show that, if $\mathcal{M}(G)$ is a complete Belyi 3-complex associated to a graph $\mathcal{G}$ with F faces and E edges, then the Ponzano-Regge partition function is

$$Z(\mathcal{M}(\mathcal{G})) = N^{F-E}. \tag{1.4.18}$$

This matches the ribbon graph evaluation of a graph, up to a normalisation factor of N^{-E}. For the case of the planar ribbon graphs, with complete Belyi 3-complexes triangulating the solid ball, we can show that the ribbon graph evaluations will be of exactly the form given in (1.3.21).

1.5 Belyi 3-complexes of planar graphs

In this section we restrict our attention to *planar* trivalent ribbon graphs generated by the fuzzy sphere matrix model. We can construct the complete Belyi 3-complex of a given planar ribbon graph $\mathcal{G}$ in two stages. First, we construct a triangulation of the solid ball with the inner Belyi triangulation (the dual of $\mathcal{G}$) on its boundary, and assign a spin label l_p to each edge of the ribbon graph. We call a labelled triangulation with the inner Belyi triangulation on its boundary an **inner Belyi 3-complex**. Any two inner Belyi 3-complexes of the same labelled graph will have the same Ponzano-Regge partition function. We review a result of Moussouris [8] which states that the Ponzano-Regge partition function of the inner Belyi 3-complex of a planar graph is equal to the evaluation of the labelled spin network dual to its boundary triangulation,

with the edge labels l_p of the spin network inherited from the triangulation.

Next, we attach tetrahedra to the outside of the inner Belyi 3-complex in such a way that the inner Belyi triangulation is moved into the interior of the manifold, and that the outer Belyi triangulation appears on the boundary of the complex. We assign a representation label j to each of the red edges and a label 0 to each of the blue edges, making the triangulation a complete Belyi 3-complex. The Ponzano-Regge partition function of the complex assigns a $6j$ symbol to each of the extra tetrahedra and sums out the labels of the inner Belyi triangulation l_p. This reproduces the ribbon graph state sum in exactly the form given in (1.3.21), up to a normalisation factor of N^{-E}.

In this section and the next section, we adopt some conventions with the edge colours drawn in the figures. Blue edges always carry the spin label 0, corresponding to the zero representation of $su(2)$. Red edges carry the spin label j, corresponding to the N-dimensional representation of $su(2)$. These edges only appear in complete Belyi 3-complexes, and will always appear on the boundary. The black edges will carry spin labels l_p, which will be constrained to be integers in the range $0 \leq l_p \leq 2j$ by the structure of the complexes. These edges appear on the boundaries of inner Belyi 3-complexes, and in the interior of complete Belyi 3-complexes. The green edges correspond to spin labels with Roman letters $a, b, c, \ldots$, which may be integers or half-integers, and may be unbounded from above. These edges always appear in the interior of the inner Belyi 3-complexes.

1.5.1 Constructing the inner Belyi 3-complex

It is straightforward to construct an inner Belyi 3-complex associated to a planar graph. Consider an embedding of the inner Belyi triangulation onto the surface of a solid ball. Add a vertex in the interior of the solid ball, and connect every vertex of the surface triangulation to the interior vertex. This gives a triangulation of the solid ball with a tetrahedron for each of the V triangles on the surface, where V is the number of vertices of the ribbon graph. We write $\mathcal{I}(\mathcal{G}, \{l_p\})$ to denote this choice of inner Belyi 3-complex with edges labelled l_p. The aim of this subsection is to show that

$$Z(\mathcal{I}(\mathcal{G}, \{l_p\}) = S(\mathcal{G}, \{l_p\}). \tag{1.5.1}$$

To do this, we first show that the partition function of the simplest inner Belyi 3-complex, corresponding to a theta graph, matches the spin network evaluation of the graph. Next, we show that modifying the graph $\mathcal{G}$ by a '3-1' or a '2-2' move

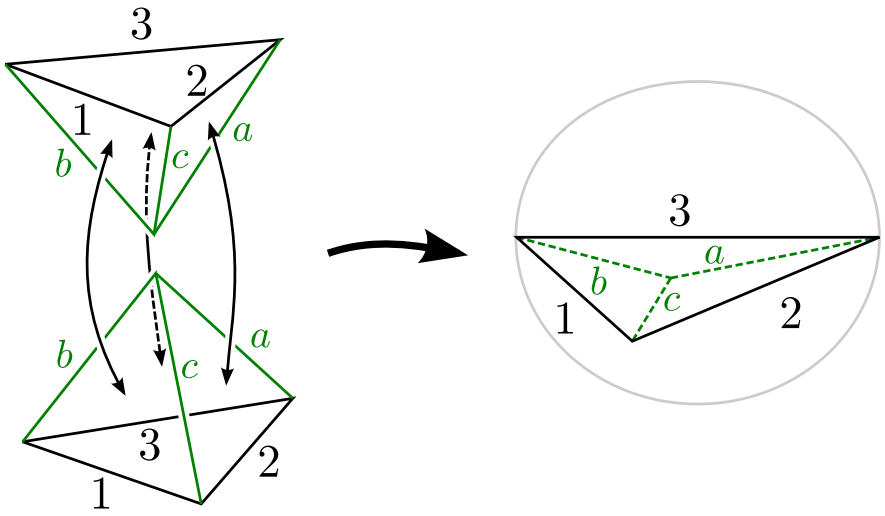

Figure 1.16: The inner Belyi 3-complex corresponding to the 'theta' graph, constructed by gluing two tetrahedra on three faces, is a two-tetrahedron triangulation of the ball.

introduces $6j$ factors and spin label sums into $Z \circ \mathcal{I}$ that match the factors given in Section 1.3.2. The 'orthogonality' move on the graph can be generated by a '3-1' and a '2-2' move whenever the graph has more than two vertices. The duals of these moves, acting on the boundary triangulation, are called the **Alexander moves**; they are the two-dimensional Pachner moves, and can be used to relate any two triangulations of the same surface. In particular, there exists a series of Alexander moves that relates any triangulation of the sphere to the dual triangulation of the theta graph [62]. (We could find such a sequence for a given triangulation by taking the dual graph and reducing down the 'polygons' of the graph, as in Section 1.3.2.) Taking this duals of this series of moves and reversing the order, we can generate any planar graph by a finite series of '3-1' and '2-2' moves on the ribbon graph. As the functions $Z \circ \mathcal{I}$ and S agree for the theta graph and are modified by the same factors when the graph is altered by any combination of '3-1' or '2-2' moves, it must be the case that $Z \circ \mathcal{I}$ and S agree for all labelled planar ribbon graphs.

In Figure 1.16 we have drawn the inner Belyi 3-complex associated to the theta graph with the boundary edges labelled l_1, l_2, l_3 (abbreviated to $1, 2, 3$ in the diagram). The complex can be constructed by taking two tetrahedra and gluing them on three faces. This gives a 'pillow' triangulation of the solid ball, with three interior edges labelled a, b, c, drawn in green. This manifold has an interior vertex, so we need to regularise the Ponzano-Regge partition function by using the Turaev-Viro model. The

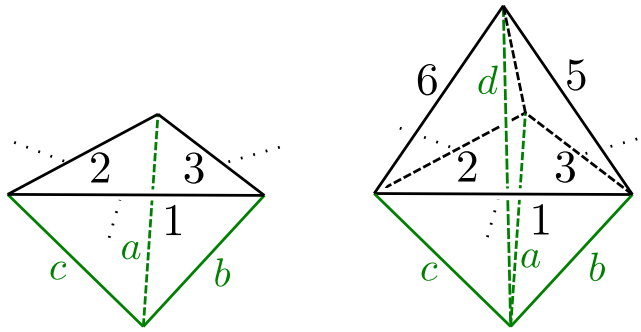

a b

Figure 1.17: A pair of inner Belyi 3-complexes of graphs related by a '3-1' move.

partition function is

$$Z_q\left(\mathcal{I}\left(\begin{array}{c}1\\2\\3\end{array}\right)\right) = w^{-2}\sum_{a,b,c}(-)^{2a+2b+2c}[2a+1][2b+1][2c+1]\left|\begin{array}{ccc} l_1 & l_2 & l_3 \\ a & b & c\end{array}\right|_q\left|\begin{array}{ccc} l_1 & l_2 & l_3 \\ a & b & c\end{array}\right|_q . \tag{1.5.2}$$

By using the orthogonality identity (1.4.14) on the sum over c and the triangle constraint sum (1.4.13), we evaluate this to

$$\begin{aligned} Z_q\left(\mathcal{I}\left(\begin{array}{c}1\\2\\3\end{array}\right)\right) &= w^{-2}\sum_{a,b}(-)^{2a+2b}\frac{[2a+1][2b+1]}{[2l_3+1]}\Delta_q(a,b,l_3)\Delta_q(l_1,l_2,l_3) \\ &= \Delta_q(l_1,l_2,l_3), \end{aligned} \tag{1.5.3}$$

which has the well-defined $q \to 1$ Ponzano-Regge limit

$$Z\left(\mathcal{I}\left(\begin{array}{c}1\\2\\3\end{array}\right)\right) = \lim_{q\to 1} Z_q\left(\mathcal{I}\left(\begin{array}{c}1\\2\\3\end{array}\right)\right) = \Delta(l_1,l_2,l_3) = S\left(\begin{array}{c}1\\2\\3\end{array}\right). \tag{1.5.4}$$

This matches the spin network evaluation of the theta graph (1.3.28).

We next consider a pair of labelled ribbon graphs $\mathcal{G}$ and $\mathcal{G}'$ which are related by a '3-1' move. Say that $\mathcal{G}$ has a vertex connecting edges with spin labels l_1, l_2, l_3, and $\mathcal{G}'$ has, in place of this vertex, a triple of vertices connecting the spin labels $l_1, l_2, \ldots, l_6$. The tetrahedra in the inner Belyi 3-complex associated to these vertices are given in Figures 1.17a and 1.17b respectively. The Turaev-Viro partition function associated

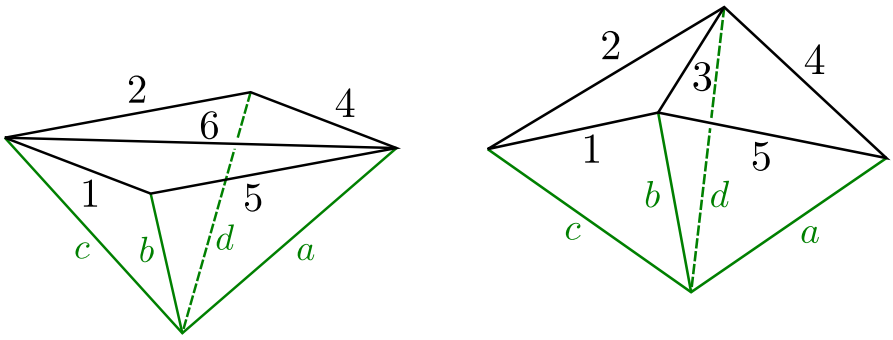

a b

Figure 1.18: A pair of inner Belyi 3-complexes of graphs related by a '2-2' move.

to the part of the manifold shown in Figure 1.17a is

$$Z_q\left(\mathcal{I}\left(\begin{array}{c}\includegraphics[height=1.2cm]{}\end{array}\right)\right) = \left|\begin{array}{ccc} l_1 & l_2 & l_3 \\ a & b & c \end{array}\right|_q , \tag{1.5.5}$$

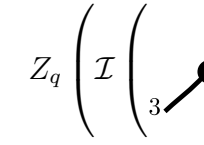

and the partition function associated to the part of the manifold shown in Figure 1.17b is

$$\begin{aligned} Z_q\left(\mathcal{I}\left(\begin{array}{c}\includegraphics[height=1.2cm]{}\end{array}\right)\right) &= \sum_d (-)^{2d}[2d+1] \left|\begin{array}{ccc} l_1 & l_6 & l_5 \\ d & b & c \end{array}\right|_q \left|\begin{array}{ccc} l_2 & l_4 & l_6 \\ d & c & a \end{array}\right|_q \left|\begin{array}{ccc} l_3 & l_5 & l_4 \\ d & a & b \end{array}\right|_q \\ &= \left|\begin{array}{ccc} l_1 & l_2 & l_3 \\ a & b & c \end{array}\right|_q \left|\begin{array}{ccc} l_1 & l_2 & l_3 \\ l_4 & l_5 & l_6 \end{array}\right|_q , \end{aligned} \tag{1.5.6}$$

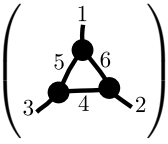

where we have used the '3-2' Pachner move identity (1.4.12) for the Turaev-Viro model. The inner Belyi triangulations of the two graphs therefore satisfy the relation

$$Z_q\left(\mathcal{I}\left(\begin{array}{c}\includegraphics[height=1.2cm]{}\end{array}\right)\right) = \left|\begin{array}{ccc} l_1 & l_2 & l_3 \\ l_4 & l_5 & l_6 \end{array}\right|_q Z_q\left(\mathcal{I}\left(\begin{array}{c}\includegraphics[height=1.2cm]{}\end{array}\right)\right) , \tag{1.5.7}$$

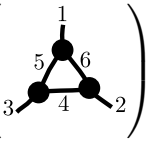

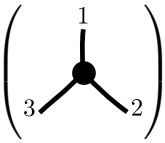

or, in terms of the complete graphs in the $q \to 1$ limit,

$$Z(\mathcal{I}(\mathcal{G}', \{l_4, l_5, l_6, l_1, \ldots\})) = \left|\begin{array}{ccc} l_1 & l_2 & l_3 \\ l_4 & l_5 & l_6 \end{array}\right| Z(\mathcal{I}(\mathcal{G}, \{l_1, \ldots\})). \tag{1.5.8}$$

This matches the relation (1.3.37) for spin networks.

Next, consider two graphs $\mathcal{G}$ and $\mathcal{G}'$ which differ by a '2-2' move at a pair of vertices of each graph. Say that the two vertices of $\mathcal{G}$ are connected by an edge labelled l_6, and the two vertices of $\mathcal{G}'$ are connected by an edge labelled l_3. The tetrahedra of the inner Belyi 3-complexes associated to the these vertices are shown in Figures 1.18a and 1.18b respectively. The Turaev-Viro partition function associated to the labelled complex in Figure 1.18a is

$Z_q\Bigg(\mathcal{I}\Bigg($ 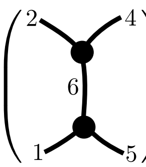 $\Bigg)\Bigg) = \begin{vmatrix} l_1 & l_6 & l_5 \\ a & b & c \end{vmatrix}_q \begin{vmatrix} l_2 & l_4 & l_6 \\ a & c & d \end{vmatrix}_q$ (1.5.9)

and the partition function associated to the complex in Figure 1.18b is

$Z_q\Bigg(\mathcal{I}\Bigg($ 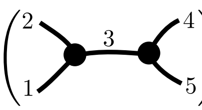 $\Bigg)\Bigg) = \begin{vmatrix} l_1 & l_2 & l_3 \\ d & b & c \end{vmatrix}_q \begin{vmatrix} l_4 & l_5 & l_3 \\ b & d & a \end{vmatrix}_q$ (1.5.10)

The '2-3' Pachner move, which is the inverse of the '3-2' Pachner move, can be applied on the two tetrahedra in Figure 1.18b; using the identity (1.4.12), the partition function becomes

$Z_q\Bigg(\mathcal{I}\Bigg($ 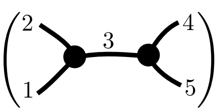 $\Bigg)\Bigg) = \sum_{l_6} (-)^{2l_6}[2l_6+1] \begin{vmatrix} l_1 & l_2 & l_3 \\ l_4 & l_5 & l_6 \end{vmatrix}_q \begin{vmatrix} l_1 & l_6 & l_5 \\ a & b & c \end{vmatrix}_q \begin{vmatrix} l_2 & l_4 & l_6 \\ a & c & d \end{vmatrix}_q$ (1.5.11)

Now, as we are only interested in inner Belyi triangulations where the spin labels l_p are integers, the phase factor drops out and we can write

$Z_q\Bigg(\mathcal{I}\Bigg($ 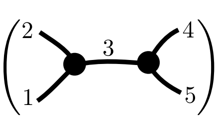 $\Bigg)\Bigg) = \sum_{l_6} [2l_6+1] \begin{vmatrix} l_1 & l_2 & l_3 \\ l_4 & l_5 & l_6 \end{vmatrix}_q Z_q\Bigg(\mathcal{I}\Bigg($ 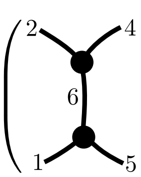 $\Bigg)\Bigg).$ (1.5.12)

In the $q \to 1$ limit, the Ponzano-Regge partition functions of the inner Belyi complexes satisfy the relation

$$Z\left(\mathcal{I}\left(\mathcal{G}', \{l_1, l_2, l_3, l_4, l_5, \ldots\}\right)\right) = \sum_{l_6} (2l_6+1) \begin{vmatrix} l_1 & l_2 & l_3 \\ l_4 & l_5 & l_6 \end{vmatrix} Z\left(\mathcal{I}\left(\mathcal{G}, \{l_1, l_2, l_4, l_5, l_6, \ldots\}\right)\right)$$

which reproduces the spin network identity (1.3.35) for $Z \circ \mathcal{I}$.

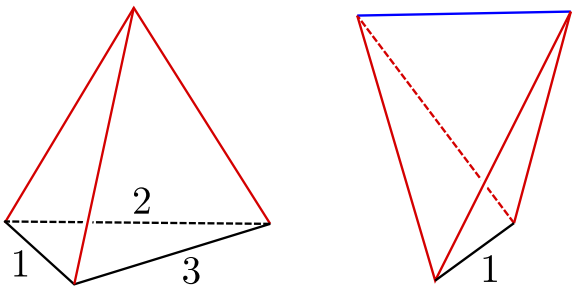

Figure 1.19: The tetrahedra glued on to each face and edge of the boundary of an inner Belyi 3-complex.

As $S(\mathcal{G}, \{l_p\})$ and $Z(\mathcal{I}(\mathcal{G}, \{l_p\}))$ agree on the theta graph and on the '3-1' and '2-2' moves, and as every planar trivalent ribbon graph can be reduced down to a theta graph by a series of '3-1' and '2-2' moves, we see that

$$Z(\mathcal{I}(\mathcal{G}, \{l_p\}) = S(\mathcal{G}, \{l_p\}) \tag{1.5.13}$$

for any planar ribbon graph $\mathcal{G}$.

1.5.2 Constructing the complete Belyi 3-complex

For any labelled ribbon graph $(\mathcal{G}, \{l_p\})$ we can construct a 3-complex, homeomorphic to a solid ball, with the dual triangulation of the ribbon graph (inner Belyi triangulation) embedded on its boundary. We can glue more tetrahedra onto this inner Belyi 3-complex to convert it into a complete Belyi 3-complex, with an outer Belyi triangulation on its boundary. To each face of the inner Belyi triangulation, we glue on the tetrahedron shown in Figure 1.19a. To each edge of the inner Belyi triangulation, which we always draw in black in the diagrams, we glue on the tetrahedron shown in Figure 1.19b. We assign the spin label j to each red edge and the spin label 0 to each blue edge of the boundary tetrahedra. The inner Belyi triangulation has been moved into the inside of the complex by this gluing, hence the name 'inner Belyi triangulation'. The labels l_p assigned to the edges of the inner Belyi triangulation are summed over in the Ponzano-Regge partition function of the complex. The outer Belyi triangulation is now embedded on the boundary of the complex, which makes this a complete Belyi 3-complex. We write $\mathcal{M}(\mathcal{G})$ to denote the complete Belyi 3-complex constructed from a planar graph $\mathcal{G}$.

Each tetrahedron of the form given in Figure 1.19a glued on to a triangle with

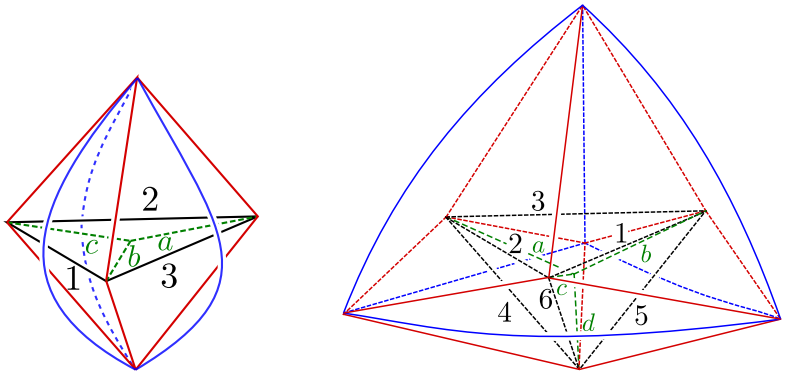

a b

Figure 1.20: Complete Belyi 3-complexes of a theta graph and a tetrahedral graph.

spin-labelled edges l_1, l_2, l_3 has the associated partition function weight

$$Z = \begin{vmatrix} l_1 & l_2 & l_3 \\ j & j & j \end{vmatrix}, \tag{1.5.14}$$

and each tetrahedron of the form in Figure 1.19a has the partition function weight

$$\begin{vmatrix} 0 & j & j \\ l_1 & j & j \end{vmatrix} = \frac{(-)^{2j}}{(2j+1)}, \tag{1.5.15}$$

where we have used an identity on $6j$ symbols from [61]. The partition function of the complete Belyi 3-complex associated to a ribbon graph $\mathcal{G}$ with vertices corresponding to the faces of the inner Belyi triangulation, is

$$\begin{aligned} Z(\mathcal{M}(\mathcal{G})) &= \sum_{\substack{l_1,l_2,\ldots \\ a,b,\ldots}} Z(\mathcal{I}(\mathcal{G},\{l_p\})) \prod_{\substack{\text{edges} \\ \text{of } \mathcal{G}}} (-)^{2l_p}(2l_p+1) \begin{vmatrix} 0 & j & j \\ l_1 & j & j \end{vmatrix} \prod_{\substack{\text{vertices} \\ \text{of } \mathcal{G}}} \begin{vmatrix} l_p & l_q & l_r \\ j & j & j \end{vmatrix} \\ &= \frac{(-)^{2jE}}{(2j+1)^E} \sum_{l_p} S(\mathcal{G},\{l_p\}) \prod_{\text{edges}} (2l_p+1) \prod_{\text{vertices}} \begin{vmatrix} l_p & l_q & l_r \\ j & j & j \end{vmatrix}. \end{aligned} \tag{1.5.16}$$

The sum matches, factor-by-factor, the ribbon graph evaluation sum given in (1.3.21), up to a power of N^E. We deduce that the Ponzano-Regge partition function of a complete Belyi 3-complex of a planar graph is

$$Z(\mathcal{M}(\mathcal{G})) = N^{-E}\mathcal{R}(G) = N^{F-E}. \tag{1.5.17}$$

We conclude this section with some examples of complete Belyi 3-complexes of planar graphs. Figure 1.20a shows the complete Belyi 3-complex corresponding to a theta graph. This is constructed from the 'pillow' triangulation given in Figure 1.16 by gluing a tetrahedron onto each of the boundary faces and a tetrahedron onto each of the boundary edges. The boundary of this manifold matches the outer Belyi triangulation of the theta graph given in Figure 1.14a. The Ponzano-Regge partition function of this manifold is

$$Z = \lim_{q\to 1} w^{-2} \sum_{\substack{l_1,l_2,l_3\\ a,b,c}} (-)^{2a+2b+2c}[2l_1+1][2l_2+1][2l_3+1][2a+1][2b+1][2c+1]$$
$$\left|\begin{matrix} l_1 & l_2 & l_3 \\ a & b & c \end{matrix}\right|_q \left|\begin{matrix} l_1 & l_2 & l_3 \\ a & b & c \end{matrix}\right|_q \left|\begin{matrix} 0 & j & j \\ l_1 & j & j \end{matrix}\right|_q \left|\begin{matrix} 0 & j & j \\ l_2 & j & j \end{matrix}\right|_q \left|\begin{matrix} 0 & j & j \\ l_3 & j & j \end{matrix}\right|_q \left|\begin{matrix} l_1 & l_2 & l_3 \\ j & j & j \end{matrix}\right|_q \left|\begin{matrix} l_1 & l_2 & l_3 \\ j & j & j \end{matrix}\right|_q$$

$$\begin{aligned} &= \frac{(-)^{2j}}{(2j+1)^3} \sum_{l_1,l_2,l_3} (2l+1)(2l_2+1)(2l_3+1) \left|\begin{matrix} l_1 & l_2 & l_3 \\ j & j & j \end{matrix}\right| \left|\begin{matrix} l_1 & l_2 & l_3 \\ j & j & j \end{matrix}\right| \\ &= N^{-3}\mathcal{R}\left(\quad\right), \end{aligned} \tag{1.5.18}$$

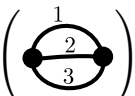

reproducing the ribbon graph sum given in Figure (1.3.43).

The complete Belyi 3-complex constructed from a tetrahedral graph is given in Figure 1.20b. This complex consists of six tetrahedra of the form in Figure 1.19a, six tetrahedra of the form in Figure 1.19b, and an inner Belyi 3-complex consisting of four tetrahedra with black and green edges. The Ponzano-Regge partition function of this complete Belyi 3-complex is

$$\begin{aligned} Z = \lim_{q\to 1} w^{-2} \sum_{\text{internal labels}} &[2l_1+1]\dots[2l_6+1](-)^{2a+2b+2c+2d}[2a+1][2b+1][2c+1][2d+1]\times \\ &\times \left|\begin{matrix} 0 & j & j \\ l_1 & j & j \end{matrix}\right|_q \left|\begin{matrix} 0 & j & j \\ l_2 & j & j \end{matrix}\right|_q \left|\begin{matrix} 0 & j & j \\ l_3 & j & j \end{matrix}\right|_q \left|\begin{matrix} 0 & j & j \\ l_4 & j & j \end{matrix}\right|_q \left|\begin{matrix} 0 & j & j \\ l_5 & j & j \end{matrix}\right|_q \left|\begin{matrix} 0 & j & j \\ l_6 & j & j \end{matrix}\right|_q \times \\ &\times \left|\begin{matrix} l_1 & l_2 & l_3 \\ j & j & j \end{matrix}\right|_q \left|\begin{matrix} l_2 & l_4 & l_6 \\ j & j & j \end{matrix}\right|_q \left|\begin{matrix} l_3 & l_4 & l_5 \\ j & j & j \end{matrix}\right|_q \left|\begin{matrix} l_1 & l_5 & l_6 \\ j & j & j \end{matrix}\right|_q \times \\ &\times \left|\begin{matrix} l_1 & l_2 & l_3 \\ a & b & c \end{matrix}\right|_q \left|\begin{matrix} l_2 & l_4 & l_6 \\ d & c & a \end{matrix}\right|_q \left|\begin{matrix} l_3 & l_4 & l_5 \\ d & b & a \end{matrix}\right|_q \left|\begin{matrix} l_1 & l_5 & l_6 \\ d & c & b \end{matrix}\right|_q \end{aligned}$$

$$= N^{-6} \sum_{\substack{l_1 l_2 l_3 \\ l_4 l_5 l_6}} (2l_1+1)(2l_2+1)(2l_3+1)(2l_4+1)(2l_5+1)(2l_6+1) \begin{vmatrix} l_1 & l_2 & l_3 \\ l_4 & l_5 & l_6 \end{vmatrix} \times$$

$$\times \begin{vmatrix} l_1 & l_2 & l_3 \\ j & j & j \end{vmatrix} \begin{vmatrix} l_2 & l_4 & l_6 \\ j & j & j \end{vmatrix} \begin{vmatrix} l_3 & l_4 & l_5 \\ j & j & j \end{vmatrix} \begin{vmatrix} l_1 & l_5 & l_6 \\ j & j & j \end{vmatrix} = N^{-6} \mathcal{R} \left(\right.$$

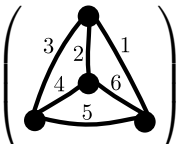

$$\left. \right). \tag{1.5.19}$$

This partition function matches the ribbon graph evaluation sum of (1.3.45).

1.6 Complete Belyi 3-complexes of non-planar graphs

In the previous section, we presented a way of constructing a complete Belyi 3-complex from any planar ribbon graph whose partition function reproduces the evaluation of the graph. We can extend this construction of Belyi 3-complexes to non-planar ribbon graphs. For a graph $\mathcal{G}$ of genus g, a complete Belyi 3-complex $\mathcal{M}(\mathcal{G})$ is a triangulation of a handlebody of genus g, with the outer Belyi triangulation of $\mathcal{G}$ embedded on the boundary, and the spin labels j and 0 assigned to the red and blue boundary edges respectively. The aim of this section is to show that, for any complete Belyi 3-complex $\mathcal{M}(\mathcal{G})$ of a graph $\mathcal{G}$,

$$Z(\mathcal{M}(\mathcal{G})) = N^{F-E} = N^{-E}\mathcal{R}(\mathcal{G}). \tag{1.6.1}$$

Unfortunately, the approach used in the previous section does not generalise to the non-planar case, as Moussouris' algorithm does not hold for non-planar graphs. The complex constructed by assigning a tetrahedron to each vertex of a graph of genus g is not a handlebody, but a three-dimensional cone over the genus g surface. The partition function associated to this conical complex does not match the spin network evaluation of the graph. The Ponzano-Regge partition function of a handlebody with an inner Belyi triangulation on its boundary does not match the spin network evaluation either. However, despite being unable to match each factor of (1.3.21) to a Ponzano-Regge partition function, we can still show that the partition function of a complete Belyi 3-complex evaluates to N^{F-E} in every case.

The approach we take is as follows. In the next subsection, we start by considering the simplest triangulation of the solid torus with an outer Belyi triangulation on its boundary, and show that its partition function evaluates to N^{F-E}. We also consider another complete Belyi 3-complex of the solid torus which is necessary for construct-

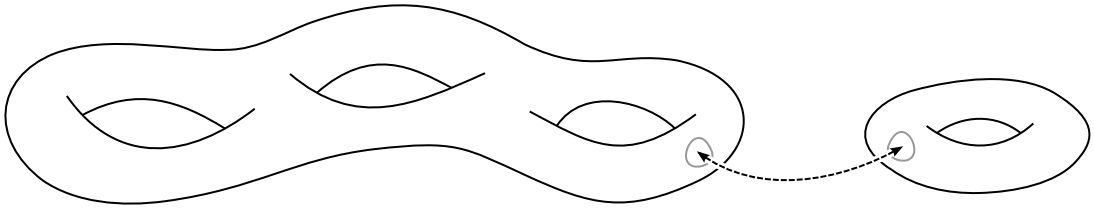

Figure 1.21: The connected sum of a genus g handlebody and a solid torus is a genus $(g+1)$ handlebody.

ing higher genus handlebodies. In the subsequent subsection, we show that any two complete Belyi 3-complexes of a pair of graphs which are related by a '3-1' or a '2-2' move will satisfy relations of the form

$$Z\left(\mathcal{M}\left(\begin{array}{c}\includegraphics[height=2.2cm]{}\end{array}\right)\right) = N^{-2}Z\left(\mathcal{M}\left(\begin{array}{c}\includegraphics[height=2.2cm]{}\end{array}\right)\right), \qquad (1.6.2)$$

$$Z\left(\mathcal{M}\left(\begin{array}{c}\includegraphics[height=2.2cm]{}\end{array}\right)\right) = Z\left(\mathcal{M}\left(\begin{array}{c}\includegraphics[height=2.2cm]{}\end{array}\right)\right). \qquad (1.6.3)$$

Any two triangulations of a surface of the same genus are related by a series of Alexander moves, which implies that any two ribbon graphs of the same genus are related by a series of '3-1', '2-2, and '1-3' moves [62]. This shows that the ribbon graph evaluation of any genus one graph agrees with the Ponzano-Regge partition function of a complete Belyi 3-complex of the graph. In the final subsection, we show how to construct a genus $(g+1)$ complete Belyi 3-complex from a genus g complete Belyi 3-complex. A genus $(g+1)$ handlebody is the *connected sum* of a genus g handlebody and a solid torus, glued together at a neighbourhood on their boundaries, as demonstrated in Figure 1.21. We glue a triangulation of the solid torus with a contractible triangle on its boundary to a general genus g handlebody, and show that the new complete Belyi 3-complex satisfies (1.6.1). This is enough to prove that (1.6.1) holds for graphs of any genus by induction on g.

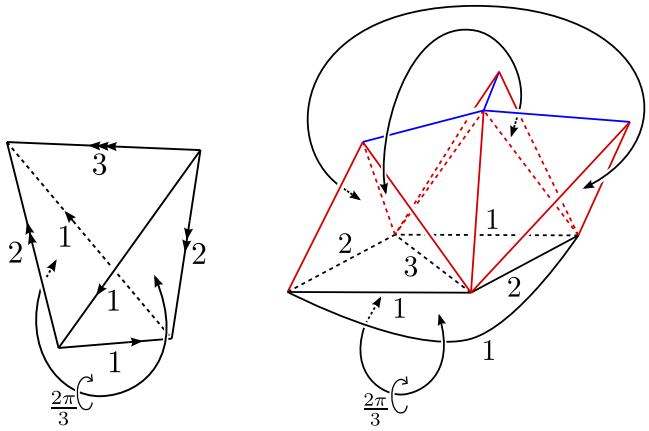

Figure 1.22: An inner and a complete Belyi 3-complex of the simplest non-planar graph.

1.6.1 Triangulations of the solid torus

We start by constructing an inner Belyi 3-complex $\mathcal{I}(\mathcal{G}, \{l_p\})$ of the simplest non-planar ribbon graph,

$$\mathcal{I}\left(\begin{array}{c}3\\2\\1\end{array}\right). \tag{1.6.4}$$

We look for a 3-complex of the solid torus with two triangles on its boundary. In fact, there exists a particularly simple triangulation, consisting of a single tetrahedron with two faces glued together after a $2\pi/3$ twist [63]. This tetrahedron is shown in Figure 1.22a. In the diagram, the triangles labelled by the triples (l_1, l_1, l_2) are identified, the edges with the same spin label are identified, and the two distinct triangles labelled (l_1, l_2, l_3) lie on the boundary. The boundary triangles of this tetrahedron form the inner Belyi triangulation shown earlier in Figure 1.15c. To convert this into a complete Belyi 3-complex, we attach two tetrahedra with black and red edges and three tetrahedra with black, red and blue edges, in an analogous manner to in the previous section. The resulting complex is shown in Figure 1.22b, and has the outer Belyi triangulation from Figure 1.15b on its boundary.

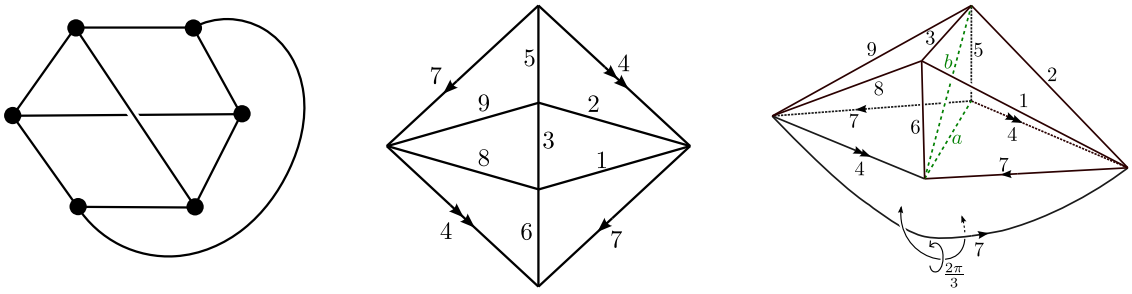

a b c

Figure 1.23: A genus one ribbon graph, with its dual triangulation and an associated inner Belyi 3-complex.

The Ponzano-Regge partition function of this complete Belyi 3-complex is

$$Z\left(\mathcal{M}\left(\begin{array}{c}\includegraphics[height=1.2em]{}\end{array}\right)\right) = \frac{(-)^{2j}}{(2j+1)^3}\sum_{l_1,l_2,l_3}(2l_1+1)(2l_2+1)(2l_3+1) \left|\begin{array}{ccc} l_1 & l_2 & l_3 \\ l_1 & l_2 & l_1 \end{array}\right| \left|\begin{array}{ccc} l_1 & l_2 & l_3 \\ j & j & j \end{array}\right| \left|\begin{array}{ccc} l_1 & l_2 & l_3 \\ j & j & j \end{array}\right| \quad (1.6.5)$$

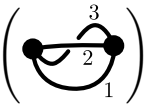

We can apply the Biedenharn-Elliot identity (1.4.12) on the sum over l_3 and the orthogonality relation (1.4.14) on the sum over l_2 to find

$$\begin{aligned} Z\left(\mathcal{M}\left(\begin{array}{c}\includegraphics[height=1.2em]{}\end{array}\right)\right) &= \frac{(-)^{2j}}{(2j+1)^3}\sum_{l_1,l_2}(2l_1+1)(2l_2+1)\left|\begin{array}{ccc} l_1 & l_1 & l_2 \\ j & j & j \end{array}\right| \left|\begin{array}{ccc} l_1 & l_1 & l_2 \\ j & j & j \end{array}\right| \\ &= \frac{1}{(2j+1)^4}\sum_{l_1}\Delta(l_1,j,j)(2l_1+1) \\ &= \frac{1}{(2j+1)^2} = N^{-2}. \end{aligned} \quad (1.6.6)$$

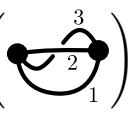

As the ribbon graph has one face and three edges, we find that $Z(\mathcal{M}(\mathcal{G}))$ matches $\mathcal{R}(\mathcal{G}) = N^{F-E}$ for this graph.

In the following subsections, we will need an inner Belyi triangulation of the solid torus in which one of the boundary triangles is homeomorphic to a disc. For this reason, we present another example of a Belyi 3-complex, associated to the ribbon graph in Figure 1.23a. This graph is of genus one and has six vertices, nine edges, and three faces, and its dual triangulation is given in Figure 1.23b with labels on the edges. By taking the one-tetrahedron triangulation of the torus from Figure 1.22a and layering four new tetrahedra onto the boundary, we can build up an inner Belyi

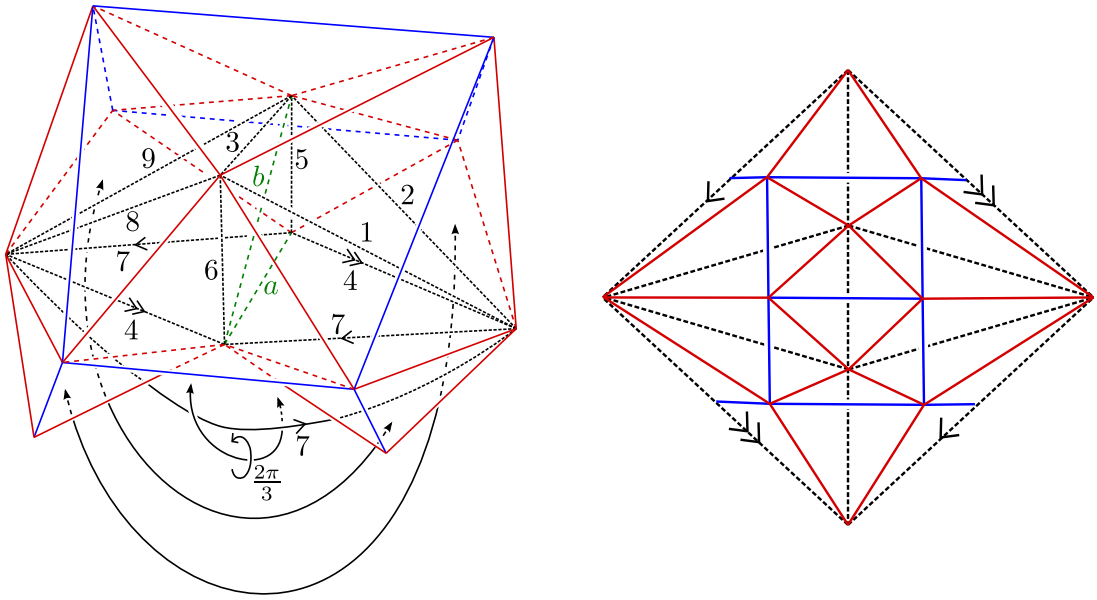

a b

Figure 1.24: A twenty-tetrahedron complete Belyi 3-complex of the ribbon graph, where three pairs of triangles are identified, and its Belyi triangulations.

3-complex of the graph, shown in Figure 1.23c.

We extend this inner Belyi 3-complex to a complete Belyi 3-complex by attaching a tetrahedron onto each face and each edge of the boundary triangulation. The complete Belyi 3-complex is shown in Figure 1.24a, along with the Belyi triangulation of the graph in Figure 1.24b. The partition function of this complex has nine $6j$ symbols corresponding to the edges of the ribbon graph, which we immediately evaluate to

$$\left| \begin{array}{ccc} 0 & j & j \\ l_p & j & j \end{array} \right| = \frac{(-)^{2j}}{(2j+1)}. \tag{1.6.7}$$

The remaining eleven tetrahedra contribute $6j$ symbols to the partition function,

$$\begin{aligned} Z(\mathcal{M}(\mathcal{G})) = \frac{(-)^{2j}}{(2j+1)^9} \sum_{a,b,l_1,\ldots} (-)^{2a+2b}(2a+1)(2b+1) \left[\prod_{p=1,\ldots,9} (2l_p+1) \right] \times \\ \times \left| \begin{array}{ccc} l_4 & l_7 & a \\ l_4 & l_7 & l_7 \end{array} \right| \left| \begin{array}{ccc} l_4 & l_7 & a \\ b & l_5 & l_2 \end{array} \right| \left| \begin{array}{ccc} l_4 & l_7 & a \\ l_5 & b & l_9 \end{array} \right| \left| \begin{array}{ccc} l_2 & l_7 & b \\ l_6 & l_3 & l_1 \end{array} \right| \left| \begin{array}{ccc} l_4 & l_9 & b \\ l_3 & l_6 & l_8 \end{array} \right| \times \\ \times \left| \begin{array}{ccc} l_2 & l_4 & l_5 \\ j & j & j \end{array} \right| \left| \begin{array}{ccc} l_5 & l_7 & l_9 \\ j & j & j \end{array} \right| \left| \begin{array}{ccc} l_3 & l_8 & l_9 \\ j & j & j \end{array} \right| \left| \begin{array}{ccc} l_4 & l_6 & l_8 \\ j & j & j \end{array} \right| \left| \begin{array}{ccc} l_1 & l_6 & l_7 \\ j & j & j \end{array} \right| \left| \begin{array}{ccc} l_1 & l_2 & l_3 \\ j & j & j \end{array} \right|. \end{aligned} \tag{1.6.8}$$

This partition function can be reduced down by successively applying the Biedenharn-Eliot and orthogonality identities. Starting with the sum over the label a, we can use the Biedenharn-Eliot identity in the form

$$\sum_a (-)^{2a}(2a+1) \begin{vmatrix} l_4 & l_7 & a \\ l_4 & l_7 & l_7 \end{vmatrix} \begin{vmatrix} l_4 & l_7 & a \\ b & l_5 & l_2 \end{vmatrix} \begin{vmatrix} l_4 & l_7 & a \\ l_5 & b & l_9 \end{vmatrix} = \begin{vmatrix} l_2 & l_7 & l_9 \\ l_7 & l_5 & l_4 \end{vmatrix} \begin{vmatrix} l_2 & l_7 & l_9 \\ l_4 & b & l_7 \end{vmatrix} \tag{1.6.9}$$

to remove the sum over a and a $6j$. This also reduces the number of $6j$s containing b by one, so we can now apply the Biedenharn-Eliot identity on the sum over the label b. In a similar manner, we can apply this identity successively on the sums over l_6, l_4, and l_8 to obtain

$$\begin{aligned} Z = \frac{(-)^{2j}}{(2j+1)^9} \sum_{\substack{l_1,l_2,l_3 \\ l_5,l_7,l_9}} & (2l_1+1)(2l_2+1)(2l_3+1)(2l_5+1)(2l_7+1)(2l_9+1)\times \\ \times & \begin{vmatrix} l_1 & l_2 & l_3 \\ j & j & j \end{vmatrix} \begin{vmatrix} l_1 & l_2 & l_3 \\ j & j & j \end{vmatrix} \begin{vmatrix} l_2 & l_7 & l_9 \\ j & j & j \end{vmatrix} \begin{vmatrix} l_2 & l_7 & l_9 \\ j & j & j \end{vmatrix} \begin{vmatrix} l_5 & l_7 & l_9 \\ j & j & j \end{vmatrix} \begin{vmatrix} l_5 & l_7 & l_9 \\ j & j & j \end{vmatrix}. \end{aligned} \tag{1.6.10}$$

Using the orthogonality relation (1.4.14) on l_5, then l_7, we obtain

$$\begin{aligned} Z &= \frac{(-)^{2j}}{(2j+1)^{11}} \sum_{l_1,l_2,l_3,l_9} (2l_1+1)(2l_2+1)(2l_3+1)(2l_9+1)\Delta(l_9,j,j) \begin{vmatrix} l_1 & l_2 & l_3 \\ j & j & j \end{vmatrix} \begin{vmatrix} l_1 & l_2 & l_3 \\ j & j & j \end{vmatrix} \\ &= \frac{(-)^{2j}}{(2j+1)^9} \sum_{l_1,l_2,l_3} (2l_1+1)(2l_2+1)(2l_3+1) \begin{vmatrix} l_1 & l_2 & l_3 \\ j & j & j \end{vmatrix} \begin{vmatrix} l_1 & l_2 & l_3 \\ j & j & j \end{vmatrix}. \end{aligned} \tag{1.6.11}$$

This $6j$ sum was evaluated in an earlier section, in equation (1.3.43). We conclude that

$$Z(\mathcal{M}(\mathcal{G})) = N^{-6}. \tag{1.6.12}$$

which confirms that the partition function of this complete Belyi 3-complex matches the ribbon graph evaluation $N^{-E}\mathcal{R}(\mathcal{G}) = N^{F-E}$ for the graph in Figure 1.23a (up to a normalisation factor of N^E).

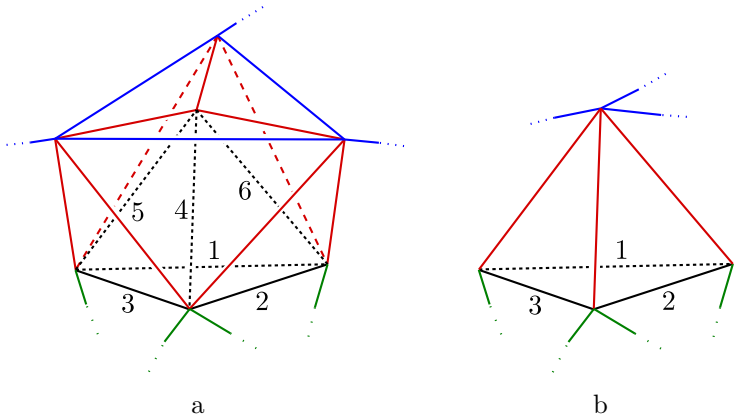

Figure 1.25: Two complete Belyi 3-complexes associated to graphs related by a '3-1' move.

1.6.2 Trivalent graph moves on complete Belyi 3-complexes

In this section we show that the Ponzano-Regge partition functions of complete Belyi 3-complexes associated to a pair of ribbon graphs related by a '3-1' move are related by a factor of N^2, and that the partition function of a pair of complete Belyi 3-complexes associated to graphs related by a '2-2' move are equal.

Consider a pair of graphs $\mathcal{G}_1$ and $\mathcal{G}_2$ which differ from each other by a '3-1' move, with $\mathcal{G}_1$ having two more vertices than $\mathcal{G}_2$. Let $\mathcal{M}_1$ be a complete Belyi 3-complex of the graph $\mathcal{G}_1$ with an inner Belyi 3-complex in its interior. Near to the part of the outer Belyi triangulation affected by the '3-1' move, the complete Belyi 3-complex takes the form shown in Figure 1.25. Let $\bar{Z}(l_1, l_2, l_3)$ refer to the partition function of the remainder of the complete Belyi 3-complex $\mathcal{M}_1$ that is not displayed in the figure. The partition function of the manifold $\mathcal{M}_1$ is then

$$Z(\mathcal{M}_1) = \frac{(-)^{2j}}{(2j+1)^3} \sum_{\substack{l_1,l_2,l_3 \\ l_4,l_5,l_6}} (2l_1+1)(2l_2+1)(2l_3+1)(2l_4+1)(2l_5+1)(2l_6+1)$$
$$\left| \begin{matrix} l_1 & l_5 & l_6 \\ j & j & j \end{matrix} \right| \left| \begin{matrix} l_2 & l_4 & l_6 \\ j & j & j \end{matrix} \right| \left| \begin{matrix} l_3 & l_4 & l_5 \\ j & j & j \end{matrix} \right| \left| \begin{matrix} l_1 & l_2 & l_3 \\ l_4 & l_5 & l_6 \end{matrix} \right| \bar{Z}(l_1, l_2, l_3). \quad (1.6.13)$$

Let $\mathcal{M}_2$ be a complex which is identical to $\mathcal{M}_1$ everywhere except at the tetrahedra shown in Figure 1.25a, which are replaced by the tetrahedron shown in Figure 1.25b.

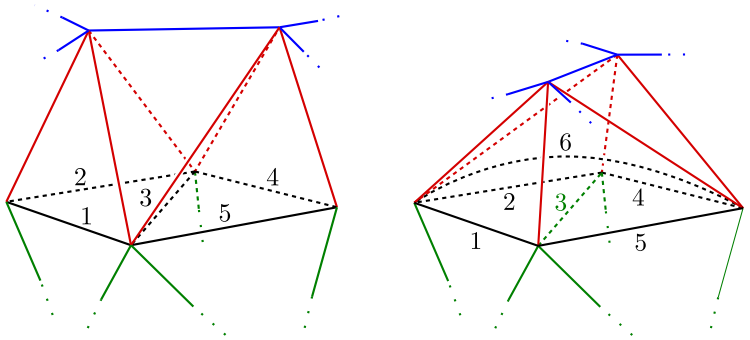

Figure 1.26: Two complete Belyi 3-complexes associated to graphs related by a '2-2' move.

This is a complete Belyi 3-complex of the graph $\mathcal{G}_2$, and has the partition function

$$Z(\mathcal{M}_2) = \sum_{l_1,l_2,l_3} (2l_1+1)(2l_2+1)(2l_3+1) \begin{vmatrix} l_1 & l_2 & l_3 \\ j & j & j \end{vmatrix} \bar{Z}(l_1,l_2,l_3). \qquad (1.6.14)$$

We can relate the partition functions of the manifolds by applying the Biedenharn-Eliot identity on the sum over l_6 in (1.6.13) and the orthogonality relation on the labels l_5 and l_4 to deduce that

$$\begin{aligned} Z(\mathcal{M}_1) &= \frac{(-)^{2j}}{(2j+1)^3} \sum_{\substack{l_1,l_2,l_3 \\ l_4,l_5}} \left[\prod_{p=1}^{5}(2l_p+1)\right] \begin{vmatrix} l_1 & l_2 & l_3 \\ j & j & j \end{vmatrix} \begin{vmatrix} l_3 & l_4 & l_5 \\ j & j & j \end{vmatrix} \begin{vmatrix} l_3 & l_4 & l_5 \\ j & j & j \end{vmatrix} \bar{Z}(l_1,l_2,l_3) \\ &= \frac{1}{(2j+1)^4} \sum_{l_1,l_2,l_3,l_4} (2l_1+1)(2l_2+1)(2l_3+1)(2l_4+1)\Delta(l_4,j,j) \begin{vmatrix} l_1 & l_2 & l_3 \\ j & j & j \end{vmatrix} \bar{Z}(l_1,l_2,l_3) \\ &= N^{-2} Z(\mathcal{M}_2). \end{aligned} \qquad (1.6.15)$$

The Ponzano-Regge partition function of the complete Belyi 3-complex $\mathcal{M}_1$ changes by a factor of N^{-2} when a '3-1' move is applied to the graph. Noting that any two triangulations of the same manifold with the same boundary data have the same Ponzano-Regge partition function, we see that any complete Belyi 3-complexes arising from graphs related by a '3-1' move are related by a factor of N^{-2}.

Next, we consider a pair of graphs $\mathcal{G}_1$ and $\mathcal{G}_2$ which are related by a '2-2' move. Let $\mathcal{M}_1$ be a complete Belyi 3-complex of the graph $\mathcal{G}_1$ with an inner Belyi 3-complex in its interior. The tetrahedra at the boundary of the complex corresponding to the affected vertices are of the form shown in Figure 1.26a. We can construct a complete

Belyi 3-complex $\mathcal{M}_2$ of the graph $\mathcal{G}_2$ by replacing these tetrahedra with the tetrahedra shown in Figure 1.26b. Let $\bar{Z}(l_1, l_2, l_3, l_4, l_5)$ be the partition function of the common remainder of the complex which is not shown in the figures. The Ponzano-Regge partition functions of the manifolds are

$$Z(\mathcal{M}_1) = \frac{(-)^{2j}}{(2j+1)} \sum_{\substack{l_1,l_2,l_3 \\ l_4,l_5}} \left(\prod_{p=1}^{5} (2l_p+1) \right) \left| \begin{array}{ccc} l_1 & l_2 & l_3 \\ j & j & j \end{array} \right| \left| \begin{array}{ccc} l_3 & l_4 & l_5 \\ j & j & j \end{array} \right| \bar{Z}(l_1, \ldots l_5),$$

$$Z(\mathcal{M}_2) = \frac{(-)^{2j}}{(2j+1)} \sum_{\substack{l_1,l_2,l_3 \\ l_4,l_5,l_6}} \left(\prod_{p=1}^{6} (2l_p+1) \right) \left| \begin{array}{ccc} l_2 & l_4 & l_6 \\ j & j & j \end{array} \right| \left| \begin{array}{ccc} l_1 & l_5 & l_6 \\ j & j & j \end{array} \right| \left| \begin{array}{ccc} l_1 & l_2 & l_3 \\ l_4 & l_5 & l_6 \end{array} \right| \bar{Z}(l_1, \ldots l_5).$$

These are related by the Biedenharn-Eliot identity on the sum over the label l_6, and so $Z(\mathcal{M}_1) = Z(\mathcal{M}_2)$. We deduce that any pair of complete Belyi 3-complexes arising from graphs related by a '2-2' move have the same Ponzano-Regge partition function.

1.6.3 Complete Belyi 3-complexes of general handlebodies

We can now show that the partition function of a complete Belyi 3-complex associated to any graph $\mathcal{G}$ matches its ribbon graph evaluation. We do this by induction on the genus. First, we show that the matching holds for all graphs of genus one. We then show that if the matching holds for all graphs of genus g, then it also holds for all graphs of genus $(g+1)$. This is enough to deduce, by induction, that the partition function of any complete Belyi 3-complex matches the ribbon graph evaluation of its graph.

First, consider a trivalent ribbon graph $\mathcal{G}$ of genus one. The Euler characteristic formula $V - E + F = 2 - 2g$ states that its ribbon graph evaluation is

$$\mathcal{R}(\mathcal{G}) = N^F = N^{E-V}. \tag{1.6.16}$$

As any two triangulations of a surface can be related by a series of Alexander moves, we know that any two ribbon graphs of the same genus can be related by a series of '3-1', '2-2' and '1-3' graph moves [62]. In particular, there exists a sequence of moves which relates the V-vertex graph $\mathcal{G}$ to the two-vertex genus one graph with the ribbon graph evaluation

$$\mathcal{R}\left(\right) = N. \tag{1.6.17}$$

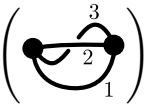

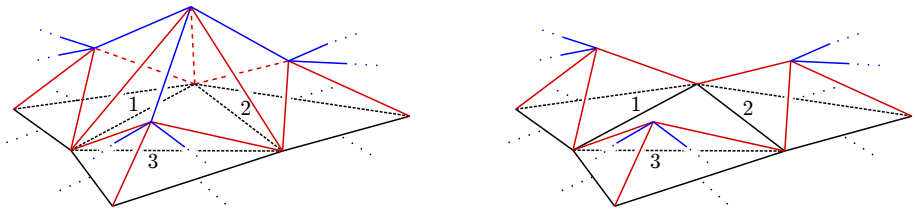

a b

Figure 1.27: The complex near the contractible triangle, and the complex after the removal of the four tetrahedra.

Consider this sequence of Alexander moves in reverse. Let $\{\mathcal{G}_i\}$ be a sequence of graphs with consecutive graphs related by a '3-1', '2-2', or '1-3' move, with $\mathcal{G}_0$ being the two-vertex graph of genus one, and $\mathcal{G}_n = \mathcal{G}$. We can choose a complete Belyi 3-complex $\mathcal{M}_i$ associated to each graph $\mathcal{G}_i$. The relations on complete Belyi 3-complexes derived in the previous section state that complete Belyi 3-complexes with graphs related by trivalent graph moves satisfy

$$Z\left(\mathcal{M}\left(\begin{array}{c}\includegraphics[height=1.2cm]{}\end{array}\right)\right) = N^{-2} Z\left(\mathcal{M}\left(\begin{array}{c}\includegraphics[height=1.2cm]{}\end{array}\right)\right), \tag{1.6.18}$$

$$Z\left(\mathcal{M}\left(\begin{array}{c}\includegraphics[height=1.2cm]{}\end{array}\right)\right) = Z\left(\mathcal{M}\left(\begin{array}{c}\includegraphics[height=1.2cm]{}\end{array}\right)\right), \tag{1.6.19}$$

from which we can see that, if V_i is the number of vertices of the graph $\mathcal{G}_i$, then the partition functions satisfy the relation

$$Z(\mathcal{M}_i) = N^{V_{i-1}-V_i} Z(\mathcal{M}_{i-1}). \tag{1.6.20}$$

This extends to a relation between the partition functions of the complete Belyi 3-complex associated to the graph $\mathcal{G}$ and the complete Belyi 3-complex discussed earlier from Figure 1.22b. We see that

$$Z(\mathcal{M}_n) = N^{V_0-V_n} Z(\mathcal{M}_0) \tag{1.6.21}$$

$$= N^{-V} = N^{-E}\mathcal{R}(\mathcal{G}). \tag{1.6.22}$$

As $\mathcal{G}$ was an arbitrary graph of genus one, this proves that equation (1.6.1) holds for all graphs of genus one.

We now know that ribbon graph evaluations match Ponzano-Regge partition functions for genus one graphs, so we assume, as an inductive hypothesis, that this is also true for all graphs of some genus g: that is, if $\mathcal{M}(\mathcal{G})$ is any complete Belyi 3-complex of a ribbon graph $\mathcal{G}$ of genus g with V vertices, then

$$Z(\mathcal{M}(\mathcal{G})) = N^{2-2g-V}. \tag{1.6.23}$$

We wish to show that this relation holds for some graph of genus $(g+1)$. Consider a V-vertex graph $\mathcal{G}$ of genus g with the property that one of its dual triangles is contractible: that is, the three vertices and three edges bounding the dual triangle are distinct. Let $\mathcal{M}(\mathcal{G})$ be a complete Belyi 3-complex of this graph with an inner Belyi triangulation in its interior. (It is always possible to construct such a triangulation of a handlebody with Belyi triangulations in the interior and on the boundary.) Near the contractible triangle of the inner Belyi triangulation, the complex takes the form shown in Figure 1.27a. By removing the tetrahedron with j labels glued to the contractible triangle with the labels (l_1, l_2, l_3), and also removing the three adjoining tetrahedra with blue edges, we create a new complex $\hat{\mathcal{M}}$, which takes the form shown in Figure 1.27b near the contractible triangle. This manifold is not a complete Belyi 3-complex or an inner Belyi 3-complex, as it does not possess either of the complete Belyi triangulations on its boundary. Writing $\hat{Z}(l_1, l_2, l_3)$ to denote the partition function of the complex $\hat{\mathcal{M}}$, then the partition function of the manifold $\mathcal{M}$ is, by the inductive hypothesis,

$$\begin{aligned} Z(\mathcal{M}(\mathcal{G})) &= \frac{(-)^{2j}}{(2j+1)^3} \sum_{l_1,l_2,l_3} \begin{vmatrix} l_1 & l_2 & l_3 \\ j & j & j \end{vmatrix} \hat{Z}(l_1, l_2, l_3) \\ &= N^{2-2g-V}. \end{aligned} \tag{1.6.24}$$

The manifold $\hat{\mathcal{M}}$ is a triangulation of a handlebody of genus g. We can create a triangulation of a handlebody of genus $(g+1)$ by gluing on a complex homeomorphic to the solid torus. Consider the triangulation of the solid torus given in the latter part of Section 1.6.1, shown in Figure 1.24a. The triangle labelled (l_1, l_2, l_3) in the interior is contractible, and borders a tetrahedron with three red edges. This tetrahedron meets three other tetrahedra with blue edges at a vertex. We remove this tetrahedron and split the vertex into three distinct boundary vertices to generate the labelled solid torus triangulation given in Figure 1.28a. The boundary of this triangulation is given in Figure 1.28b, with the interior Belyi triangulation projected onto the surface in dashed lines.

We can glue this solid torus triangulation onto the handlebody triangulation by

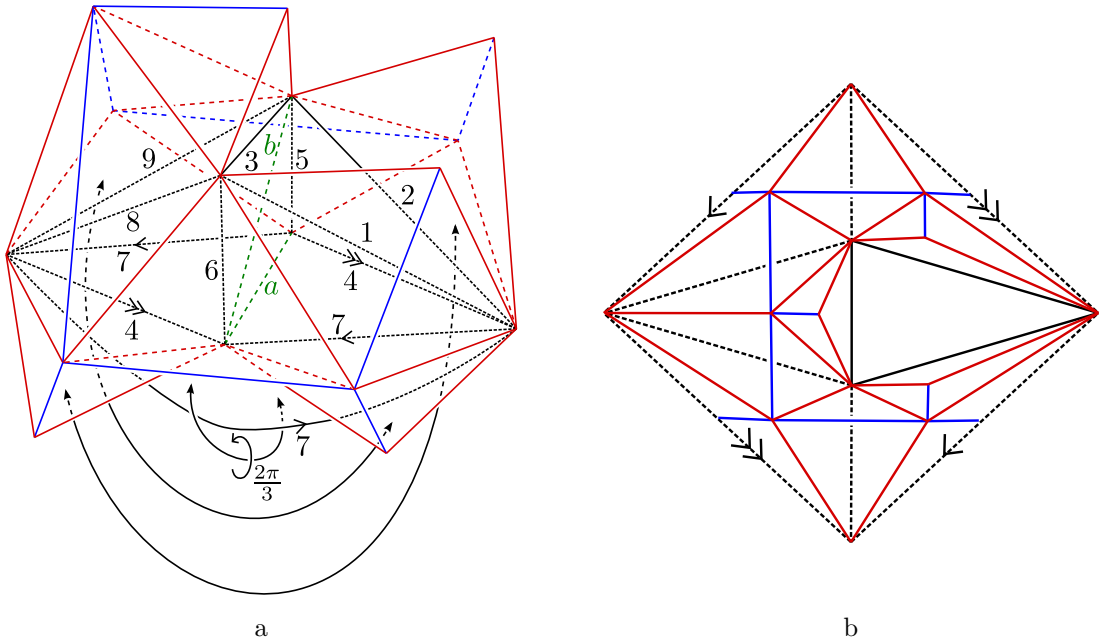

Figure 1.28: A triangulation of the solid torus and its boundary triangulation with the inner Belyi triangulation.

identifying the four pairs of triangles on the boundary of each manifold which bound the labels l_1,l_2, and l_3. These black edges are moved into the interior of the glued manifold. The blue edges of the glued complex trace out an embedded graph $\mathcal{G}'$ on the surface of the glued manifold $\mathcal{M}'$, which has genus $(g+1)$ and $V' = V+4$ vertices. The boundary of the glued triangulation is an outer Belyi triangulation, so this complex is a complete Belyi 3-complex of genus $(g+1)$. Using the partition function of the solid torus (1.6.8) and $\hat{\mathcal{M}}$, then the glued Belyi 3-complex has the partition function

$$Z(\mathcal{M}'(\mathcal{G}')) = \frac{(-)^{2j}}{(2j+1)^9} \sum_{a,b,l_1,\ldots} (-)^{2a+2b}(2a+1)(2b+1)\left[\prod_{p=1,\ldots,9}(2l_p+1)\right] \times$$
$$\times \begin{vmatrix} l_4 & l_7 & a \\ l_4 & l_7 & l_7 \end{vmatrix} \begin{vmatrix} l_4 & l_7 & a \\ b & l_5 & l_2 \end{vmatrix} \begin{vmatrix} l_4 & l_7 & a \\ l_5 & b & l_9 \end{vmatrix} \begin{vmatrix} l_2 & l_7 & b \\ l_6 & l_3 & l_1 \end{vmatrix} \begin{vmatrix} l_4 & l_9 & b \\ l_3 & l_6 & l_8 \end{vmatrix} \times$$
$$\times \begin{vmatrix} l_2 & l_4 & l_5 \\ j & j & j \end{vmatrix} \begin{vmatrix} l_5 & l_7 & l_9 \\ j & j & j \end{vmatrix} \begin{vmatrix} l_3 & l_8 & l_9 \\ j & j & j \end{vmatrix} \begin{vmatrix} l_4 & l_6 & l_8 \\ j & j & j \end{vmatrix} \begin{vmatrix} l_1 & l_6 & l_7 \\ j & j & j \end{vmatrix} \hat{Z}(l_1, l_2, l_3)$$

$$= \frac{(-)^{2j}}{(2j+1)^9} \sum_{l_1,l_2,l_3} (2l_1+1)(2l_2+1)(2l_3+1) \begin{vmatrix} l_1 & l_2 & l_3 \\ j & j & j \end{vmatrix} \hat{Z}(l_1,l_2,l_3)$$
$$= N^{-6} N^{2-2g-V} = N^{2-2(g+1)-(V+4)}. \quad (1.6.25)$$

This evaluation matches the formula (1.6.23) for a genus $(g+1)$ graph with $V' = V+4$ vertices, as required.

We have shown that there is a genus $(g+1)$ graph with a complete Belyi 3-complex matching the ribbon graph evaluation. We can relate the partition functions of all genus $(g+1)$ graphs by using similar arguments as those used in the genus one case. If $\mathcal{G}''$ is another graph of genus $(g+1)$, then there exists a sequence of trivalent graph moves relating the graphs $\mathcal{G}'$ and $\mathcal{G}''$ with an associated sequence of complete Belyi 3-complexes. Say that $\mathcal{G}''$ has V'' vertices and an associated complete Belyi 3-complex $\mathcal{M}''$. The partition functions of the complexes are related by (1.6.21),

$$Z(\mathcal{M}'') = N^{V'-V''} Z(\mathcal{M}')$$
$$= N^{2-2(g+1)-V''}. \quad (1.6.26)$$

As $\mathcal{G}''$ was an arbitrary genus $(g+1)$ graph, this tells us that the matching holds for all genus $(g+1)$ graphs. This is enough to prove the inductive hypothesis, and so we deduce that the matching of ribbon graph evaluations and Ponzano-Regge partition functions of complete Belyi 3-complexes holds for all ribbon graphs.

1.7 Discussion

We have linked the Gaussian Hermitian matrix model with the fuzzy sphere matrix algebra, and interpreted this framework as a spacetime field theory on the S^2 target space of the Belyi string. The correlators of the matrix model can be expanded into a series of trivalent ribbon graphs, each of which corresponds to a weighted sum over the representations of $su(2)$, in a manner resembling the evaluations of spin networks. The Ponzano-Regge model reproduces these spin label sums for a class of triangulated 3-manifolds with a particular set of boundary data, which we called complete Belyi 3-complexes. This suggests an interpretation of the Ponzano-Regge model as a 'lift' to three dimensions of the two-dimensional Belyi string theory.

The Ponzano-Regge partition functions generated by planar graphs take a different form to those generated for non-planar graphs. For planar graphs, it is possible to

choose Belyi 3-complexes of graphs such that partition functions take the form

$$Z(\mathcal{M}(\mathcal{G})) = \left(\frac{(-)^{2j}}{2j+1}\right)^{E} \sum_{l_p} S(\mathcal{G}, \{l_p\}) \prod_{\substack{\text{graph} \\ \text{edges}}} (2l_p{+}1) \prod_{\substack{\text{graph} \\ \text{vertices}}} \begin{vmatrix} l_p & l_q & l_r \\ j & j & j \end{vmatrix} = N^{-E} \mathcal{R}(\mathcal{G}). \tag{1.7.1}$$

The spin network evaluation $S(\mathcal{G}, \{l_p\})$ of a graph corresponds to the partition function $Z_{\text{in}}(\mathcal{G}, \{l_p\})$ of the inner Belyi 3-complex, contained within the complete Belyi 3-complex, with the dual graph to $\mathcal{G}$ embedded on its boundary. The matching of the partition function and ribbon graph evaluations at the level of the individual factors in the state sum weight provides a strong link between the two models in the planar case.

While we have successfully matched the values of the partition functions and the ribbon graphs in all cases, this factor-by-factor matching does not extend to the non-planar case. This is a direct consequence of the fact that Moussouris' algorithm, which identified $Z_{\text{in}}(\mathcal{G}, \{l_p\})$ and $S(\mathcal{G}, \{l_p\})$ for planar graphs, does not generalise to non-planar graphs. To solve the discrepancy between the weight factors in the two spin label sums would be tantamount to extending Moussouris' algorithm to non-planar graphs. The algorithm of Section 1.3.2 gives an expression for any spin network in terms of $6j$s and representation dimensions, with phase factors introduced in the reduction of non-planar graphs. It is possible that there exists a class of triangulated 3-manifolds or 3-conifolds, which are neither handlebodies nor simply cones over a genus g surface, whose Ponzano-Regge partition functions reproduce the spin network evaluations of non-planar graphs. This is an open problem in our scenario and in the spin network literature [64]. It seems plausible that the difficulties of the non-planar case are related to the fact that the topological A-string/matrix model matching is only known to hold at the planar level [4, 5].

The Ponzano-Regge partition functions of complete Belyi 3-complexes and the ribbon graph evaluations differ by a factor of N^E. We interpreted this discrepancy as a relic of our choices of normalisation. Indeed, if we take the generating function Z_{HMM} of the trivalent ribbon graph correlators (1.2.38) with the coupling rescaled by $\lambda \mapsto N^{-2}\lambda$, then the Ponzano-Regge partition functions Z_{PR} appear in the series

expansion with matching normalisations:

$$\begin{aligned} Z_{\mathrm{HMM}}(\lambda, N) &= \int Da\; e^{-\frac{1}{2}\mathrm{tr}X^2+\lambda N^{-3/2}\mathrm{tr}X^3} = \sum_{k\geq 0} \frac{\lambda^{2k}}{(2k)!} N^{-3k} \langle (\mathrm{tr}X^3)^{2k} \rangle \\ &= \sum_{k\geq 0} \frac{\lambda^{2k}}{(2k)!} \sum_{\tau\in[2^{3k}]} Z_{\mathrm{PR}}(\mathcal{M}(\mathcal{G}(\sigma_k, \tau))). \end{aligned} \tag{1.7.2}$$

In this expression, each pair of S_{6k} permutations (σ_k, τ), with $\sigma_k \in [3^{2k}]$, specifies a trivalent ribbon graph $\mathcal{G}$ with $V = 2k$ vertices and $E = 3k$ edges, and $\mathcal{M}$ is any choice of complete Belyi 3-complex of the graph $\mathcal{G}$. This matching of the matrix model with the Ponzano-Regge model holds at a graph-by-graph level. It is an open question as to whether there exists a matching of the matrix model correlators, or the generating functions of the correlators, to partition functions in higher-dimensional gravity.

The Belyi maps string theory discussed in this chapter was realised within a more conventional string theory in [4]. An interesting direction for future research would be to seek a realisation of the Ponzano-Regge state sums of complete Belyi 3-complexes within more conventional constructs in string theory. The Ponzano-Regge model is known to be equivalent to Chern-Simons theory with $ISO(3)$ gauge group [12, 13], and Chern-Simons terms are known to arise in the worldvolumes of membranes in M-theory [65]. It seems plausible to expect there to be an embedding of our triangulated 3-manifolds within membrane constructions, giving an M-theory interpretation of the Belyi string.

Chapter 2

Thresholds of factorisation in the AdS/CFT correspondence

The original AdS/CFT correspondence of Maldacena proposes that type IIB string theory on an $AdS_5 \times S^5$ background is dual to $\mathcal{N} = 4$ super Yang-Mills in four dimensions in the large N limit [14]. In the half-BPS sector, the three-point correlators of $\mathcal{N} = 4$ super Yang-Mills are not renormalised, and can be matched exactly to Kaluza-Klein graviton correlators in supergravity [17]. These correlators tend to zero in the large N limit when the graviton energies are small, which is a manifestation of *large N factorisation*.

If the graviton energies are chosen to grow at a large enough rate with respect to N, then the three-point correlator does not tend to zero and diverges in the large N limit. This divergence is due to the $1/N$ quantum corrections to the correlator becoming large. We interpret this breakdown of large N factorisation as a result of non-local effects emerging in the gravitational theory at high energy. While we cannot yet formulate an effective field theory on the gravity side which reproduces the breakdown of factorisation in the gauge theory correlators, we believe that studying the limits of factorisation in the gauge theory provides hints towards the nature of non-locality in quantum gravity.

The aim of this chapter is to provide a systematic study of the threshold energies at which large N factorisation fails to hold by careful analysis of the gauge theory correlators. The explicit finite N form of the CFT correlator allows us to investigate the regime of graviton energies at which the correlators become non-vanishing in the large N limit. We define the *factorisation threshold* to be the submanifold of the parameter space $\{J_1, J_2, N\}$ on which the position-independent free field CFT correlator $\langle \mathrm{tr} Z^{J_1} \mathrm{tr} Z^{J_2} \mathrm{tr} Z^{\dagger J_1 + J_2} \rangle$ evaluates to a constant c, chosen for convenience to be one in most formulae. At energies below and near the threshold, we associate single-traces to

single objects and multi-traces to multiple objects. However, a standard Fock space structure is not really appropriate at the threshold, as composite states made of a pair of gravitons have non-vanishing quantum correlations with states consisting of a single graviton, even as N is taken to infinity. Above the threshold, associating single traces to single objects of any sort probably does not make sense. Certainly, for J_i of order N, it is known that the gravitons are represented semiclassically by D3-branes wrapping a sphere [66], and cannot be represented as single traces [24]. The correct basis for single and giant gravitons is given by Schur polynomials, indexed by Young diagrams [25].

We focus on three types of correlator in particular: an extremal three-point correlator with one independent operator dimension J, an extremal three-point correlator with two independent operator dimensions J_1 and J_2, and a 'near-extremal' three-point correlator. We also consider some extensions concerning extremal correlators on non-trivial backgrounds and extremal correlators with a large number of operators. We find, quite generally, that the threshold occurs when the product of two of the dimensions is of order $N \log N$.

The outline of this chapter is as follows. In Section 2.1 we give an overview of our results, introducing the definition of the factorisation threshold and stating without detailed calculation the form of the threshold in the simplest case. The local gauge invariant operators are functions of a four-dimensional spacetime position and an energy J, which is equal to angular momentum because of the BPS condition. We explain an interesting aspect of our results, namely the similarity of the dependence of the threshold on separations in spacetime and on differences in energy. We elaborate on the departure from the usual Fock space structure associated with traces at large N and raise the question of a spacetime effective field theory derivation of the properties of the threshold. This is one of our motivations for performing detailed studies of the threshold.

In the subsequent sections, we present the details of the calculations of the thresholds. In Section 2.2 we review and introduce some notation on large N asymptotics for describing the thresholds precisely, and give a complete calculation of the extremal three-point correlator with one independent angular momentum J. We also discuss in this section some links between the form of the threshold equations with running gauge coupling equations and instanton expansions. In Section 2.3, we present a calculation of the three-point extremal correlator when the operator dimensions are not equal. In Section 2.4, we calculate a non-extremal three-point correlator, and discuss how it differs from the extremal cases.

We discuss in Section 2.5 some other tractable examples of extremal correlators that could shed more light on the general nature of factorisation thresholds. We consider the case of a correlator with k holomorphic insertions, and also the case of a three-point correlator on a non-trivial background dual to an LLM geometry [67]. We conclude by summarising what has been shown about factorisation within this chapter, and discussing some other examples of correlators that could tell us more about the general nature of factorisation thresholds in the future.

2.1 Factorisation thresholds and bulk interpretations

In this section we describe the factorisation threshold for the simplest case: the transition of two gravitons with the same angular momentum J going to a single graviton of angular momentum $2J$. This is followed by a discussion of the physics at the threshold in the bulk AdS space. This motivates further investigations of thresholds, which we outline, along with the qualitative results. The details of these investigations are presented in subsequent sections.

2.1.1 Thresholds of factorisation in the gauge theory

Our starting point is the three-point correlator of two holomorphic single trace operators and an antiholomorphic single trace operator,

$$\langle \mathrm{tr} Z^{J_1}(x_1) \mathrm{tr} Z^{J_2}(x_2) \mathrm{tr} Z^{\dagger J_1+J_2}(y) \rangle. \tag{2.1.1}$$

This correlator is not renormalised [17], and so a calculation in the free field limit will hold for all values of the coupling g^2_{YM}. The position-dependence of the correlator can be factored out by conformal symmetry:

$$\langle \mathrm{tr} Z^{J_1}(x_1) \mathrm{tr} Z^{J_2}(x_2) \mathrm{tr} Z^{\dagger J_1+J_2}(y) \rangle = \frac{\langle \mathrm{tr} Z^{J_1} \mathrm{tr} Z^{J_2} \mathrm{tr} Z^{\dagger J_1+J_2} \rangle}{|x_1-y|^{2J_2}|x_2-y|^{2J_2}}. \tag{2.1.2}$$

The factor in the numerator of this expression is position-independent and can be calculated using character expansions [27]. If we apply an inversion $y' = \frac{y}{|y|^2}$, and transform the anti-holomorphic operator to the primed frame, while taking $|x_1 - x_2| \to 0$, $y' \to 0$, then the position dependence vanishes, and we are left with the purely combinatoric factor which can be interpreted as an inner product of the double

trace state and the single trace state. This correlator is *extremal* as the sum of the holomorphic operator dimensions $(J_1 + J_2)$ is equal to the antiholomorphic operator dimension. In the following sections, we focus on the inner product

$$\langle \mathrm{tr} Z^{J_1} \mathrm{tr} Z^{J_2} \mathrm{tr} Z^{\dagger J_1 + J_2} \rangle. \tag{2.1.3}$$

A natural normalisation for these correlators is the *multiparticle normalisation*, in which each operator is divided by the square root of its two-point function,

$$\langle\langle \mathrm{tr} Z^{J_1} \mathrm{tr} Z^{J_2} \mathrm{tr} Z^{\dagger J_1 + J_2} \rangle\rangle := \frac{\langle \mathrm{tr} Z^{J_1} \mathrm{tr} Z^{J_2} \mathrm{tr} Z^{\dagger J_1 + J_2} \rangle}{\sqrt{\langle \mathrm{tr} Z^{J_1} \mathrm{tr} Z^{\dagger J_1} \rangle \langle \mathrm{tr} Z^{J_2} \mathrm{tr} Z^{\dagger J_2} \rangle \langle \mathrm{tr} Z^{J_1 + J_2} \mathrm{tr} Z^{\dagger J_1 + J_2} \rangle}}. \tag{2.1.4}$$

This normalisation is used in comparing supergravity and conformal field theory calculations of the three-point functions [17]. We have introduced the double-bracket notation $\langle\langle \cdot \rangle\rangle$ to refer to a multiparticle-normalised correlator. When the operator dimensions J_i are sufficiently small, then

$$\langle\langle \mathrm{tr} Z^{J_1} \mathrm{tr} Z^{J_2} \mathrm{tr} Z^{\dagger J_1 + J_2} \rangle\rangle \simeq \frac{\sqrt{J_1 J_2 (J_1 + J_2)}}{N} \tag{2.1.5}$$

in the large N limit [17, 68]. This clearly tends to zero at large N, and so the single trace and double trace operators are orthogonal at large N.

Large N orthogonality of the operators can still hold when J_1 and J_2 increase with N. By calculating the correlator explicitly at finite N, it can be shown that (2.1.5) is still valid when J_1 and J_2 are functions of N, provided that $J_1, J_2 \leq \sqrt{N}$ at large N. However, this formula is not valid when J_1 and J_2 grow large enough with N. For large enough J_i, the normalised correlator grows exponentially with N, and factorisation of the operators no longer holds. The aim of this chapter is to investigate and interpret the threshold partitioning these two distinct large N limits of the normalised correlator.

For simplicitly, we initially consider in Section 2.2 a correlator in which the holomorphic operator dimensions are equal. Setting $J_1 = J_2 = J$, we define

$$G_3(J, N) = \langle\langle \mathrm{tr} Z^J \mathrm{tr} Z^J \mathrm{tr} Z^{\dagger 2J} \rangle\rangle. \tag{2.1.6}$$

To gain some insight into the large N behaviour of this correlator when J depends on N, we can plug in a simple trial function $J(N)$ and find the asymptotic behaviour of the correlator when N is large. If we set $J = N^\alpha$, where α is a constant, then a finite

N calculation [68] shows that

$$\boxed{\begin{aligned} G_3(N^\alpha, N) &\to 0, \qquad 0 < \alpha \leq \frac{1}{2}, \\ G_3(N^\alpha, N) &\to \infty, \qquad \frac{1}{2} < \alpha < 1. \end{aligned}} \tag{2.1.7}$$

If J grows as a power of N larger than $\frac{1}{2}$, then the correlator will diverge and factorisation breaks down. However, a simple power-law scaling is not sufficient to deduce the exact growth of J that is required for the correlator to diverge. A more general N-dependence can be found, intermediate between the cases $\alpha = \frac{1}{2}$ and $\alpha > \frac{1}{2}$, for which the correlator tends to a constant value.

Our main approach to considering the threshold between factorisation and breakdown is to look for a solution to the equation

$$G_3(J, N) = 1. \tag{2.1.8}$$

We call this the *factorisation threshold equation*. It defines a curve $J(N)$ in the parameter space with axes labelled (J, N). For large enough N, this curve divides the parameter space into two regions: the factorisation region, where the correlator is less than one, and the breakdown region, where the correlator is greater than one. The *threshold* $J_t(N)$ is the exact solution of the equation $G_3(J_t(N), N) = 1$. A sketch of this threshold curve in (J, N) parameter space is shown in Figure 2.1.

The trial function approach shows that the threshold must scale with N at a faster rate than $\sqrt{N}$, but at a slower rate than $N^{\frac{1}{2}+\delta}$ for any constant δ. Provided that J lies in the range $N^{\frac{1}{2}} < J < N^{\frac{1}{2}+\delta}$, we show in Section 2.2.2 that the correlator G_3 has the asymptotic behaviour

$$G_3(J, N) \simeq \sqrt{\frac{J}{2N}} \exp\left(\frac{J^2}{2N}\right). \tag{2.1.9}$$

Using this asymptotic form of the correlator, we can invert the equation $G_3(J_t(N), N) = 1$ to derive an asymptotic solution of $J_t(N)$, the threshold of factorisation. In Section 2.2.3 we show that the large N solution is

$$J_t(N) = \sqrt{\frac{1}{2} N \log N}\left[1 - \frac{\log\log N}{2\log N} + \frac{\log 8}{2\log N} + \mathcal{O}\left(\frac{\log\log N}{\log N}\right)^2\right]. \tag{2.1.10}$$

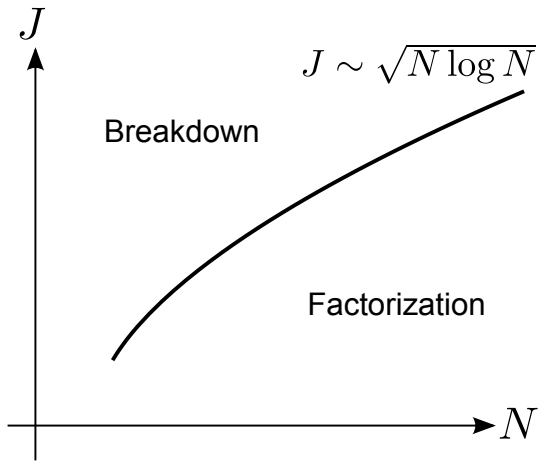

Figure 2.1: A sketch of the threshold curve $J_t(N)$ in (J, N) parameter space for large N. Away from the origin, the curve partitions the parameter space into the factorisation region $G_3(J_t(N), N) < 1$, and the breakdown region $G_3(J_t(N), N) > 1$.

Neglecting the constant term, the leading-order behaviour is simply

$$J_t^2 \sim N \log N. \tag{2.1.11}$$

This is the solution that divides (J, N)-space into the regions where factorisation holds and breaks down.

2.1.2 The breakdown of bulk effective field theory at the threshold

The correlator $\langle\langle \mathrm{tr}Z^J \mathrm{tr}Z^J (\mathrm{tr}Z^\dagger)^{2J}\rangle\rangle$ is not renormalised [17]. It is an inner product of the double trace state with the single trace state, normalised by the appropriate factors given above. A sketch of these two states in energy space is given in Figure 2.2. At finite N, this inner product is non-trivial and mixes trace structures according to a non-trivial function of J and N. The matching supergravity correlator can be computed for J of order one in the large N limit. The supergravity computation can be understood as relying on a Fock space structure for gravitons, where at leading large N single gravitons are orthogonal to multi-gravitons, hence single traces are orthogonal to multi-traces. This Fock space structure is used to set up perturbation theory where there are $\frac{1}{N}$ interactions. The N-corrected inner product coming from CFT is then recovered with the help of the supergravity interactions.

At the factorisation threshold, the leading large N overlap is not vanishing; it is

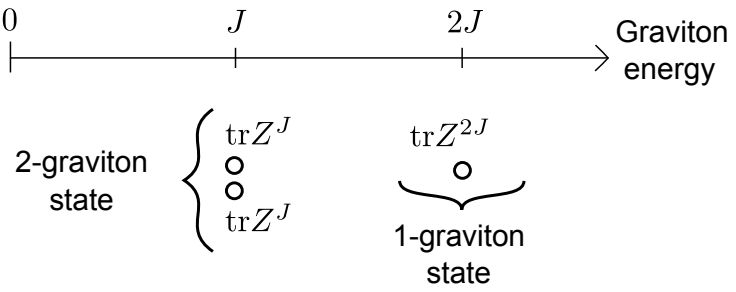

Figure 2.2: The single and multi-graviton states within energy space.

order one. At this regime, a Fock space structure with single gravitons corresponding to single traces, being orthogonal to multi-gravitons corresponding to multi-traces, cannot be the right spacetime structure for computing the leading large N behaviour of the correlator. There should be a modification of the spacetime effective field theory which reproduces the correlators at threshold. This modification is unknown, but hints about its nature can be obtained by studying the detailed properties of the threshold.

Once the angular momenta J are sufficiently large that we are well past the threshold and into the region of broken factorisation, we eventually reach the region of $J \sim N$, where the best way to think about the physics is in terms of giant gravitons [24]. The basis of Schur polynomial operators, which are non-trivial linear combinations of multi-traces, becomes the best way to match bulk states and CFT states [25]. The region where $J \sim N$ was indeed earlier identified as an interesting region in connection with the fact that finite N relations allow single traces to be expressed in terms of multi-traces via Cayley-Hamilton relations [69]. This lead to a stringy exclusion principle, suggestive of some form of algebraic deformation of the spacetime algebra of functions [70].

Here we focus instead on the threshold near $J \sim \sqrt{N \log N}$, where the large N correlator is not infinite, but fixed at $G_3 = 1$. We could even take $G_3 = c$ for a small c, say 10^{-5}, but not going to zero as N approaches infinity. This suggests that a spacetime picture in terms of elementary objects matching the number of traces, such as gravitons stretched into BMN strings, is the right framework for understanding the precise nature of the threshold and the form of the interactions in this threshold region.

With these motivations spelt out, we turn to some qualitative outcomes of our detailed studies of how the thresholds are approached when various parameters in the graviton system are tuned. An intriguing result we find is that, as we explain further in the next subsection, in some of its effects on the factorisation threshold, separation

in J-space is similar to separation in coordinate space. One possible interpretation of this is that the spatial extents of the bulk gravitons are related to their energies, in the spirit of the UV-IR relation [71, 72]. We can make such an argument by considering the gravitons in the context of the LLM picture [67]. A trace operator is a superposition of Schur polynomials corresponding to hook representations, interpolating between a single row and a single column Young diagram. This is a superposition of states in the free fermion picture involving excitation of a fermion from some depth k below the top of the Fermi sea to a level $(J-k)$ above the Fermi sea, with k varying from 0 to $(J-1)$. Since the fermion energy levels translate to radial positions in the LLM plane, with large radial positions of the excited fermion being closer to the boundary, this is in line with the UV-IR interpretation. However, consideration of normalisable modes in the global coordinates shows that gravitons at higher energy J become more localised near the centre [73]. This suggests that the interpretation of half-BPS correlators in terms of gravitons requires care regarding the distinction between normalisable and non-normalisable modes of the same field, and between the Lorentzian versus Euclidean picture of AdS. It is therefore prudent to postpone a detailed spacetime interpretation of the thresholds at this stage. Nethertheless, it is clear that this breakdown of the standard Fock space structure of effective spacetime field theory is an important new window where the gauge theory can provide valuable information towards the spacetime understanding.

2.1.3 Refined investigations of the factorisation thresholds

In Section 2.3 we investigate the more general extremal normalised three-point correlator

$$G_3(J_1, J_2, N) = \langle\langle \mathrm{tr} Z^{J_1} \mathrm{tr} Z^{J_2} \mathrm{tr} Z^{\dagger J_1+J_2} \rangle\rangle \tag{2.1.12}$$

where $J_1 \neq J_2$. We define the threshold to be the surface in the three-dimensional parameter space (J_1, J_2, N) that satisfies

$$G_3(J_1, J_2, N) = 1. \tag{2.1.13}$$

Making the assumption that both J_1 and J_2 grow at least as large as a positive power of N, then we find in Section 2.3 that the correlator decays to zero if the product of the angular momenta $J_1 J_2$ is less than N at large N, and grows exponentially if $J_1 J_2$ grows faster than $N^{1+\delta}$ with N, where δ is any positive constant. If the angular momenta

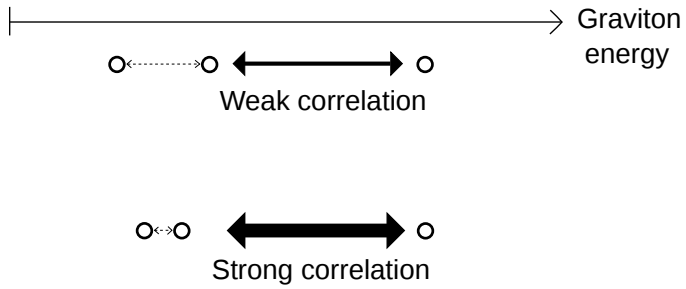

Figure 2.3: Two systems of gravitons with different energy differences but the same total energy. Graviton states become strongly correlated when the separation of the graviton energies decreases.

are constrained to lie in the range $N < J_1 J_2 < N^{1+\delta}$, then an asymptotic form of the correlator can be found. We find that at large N in this regime, the threshold lies at

$$J_1 J_2 \sim N \log N, \tag{2.1.14}$$

where we have dropped a constant multiplicative factor.

In the bulk picture, single trace operators with different dimensions correspond to gravitons at different energies. The combined energy of the two gravitons with energies J_1 and J_2 is equal to the energy of the other graviton $(J_1 + J_2)$. If we fix N and the energy $(J_1 + J_2)$ of the more energetic graviton, but vary the *difference* in the energies of the less energetic gravitons $\Delta J = |J_1 - J_2|$, then we find that we can move within parameter space *from the factorisation region to the threshold by decreasing the difference in energies of the two gravitons*. This is illustrated in Figure 2.3.

Another related set-up is a strongly-correlated system of gravitons at the threshold in which N and the value of the correlator $G_3(J_1, J_2, N) = 1$ are fixed but the separation of the graviton energies is varied. Once N is fixed and we are constrained to the threshold surface, there is only one available free parameter in the system, which we take to be the separation of the graviton energies $|J_1 - J_2|$. It can be shown that *increasing the separation in energies* $|J_1 - J_2|$ *of the two gravitons at the threshold corresponds to an increase in the energy* $(J_1 + J_2)$ *of the single graviton state.* This system is shown in Figure 2.4.

We extend the investigation of factorisation thresholds to the case of non-extremal correlators. In particular we study in detail the multiparticle-normalised correlator

$$\langle\langle \mathrm{Str}(Z^{J_1} Y)\mathrm{Str}(Z^{J_2} Y^\dagger)\mathrm{tr}(Z^{\dagger J_1 + J_2})\rangle\rangle \tag{2.1.15}$$

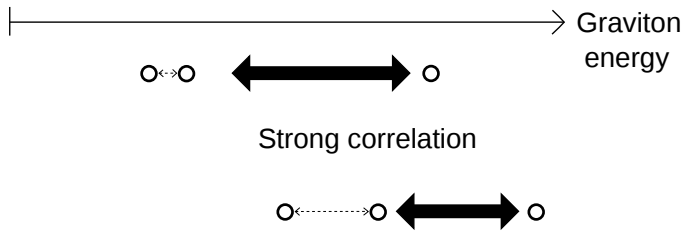

Figure 2.4: Two systems of gravitons at the threshold with different energy separations. Graviton states become strongly correlated at lower energies (further from the boundary) when the separation of the graviton energies is smaller.

and find a sensible extension of the discussion of factorisation thresholds from the extremal case. In the discussion of extremal correlators above, we did not pay much attention to the spatial dependences of correlators. There is a simple reason for this. In the extremal case, we can set the two holomorphic operators at one point x_1 and the anti-holomorphic operator at another point x_2. This has the standard spatial dependence $|x_1 - x_2|^{-2(J_1+J_2)}$. The spatial dependence can be removed by taking the anti-holomorphic operator to infinity, changing frame by the inversion $y = \frac{x_2}{|x_2|^2}$. In this limit the correlator is computing an inner product of states and all position dependences vanish after we take into account the conformal transformation of the anti-holomorphic operator. In the above non-extremal case we can set the first operator at x_1, the second at $x_1 + \epsilon$ and take the third operator to infinity by applying an inversion. The only position dependence left is ϵ^{-2}, so the above correlator is a dimensionful quantity, and it does not make sense to ask when it is equal to one in the large N limit.

We can introduce a dimensionful energy cutoff Λ in the CFT. This dimensional cutoff will not change the CFT calculation if we take $\epsilon\Lambda \gg 1$. The correct quantity to use to define the threshold is then Λ^{-2} times the non-extremal correlator above. This will be dimensionless, will contain the dimensionless parameter $\epsilon\Lambda \equiv \mathcal{R}$ and can be compared to one to define a factorisation threshold. In the region of J_i of order one and $\mathcal{R} \sim 1$ there is factorisation, but appropriate growth of J_i with N can cause breakdown of factorisation, with the details of the threshold depending on the dimensionless $\mathcal{R}$. We find that *decreasing $\epsilon\Lambda$, within the regimes where the correlator calcuations are valid, can cause the transition from factorisation to breakdown.* This is in line with the discussion in [74], where short distances were argued to explore large energies which have to be low enough in relation to N for factorisation to hold. Another interesting aspect of this nearly-extremal correlator is that when $\mathcal{R} = \epsilon\Lambda$ is large and fixed, or only varies with N as a power or less, then the threshold is of the

same form as the extremal correlator; we find the threshold lies at $J_1 J_2 \sim N \log N$.

Later in this chapter, we consider the transition from multiple holomorphic traces to a single anti-holomorphic trace, or equivalently multiple gravitons going to a single graviton. If we have k starting gravitons, with k order one, we find that the threshold depends on the *largest pairwise product* $J_i J_j$, and occurs at $J_i J_j \simeq k^{-1} N \log N$. The threshold of factorisation *decreases* as the number of gravitons in the multi-graviton state *increases*.

Another generalisation of the threshold investigation involves considering three-point extremal correlators corresponding to graviton scatterings on an LLM background given by M maximal giant gravitons, as in [75]. When M is of the same order as N, then the factorisation threshold is $J_1 J_2 \sim (M+N)\log(M+N)$. If M is chosen to have a fixed linear dependence on N, then the leading order behaviour of the threshold is again $J_1 J_2 \sim N \log N$, up to a constant factor.

We conclude that another striking property of the thresholds is the universality of the leading large N behaviour of the form $J_i J_j \simeq N \log N$.

2.2 The extremal three-point correlator with $J_1 = J_2$

In this section we present a detailed calculation of the asymptotic form of the three-point correlator

$$G_3(J,N) = \langle\langle \mathrm{tr} Z^J \mathrm{tr} Z^J \mathrm{tr} Z^{\dagger 2J} \rangle\rangle \tag{2.2.1}$$

in the relevant region $N^{\frac{1}{2}} < J < N^{\frac{1}{2}+\delta}$, where δ is any small positive constant. We then asymptotically solve the threshold equation

$$G_3(J_t(N), N) = 1 \tag{2.2.2}$$

in the large N limit, deducing that at leading order the threshold behaves as

$$J_t \simeq \sqrt{\frac{N}{2} \log N}. \tag{2.2.3}$$

Further, we discuss some links between the form of the threshold solution and running couplings in QCD. Finally, we find explicitly the all-orders asymptotic expansion of the threshold, and attempt to extend this result past perturbation theory by deriving

a transseries expansion.

2.2.1 Review of asymptotics and series

We start by briefly reviewing and clarifying some definitions, and introducing some new notation. Throughout this chapter, we will be using precise definitions of the asymptotic symbols '$\sim$' and '$\simeq$', the 'little o' order symbol o, and asymptotic series. We will also be using a precise definition of the 'big O' order symbol $\mathcal{O}$ that differs slightly from that used in the literature, but which is stronger than the commonly-used definition.

For two N-dependent functions $f(N)$ and $g(N)$, then we say that $f \simeq g$ at large N if

$$\lim_{N\to\infty} \frac{f(N)}{g(N)} = 1. \tag{2.2.4}$$

Note that with this definition the ratio of these two functions must tend to one, and not to any other constant. We use the notation $f = o(g)$ if f is a function that satisfies

$$\lim_{N\to\infty} \frac{f(N)}{g(N)} = 0, \tag{2.2.5}$$

i.e. if f is much smaller than g at large N. From these definitions, the following two statements are equivalent:

$$\begin{aligned} f(N) &\simeq g(N) \\ f(N) &= g(N)(1 + o(1)). \end{aligned} \tag{2.2.6}$$

We shall also use the notation $f \ll g$ if $f = o(g)$, and similarly $f \gg g$ if $g = o(f)$. An *asymptotic series* at large N is formally defined by a set of functions $\{\phi_k(N)\}$ and constant coefficients $\{a_k\}$ with the property that

$$\phi_{k+1} = o(\phi_k) \tag{2.2.7}$$

for any $k \geq 0$. We say that

$$f(N) \simeq \sum_{k=0}^{\infty} a_k \phi_k \tag{2.2.8}$$

if, for any $n \geq 0$, we have

$$f - \sum_{k=0}^{n} a_k \phi_k = o(\phi_n). \tag{2.2.9}$$

This definition of an asymptotic series does not allow for terms which are subleading to all the ϕ_k. Later, we shall also employ an extended version of an asymptotic series called a *transseries*. This type of series contains extra terms that tend to zero faster than all terms in a classical asymptotic series, but can still be assigned meaning when considered as a formal sum. Transseries are commonly used in describing instanton corrections to series expansions generated in QFTs, in which the instanton-dependent terms are exponentially suppressed in the coupling constant. We discuss this more in Section 2.2.5.

In this thesis we write $f \sim g$ if there exists some positive constant C such that

$$\lim_{N\to\infty} \frac{|f(N)|}{|g(N)|} = C. \tag{2.2.10}$$

This notation is commonly used in the physics literature, but not often in the mathematical literature; in the latter, the constant C in this definition is required to be one. Equivalently, we write $f = \mathcal{O}(g)$ if $f \sim g$. This is a departure from the conventional $\mathcal{O}$-notation, which only requires the ratio f/g to be bounded from above at large N. This modified definition is a stronger condition, as it not only implies that f/g is bounded from above, but is also bounded from below too. This is useful for keeping track of the errors and assumptions made at each step within our calculations.

'Big O' notation is used for expressing the errors of an N-dependent function, or corrections to an asymptotic series, or for giving a coarse expression of the leading-order behaviour of a function. It is useful in the following for representing functions whose explicit forms are unknown or irrelevant, but whose leading-order behaviours at large N are important. Generally, when an upper bound on the leading-order behaviour of a correction is known but a lower bound is not, then we will use the o (little o) symbol. In general, we shall write equations as equalities when the corrections or errors are present, and use '$\simeq$' for equations when the error terms have been dropped.

2.2.2 Asymptotics of the three-point correlator

To solve the threshold equation (2.2.2), we need to find an asymptotic form of the normalised correlator (2.2.1) at large N and large J, with small J/N. The form of this

expression will change depending on how quickly J grows with N, so it is necessary to carefully specify at each stage what possible behaviour J can take. We will find that the breakdown threshold is located at J just larger than $\mathcal{O}(\sqrt{N})$, and so we will look for a large N asymptotic form of the correlator $G_3(J,N)$ that is valid in this region. It suffices to impose $J \ll N^{2/3}$ to describe the asymptotic form of the correlator around the threshold.

The position-independent two-particle and three-particle correlators are known precisely for finite N [27]. We recall that the two-point function at zero coupling is

$$\langle \mathrm{tr} Z^J \mathrm{tr} Z^{\dagger J} \rangle = J! \left[\binom{N+J}{J+1} - \binom{N}{J+1} \right], \tag{2.2.11}$$

and the three-point function (for general operator dimensions J_1 and J_2) is

$$\begin{aligned} \langle \mathrm{tr} Z^{J_1} \mathrm{tr} Z^{J_2} \mathrm{tr} Z^{\dagger J_1+J_2} \rangle = (J_1+J_2)! \Bigg[& \binom{N+J_1+J_2}{J_1+J_2+1} - \binom{N+J_1}{J_1+J_2+1} \\ & - \binom{N+J_2}{J_1+J_2+1} + \binom{N}{J_1+J_2+1} \Bigg], \end{aligned} \tag{2.2.12}$$

All the terms in the finite N correlator expressions are of the form

$$J! \binom{N+\Lambda}{J+1} = \frac{(N+\Lambda-J)}{(J+1)} \frac{(N+\Lambda)!}{(N+\Lambda-J)!}, \tag{2.2.13}$$

where Λ is either 0 or J for the terms in the two-point function. Taking N and J to be large, but keeping J/N small, we apply Stirling's approximation

$$n! = e^{-n} n^{n+\frac{1}{2}} \sqrt{2\pi} \left(1 + \mathcal{O}\left(\frac{1}{n}\right) \right) \tag{2.2.14}$$

to find that

$$\begin{aligned} J! \binom{N+\Lambda}{J+1} &\simeq \frac{(N+\Lambda-J)}{J+1} N^J e^{-J} \sqrt{1+\frac{\Lambda}{N}} \sqrt{1+\frac{\Lambda-J}{N}} \left(1+\frac{\Lambda}{N}\right)^{N+\Lambda} \left(1+\frac{\Lambda-J}{N}\right)^{-N-\Lambda+J} \\ &\simeq \frac{N^{J+1} e^{-J}}{J} \left(1+\frac{\Lambda}{N}\right)^{N+\Lambda} \left(1+\frac{\Lambda-J}{N}\right)^{-N-\Lambda+J}. \end{aligned} \tag{2.2.15}$$

Here, we have dropped some error terms of order $\mathcal{O}\left(\frac{1}{J}\right)$ and $\mathcal{O}\left(\frac{J}{N}\right)$. We expand the terms in the brackets by taking logs, and using the fact that $\Lambda < N$ to perform a series

expansion. We find that

$$\begin{aligned}\log\left(1+\frac{\Lambda}{N}\right)^{N+\Lambda} &= -N\left(1+\frac{\Lambda}{N}\right)\sum_{k=1}^{\infty}\frac{(-\Lambda)^k}{kN^k} \\ &= \Lambda+\sum_{k=1}^{\infty}\frac{(-\Lambda)^{k+1}}{k(k+1)N^k}. \end{aligned} \tag{2.2.16}$$

Hence, replacing Λ with $\Lambda - J$ in the second bracketed factor of (2.2.15), we find

$$J!\binom{N+\Lambda}{J+1} \simeq \frac{N^{J+1}}{J}\exp\left(\sum_{k=1}^{\infty}\frac{(-\Lambda)^{k+1}-(-\Lambda+J)^{k+1}}{k(k+1)N^k}\right). \tag{2.2.17}$$

We can simplify this expression by dropping the terms in the infinite sum that tend to zero with large N. The kth term in the sum scales like J^{k+1}/N^k for some integer k, so if we impose that $J \ll N^{2/3}$, then all terms with $k \geq 2$ are small. With this condition, we can drop the subleading terms of order $\mathcal{O}(J^3/N^2)$ and write

$$\boxed{J!\binom{N+\Lambda}{J+1} \simeq \frac{N^{J+1}}{J}\exp\left(\frac{-J^2}{2N}+\frac{J\Lambda}{N}\right).} \tag{2.2.18}$$

This expression, which is valid for any $\Lambda \leq J \ll N^{2/3}$, is used repeatedly in the following sections to derive the asymptotics of finite N correlators. Including both terms in (2.2.11) with $\Lambda = J$ and $\Lambda = 0$ respectively, we can now state that two-point function has the asymptotic form

$$\langle \mathrm{tr}Z^J \mathrm{tr}Z^{\dagger J}\rangle \simeq \frac{N^{J+1}}{J}e^{\frac{J^2}{2N}}\left(1-e^{-\frac{J^2}{N}}\right). \tag{2.2.19}$$

This approach generalises in a straightforward manner to the three-point function. Replacing J with $2J$ and allowing Λ to take the values 0, J, and $2J$, we find that (2.2.12) becomes

$$\begin{aligned}\langle \mathrm{tr}Z^J \mathrm{tr}Z^J \mathrm{tr}Z^{\dagger 2J}\rangle &\simeq \frac{N^{2J+1}}{2J}\left(e^{\frac{2J^2}{N}}-2+e^{\frac{-2J^2}{N}}\right) \\ &\simeq \frac{N^{2J+1}}{2J}e^{\frac{2J^2}{N}}\left(1-e^{-\frac{2J^2}{N}}\right)^2. \end{aligned} \tag{2.2.20}$$

These expressions allow us to read off the asymptotic form of the normalised three-

point function (2.2.1). We find that

$$G_3 \simeq \sqrt{\frac{J}{2N}} \exp\left(\frac{J^2}{2N}\right) \frac{\left(1-e^{-\frac{2J^2}{N}}\right)^2}{(1-e^{-\frac{J^2}{N}})\sqrt{(1-e^{-\frac{4J^2}{N}})}}. \tag{2.2.21}$$

This expression is valid for any behaviour of J provided that $J \ll N^{2/3}$.

To find a more tractable version of this formula at large N, we need to state how J^2/N grows with N. There are three cases to consider: J^2/N going to zero with large N, J^2/N going to a constant, and J^2/N going to infinity. In the first case where J^2/N is small, we can use

$$(1-e^{-\frac{kJ^2}{N}}) \simeq \frac{kJ^2}{N}, \qquad \exp\left(\frac{J^2}{2N}\right) \simeq 1, \tag{2.2.22}$$

where $k \in \{1,2,4\}$, to see that

$$G_3 \simeq \frac{\sqrt{JJ(2J)}}{N}, \tag{2.2.23}$$

which is the known behaviour of the normalised three-point correlator for $J \ll \sqrt{N}$. The assumption $J^2/N \to 0$ means that the correlator will tend to zero in this limit, and so factorisation holds in this case. Alternatively, in the case that J^2/N tends to a constant value, i.e. $J = \mathcal{O}(\sqrt{N})$, then (2.2.21) will scale as $\mathcal{O}(N^{-\frac{1}{4}})$ with large N. This means that factorisation will still hold in this case. However, in the case that J^2/N grows large with N, then we have

$$(1-e^{-\frac{kJ^2}{N}}) \simeq 1, \qquad \exp\left(\frac{J^2}{2N}\right) \to \infty, \tag{2.2.24}$$

and thus

$$\boxed{G_3 = \langle\langle \mathrm{tr}Z^J \mathrm{tr}Z^J \mathrm{tr}Z^{\dagger 2J}\rangle\rangle \simeq \sqrt{\frac{J}{2N}} \exp\left(\frac{J^2}{2N}\right).} \tag{2.2.25}$$

This correlator will grow to infinity if J grows quickly enough with N. In particular, if $J \geq N^{\frac{1}{2}+\delta}$ for some small constant $\delta > 0$ at large enough N i.e. if J grows faster than $\sqrt{N}$ by a positive power, then the exponential term dominates and the correlator will tend to infinity. We deduce that the threshold - that is, the growth of J with N

which keeps the correlator finite and non-zero at large N - lies in the range

$$N^{\frac{1}{2}} < J < N^{\frac{1}{2}+\delta}, \tag{2.2.26}$$

where δ is any small positive number. This is the relevant region for solving asymptotically the factorisation threshold equation

$$G_3(J_t(N), N) = 1. \tag{2.2.27}$$

2.2.3 Solving the factorisation threshold equation

We can use (2.2.25) in the region (2.2.26) to find a function $J(N)$ that solves the threshold equation (2.2.27) at large N. To do this, we write down the *exact* equation

$$G_3 = \sqrt{\frac{J}{2N}} \exp\left(\frac{J^2}{2N}\right) e^{-\frac{1}{4}r}, \tag{2.2.28}$$

where the error function $r(J, N)$ is implicitly defined by this equation (the factor of $\frac{1}{4}$ here is chosen for later convenience). All the large N approximations that were taken in generating the asymptotic expression (2.2.25) are encoded in this error function, so it must tend to zero with N (provided that we remain in the range (2.2.26)). To find the leading-order behaviour of r, we collate the terms dropped at various stages in the previous section. In (2.2.15) and (2.2.18), we have dropped terms of order $\mathcal{O}\left(\frac{1}{J}\right)$, $\mathcal{O}\left(\frac{J}{N}\right)$, and $\mathcal{O}\left(\frac{J^3}{N^2}\right)$. As J^2/N is large, all these errors are $\mathcal{O}\left(\frac{J^3}{N^2}\right)$. Also, in performing the approximation

$$\left(1 - e^{-\frac{kJ^2}{N}}\right) \simeq 1 \tag{2.2.29}$$

for various values of k, we have dropped terms of order $\mathcal{O}(e^{-\frac{J^2}{N}})$. At present, we have not specified tight enough constraints on J to determine which is the larger, so we keep both remainders. We write

$$G_3 = \sqrt{\frac{J}{2N}} \exp\left(\frac{J^2}{2N}\right) \left(1 + \mathcal{O}\left(\frac{J^3}{N^2}\right) + \mathcal{O}\left(e^{-\frac{J^2}{N}}\right)\right) \tag{2.2.30}$$

and so we have

$$e^{-\frac{1}{4}r} = 1 + \mathcal{O}\left(\frac{J^3}{N^2}\right) + \mathcal{O}\left(e^{-\frac{J^2}{N}}\right) \tag{2.2.31}$$

This means that the error function r is bounded by

$$r = \mathcal{O}\left(\frac{J^3}{N^2}\right) + \mathcal{O}\left(e^{-\frac{J^2}{N}}\right). \tag{2.2.32}$$

Again, we know that this function tends to zero, but cannot yet deduce its leading-order behaviour before solving the threshold equation. Rearranging (2.2.28), we can write the threshold equation $G_3(J_t(N), N) = 1$ as

$$\left(\frac{2J_t^2}{N}\exp\left(\frac{2J_t^2}{N}\right)\frac{1}{8Ne^r}\right)^{\frac{1}{4}} = 1. \tag{2.2.33}$$

This equation cannot be solved exactly in terms of elementary functions (i.e. exponentials, logarithms and powers of z), but it can be rewritten and approximated by using the Lambert W-function. The Lambert W-function is defined by the equation

$$W(z)e^{W(z)} = z. \tag{2.2.34}$$

It is a multivalued function, but here we just consider the principle branch of the function, where $W(z)$ is positive and real for positive real z. In this regime, a large z asymptotic expansion of the function is known to all orders [76, 77]. More discussion of the Lambert W-function is given in Appendix C. Equation (2.2.33) is solved in terms of the W-function by

$$\frac{2J_t^2}{N} = W(8Ne^r), \tag{2.2.35}$$

which can be written

$$J_t = \sqrt{\frac{N}{2}W(8Ne^r)}. \tag{2.2.36}$$

To find a more tractable version of the threshold expressed in terms of elementary functions, we can expand the W-function by using its asymptotic series. The large z expansion of the W-function is [77]

$$W(z) \simeq \log z - \log\log z + \sum_{n=1}^{\infty}\left(\frac{-1}{\log z}\right)^n \sum_{k=0}^{n}\begin{bmatrix} n \\ n-k+1 \end{bmatrix}\frac{(-\log\log z)^k}{k!}, \tag{2.2.37}$$

where the coefficients in the square brackets are the Stirling cycle numbers (of the first kind); the notation $\begin{bmatrix} n \\ k \end{bmatrix}$ denotes the number of permutations of n elements composed

of k disjoint cycles. We can find the leading-order behaviour of the threshold by truncating this series. However, to guarantee that the truncated solution still satisfies $G_3(J_t(N), N) = 1$ in the large N limit, we need to keep all the terms in the series that do not tend to zero. The first two terms in the series are large as $z \to \infty$, and the remaining terms in the infinite series all go to zero, and so we keep the first two terms and find that the large N solution of (2.2.36) is

$$\frac{J_t^2}{N} = \frac{1}{2}\left[\log(8Ne^r) - \log\log(8Ne^r) + \mathcal{O}\left(\frac{\log\log N}{\log N}\right)\right]. \tag{2.2.38}$$

We can now extract out the N-dependence of the remainder function at the threshold, $r(J_t(N), N)$. Since

$$\frac{J_t^2}{N} = \frac{1}{2}\left(\log 8N - \log\log N + o(1)\right), \tag{2.2.39}$$

we find that

$$e^{-\frac{J_t^2}{N}} \simeq \sqrt{\frac{\log N}{8N}}, \qquad \frac{J_t^3}{N^2} \simeq \sqrt{\frac{(\log N)^3}{8N}}, \tag{2.2.40}$$

and so to leading order in N,

$$r(J_t(N), N) = \mathcal{O}\left(\sqrt{\frac{(\log N)^3}{N}}\right). \tag{2.2.41}$$

This term is smaller than $N^{-\frac{1}{2}+\delta}$ for any constant $0 < \delta < \frac{1}{2}$, and so all powers of r are subleading to all logarithm-dependent terms in the expansion. We can therefore discard these r-dependent terms as they are 'exponentially suppressed' in terms of the parameter $\log N$. The full asymptotic series expansion of the threshold is

$$J_t^2 \simeq \frac{1}{2}N\left[\log(8N) - \log\log(8N) + \sum_{n=1}^{\infty}\left(\frac{-1}{\log(8N)}\right)^n \sum_{k=0}^{n}\begin{bmatrix} n \\ n-k+1 \end{bmatrix}\frac{(-\log\log(8N))^k}{k!}\right]. \tag{2.2.42}$$

Taking square roots and moving out the constant factors in the logs, we deduce that the leading-order terms in the expansion of the threshold are

$$J_t = \sqrt{\frac{1}{2}N\log N}\left[1 - \frac{\log\log N}{2\log N} + \frac{\log 8}{2\log N} + \mathcal{O}\left(\frac{(\log\log N)^2}{(\log N)^2}\right)\right]. \tag{2.2.43}$$

This is the leading-order solution to

$$G_3(J_t(N), N) := \langle\langle \mathrm{tr} Z^{J_t} \mathrm{tr} Z^{J_t} \mathrm{tr} Z^{2J_t} \rangle\rangle = 1 \tag{2.2.44}$$

for large N and large J_t.

In (2.2.43), we have given the first three terms in the expansion of the threshold. This is the necessary degree of accuracy of the threshold $J_t(N)$ for which the truncated series still satisfies the threshold equation in the large N limit. That is, if we take the truncated threshold

$$\tilde{J}(N) = \sqrt{\frac{1}{2} N \log N} \left[1 - \frac{\log\log N}{2 \log N} + \frac{\log 8}{2 \log N} \right] \tag{2.2.45}$$

and plug this into the exact expression (2.2.28), we have

$$G_3(\tilde{J}(N), N) = \exp\left[\frac{1}{16 \log N} \left(\log\left(\frac{8}{\log N} \right) \right)^2 - \frac{1}{4} r \right], \tag{2.2.46}$$

which tends to one in the large N limit. If we had only taken the first term in the threshold solution $\tilde{J} = \sqrt{\frac{1}{2} N \log N}$ and plugged this into (2.2.28), we would have found that $G_3(\tilde{J}(N), N)$ actually grows logarithmically with N, and so the threshold equation cannot hold for arbitrarily large N. Similarly, truncating the series at the second term causes the correlator $G_3(\tilde{J}(N), N)$ to converge to a different constant than 1 at large N.

We remark that the factors of 8 appearing in the logs have come from choosing the factorisation threshold to be at $G_3 = 1$. If we had instead chosen $G_3(J, N) = c$ for some constant c, then the threshold solution would be

$$\frac{J_t^2}{N} = \frac{1}{2} W(8 c^4 N e^r), \tag{2.2.47}$$

and the leading-order behaviour after expansion would be

$$J_t = \sqrt{\frac{1}{2} N \log N} \left[1 - \frac{\log\log N}{2 \log N} + \frac{\log 8 + 4 \log c}{2 \log N} + \mathcal{O}\left(\frac{\log\log N}{\log N} \right)^2 \right]. \tag{2.2.48}$$

2.2.4 Similarities to the running coupling of gauge theories

We pause here to discuss some similarities between our threshold solution and the the running coupling of non-abelian gauge theories. The beta function of $\alpha_s(Q^2)$ from

QCD gauge theory is

$$Q^2\frac{d\alpha_s}{dQ^2} = \frac{d\alpha_s}{dL} = \beta_0\alpha_s^2 + \beta_1\alpha_s^3 + \beta_2\alpha_s^3 + \mathcal{O}(\alpha_s^4), \tag{2.2.49}$$

where Q^2 is the energy scale, β_i is the beta function at loop order $(i+1)$, and $L = \log(\frac{Q^2}{\Lambda^2})$. This has been solved perturbatively [78, 79] for the running coupling $\alpha_s(Q^2)$,

$$\begin{aligned}\alpha_s(Q^2) + \frac{1}{\beta_0\log L} &= \frac{\beta_1}{\beta_0^2 L}(\log L) + \frac{\beta_1^2}{\beta_0^4 L^2}\left((\log L)^2 - \log L - 1 + \frac{\beta_0\beta_2}{\beta_1^2}\right) \\ &+ \frac{\beta_1^3}{\beta_0^6 L^3}\left((\log L)^3 - \frac{5}{2}(\log L)^2 - (2 - 3\frac{\beta_0\beta_2}{\beta_1^2})\log L + \frac{1}{2} - \frac{\beta_0^2\beta_3}{\beta_1^3}\right) + \mathcal{O}\left(\frac{(\log L)^4}{L^4}\right).\end{aligned} \tag{2.2.50}$$

The threshold solution can be recast into a form which reveals a striking similarity with the expansion of $\alpha_s(Q^2)$. Starting from the definition of the W-function and its asymptotic series (2.2.37), we can write

$$\begin{aligned}\log W(z) &= \log z - W(z) \\ &\simeq \log\log z - \sum_{n=1}^{\infty}\left(\frac{-1}{\log z}\right)^n \sum_{k=0}^{n}\begin{bmatrix} n \\ n-k+1\end{bmatrix}\frac{(-\log\log z)^k}{k!},\end{aligned} \tag{2.2.51}$$

where the factors $\begin{bmatrix} n \\ k\end{bmatrix}$ are Stirling cycle numbers of the first kind. Introducing the new variables $y = \log J_t$ and $v = \log N$, we can take logs of the exact solution

$$J_t = \sqrt{\frac{N}{2}W(8Ne^r)} \tag{2.2.52}$$

and plug in the first few Stirling numbers to find

$$\begin{aligned}2y &= v + \log v - \log 2 + \frac{1}{v}\left(-\log v + \log 8\right) \\ &+ \frac{1}{v^2}\left[-\frac{1}{2}(\log v)^2 + (1+\log 8)\log v - \frac{1}{2}(\log 8)(\log 8 + 2)\right] + \mathcal{O}\left(\frac{(\log v)^3}{v^3}\right)\end{aligned} \tag{2.2.53}$$

$$\simeq v + \log v - \log 2 + \sum_{l=1}^{\infty}\frac{P_0^l(\log v)}{v^l}, \tag{2.2.54}$$

where P_0^l are polynomials of order l, and we have dropped the subleading r-dependent terms. All but the first three terms in this sum tend to zero in the large v (i.e. large N) limit, so we can define the variable $Y = 2y - v - \log v + \log 2$, which has the

perturbative expansion

$$Y = \frac{1}{v}\left(-\log v + \log 8\right) + \frac{1}{v^2}\left[-\frac{1}{2}(\log v)^2 + (1+\log 8)\log v - \frac{1}{2}(\log 8)(\log 8 + 2)\right] + \mathcal{O}\left(\frac{(\log v)^3}{v^3}\right). \quad (2.2.55)$$

We can now see that both (2.2.50) and (2.2.55) are manifestly of the same form. Each bracketed term in the first series can be written $L^{-n}\tilde{P}^n(\log L)$, and each bracketed term in the second series can be written $v^{-n}P^n(\log v)$, where $\tilde{P}^n$ and P^n are polynomials of order n. The similarity between these series is intriguing, and it would be of interest to find out if there is a physical explanation.

2.2.5 Expansion of the threshold as a transseries

We have given in equation (2.2.42) an infinite asymptotic series expansion of the threshold $J_t(N)$ in terms of powers of $\log N$ and $\log\log N$. We can go beyond this classical asymptotic series approach to the threshold by considering the *non-perturbative corrections*, generated by the subleading terms in r that were previously neglected. This type of series is known as a *transseries*, and is perhaps most commonly seen in theoretical physics to describe instanton corrections in quantum field theory.

When considering asymptotic expansions from path integrals in quantum field theory, we are interested in not only the original perturbative series in the coupling constant, but also the exponentially-suppressed instanton correction terms. These typically come from saddle-points in the path integral. A typical asymptotic series in a quantum field theory with small coupling constant $g \to 0$ and instanton corrections has the form

$$\sum_n a_n g^n + e^{-A/g}\sum_n a_n^{(1)} g^n + \mathcal{O}\left(e^{-2A/g}\right). \quad (2.2.56)$$

The definition of an asymptotic series given in Section 2.2.1 cannot be used to describe the exponential contributions, as they are subleading to all powers of the coupling g. We make sense of a series with instanton corrections by thinking of it as a purely formal sum, in which g and $e^{-A/g}$ are treated as independent variables. Once the formal transseries is constructed, there are approaches that can recover the *exact* full form of the path integral from the series; this is called the theory of *resurgence*. The lecture notes [80] give a review of transseries and resurgence in QFT and string theory.

In our analysis of the threshold, the series we have found has not come from a path integral, but still has exponentially-suppressed corrections. Rather than corresponding to saddle-points, the exponential corrections arise from the corrections to the asymptotics of the finite N correlators. We can see the analogy between thresholds and instanton expansions by changing variables from N to $v = \log N$ in our threshold expressions; the remainder term r is then proportional to $e^{-v/2}$. We show in the following that the general form of a transseries of the threshold can be found, in terms of $e^{-v/2}$, v and $\log v$.

An interesting possible future research direction would be to use the transseries expansion to search for an effective field theory description of gravitons at the threshold. The threshold expansions with exponential corrections strongly resemble instanton expansions of field theoretic partition functions, and so they could well contain valuable hints about the nature of such an effective field theory.

We start by writing the threshold in terms of the variables $y = \log J_t$ and $v = \log N$ introduced in the previous section, but retain the r-dependent terms in the series expansion. With the r-corrections, the series (2.2.53) becomes

$$\begin{aligned} 2y &= v + \log v - \log 2 + \frac{1}{v}\left(-\log v + \log 8\right) + \frac{r}{v} + \mathcal{O}\left(\frac{r^2}{v^2}\right) \\ &+ \frac{1}{v^2}\left[-\frac{1}{2}(\log v)^2 + (1+\log 8)\log v - \frac{1}{2}(\log 8)(\log 8 + 2)\right] + \mathcal{O}\left(\frac{(\log v)^3}{v^3}\right) \quad (2.2.57) \\ &\simeq v + \log v - \log 2 + \sum_{l=1}^{\infty} \frac{P_0^l(\log v)}{v^l} + \mathcal{O}\left(\frac{r}{v}\right), \quad (2.2.58) \end{aligned}$$

All the terms that depend on the error function r are subleading to any power of $\log v$ and v. To find the exponentially-supressed contributions to the threshold and extend the asymptotic series to a transseries, we need to find a more precise expression for r near the threshold. In the previous section, the function $r(J, N)$ was defined by the exact equation

$$G_3 = \sqrt{\frac{J}{2N}} \exp\left(\frac{J^2}{2N}\right) e^{-\frac{1}{4}r}. \quad (2.2.59)$$

The next-to-leading order corrections to the remainder function r were estimated in (2.2.32). A more careful calculation shows that the next-to-leading order behaviour of

the correlator near the threshold is

$$G_3 = \sqrt{\frac{J}{2N}} \exp\left(\frac{J^2}{2N}\right)\left[1 - \frac{J^3}{N^2} + e^{-\frac{J^2}{N}} + \mathcal{O}\left(\frac{J^6}{N^4}\right)\right], \tag{2.2.60}$$

and so

$$r(J,N) \;=\; 4\left(\frac{J^3}{N^2} - e^{-\frac{J^2}{N}} + \mathcal{O}\left(\frac{J^6}{N^4}\right)\right). \tag{2.2.61}$$

Plugging in the leading-order behaviour of the threshold $J \simeq \sqrt{\frac{1}{2}N\log N}$ gives us the leading-order behaviour of r as a function purely of N, or as a function of v. We find

$$\begin{aligned} r(J_t(N),N) &= \sqrt{\frac{2(\log N)^3}{N}}\left[1 - \frac{1}{\log N}\left(\log\log N - \frac{3}{2}\log 8 + 1\right) + \mathcal{O}\left(\frac{\log\log N}{\log N}\right)^2\right] \\ &= \sqrt{2}v^{\frac{3}{2}}e^{-\frac{v}{2}}\left[1 - \frac{1}{v}\left(\log v - \frac{3}{2}\log 8 + 1\right) + \mathcal{O}\left(\frac{\log v}{v}\right)^2\right] \end{aligned} \tag{2.2.62}$$

This correction can be reintroduced into (2.2.57) to give the first exponential correction of the threshold,

$$\begin{aligned} 2y = v + \log v - \log 2 + \frac{1}{v}\left(-\log v + \log 8\right) + \mathcal{O}\left(\frac{\log v}{v}\right)^2 \\ + \sqrt{2ve^{-v}}\left[1 + \frac{1}{v}\left(\frac{3}{2}\log 8 - 2 - \log v\right) + \mathcal{O}\left(\frac{\log v}{v}\right)^2\right] + \mathcal{O}\left(ve^{-v}\right). \end{aligned} \tag{2.2.63}$$

The remainder r has an asymptotic expansion at the threshold as a series of powers of $v^{\frac{3}{2}}e^{-\frac{v}{2}}$ multiplied by powers of $\log v$ and inverse powers of v. From considering the structure of the terms in (2.2.51), and writing $8Ne^r = e^{v+\log 8+r}$, it can be seen that a kth power of r in the asymptotic expansion of $W(8Ne^r)$ is accompanied by a kth inverse power of v, followed by positive powers of $\log v$ and inverse powers of v. Noting that the subleading terms in the asymptotic expansion of r can also contribute, we can deduce the all-orders form of the asymptotic series with exponential corrections, although it is difficult to calculate coefficients explicitly beyond the first few terms. The general form of the transseries form of the threshold is

$$2y \simeq v + \log v - \log 2 + \sum_{k=0}^{\infty}\sum_{n=0}^{\infty}(\sqrt{ve^{-v}})^k \frac{P_k^n(\log v)}{v^n}, \tag{2.2.64}$$

where the P_k^n are polynomials of order n, and $P_0^0(\log v) = 0$.

This series gives an alternative expression for the threshold $J_t = e^y$ in terms of $v = \log N$. Only the first three terms do not go to zero in the large N limit, so we can exponentiate this expression to derive an infinite asymptotic series for the threshold. We find that

$$J_t \simeq \sqrt{\frac{1}{2}N\log N}\left[1+\sum_{k=0}^{\infty}\sum_{n=0}^{\infty}\left(\sqrt{\frac{\log N}{N}}\right)^k \frac{P_k'^n(\log\log N)}{(\log N)^n}\right] \tag{2.2.65}$$

where the polynomials have been modified, but the form of the series has not. As remarked at the end of subsection 2.2.3, for a truncated threshold series $\tilde{J}_t(N)$ to satisfy $G_3(\tilde{J}_t(N), N) \to 1$ at large N, we must include the next-to-leading order term,

$$\frac{P_0'^1(\log\log N)}{\log N} = \frac{-\log\log N}{2\log N} + \frac{\log 8}{2\log N}. \tag{2.2.66}$$

As a final remark, we note again that changing the threshold from $G_3 = 1$ to $G_3 = c$ will not alter the form of the series, but will modify the polynomials and constants. From (2.2.47), we see that shifting the threshold equation to $G_3 = c$ will transform the series as

$$2y \simeq v + \log v - \log 2 + \sum_{k=0}^{\infty}\sum_{n=0}^{\infty}(\sqrt{v+c^4}e^{-\frac{v+c^4}{2}})^k \frac{P_k^n(\log(v+c^4))}{(v+c^4)^n} \tag{2.2.67}$$

$$\simeq v + \log v - \log 2 + \sum_{k=0}^{\infty}\sum_{n=0}^{\infty}(\sqrt{v}e^{-\frac{v}{2}})^k \frac{\tilde{P}_k^n(\log v)}{v^n}. \tag{2.2.68}$$

The three leading-order terms and the highest-order terms in the polynomials are unaffected by the shift.

2.3 The extremal three-point correlator with $J_1 \neq J_2$

In the previous section we solved the equation $G_3(J(N), N) = 1$ at large N by finding the asymptotic form of the three-point function G_3 and solving for $J(N)$. In this section we consider the threshold of factorisation for the more general three-point

function,

$$\begin{aligned} G_3(J_1,J_2,N) &:= \langle\langle \mathrm{tr}Z^{J_1}\mathrm{tr}Z^{J_2}\mathrm{tr}Z^{\dagger J_1+J_2}\rangle\rangle \\ &= \frac{\langle \mathrm{tr}Z^{J_1}\mathrm{tr}Z^{J_2}\mathrm{tr}Z^{\dagger J_1+J_2}\rangle}{\sqrt{\langle \mathrm{tr}Z^{J_1}\mathrm{tr}Z^{\dagger J_1}\rangle\langle \mathrm{tr}Z^{J_2}\mathrm{tr}Z^{\dagger J_2}\rangle\langle \mathrm{tr}Z^{J_1+J_2}\mathrm{tr}Z^{\dagger J_1+J_2}\rangle}}, \end{aligned} \tag{2.3.1}$$

and examine the behaviour of $J_1(N)$, $J_2(N)$ with N for which the threshold equation

$$G_3(J_1(N),J_2(N),N)=1 \tag{2.3.2}$$

is satisfied at large N. Using similar methods as in the previous section, the asymptotic form of $G_3(J_1(N),J_2(N),N)$ can be found at large N, and can be used to invert the threshold equation (2.3.2) to retrieve a simple leading-order constraint on the functions $J_1(N),J_2(N)$ at the threshold. We find quite generally that (2.3.2) is solved in the large N limit by solutions $J_1(N),J_2(N)$ that have the leading-order behaviour

$$J_1J_2 \sim N\log N, \tag{2.3.3}$$

where we have omitted a constant of proportionality. In fact, this constant of proportionality depends on the N-dependent behaviour of the *smaller* of the two angular momenta J_1 and J_2.

In the following subsection, we present the calculation of the large N behaviour of the correlator $G_3(J_1,J_2,N)$, and invert the threshold equation $G_3(J_1(N),J_2(N),N)=1$ to find the result $J_1J_2=\mathcal{O}(N\log N)$. Following that, we discuss how the threshold from the bulk perspective relates the separation of the graviton energies $\Delta J=|J_1-J_2|$ to the energy of the single graviton $E=(J_1+J_2)$.

2.3.1 Scaling limits and the threshold equation

We start from the expressions for the two and three-point correlators in Section 2.2.2. These generalise in a straightforward manner to give the expression, valid for large N and $1\ll J_1,J_2\ll N^{\frac{2}{3}}$:

$$G_3(J_1,J_2,N)\simeq\sqrt{\frac{J_1J_2}{(J_1+J_2)N}}\exp\left(\frac{J_1J_2}{2N}\right)\frac{(1-e^{-\frac{J_1(J_1+J_2)}{N}})(1-e^{-\frac{J_2(J_1+J_2)}{N}})}{\sqrt{(1-e^{-\frac{J_1^2}{N}})(1-e^{-\frac{J_2^2}{N}})(1-e^{-\frac{(J_1+J_2)^2}{N}})}}. \tag{2.3.4}$$

Without loss of generality, we assume throughout that $J_1\leq J_2$.

We can find bounds on the threshold region by considering the large N behaviour of the product of the angular momenta $J_1 J_2$. If $J_1 J_2/N$ goes to zero with N, then the assumption $J_1 \leq J_2$ means that J_1^2/N must also go to zero with N. We use

$$\begin{aligned} 1 - e^{-\frac{J_1^2}{N}} &\simeq \frac{J_1^2}{N}, \\ 1 - e^{-\frac{J_1(J_1+J_2)}{N}} &\simeq \frac{J_1(J_1+J_2)}{N}, \\ 1 - e^{-\frac{J_2(J_1+J_2)}{N}} &\simeq 1 - e^{-\frac{J_2^2}{N}}, \\ 1 - e^{-\frac{(J_1+J_2)^2}{N}} &\simeq 1 - e^{-\frac{J_2^2}{N}} \end{aligned} \tag{2.3.5}$$

to deduce that the the correlator behaves as

$$G_3 \simeq \sqrt{\frac{J_1 J_2}{N}} \sqrt{\frac{J_1 + J_2}{N}} \ll 1. \tag{2.3.6}$$

The correlator thus decays to zero at large N. On the other hand, if $J_1 J_2/N$ grows with N to infinity at a faster rate than some small positive power of N, i.e. $J_1 J_2 \geq N^{1+\delta}$ for some small positive constant δ, then the $\exp(J_1 J_2/2N)$ factor scales at least as quickly as $\exp(N^\delta)$, an exponential of a positive power of N. All other factors in the expression are bounded by powers of N, and so the exponential term dominates and G_3 must tend to infinity. Summarizing the above, we have

$$\boxed{\begin{aligned} G_3(J_1, J_2, N) \to 0, \qquad & \frac{J_1 J_2}{N} \to 0, \\ G_3(J_1, J_2, N) \to \infty, \qquad & \frac{J_1 J_2}{N^{1+\delta}} \to \infty \ \text{ for some } \delta > 0. \end{aligned}} \tag{2.3.7}$$

These limits extend the relations given in (2.1.7) to the more general case. We deduce that a large N solution to the equation $G_3 = 1$ could only exist when the product $J_1 J_2$ lies somewhere in the range

$$N < J_1 J_2 < N^{1+\delta}, \tag{2.3.8}$$

for any small positive constant δ.

By constraining $J_1 J_2$ to lie within this range, the expression for the three-point correlator (2.3.4) can be simplified. Since we require $J_1 J_2$ to be grow larger than N, and have constrained both J_1 and J_2 to be less than $N^{\frac{2}{3}}$, we must have that $J_1 \gg N^{\frac{1}{3}}$, i.e. J_1 grows at least as quickly as a positive power of N. Also, the factors of the form

$(1 - e^{-x})$ in (2.3.4) tends to one if x tends to infinity, so we can use the facts that $J_1 J_2/N \to \infty$ near the threshold and $J_1 \leq J_2$ to neglect several factors and write

$$G_3 \simeq \sqrt{\frac{J_1 J_2}{(J_1 + J_2)N}} \exp\left(\frac{J_1 J_2}{2N}\right) \left(1 - e^{-\frac{J_1^2}{N}}\right)^{-\frac{1}{2}}. \tag{2.3.9}$$

We can keep track of the errors generated in approximating the asymptotic form of the correlator by writing the *exact* expression,

$$G_3 = \sqrt{\frac{J_1 J_2}{(J_1 + J_2)N}} \exp\left(\frac{J_1 J_2}{2N}\right) \left(1 - e^{-\frac{J_1^2}{N}}\right)^{-\frac{1}{2}} e^{-\frac{r}{2}}, \tag{2.3.10}$$

where again the remainder function $r(J_1, J_2, N)$ is defined implicitly by this equation, and the J_i scale with N in the range $N^{\frac{1}{3}} \ll J_1 \leq J_2 \ll N^{\frac{2}{3}}$. This remainder function tends to zero with N, but its leading-order behaviour will in general change depending on the scaling behaviour of J_1 and J_2. We will later show that, near the threshold, the remainder function is of the order

$$r = \mathcal{O}\left(\frac{(\log N)^2}{J_1}\right), \tag{2.3.11}$$

and so decays to zero at a faster rate than some inverse power of N.

We wish to simplify the equation

$$G_3 = \sqrt{\frac{J_1 J_2}{(J_1 + J_2)N}} \exp\left(\frac{J_1 J_2}{2N}\right) \left(1 - e^{-\frac{J_1^2}{N}}\right)^{-\frac{1}{2}} e^{-\frac{r}{2}} = 1 \tag{2.3.12}$$

in the large N limit. A convenient way to do this is by using the Lambert W-function, and its large argument expansion. Equation (2.3.12) is solved exactly (with the implicit remainder term r) by

$$\frac{J_1 J_2}{N} = W\left((J_1 + J_2)(1 - e^{-\frac{J_1^2}{N}})e^r\right). \tag{2.3.13}$$

The argument of the W-function changes depending on the behaviour of J_1^2/N with increasing N, but will grow to infinity in all relevant cases, allowing us to use the large argument asymptotic expansion of the W-function,

$$W(z) = \log z - \log\log z + \mathcal{O}\left(\frac{\log\log z}{\log z}\right). \tag{2.3.14}$$

To proceed, we must consider three possible scaling behaviours of J_1^2/N in turn: the case when J_1^2/N tends to zero, the case when J_1^2/N tends to a constant, and the case when J_1^2 tends to infinity.

First, consider the case where $J_1^2/N \to 0$. We have

$$(1 - e^{-\frac{J_1^2}{N}}) = \frac{J_1^2}{N} + \mathcal{O}\left(\frac{J_1^2}{N}\right)^2 \tag{2.3.15}$$

so

$$(J_1 + J_2)(1 - e^{-\frac{J_1^2}{N}}) = \frac{J_1 J_2}{N} J_1 \left(1 + \frac{J_1}{J_2}\right)\left(1 + \mathcal{O}\left(\frac{J_1^2}{N}\right)\right) \tag{2.3.16}$$

which must tend to infinity since $J_1 J_2/N$ and J_1 are large. Neglecting the remainder term r for the moment, we expand out the W-function to find the threshold equation

$$\begin{aligned}\frac{J_1 J_2}{N} = \log J_1 - \log\log J_1 + \log\left(\frac{J_1 J_2}{N}\right) \\ + \log\left(1 + \frac{J_1}{J_2}\right) - \log\left[1 + \frac{1}{\log J_1}\left(\log\left(\frac{J_1 J_2}{N}\right) + \log\left(1 + \frac{J_1}{J_2}\right)\right)\right] \\ + \mathcal{O}\left(\frac{J_1^2}{N}\right) + \mathcal{O}\left(\frac{\log\log(J_1 + J_2)(1 - e^{-\frac{J_1^2}{N}})}{\log(J_1 + J_2)(1 - e^{-\frac{J_1^2}{N}})}\right).\end{aligned} \tag{2.3.17}$$

This fairly involved expression can be substantially simplified as follows: first, we simplify the final error term by giving its leading behaviour in terms of N. Next, we show that all terms on the second line are small at large N, which allows us to deduce that the leading-order behaviour of the expression is $\log J_1$. Finally, by plugging in $\log J_1(1 + o(1))$ into the expressions for $J_1 J_2/N$ on the RHS of (2.3.17), we will find that the $\log\log J_1$ term cancels, and that only one large term remains in its asymptotic series expansion.

First, we consider the latter remainder term. We know that J_1 and J_2 scale with N at a larger rate than some positive power of N, so $\log J_1$ is $\mathcal{O}(\log N)$ to leading order. We have also required $J_1 J_2/N$ to scale to infinity at a slower rate than any positive power of N, as this is required for the threshold solution to $G_3 = 1$ to be valid at large N. This means that $\log(J_1 J_2/N)$ must be $o(\log N)$. We deduce that

$$\begin{aligned}\log\left[(J_1 + J_2)(1 - e^{-\frac{J_1^2}{N}})\right] &= \log J_1 + \log\left(\frac{J_1 J_2}{N}\right) + \log\left(1 + \frac{J_1}{J_2}\right) + \mathcal{O}\left(\frac{J_1^2}{N}\right) \\ &= \mathcal{O}(\log N),\end{aligned} \tag{2.3.18}$$

and hence

$$\mathcal{O}\left(\frac{\log\log(J_1+J_2)(1-e^{-\frac{J_1^2}{N}})}{\log(J_1+J_2)(1-e^{-\frac{J_1^2}{N}})}\right)=\mathcal{O}\left(\frac{\log\log N}{\log N}\right). \tag{2.3.19}$$

Both this term and the $\mathcal{O}\left(\frac{J_1^2}{N}\right)$ term are small in the large N limit. Next, we can see that all terms on the second line of (2.3.17) must be small. Noting that

$$\frac{J_1}{J_2} \;=\; \frac{J_1^2}{N}\frac{N}{J_1J_2}\to 0 \tag{2.3.20}$$

since $J_1^2/N\to 0$ and $J_1J_2/N\to\infty$, we have that

$$\log\left(1+\frac{J_1}{J_2}\right)\to 0. \tag{2.3.21}$$

Also, it was required that J_1J_2/N grows to infinity with N, but not as a positive power of N or greater, so $\log(J_1J_2/N)=o(\log N)$. Since $\log J_1=\mathcal{O}(\log N)$, this means that

$$\frac{1}{\log J_1}\log\left(\frac{J_1J_2}{N}\right)\to 0, \tag{2.3.22}$$

and so the second term in the second line of (2.3.17) is also small. The largest term in (2.3.17) must therefore be $\log J_1$, which is of order $\mathcal{O}(\log N)$. Using this and (2.3.20), we see that J_1/J_2 must be smaller than $\mathcal{O}(1/\log N)$, and so we can collate all the remainders in the threshold expression into two terms; we find

$$\frac{J_1J_2}{N}=\log J_1-\log\log J_1+\log\left(\frac{J_1J_2}{N}\right)+\mathcal{O}\left(\frac{\log\log N}{\log N}\right)+\mathcal{O}\left(\frac{J_1^2}{N}\right). \tag{2.3.23}$$

By plugging in this expression for J_1J_2/N into the third term, we can cancel the $\log\log J_1$ and obtain the leading-order threshold equation

$$\frac{J_1J_2}{N}=\log J_1+\mathcal{O}\left(\frac{\log\log N}{\log N}\right)+\mathcal{O}\left(\frac{J_1^2}{N}\right). \tag{2.3.24}$$

This formula is valid at the threshold, provided that $J_1^2/N\to 0$ with large N. There are two different remainder terms in this expression as we have not imposed enough conditions on J_1 to state which term is larger. Constraining the scaling behaviour of J_1 with N would allow us to deduce which term is subleading. For example, if we set $J_1\simeq\sqrt{N}(\log\log N)/\sqrt{\log N}$, then the $\mathcal{O}(J_1^2/N)$ term is the leading error, but if

$J_1 \simeq N^{5/12}$ then the $\mathcal{O}\left(\frac{\log\log N}{\log N}\right)$ term is the largest error.

Next, we consider the case where J_1^2/N tends to a constant. Starting from threshold equation

$$\frac{J_1 J_2}{N} = W((J_1+J_2)(1-e^{-\frac{J_1^2}{N}})e^r), \tag{2.3.25}$$

the argument of the W-function is clearly large since (J_1+J_2) grows with N. Again neglecting the remainder term, we can use the large argument expansion of the W-function and write

$$\frac{J_1 J_2}{N} \simeq \log\left((J_1+J_2)(1-e^{-\frac{J_1^2}{N}})\right) - \log\log\left((J_1+J_2)(1-e^{-\frac{J_1^2}{N}})\right) + \mathcal{O}\left(\frac{\log\log\left((J_1+J_2)(1-e^{-\frac{J_1^2}{N}})\right)}{\log\left((J_1+J_2)(1-e^{-\frac{J_1^2}{N}})\right)}\right). \tag{2.3.26}$$

Since $\log((J_1+J_2)(1-e^{-\frac{J_1^2}{N}})) = \mathcal{O}(\log N)$, we can simplify this remainder term and expand out the second term to write

$$\frac{J_1 J_2}{N} \simeq \log(J_1+J_2) - \log\log(J_1+J_2) + \log\left(1-e^{-\frac{J_1^2}{N}}\right) + \mathcal{O}\left(\frac{\log\log N}{\log N}\right). \tag{2.3.27}$$

In writing this expression, we have dropped a term of $\mathcal{O}\left(\frac{1}{\log N}\right)$ as it is subleading to the $\mathcal{O}\left(\frac{\log\log N}{\log N}\right)$ remainder term. The first two terms in this expression grow large with increasing N, and the third term tends to a constant.

Finally, we consider the case where J_1^2/N tends to infinity with N. Again we find that (2.3.27) still holds, but that the third term now tends to zero. From the series expansion of the logarithm, we have

$$\log\left(1-e^{-\frac{J_1^2}{N}}\right) = \mathcal{O}\left(e^{-\frac{J_1^2}{N}}\right), \tag{2.3.28}$$

so we write the final expression

$$\frac{J_1 J_2}{N} \simeq \log(J_1+J_2) - \log\log(J_1+J_2) + \mathcal{O}\left(e^{-\frac{J_1^2}{N}}\right) + \mathcal{O}\left(\frac{\log\log N}{\log N}\right). \tag{2.3.29}$$

Again, we have two remainder terms, as we have not specified how quickly J_1^2/N scales to infinity with N and so cannot state which is the larger.

Summarizing the above, we have three different threshold equations for the different regimes of J_1^2/N. Listed in order of increasing J_1^2/N, we have:

$$\frac{J_1 J_2}{N} = \begin{cases} \log J_1 + \mathcal{O}\left(\frac{\log\log N}{\log N}\right) + \mathcal{O}\left(\frac{J_1^2}{N}\right) & \frac{J_1^2}{N} \to 0 \\ \log(J_1+J_2) - \log\log(J_1+J_2) + \log\left(1 - e^{-\frac{J_1^2}{N}}\right) + \mathcal{O}\left(\frac{\log\log N}{\log N}\right) & \frac{J_1^2}{N} \to \text{const.} \\ \log(J_1+J_2) - \log\log(J_1+J_2) + \mathcal{O}\left(\frac{\log\log N}{\log N}\right) + \mathcal{O}\left(e^{-\frac{J_1^2}{N}}\right) & \frac{J_1^2}{N} \to \infty. \end{cases} \tag{2.3.30}$$

In all cases, the explicitly-given terms are non-zero in the large N limit, and the higher-order terms are small. All these large terms are necessary to describe the threshold accurately at large N; if we plug (2.3.30) into (2.3.12) with the remainder terms and r discarded, then the correlator tends to one at large N in each case.

The angular momenta J_1 and J_2 grow at least as quickly as a positive power of N, so the leading-order term in the threshold is always proportional to $\log N$. If we assume that the power-dependence of J_1 on N is simple enough that it can be separated out into the form $J_1 = N^{\alpha_1} e^{\delta_1}$, where α_1 is a constant and $|\delta_1(N)| \ll \log N$, then the leading-order term of the threshold solution is

$$J_1 J_2 \simeq \alpha_1 N \log N. \tag{2.3.31}$$

We have so far neglected the error parameter r without discussion, but we can now justify this. To derive the equation

$$G_3 \simeq \sqrt{\frac{J_1 J_2}{(J_1+J_2)N}} \exp\left(\frac{J_1 J_2}{2N}\right) \left(1 - e^{-\frac{J_1^2}{N}}\right)^{-\frac{1}{2}} \tag{2.3.32}$$

near the threshold, we have dropped corrections of at most order $\mathcal{O}(1/J_1)$ and $\mathcal{O}(J_1 J_2 (J_1 + J_2)/N^2)$. Near the threshold, J_1 and J_2 satisfy

$$\frac{J_1 J_2 (J_1+J_2)}{N^2} \simeq \frac{1}{J_1}\left(\frac{J_1 J_2}{N}\right)^2 = \mathcal{O}\left(\frac{(\log N)^2}{J_1}\right). \tag{2.3.33}$$

The remainder parameter r, defined in (2.3.12), must contain all the corrections to the correlator near the threshold. We can therefore state that, near the threshold, the largest corrections to r must be

$$r = \mathcal{O}\left(\frac{(\log N)^2}{J_1}\right), \tag{2.3.34}$$

which decays to zero with N at a faster rate than some inverse power of N. If we reintroduce this remainder when expanding out the W-function in (2.3.13), we will modify each equation in (2.3.30) by the addition of an r term, plus $\mathcal{O}(r^2)$ corrections. However, this term must be smaller than $\mathcal{O}\left(\frac{\log\log N}{\log N}\right)$, and in fact is smaller than any power of $(\log\log N/\log N)$: in terms of the parameter $v = \log N$, the contributions from r are exponentially suppressed in v. As a consequence, we can always drop these terms from the solution.

2.3.2 A change of variables

The threshold equation $G_3(J_1, J_2, N) = 1$ defines a two-dimensional threshold surface in three-dimensional (J_1, J_2, N)-space. We can develop some insight into the relation between this surface and the physical properties of the correlator by changing the parameter space variables. If we take N to be fixed but large enough that the remainder $\mathcal{O}\left(\frac{\log\log N}{\log N}\right)$ is small, then we can use (2.3.30) to rewrite the threshold as a curve in $E = J_1 + J_2$ and $\Delta J = |J_2 - J_1|$. For the region where $J_1^2/N \to 0$, i.e. $(E^2 - \Delta J^2)/N \to 0$, then the threshold of factorisation is

$$\frac{E^2 - \Delta J^2}{4N \log(E - \Delta J)} \simeq 1 + \mathcal{O}\left(\frac{\log\log N}{\log N}\right), \tag{2.3.35}$$

and for the region where $J_1^2/N = (E^2 - \Delta J^2)/N$ does not tend to zero, then the threshold is

$$\frac{E^2 - \Delta J^2}{4N(\log E - \log\log E)} \simeq 1 + \mathcal{O}\left(\frac{\log\log N}{\log N}\right), \tag{2.3.36}$$

where all the discarded terms are small.

We can say something about how perturbations away from the threshold in $(E, \Delta J, N)$ space affect the factorisation of the correlator by rewriting the correlator in the form

$$G_3(E, \Delta J, N) = \left[\frac{E^2 - \Delta J^2}{4NE} \exp\left(\frac{E^2 - \Delta J^2}{4N}\right)\left(1 - e^{-\frac{1}{4N}(E-\Delta J)^2}\right)^{-1} e^{-r}\right]^{\frac{1}{2}}. \tag{2.3.37}$$

It is convenient to work with $\log(G_3)^2$, and allow E and ΔJ to be independent of N. Taking the differential of $\log(G_3)^2$, we have

$$d\log(G_3)^2 = \frac{2}{G_3} dG_3 = \frac{2}{G_3}\left[\frac{\partial G_3}{\partial E} dE + \frac{\partial G_3}{\partial(\Delta J)} d(\Delta J) + \frac{\partial G_3}{\partial N} dN\right], \tag{2.3.38}$$

Expressing the coefficients of the differentials in terms of J_1, J_2 and N for convenience, we have

$$\begin{aligned} d\log(G_3)^2 = \frac{1}{2}dE\left[\frac{J_2}{N}+\frac{1}{J_1}+\frac{J_1}{N}+\frac{1}{J_2}-\frac{2}{J_1+J_2}-\frac{2J_1}{N(e^{\frac{J_1^2}{N}}-1)}\right] \\ +\frac{1}{2}d(\Delta J)\left[-\frac{J_2}{N}-\frac{1}{J_1}+\frac{J_1}{N}+\frac{1}{J_2}+\frac{2J_1}{N(e^{\frac{J_1^2}{N}}-1)}\right] \\ -\frac{dN}{N}\left[\frac{J_1J_2}{N}+1-\frac{J_1^2}{N(e^{\frac{J_1^2}{N}}-1)}\right]-dr. \end{aligned} \quad (2.3.39)$$

At large N and near the threshold $J_1J_2 = \mathcal{O}(N\log N)$, the largest term in the coefficient of dE is J_2/N, which is of order $\mathcal{O}\left(\frac{\log N}{J_1}\right)$. This means that $\frac{\partial G_3}{\partial E}$ is positive at large N. Similarly, the largest term in the coefficient of $d(\Delta J)$ is $-J_2/N$, which is order $\mathcal{O}\left(\frac{\log N}{J_1}\right)$, and so $\frac{\partial G_3}{\partial \Delta J}$ is negative at large N. The corrections to dE and $d(\Delta J)$ from the differential of the error function dr are order $\mathcal{O}\left(\frac{\log N}{J_1^2}\right)$ at the threshold, and so are subleading.

The signs of the partial derivates of G_3 with respect to E and ΔJ gives us some interesting insights into factorisation near the threshold. If we consider N to be large and fixed, and take E and ΔJ near to the threshold, then a small increase in the energy of the single graviton E will increase the correlator G_3, and move the correlator into the breakdown region. On the other hand, if the separation between the gravitons ΔJ in the multi-graviton state is increased by a small amount, then G_3 will decrease, and the correlator will move into the factorisation region.

2.4 Non-extremal correlators

We can consider the existence of a threshold of factorisation for a non-extremal three-point function with operators formed from the complex scalar fields $Z = \phi_5 + i\phi_6$ accompanied by a small number of $Y = \phi_3 + i\phi_4$ insertions. Consider a correlator of symmetrised trace operators inserted at the points x_1, x_2, and y:

$$\langle \mathrm{Str}(Z^{J_1}Y^{J_3})(x_1)\mathrm{Str}(Z^{J_2}Y^{\dagger J_3})(x_2)\mathrm{tr}(Z^{\dagger J_1+J_2})(y)\rangle. \quad (2.4.1)$$

In a similar manner to the extremal correlator consisting of only Z-fields, we can use the conformal symmetry to separate out a position-independent correlator by a

particular choice of operator insertion locations. Under the inversion $y \to y' = y/|y|^2$, the antiholomorphic operator transforms as

$$\begin{aligned} \mathrm{tr}(Z^{\dagger J_1+J_2})(y) &\to \mathrm{tr}'(Z^{\dagger J_1+J_2})(y') \\ &= |y|^{J_1+J_2}\mathrm{tr}(Z^{\dagger J_1+J_2})(y). \end{aligned} \tag{2.4.2}$$

By taking $x_1 \to 0$ and $y' \to 0$ i.e. $y \to \infty$, the correlator becomes

$$\begin{aligned} &\langle \mathrm{Str}(Z^{J_1}Y^{J_3})(0)\mathrm{Str}(Z^{J_2}Y^{\dagger J_3})(x_2)\mathrm{tr}'(Z^{\dagger J_1+J_2})(0)\rangle \\ &\quad = \frac{\langle \mathrm{Str}(Z^{J_1}Y^{J_3})\mathrm{Str}(Z^{J_2}Y^{\dagger J_3})\mathrm{tr}(Z^{\dagger J_1+J_2})\rangle}{|x_2|^{2J_3}}. \end{aligned} \tag{2.4.3}$$

We have separated out a combinatoric factor which can be evaluated by a matrix model calculation. Unlike the extremal correlator, however, the separation $|x_2|$ between the operators inserted at $\mathrm{Str}(Z^{J_1}Y^{J_3})$ and $\mathrm{Str}(Z^{J_2}Y^{\dagger J_3})$ is still present in this correlator. Introducing the notation $\epsilon \equiv |x_2|$ for the magnitude of the separation between these two operators, and $\| \mathcal{O} \| = \sqrt{\langle \mathcal{O}\mathcal{O}^\dagger \rangle}$ for the norm of a matrix model operator $\mathcal{O}$, then the multiparticle-normalised correlator is

$$G_3(J_i, N; \epsilon) = \frac{\langle \mathrm{Str}(Z^{J_1}Y^{J_3})\mathrm{Str}(Z^{J_2}Y^{\dagger J_3})\mathrm{tr}(Z^{\dagger J_1+J_2})\rangle}{\epsilon^{2J_3} \,\|\, \mathrm{Str}(Z^{J_1}Y^{J_3}) \,\| \| \,\mathrm{Str}(Z^{J_2}Y^{J_3}) \,\| \| \,\mathrm{tr}(Z^{J_1+J_2}) \,\|} \tag{2.4.4}$$

The appearance of this position-dependence means that the three-point correlator is dimensionful, and so it is not meaningful to define the threshold as being when the correlator approaches a fixed number at large N. However, if we introduce an arbitrary mass scale Λ, then we can instead consider the combination $\Lambda^{-2J_3}G_3(J_i, N; \epsilon)$, which is dimensionless. We define the *non-extremal threshold* as the solution to the equation

$$\Lambda^{-2J_3}G_3(J_i, N; \epsilon) = 1. \tag{2.4.5}$$

A natural choice of Λ would be a UV cutoff of the CFT. This will modify correlators in general, and the ϵ^{-2J_3} factor will be modified to

$$\frac{1}{\epsilon^{2J_3}}\left(1 + o(\epsilon^{-1}\Lambda^{-1})\right). \tag{2.4.6}$$

The higher-order corrections can be neglected if we require that the separation ϵ is much larger than the cutoff length Λ^{-1}. We can do this by setting $\epsilon\Lambda$ to be large and independent of N, or by allowing $\epsilon\Lambda$ to grow large with N. It is convenient in the following to define $\mathcal{R} := \epsilon\Lambda$ as the dimensionless ratio between the cutoff separation

and the length scale. This is required to be large for the higher-order corrections to ϵ to be absent. The non-extremal threshold equation can then be written in the form

$$\Lambda^{-2J_3} G_3(J_i, N; \epsilon) = \mathcal{R}^{-2J_3} \frac{\langle \mathrm{Str}(Z^{J_1} Y^{J_3}) \mathrm{Str}(Z^{J_2} Y^{\dagger J_3}) \mathrm{tr}(Z^{\dagger J_1 + J_2}) \rangle}{\| \mathrm{Str}(Z^{J_1} Y^{J_3}) \| \| \mathrm{Str}(Z^{J_2} Y^{J_3}) \| \| \mathrm{tr}(Z^{J_1+J_2}) \|} = 1. \quad (2.4.7)$$

To investigate the threshold of this non-extremal correlator, we look for an exact finite N expression of the correlator that is valid when some of the operator dimensions are large. There are three matrix model correlator expressions that we need in order to evaluate the correlator:

$$\begin{aligned} \| \mathrm{Str}(Z^{J_1} Y^{J_3}) \|^2 &= \langle \mathrm{Str}(Z^{J_1} Y^{J_3}) \mathrm{Str}(Z^{\dagger J_1} Y^{\dagger J_3}) \rangle, \\ \| \mathrm{tr}(Z^{J_1+J_2}) \|^2 &= \langle \mathrm{tr}(Z^{J_1+J_2}) \mathrm{tr}(Z^{\dagger J_1+J_2}) \rangle, \\ & \langle \mathrm{Str}(Z^{J_1} Y^{J_3}) \mathrm{Str}(Z^{J_2} Y^{\dagger J_3}) \mathrm{tr}(Z^{\dagger J_1+J_2}) \rangle. \end{aligned} \quad (2.4.8)$$

The norm $\| \mathrm{tr}(Z^{J_1+J_2}) \|^2$ is known explicitly, but we have not found a closed form of the other correlators for general operator dimensions. However, exact evaluations of the correlator can be found for small values of J_3, where there is only a small number of Y-insertions; in the following we focus on the 'near-extremal' case when $J_3 = 1$.

2.4.1 The 'near-extremal' correlator

We set $J_3 = 1$ in (2.4.7) and consider the correlator

$$G_3(J_i, N; \epsilon) = \frac{\langle \mathrm{Str}(Z^{J_1} Y) \mathrm{Str}(Z^{J_2} Y^\dagger) \mathrm{tr}(Z^{\dagger J_1+J_2}) \rangle}{\epsilon^2 \| \mathrm{Str}(Z^{J_1} Y) \| \| \mathrm{Str}(Z^{J_2} Y) \| \| \mathrm{tr}(Z^{J_1+J_2}) \|}. \quad (2.4.9)$$

The norm $\| \mathrm{tr}(Z^{J_1+J_2}) \|^2$ was known previously [27] and used in Sections 2.2 and 2.3:

$$\langle \mathrm{tr}(Z^{J_1+J_2}) \mathrm{tr}(Z^{\dagger J_1+J_2}) \rangle = (J_1+J_2)! \left[\binom{N+J_1+J_2}{J_1+J_2+1} - \binom{N}{J_1+J_2+1} \right]. \quad (2.4.10)$$

For $J_3 = 1$, there is only one pair of Y-matrices, so the contraction of the three-point function can be performed immediately. The unnormalised three-point correlator becomes

$$\langle \mathrm{Str}(Z^{J_1} \overbrace{Y) \mathrm{Str}(Z^{J_2} Y^\dagger}) \mathrm{tr}(Z^{\dagger J_1+J_2}) \rangle = \langle \mathrm{tr}(Z^{J_1+J_2}) \mathrm{tr}(Z^{\dagger J_1+J_2}) \rangle, \quad (2.4.11)$$

where we have used the fact that $\mathrm{Str}(Z^{J_1+J_2}) = \mathrm{tr}(Z^{J_1+J_2})$. This means that (2.4.9) reduces to

$$G_3(J_i, N; \epsilon) = \frac{\| \mathrm{tr}(Z^{J_1+J_2}) \|}{\epsilon^2 \| \mathrm{Str}(Z^{J_1}Y) \| \| \mathrm{Str}(Z^{J_2}Y) \|}. \tag{2.4.12}$$

The other correlators can be determined by tensor space methods. In Appendix D, we have derived the equation

$$\langle \mathrm{Str}(Z^{J_1}Y^{J_2}) \mathrm{Str}(Z^{\dagger J_1}Y^{\dagger J_2}) \rangle = J_1! J_2! \left[\binom{N+J_1+J_2}{J_1+J_2+1} - \binom{N}{J_1+J_2+1} \right]. \tag{2.4.13}$$

Substituting in the relevant values of J_1 and J_2 in to the correlators in the denominators of (2.4.9), we find that

$$\| \mathrm{Str}(Z^{J_1}Y) \| = \sqrt{J_1!} \left[\binom{N+J_1+1}{J_1+2} - \binom{N}{J_1+2} \right]^{\frac{1}{2}}, \tag{2.4.14}$$

$$\| \mathrm{Str}(Z^{J_2}Y) \| = \sqrt{J_2!} \left[\binom{N+J_2+1}{J_2+2} - \binom{N}{J_2+2} \right]^{\frac{1}{2}}, \tag{2.4.15}$$

and so

$$\Lambda^{-2} G_3(J_i, N; \epsilon) = \mathcal{R}^{-2} \left(\frac{(J_1+J_2)!}{J_1! J_2!} \right)^{\frac{1}{2}} \left[\binom{N+J_1+J_2}{J_1+J_2+1} - \binom{N}{J_1+J_2+1} \right]^{\frac{1}{2}} \times$$
$$\times \left[\binom{N+J_1+1}{J_1+2} - \binom{N}{J_1+2} \right]^{-\frac{1}{2}} \left[\binom{N+J_2+1}{J_2+2} - \binom{N}{J_2+2} \right]^{-\frac{1}{2}}. \tag{2.4.16}$$

This is the finite N expression of the non-extremal correlator when $J_3 = 1$. It is valid for small or large J_1 and J_2, provided that $J_1, J_2 \ll N$. As in the extremal case, we wish to find the asymptotic form of this expression when J_1, J_2, and N are large, but the ratios J_1/N and J_2/N are small. Making the assumptions that $J_1 \leq J_2 \ll N^{\frac{2}{3}}$, then equation (2.2.18) still holds with J replaced by (J_1+1). Dropping the subleading corrections, we find that

$$J_1! \left[\binom{N+J_1+1}{J_1+2} - \binom{N}{J_1+2} \right] \simeq \frac{N^{J_1+2}}{J_1^2} \exp\left(\frac{J_1^2}{2N} \right) \left(1 - e^{-\frac{J_1^2}{N}} \right), \tag{2.4.17}$$

and similarly for J_2. The full large N expression for the correlator for $1 \ll J_1 \leq J_2 \ll$

N is therefore

$$\Lambda^{-2}G_3 \simeq \mathcal{R}^{-2}\sqrt{\frac{J_1^2J_2^2}{(J_1+J_2)N^3}}\exp\left(\frac{J_1J_2}{2N}\right)\sqrt{\frac{\left(1-e^{-\frac{(J_1+J_2)^2}{N}}\right)}{\left(1-e^{-\frac{J_1^2}{N}}\right)\left(1-e^{-\frac{J_2^2}{N}}\right)}} \tag{2.4.18}$$

We can argue that the correlator must decay to zero if J_1J_2/N is small as follows: If J_1J_2/N tends to zero with N, then the exponential term tends to 1. The factor $\mathcal{R}^{-2}$ has already been taken to be small. Since J_1J_2/N is small and we have assumed that $J_1 \leq J_2$, we know that J_1^2/N is also small and so

$$\begin{aligned} 1-e^{-\frac{(J_1+J_2)^2}{N}} &\simeq 1-e^{-\frac{J_2^2}{N}}, \\ \frac{J_1^2/N}{1-e^{-\frac{J_1^2}{N}}} &\simeq 1, \end{aligned} \tag{2.4.19}$$

and thus we can deduce that

$$\Lambda^{-2}G_3 \simeq \mathcal{R}^{-2}\frac{J_2}{N}\frac{1}{\sqrt{J_1+J_2}}. \tag{2.4.20}$$

The correlator must therefore tend to zero when J_1J_2/N is small.

On the other hand, consider the case when J_1J_2/N grows larger than a positive power of N, i.e. $J_1J_2 > N^{1+\delta}$ for some $\delta > 0$. The exponential term will dominate the expression, as it will grow to infinity exponentially quickly with N as compared to the other factors of J_1, J_2, and N outside of the exponential. In this case, the correlator must definitely grow to infinity (provided that $\mathcal{R}$ is does not grow with N at a faster than a power of N). Summarizing the above, we have

$$\boxed{\begin{aligned} &G_3(J_1,J_2,N;\mathcal{R}) \to 0, \qquad \frac{J_1J_2}{N} \to 0, \\ &G_3(J_1,J_2,N;\mathcal{R}) \to \infty, \qquad \frac{J_1J_2}{N^{1+\delta}} \to \infty \ \text{ for some } \delta > 0. \end{aligned}} \tag{2.4.21}$$

The threshold must therefore be constrained to lie in the region

$$N < J_1J_2 < N^{1+\delta}. \tag{2.4.22}$$

In this range, the large N behaviour of the correlator is simply

$$\Lambda^{-2}G_3(J_1,J_2,N;\epsilon) \simeq \mathcal{R}^{-2}\sqrt{\frac{J_1^2J_2^2}{(J_1+J_2)N^3}}\exp\left(\frac{J_1J_2}{2N}\right)\left(1-e^{-\frac{J_1^2}{N}}\right)^{-\frac{1}{2}}. \quad (2.4.23)$$

We can encompass all the errors present in approximating this expression by the function r, defined by the equation

$$\Lambda^{-2}G_3(J_1,J_2,N;\epsilon) = \mathcal{R}^{-2}\sqrt{\frac{J_1^2J_2^2}{(J_1+J_2)N^3}}\exp\left(\frac{J_1J_2}{2N}\right)\left(1-e^{-\frac{J_1^2}{N}}\right)^{-\frac{1}{2}}e^{-\frac{r}{2}}, \quad (2.4.24)$$

and attempt to solve asymptotically the threshold equation

$$\Lambda^{-2}G_3(J_1,J_2,N;\epsilon) = 1. \quad (2.4.25)$$

We consider the cases $J_1 = J_2$ and $J_1 \neq J_2$ separately.

2.4.2 $J_1 = J_2$

If we consider the non-extremal correlator when $J_1 = J_2 = J$, then the threshold equation with error function r becomes

$$\mathcal{R}^{-2}\sqrt{\frac{J^3}{2N^3}}\exp\left(\frac{J^2}{2N}\right)\left(1-e^{-\frac{J^2}{N}}\right)^{-\frac{1}{2}}e^{-\frac{r}{2}} = 1. \quad (2.4.26)$$

This has an exact solution in term of the W-function,

$$\frac{J_t^2}{N} = \frac{3}{2}W\left[\frac{2^{5/3}}{3}N\mathcal{R}^{8/3}\left(1-e^{-\frac{J_t^2}{N}}\right)^{\frac{2}{3}}e^{\frac{2r}{3}}\right]. \quad (2.4.27)$$

The argument of the W-function must be large, so we can again expand it in terms of logarithms. The factors of $(1-e^{-\frac{J^2}{N}})$ and $e^{\frac{2r}{3}}$ must be subleading, and so a short calculation shows that the threshold expands out to

$$\frac{J_t^2}{N} = \frac{3}{2}\log N + 4\log\mathcal{R} - \frac{3}{2}\log\left[\log N + \frac{8}{3}\log\mathcal{R}\right] + \frac{1}{2}\log\left(\frac{32}{27}\right) + o(1). \quad (2.4.28)$$

In this large N expansion of the threshold, we have the two parameters N and $\mathcal{R} \equiv \epsilon\Lambda$. If we take $\mathcal{R}$ to be large but independent of N, then it must become

subleading in the large N limit, and the threshold becomes

$$\frac{J_t^2}{N} = \frac{3}{2}\log N - \frac{3}{2}\log\log N + 4\log\mathcal{R} + \frac{1}{2}\log\left(\frac{32}{27}\right) + o(1) \tag{2.4.29}$$

$$\simeq \frac{3}{2}\log N. \tag{2.4.30}$$

Alternatively, we can allow the ratio $\mathcal{R}$ to grow large with N, by letting either the separation of the operators ϵ or the cutoff scale Λ grow with N. The $\log\mathcal{R}$ terms are subleading and the above expression still holds if $\mathcal{R}$ scales to infinity at a slower rate than a power of N. If $\mathcal{R}$ grows like a power of N, then it can influence the leading constant of the threshold, but it is still logarithmically dependent on N. In all these cases, the leading-order behaviour of the threshold is simply

$$J^2 = \mathcal{O}(N\log N), \tag{2.4.31}$$

as was the case for the extremal correlator.

The expansion of the threshold given in (2.4.29) tells us something new about the factorisation thresholds for non-extremal correlators. The $(4\log\mathcal{R})$ term, which did not appear in the extremal threshold, means that the threshold in the non-extremal case depends on the separation of the correlators in the boundary directions. If we considered a system at the threshold at fixed large N and fixed large $\mathcal{R}$, then a decrease in $\mathcal{R}$ will lead to an increase in $\Lambda^{-2}G_3$, and an increase in $\mathcal{R}$ will lead to a decrease in $\Lambda^{-2}G_3$. From the bulk AdS perspective, this means that we move from factorisation to breakdown when the gravitons are moved closer together in the boundary directions, perpendicular to the AdS radius.

2.4.3 $J_1 \neq J_2$

When J_1 and J_2 are not equal, but lie in the region $N^{\frac{1}{3}} \ll J_1 \leq J_2 \ll N^{\frac{2}{3}}$, then equation (2.4.24) has the solution

$$\frac{J_1 J_2}{N} = 2W\left[\sqrt{\frac{1}{4}\mathcal{R}^4 N(J_1+J_2)(1-e^{-\frac{J_1^2}{N}})e^r}\right]. \tag{2.4.32}$$

The form of the expansion of the W-function depends on the scaling behaviour of the smallest angular momentum with N, which we have chosen to be J_1. We consider separately three cases: J_1^2/N tends to zero, J_1^2/N tends to a constant, and J_1^2/N tends to infinity.

If $J_1^2/N \to 0$, then the leading terms in the expansion of the W-function are

$$\begin{aligned}\frac{J_1 J_2}{2N} &\simeq \frac{1}{2}\log\left[\frac{1}{4}\mathcal{R}^4 N(J_1+J_2)\frac{J_1^2}{N}\right] - \log\left[\frac{1}{2}\log\left[\frac{1}{4}\mathcal{R}^4 N(J_1+J_2)\frac{J_1^2}{N}\right]\right] + o(1)\\ &= \frac{1}{2}\log\left(\frac{J_1 N\mathcal{R}^4}{4}\right) + \log\left(1+\frac{J_1}{J_2}\right) + \log\left(\frac{J_1 J_2}{N}\right) - \log\left[\frac{1}{2}\log\left[\frac{1}{4}\mathcal{R}^4 N(J_1+J_2)\frac{J_1^2}{N}\right]\right]\end{aligned} \tag{2.4.33}$$

Plugging in $J_1 J_2/N$ into the third term, the log-log cancels and we have

$$\frac{J_1 J_2}{2N} = \frac{1}{2}\log\left(\frac{J_1 N\mathcal{R}^4}{4}\right) + \log\left(1+\frac{J_1}{J_2}\right) + \mathcal{O}(1). \tag{2.4.34}$$

Since $J_1 \leq J_2$, the second term is $\mathcal{O}(1)$, hence

$$\frac{J_1 J_2}{N} = \log(J_1 N) + 4\log\mathcal{R} + \mathcal{O}(1). \tag{2.4.35}$$

If J_1^2/N tends to a constant at large N, then the expansion becomes

$$\frac{J_1 J_2}{2N} \;=\; \frac{1}{2}\log\left[\frac{\mathcal{R}^4 N}{4}(J_1+J_2)\right] \;+\; c \;-\; \log\left[\frac{1}{2}\log\left[\frac{\mathcal{R}^4 N}{4}(J_1+J_2)\right]+c\right] \;+\; o(1), \tag{2.4.36}$$

where c is some constant (order 1 with respect to N). Hence

$$\frac{J_1 J_2}{N} = \log((J_1+J_2)N) + 4\log\mathcal{R} - \log\log((J_1+J_2)N) + \mathcal{O}(1). \tag{2.4.37}$$

If J_1^2/N tends to infinity with N, then the above equation also holds but with c replaced by zero.

We can collate these three cases into a single equation by taking the leading scaling-behaviour of J_1 to be fixed, i.e. assuming $J_1 = N^{\alpha_1} e^{\delta_1}$ for subleading δ_1 and constant α_1. The threshold can then be written in all cases as

$$\frac{J_1 J_2}{N} = (1+\alpha_1)\log N + 4\log\mathcal{R} + o(\log N). \tag{2.4.38}$$

As in the extremal case, decreasing the difference between the angular momenta $\Delta J = |J_2 - J_1|$ will move the correlator from the threshold to the breakdown region. In addition, from the structure of the correlator in (2.4.24), it is clear that decreasing $\mathcal{R}$ while fixing N, J_1, and J_2 will move the correlator from the threshold to the breakdown

region. From the bulk AdS point of view, non-extremal correlators correspond to the interactions of Kaluza-Klein gravitons with angular momenta in perpendicular directions in the S^5. We can move from the threshold to the breakdown region by moving the gravitons closer together in the boundary directions, or by decreasing the separation in the graviton energies.

2.5 Multi-gravitons and non-trivial backgrounds

In the previous sections we have studied in detail the thresholds of some simple extremal and non-extremal three-point functions. In this section we briefly discuss two other examples of extremal correlators for which we have found explicit expressions of the threshold: a correlator corresponding to a $(k+1)$-graviton system, and a correlator corresponding to gravitons in an LLM background. We find a very similar form of the thresholds to the previous examples in both cases. In the future, developing the tools to calculate more general correlators in the half-BPS sector could give us more insight into general properties of thresholds, and thus also shed light on the behaviour of high-momentum graviton systems in supergravity.

2.5.1 The $(k+1)$-graviton correlator

We can calculate the extremal correlator associated to k gravitons scattering into a single graviton,

$$\langle\langle\prod_{i=1}^{k}(\mathrm{tr}Z^{J_i})\mathrm{tr}Z^{\dagger\sum J_i}\rangle\rangle \tag{2.5.1}$$

and take the large dimensions limit using similar techniques. We find that the correlator evaluates to

$$\langle\prod_{i=1}^{k}(\mathrm{tr}Z^{J_i})\mathrm{tr}Z^{\dagger J}\rangle = J!\sum_{t=0}^{k}\sum_{\substack{S\subseteq\{1,\ldots,k\}\\|S|=t}}(-)^{k-t}\binom{N+\sum_{i\in S}J_i}{J+1}, \tag{2.5.2}$$

where the sum is performed over all subsets of the k-element set $\{1,2,\ldots,k\}$, and $J=\sum_i J_i$. An outline of the derivation of this result is given in Appendix D.

In this section, we we derive the asymptotic form of the $(k+1)$-point function (2.5.2). Assuming that $J_i \ll N^{\frac{2}{3}}$ and that Λ is some sum of the J_i, we have from

Section 2.2

$$J!\binom{N+\Lambda}{J+1} \simeq \frac{N^{J+1}}{J}\exp\left(\frac{J(2\Lambda-J)}{2N}-\mathcal{O}\left(\frac{J^3}{N^2}\right)\right). \tag{2.5.3}$$

We can then write (2.5.2) as

$$\begin{aligned}\langle\prod_{i=1}^{k}(\mathrm{tr}Z^{J_i})\mathrm{tr}Z^{\dagger J}\rangle &\simeq \frac{N^{J+1}}{J}\sum_{S\subseteq\{1\ldots k\}}(-)^{k-|S|}e^{-\frac{J^2}{2N}+\mathcal{O}(J^3/N^2)}e^{\frac{J}{N}\sum_{i\in S}J_i}\\ &\simeq \frac{N^{J+1}}{J}e^{-\frac{J^2}{2N}+\mathcal{O}(J^3/N^2)}(-)^k\sum_{S\subseteq\{1\ldots k\}}\prod_{i\in S}\left(-e^{\frac{J}{N}J_i}\right)\end{aligned} \tag{2.5.4}$$

We can evaluate this sum over subsets explicitly by first partitioning the sum into two; one sum over the subsets including the element k, and one over the subsets not including k. We can then apply this for each integer from 1 to k. We have

$$\begin{aligned}\sum_{S\subseteq\{1\ldots k\}}\prod_{i\in S}\left(-e^{\frac{J}{N}J_i}\right) &= \left(-e^{\frac{J}{N}J_k}\right)\sum_{S\subseteq\{1\ldots k-1\}}\prod_{i\in S}\left(-e^{\frac{J}{N}J_i}\right)+1\sum_{S\subseteq\{1\ldots k-1\}}\prod_{i\in S}\left(-e^{\frac{J}{N}J_i}\right)\\ &= (-e^{\frac{J}{N}J_1}+1)(-e^{\frac{J}{N}J_2}+1)\ldots(-e^{\frac{J}{N}J_k}+1).\end{aligned} \tag{2.5.5}$$

Taking out a factor of $e^{J^2/N}$ from this product, we have the asymptotic form of the unnormalised correlator,

$$\langle\prod_{i=1}^{k}(\mathrm{tr}Z^{J_i})\mathrm{tr}Z^{\dagger J}\rangle \simeq \frac{N^{J+1}}{J}\exp\left(\frac{J^2}{2N}+\mathcal{O}\left(\frac{J^3}{N^2}\right)\right)\prod_{i=1}^{k}\left(1-e^{-\frac{JJ_i}{N}}\right). \tag{2.5.6}$$

Together with the known asymptotic form of the 2-point function

$$\langle\mathrm{tr}Z^{J_i}\mathrm{tr}Z^{\dagger J_i}\rangle \simeq \frac{N^{J_i+1}}{J_i}e^{\frac{J_i^2}{2N}}\left(1-e^{-\frac{J_i^2}{N}}\right), \tag{2.5.7}$$

we can therefore write the full correlator in the large J, small J^3/N^2 limit,

$$\begin{aligned}\langle\langle\prod_{i=1}^{k}(\mathrm{tr}Z^{J_i})\mathrm{tr}Z^{\dagger J}\rangle\rangle &\simeq \sqrt{\frac{J_1\ldots J_k}{JN^{k-1}}}e^{\frac{J^2}{4N}-\frac{J_1^2}{4N}-\ldots-\frac{J_k^2}{4N}}\frac{\prod_{i=1}^{k}(1-e^{-JJ_1/N})}{\sqrt{(1-e^{-J^2/N})\prod_{i=1}^{k}(1-e^{-J_1^2/N})}}\\ &\simeq \sqrt{\frac{J_1\ldots J_k}{JN^{k-1}}}\frac{(1-e^{-\frac{JJ_1}{N}})\ldots(1-e^{-\frac{JJ_k}{N}})}{\sqrt{(1-e^{-\frac{J_1^2}{N}})\ldots(1-e^{-\frac{J_k^2}{N}})(1-e^{-\frac{J^2}{N}})}}\exp\left(\sum_{i<j}\frac{J_iJ_j}{2N}+\mathcal{O}\left(\frac{J^3}{N^2}\right)\right).\end{aligned} \tag{2.5.8}$$

In the regime where all $J_i \ll N^{\frac{2}{3}}$ for all $i = 1, 2, \dots k$, then the correlator is asymptotic to

$$\sqrt{\frac{J_1 \dots J_k}{N^{k-1} \sum_i J_i}} \frac{(1 - e^{-\frac{J_1 \sum J_i}{N}}) \dots (1 - e^{-\frac{J_k \sum J_i}{N}})}{\sqrt{(1 - e^{-\frac{J_1^2}{N}}) \dots (1 - e^{-\frac{J_k^2}{N}})(1 - e^{-\frac{(\sum J_i)^2}{N}})}} \exp\left(\sum_{i<j} \frac{J_i J_j}{2N}\right). \quad (2.5.9)$$

The factors in front of the exponential tend to zero as a power of N when $1 \ll J_i \ll N^{\frac{2}{3}}$. If *all* pairs of dimensions satisfy $J_i J_j \lesssim N$, then the exponential term is small, and the correlator decays to zero. However, if *any* pair of distinct dimensions satisfy $J_i J_j \geq N^{1+\delta}$ for some $\delta > 0$, then the exponential term dominates any power of N, and so the correlator tends to infinity. We can deduce that the factorisation threshold when $G_3 = 1$ should be located when the product of the largest two operators grows logarithmically larger than N:

$$J_i J_j = \mathcal{O}(N \log N). \quad (2.5.10)$$

In the case when all the J_i are taken to be equal to J, then we can solve the threshold explictly at leading order. The correlator for $N^{\frac{1}{2}} < J < N^{\frac{1}{2}+\delta}$ is asymptotically

$$G_{k+1} \simeq \sqrt{\frac{J^{k-1}}{kN^{k-1}}} \exp\left(\frac{k(k-1)}{4} \frac{J^2}{N}\right), \quad (2.5.11)$$

and the leading-order terms in the expansion of the threshold satisfying $G_{k+1}(J_t(N), N) = 1$ are

$$J_t^2 = \frac{N}{k}\left[\log N - \log\log N + \left(\frac{k+1}{k-1}\right)\log k + o(1)\right]. \quad (2.5.12)$$

This can be interpreted as saying that as the number of gravitons *increases*, the region in which factorisation holds *shrinks*. When more gravitons are added to a system, they will start behaving like a single particle located further away from the boundary.

2.5.2 Factorisation thresholds for large backgrounds

Thresholds of factorisation can be considered in more general half-BPS bulk backgrounds, specified in the dual description by Schur Polynomials. For a background described by a Young tableau B with n boxes, the associated Schur polynomial χ_B is

a $U(N)$ character [25],

$$\chi_B(Z) = \frac{1}{n!}\sum_{\sigma\in S_n}\chi_B(\sigma)\mathrm{tr}(\sigma Z^{\otimes n}). \tag{2.5.13}$$

The CFT state corresponding to such a background is $|B\rangle = \chi_B(Z^\dagger)|0\rangle$, and the operator in this background are defined by [75]

$$\langle \mathcal{O}\dots\mathcal{O}\rangle_B = \frac{\langle B|\mathcal{O}\dots\mathcal{O}|B\rangle}{\langle B|B\rangle}. \tag{2.5.14}$$

This gives us the definition of a three-particle normalised correlator in the state,

$$\begin{aligned} G_3(J_1,J_2;N,M)_B &= \frac{\langle \mathrm{tr}Z^{J_1}\mathrm{tr}Z^{J_2}\mathrm{tr}Z^{\dagger J_1+J_2}\rangle_B}{\sqrt{\langle \mathrm{tr}Z^{J_1}\mathrm{tr}Z^{\dagger J_1}\rangle_B\langle \mathrm{tr}Z^{J_2}\mathrm{tr}Z^{\dagger J_2}\rangle_B\langle \mathrm{tr}Z^{J_1+J_2}\mathrm{tr}Z^{\dagger J_1+J_2}\rangle_B}} \\ &= \sqrt{\langle B|B\rangle}\frac{\langle B|\mathrm{tr}Z^{J_1}\mathrm{tr}Z^{J_2}\mathrm{tr}Z^{\dagger J_1+J_2}|B\rangle}{\sqrt{\langle B|\mathrm{tr}Z^{J_1}\mathrm{tr}Z^{\dagger J_1}|B\rangle\langle B|\mathrm{tr}Z^{J_2}\mathrm{tr}Z^{\dagger J_2}|B\rangle\langle B|\mathrm{tr}Z^{J_1+J_2}\mathrm{tr}Z^{\dagger J_1+J_2}|B\rangle}}. \end{aligned} \tag{2.5.15}$$

One of the easiest ones backgrounds in which to perform the threshold calculation is the background corresponding to a large rectangular Young diagram with N rows of length M, where M is of the same order as N. In [75], it was shown by performing manipulations of Schurs that the large rectangular background modifies the normalised correlator by shifting the matrix rank parameter from N to $M+N$. That is, we have

$$\begin{aligned} G_3(J_1,J_2;N,M)_B &= \left[\frac{\langle \mathrm{tr}Z^{J_1}\mathrm{tr}Z^{J_2}\mathrm{tr}Z^{\dagger J_1+J_2}\rangle}{\sqrt{\langle \mathrm{tr}Z^{J_1}\mathrm{tr}Z^{\dagger J_1}\rangle\langle \mathrm{tr}Z^{J_2}\mathrm{tr}Z^{\dagger J_2}\rangle\langle \mathrm{tr}Z^{J_1+J_2}\mathrm{tr}Z^{\dagger J_1+J_2}\rangle}}\right]_{N\to N+M} \\ &= G_3(J_1,J_2,N+M). \end{aligned} \tag{2.5.16}$$

Hence, the correlator in a large rectangular background only differs from the normalised correlator in that the argument N is replaced by $N+M$. This means that, in this background, the threshold of factorisation is at

$$J_1J_2 \sim (N+M)\log(N+M). \tag{2.5.17}$$

We interpret this as evidence that the presence of a background can *increase* the size of the region in which factorisation is valid.

2.6 Discussion

We have undertaken a detailed study, via gauge theory calculations, of the thresholds where multi-particle Kaluza-Klein gravitons have order one correlations at large N with single gravitons. The angular momenta of the gravitons in $AdS_5 \times S^5$ must grow large with N for the correlator to approach the threshold, and the precise form of this growth was worked out in several cases. The large N growth at the threshold region for the case of two gravitons of angular momentum J being correlated with a single graviton of angular momentum $2J$ is $J \sim \sqrt{N \log N}$. The breakdown of factorisation is a breakdown of the usual perturbative scheme for computing graviton interactions in spacetime, which relies on a multi-graviton Fock space with states of different particle number being orthogonal. In this usual framework, the mixing between different particle numbers arises in $1/N$ corrections which are suppressed at large N for small enough J. We have found quantitative description of several factors which can move a correlator from the regime factorisation to the threshold, such as:

- Increasing the total energy of the gravitons,
- Decreasing the separation in the energies of the two gravitons,
- Decreasing the separation of gravitons in the boundary directions,
- Increasing the number of gravitons.

Another qualitative outcome of interest is that for k gravitons being correlated with a single graviton, the threshold can be expressed in terms of the two largest momenta among the k gravitons, taking the form $J_i J_j \sim N \log N$. In these investigations, we have found a rich variety of applications of the Lambert W-function. We have seen intriguing similarities between asymptotic threshold equations and running gauge couplings in non-abelian gauge theories. The large N approximations have also involved transseries of the kind seen in instanton-corrected perturbation expansions of quantum field theory.

We also investigated the factorisation thresholds in the presence of LLM backgrounds associated with rectangular Young diagram backgrounds. The presence of these backgrounds *increases* the region of graviton momenta that are consistent with factorisation. There are indications that triangular Young diagrams can be used to model thermal black hole-like backgrounds [81]. We expect that, in the presence of black holes, the regime of validity of effective field theory should be smaller than in the

absence of black holes. This would suggest that factorisation in triangular Young diagram backgrounds should occur in a more limited regime of graviton angular momenta than factorisation in the vacuum. This is a very concrete problem in the combinatorics of CFT correlators, and an interesting research direction for the future.

In the study of factorisation thresholds, we have consistently found thresholds when the angular momenta are of the form $J_i J_j \sim N \log N$, which suggests that there is some form of *universality* of the threshold. An interesting future direction would be to consider the thresholds calculated in the 'overlap-of-states' norm from [24, 82], as opposed to the 'multiparticle' norm used in this thesis. In the overlap normalisation, the correlators are bounded by one from above and cannot grow exponentially with N, but they may well tend to a finite non-zero constant at large N if their angular momenta grow quickly enough. We could define a threshold in the overlap normalisation as the surface where a correlator is equal to some fixed constant between zero and one. Evidence from shifting the factorisation threshold at the end of Section 2.2.3 suggests that the form of the threshold will not change when going to the overlap norm, and will remain $J^2 \sim N \log N$. This is another interesting problem for the future that involves non-trivial asymptotics of finite N CFT correlators, and could well provide further evidence for the universality of the $N \log N$ threshold.

In Section 2.4 we showed how the 'near-extremal' correlator has a threshold which depends on the separation of the CFT insertions in the 4d spacetime directions, as well as exhibiting the dependences on total energy and energy differences of the corresponding gravitons. We considered two gravitons in AdS with angular momenta $(J_3, J_1), (-J_3, J_2)$ where the first entry refers to the Y-plane and the second to the Z-plane. We studied the correlation with a single graviton with angular momenta $(J_1 + J_2, 0)$. The explicit calculations were done for $J_3 = 1$, with J_1, J_2 growing with N. A generalisation to the case of J_3 also growing with N would be very interesting, as it would show the effect on the quantum correlations at threshold between two gravitons and a single graviton, when the two gravitons annihilate a large amount of Y-momentum and the correlator is no longer near-extremal.

We hope to have convinced the reader that the theme of thresholds between different behaviours is a fruitful way to explore the bulk AdS physics encoded in the correlators of the CFT. Since the string coupling parameters are related as

$$\frac{1}{N} = g_s \frac{l_s^4}{R^4} \tag{2.6.1}$$

for fixed R/l_s, finite N is finite string coupling, and is non-perturbative from the point of view of strings in the bulk spacetime. Hence, finite N calculations in CFT contain valuable information about strongly quantum gravitational effects. The generic $J_iJ_j \sim N \log N$ we found, which in spacetime variables is

$$J_iJ_j \sim N \log N = \left(\frac{R^4}{g_s l_s^4}\right) \log \left(\frac{R^4}{g_s l_s^4}\right), \tag{2.6.2}$$

is an intriguing result that should be understood better from the bulk point of view, either from a first principles string calculation in $AdS_5 \times S^5$ or from a phenomenological model of quantum gravitational spacetime constructed to reproduce the CFT result. As we observed, the threshold corresponds to a region where the Fock space of spacetime field modes breaks down. The broader issue of the breakdown of perturbative effective field theory is central to questions in black hole physics [74, 83, 84]. In particular, black hole complementarity is related to the structure of Hilbert spaces needed to describe infalling observers and outgoing radiation. We propose that a convincing spacetime understanding of the thresholds derived here would be a highly instructive step in understanding the departures from effective field theory in quantum gravity. Insights from earlier work on bulk spacetime in AdS in connection with gauge-string duality, such as in [85, 86], might be useful. Alternatively, the methods of collective field theory [87] could help with a derivation of the large N effective field theory. Another possible approach towards better understanding the thresholds from the spacetime point of view would be to make use of a combination of semi-classical tools, exploiting high energy eikonal approximations or physical effects such as the tidal stretching of high energy gravitons into strings, for example along the lines of [88, 89].

The study of Schur operators as the description of giant gravitons was motivated by the observed departure from orthogonality between multi-graviton and single graviton states at large J [24]. Schur operators give a weakly-coupled description of giant gravitons in the regime of $J \sim N$, but become strongly-interacting as J is decreased [68]. In this chapter, we have focused on the approach to the threshold in the regime near $J \sim \sqrt{N}$ by studying single and multi-trace graviton operators. It would be very interesting to study thresholds between weak and strong interactions in giant graviton physics as the angular momenta are decreased from $J \sim N$. The detailed investigations of the one-loop and multi-loop dilatation operators around giant graviton backgrounds should provide useful data for this purpose [90, 91, 92].

The fact that the thresholds are near $\sqrt{N}$ rather than $N^{1/4}$ is rather intriguing. This has been discussed in [68]. Angular momenta of $J \sim N^{1/4}$ correspond to momenta comparable to the ten-dimensional Planck scale. This may be a sign that $AdS_5 \times S^5$ physics is just very different from expectations derived from effective field theory in flat space $\mathbb{R}^{9,1}$. On the other hand, it could be that a clever interpretation of the link between the extremal correlators and flat space scattering would account for the thresholds we see from the CFT. Potentially, the correct interpretation has to recognise that extremal correlators correspond to collinear graviton scatterings. We would need to consider the flat space expectations in the light of collinear effective theories of gravitons, along the lines developed in [93], to understand the difference between the threshold scale and the Planck scale. An early discussion of the subtleties of connecting bulk AdS spacetime physics to the flat space limit is given in [94].

There is a great deal of quantitative information about graviton correlations at the factorisation threshold which is available via finite N CFT computations and their large N asymptotics. The lessons we draw from these are very likely to be important for questions we would like to answer in black hole physics and quantum gravity.

Chapter 3

The light-cone cell decomposition of moduli space

Moduli spaces of Riemann surfaces appear in the ranges of integration for bosonic string amplitudes. Distinct points in the same moduli space correspond to inequivalent Riemann surfaces with the same topology and number of punctures. However, moduli spaces are very difficult to describe explicitly in all but the simplest cases, where the Riemann surfaces have low genus and few punctures.

A detailed understanding of moduli spaces is fundamental both in pure mathematics and in string theory. The aim of this chapter is to develop the understanding of moduli spaces via the *light-cone cell decomposition* of Giddings, Wolpert, and Nakamura [30, 31]. In the light-cone cell decomposition, each cell is associated to a particular type of ribbon graph embedded on the surface, which we call a *Nakamura graph*. We undertake a systematic study of Nakamura graphs and their associated cells by introducing a description of the graphs in terms of equivalence classes of permutation tuples. These tuples precisely describe the structure of the cells in moduli space, their boundaries, and their automorphism groups. We use this tuples description to develop powerful computational tools to catalogue Nakamura graphs, and demonstrate this approach by finding the orbifold Euler characteristic of the moduli spaces $\mathcal{M}_{g,n}$ with $(2g-2+n) \leq 7$.

The outline of this chapter is as follows. In Section 3.1, we start by recalling the properties of the Giddings-Wolpert differential and explaining how Nakamura associated a graph to each differential. The Giddings-Wolpert differential of a surface is a meromorphic one-form with purely imaginary periods and residues at the punctures which sum up to zero. The Nakamura graph associated to the surface has vertices at the poles and zeroes of the differential, and edges on the real trajectories extending from the zeroes. We introduce some parameters to describe the graphs and their as-

sociated cells in the light-cone cell decomposition. We review an alternative definition of moduli space, which was used in [31], describing the equivalence classes of Riemann surfaces in which some of the punctures may be permuted.

In Section 3.2, we develop a new permutation description of Nakamura graphs by considering branched covering maps from the worldsheet onto the Riemann sphere. The branching determines a Hurwitz class associated to the graph, and the ramification points correspond to vertices of the graph. Each Hurwitz class determines a unique Nakamura graph, but there can be multiple Hurwitz classes corresponding to a given Nakamura graph. To solve this redundancy, we introduce an equivalence relation on the space of Hurwitz classes which we call *slide-equivalence*. There is a one-to-one correspondence between slide-equivalence classes and Nakamura graphs. These Hurwitz classes and slide-equivalence classes describe cells in the moduli space of Riemann surfaces in which the punctures on the surfaces can be permuted. To describe cells in the moduli space with fixed punctures, we introduce *split tuples* which encode a labelling of the punctures.

In Section 3.3 we explain how the permutation tuples can be used to generate the cells in moduli space explicitly. The faces of a Nakamura graph are holomorphic to strips in the complex plane. Each of the d strips has a width b_j, and each of the l zeroes has a time coordinate t_k, and so a point in the cell is determined by a point in $\mathbb{R}^{d+l}$. These parameters are constrained by the residues of the poles and the time-ordering of the zeroes determined by the graph, forming a $(d + l - n)$-dimensional subset. These constraints, and the automorphism group of the graph, can be read off from the permutation tuple. This approach also shows how the automorphism group of the graph acts on the parameter space, which gives the orbifold quotienting of the cell explicitly. The boundaries of this cell can be found from the tuple, corresponding to the collapse of a strip or the merging of a pair of interaction points. We show how this procedure works for some simple examples of low-dimensional moduli spaces. The cell decomposition of moduli space is preserved by the action of the mapping class group; we demonstrate this in Section 3.4 by extending the cell decomposition to a cell decomposition of Teichmüller space.

In Section 3.5 we discuss the orbifold Euler characteristic of moduli space. This was used by Nakamura as a method of verifying that the graphs gave a cell decomposition. We explore some links between the counting of cells in the moduli space and the correlators of matrix models. Cells of top dimension in the light-cone cell decomposition are specified by Nakamura graphs with simple zeroes and no internal edges, i.e. graphs where all zeroes have valency four and connect only to the poles.

Within the slide-equivalence class of a top-dimensional graph, there is a unique Hurwitz class consisting of a tuple of three permutations, which naturally corresponds to a Belyi map. This allows us to use known exact results from Hermitian matrix model correlators [34] to obtain all-orders analytic formulae for the contribution to the Euler characteristic from the top-dimensional cells. These results agree with the tables given by Nakamura for small g and n. We can also consider cells with lower dimension corresponding to graphs with no internal edges In this case, we can use complex matrix models to derive analytic formulae for the contributions to the Euler characteristic from lower-dimension cells. We conclude this section by briefly discussing our computational approach to testing the validity of the light-cone cell decomposition. Using the group theory software GAP, we were able to reproduce and extend the tables of cells, dimensions, and automorphism groups found in [31]. The full details of the algorithm are presented in Appendix F. We conclude this chapter with some discussion of our results and future applications.

3.1 Nakamura graphs

The key aim of this chapter is to develop a cell decomposition of the moduli space of Riemann surfaces by using a family of graphs which we call *Nakamura graphs*. In this section, we introduce the definition of Nakamura graphs via the Giddings-Wolpert differential on a Riemann surface, and discuss their properties and parameters. More discussion and definitions of moduli spaces of Riemann surfaces are given in Appendix E.

3.1.1 Giddings-Wolpert differentials

Consider a Riemann surface X with n distinguished labelled points $P_1, P_2, \ldots, P_n$ and genus g, where $n \geq 2$. Associate a set of real numbers $r_1, r_2, \ldots r_n$ respectively to the n labelled points, which satisfy $\sum_i r_i = 0$. Giddings and Wolpert proved in [30] that there exists a unique abelian differential ω on the Riemann surface X such that ω has n simple poles at the points P_i with respective residues r_i and pure imaginary periods on any closed integral on the surface. This is the **Giddings-Wolpert** differential of the surface. This differential restricts to a holomorphic differential on $\hat{X}$, the punctured Riemann surface with the n labelled points removed.

The Giddings-Wolpert differential yields a global time coordinate on the Riemann surface X, up to an overall constant representing the time translation symmetry. If we

fix a point z_0 on the surface which is not a pole of ω, then we can define the global time coordinate of a generic point z on the surface to be $T := \mathrm{Re}(\int_{z_0}^{z} \omega)$. This expression does not depend on the choice of integration contour from z_0 to z, since any two paths from z_0 to z differ only by a closed contour, and the integral of the differential along any closed contour is imaginary. The global time coordinate tends to negative infinity as we approach the poles with positive residue, and to positive infinity as we approach the poles with negative residues. We call the poles with positive residue the **incoming poles**, and the poles with negative residue the **outgoing poles**.

For the cases of the sphere and the torus, it is not too difficult to construct the differential of a given marked surface and its time coordinate explicitly. Take a sphere with n marked points P_i and associated reals r_i, where $\sum_i r_i = 0$. We can choose coordinates z on the sphere such that the marked points P_i are located at $z = p_i$ for some $p_i \in \mathbb{C}$. In this chart, the Giddings-Wolpert differential can be explicitly written as

$$\omega(z; p_i) := \sum_{i=1}^{n} \frac{r_i dz}{z - p_i}. \tag{3.1.1}$$

It is clear that this differential has residue r_i at each point P_i. The integral of the differential along any closed contour $\mathcal{C}$ is $\oint_{\mathcal{C}} \omega = 2\pi i \sum_{P_i \in \mathcal{C}} r_i$, summed over the points P_i enclosed in the contour $\mathcal{C}$, and this integral is purely imaginary. The global time coordinate is

$$T(z) = \ln \left(\prod_i |z - p_i|^{r_i} \right) + T_0, \tag{3.1.2}$$

where T_0 is an arbitrary constant.

Now consider a torus with n marked points P_i, associated real values r_i with $\sum_i r_i = 0$, and modular parameter τ with $\mathrm{Im}(\tau) > 0$. This torus can be realised as the quotient of the complex plane $\mathbb{C}$ by the equivalence relation $z \sim z + n + m\tau$ for all integers n and m. In these coordinates, the marked points P_i are located respectively at $z = p_i$ for some $p_i = a_i + b_i\tau$, where $0 \leq a_i, b_i < 1$. To define the Giddings-Wolpert differential on this surface, we use the Jacobi theta function $\theta_{11}(z; \tau)$, which is a holomorphic quasi-periodic function on the complex z plane satisfying

$$\begin{aligned} \theta_{11}(z+1;\tau) &= \theta_{11}(z;\tau), & \theta_{11}(z+\tau;\tau) &= e^{-2\pi i(z+1/2)}\theta_{11}(z;\tau), \\ \theta_{11}(z;\tau+1) &= \sqrt{i}\theta(z;\tau), & \theta_{11}(z/\tau;-1/\tau) &= (-i)\sqrt{i\tau}e^{i\pi z^2/\tau}\theta_{11}(z;\tau), \end{aligned} \tag{3.1.3}$$

and behaves like $\theta_{11}(z;\tau) \approx z$ for small values of z. The differential on this surface is

$$\omega(z; p_i, \tau) := dz \sum_{i=1}^{n} r_i \left(-2\pi i \frac{\mathrm{Im}(p_i)}{\mathrm{Im}(\tau)} + \frac{\theta'_{11}(z-p_i;\tau)}{\theta_{11}(z-p_i;\tau)} \right), \tag{3.1.4}$$

and the associated global time coordinate on the surface is

$$T(z) = \sum_i r_i \left[2\pi \frac{\mathrm{Im}(p_i)}{\mathrm{Im}(\tau)} \mathrm{Im}(z) + \log|\theta_{11}(z-p_i;\tau)| \right] + T_0, \tag{3.1.5}$$

where T_0 is an arbitrary constant. It can be shown from the above properties and relations of the Jacobi theta function that $\omega(z;p_i)$ and $T(z)$ are well-defined on the torus, i.e. these definitions are invariant under the coordinate shifts $z \to z + m + n\tau$ and under the modular transformations $(\tau, p_i) \to (\tau+1, p_i)$, $(\tau, p_i) \to (-1/\tau, p_i/\tau)$. The integrals of the differential along the cycles $a : z \to z+1$ and $b : z \to z+\tau$ are imaginary, as are the integrals around each pole p_i, and so all periods of the differential are pure imaginary.

Formulae for Giddings-Wolpert differentials in terms of theta functions at genus one and higher can be found in recent work [95].

3.1.2 Graphs and strip decompositions

The Giddings-Wolpert differential associated to a marked Riemann surface naturally gives rise to an embedded ribbon graph on the surface. This construction was developed by Nakamura in [31], and leads to a cell decomposition of the moduli space of Riemann surfaces in which each cell is specified by a graph. In this subsection we review the basic properties of these graphs, which we call *Nakamura graphs*.

The Giddings-Wolpert differential ω has a set of zeroes $Q_1, \ldots, Q_l$, around which there exist complex coordinates z such that $\omega = d(z^{p+1})$ for some positive p. This integer p is the **order** of the zero: if $p = 1$, the zero is **simple**. For each point on the surface, there exists a finite set of directions in which z^{p+1} is real. These are the **real trajectories** that extend out from the point. There are two real trajectories extending out from a generic point on the surface, and $2(p+1)$ real trajectories extending out from a zero of order p. The real trajectories that extend out from the zeroes of the differential will only meet at the poles and zeroes of the differential.

The set of real trajectories extending out from all the zeroes of the differential defines a ribbon graph embedded onto the surface, with the vertices of the graph corresponding to the poles and zeroes of ω, and the edges of the graph corresponding

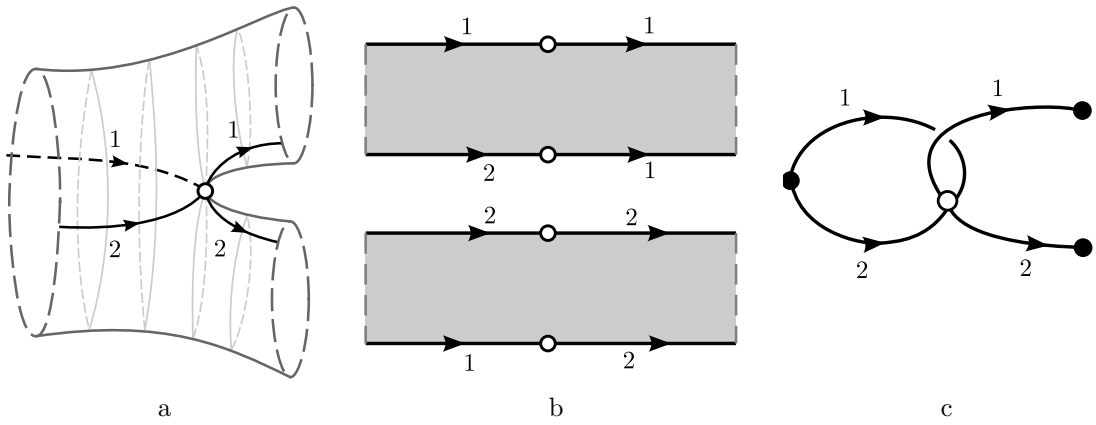

Figure 3.1: The real trajectories of a Giddings-Wolpert differential on a three-punctured sphere, the associated strip-decomposition, and the Nakamura graph.

to the real trajectories extending out from zeroes. The edges also inherit an orientation from the Giddings-Wolpert differential: they are oriented in the direction along which the global time coordinate increases. It was shown in [31] that this graph has the following properties:

- The graph is connected, oriented, and cyclically ordered at the vertices.
- The edges connecting to an incoming pole are all oriented away from the pole, and the edges corresponding to an outgoing pole are all oriented towards the pole.
- A zero connects to cyclically alternating incoming and outgoing edges, and has a valency of at least four.
- No edge connects to the same end point twice, and no edge has only poles as its end points.
- Every face of the ribbon graph contains on its boundary exactly two poles, one incoming and one outgoing.

The unique oriented graph $\mathcal{G}$ associated to the surface with labelled points and residues (X, P_i, r_i) is the **Nakamura graph** of the surface. We can also assign a labelling to the n poles of the graph, coming from the labelling of the points on the Riemann surface. This is the **pole-labelled Nakamura graph** $\bar{\mathcal{G}}$ of the surface.

Each face of the graph is bounded by two extended real trajectories of the differential. It is possible to choose local coordinates z on each face such that $\omega = dz$ within the face, with z in the range $0 < \mathrm{Im}(z) < b_j$ for some b_j. Each face of the

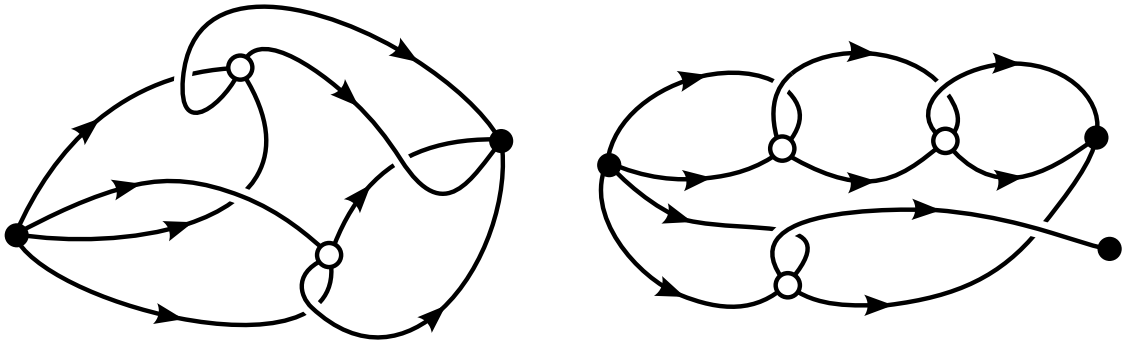

a b

Figure 3.2: Two examples of Nakamura graphs.

graph is holomorphic to a strip $\mathbb{R} \times (0, b_j)$ in the complex plane, and each strip has a width b_j which is determined by the differential. The zeroes of the differential lie on the boundaries of the strips. We can consistently choose complex coordinates on each strip such that the real coordinates of the zeroes on the boundary of the strip match the global time coordinates of the zeroes. The global time coordinates t_k of the zeroes Q_k are unique up to a simultaneous time translation of all the zeroes, $t_k \mapsto t_k + c$. This time-translation symmetry can be fixed by putting a constraint on the time coordinates, such as requiring that $\sum_k t_k = 0$. In this way, each punctured Riemann surface with residues $(\hat{X}, r_i)$ has a unique decomposition into strips via the Giddings-Wolpert differential, and with the gluing at the strip boundaries determined by the Nakamura graph. We call this the **strip decomposition** of the surface. The surface (X, P_i, r_i) with labelled points can be recovered from $\hat{X}$ by reintroducing points at $t = \pm\infty$ on the strips, corresponding to the poles of the Giddings-Wolpert differential.

An example of a Nakamura graph and a strip decomposition of a surface of genus zero with three punctures is given in Figure 3.1. In the first figure, the three boundary circles represent the removed points from the surface, taken to infinity, which correspond to the poles of the Giddings-Wolpert differential. The white vertices represent the zero of the differential. We label the graph edges by assigning the same label to all the edges on the upper boundary of a given strip. This graph decomposes the surface into two strips in the complex plane, which we have drawn in the second figure. The bounding edges with the same label *and the same real coordinate range* are identified. The third figure shows the Nakamura graph without an embedding into a surface. The black vertices represent the poles of the differential, which are at the labelled points of the surface. Two more examples of Nakamura graphs are given in Figure 3.2.

Once we have fixed a set of n residues r_i, then for each distinct Riemann surface

X with n labelled points there is a unique pole-labelled Nakamura graph $\bar{\mathcal{G}}$, set of strip widths b_j, and set of interaction times t_k, up to relabellings of the parameters. Alternatively, given a Nakamura graph $\bar{\mathcal{G}}$ and a consistent set of strip widths b_j and interaction times t_k, then we can uniquely reconstruct the associated Riemann surface by constructing and gluing together the holomorphic strips. For a given graph $\bar{\mathcal{G}}$, the set $C(\bar{\mathcal{G}})$ of Riemann surfaces with this graph can be parametrised by the admissible strip widths b_j and interaction times t_k. One of the main goals of this chapter is to specify the set $C(\bar{\mathcal{G}})$ explicitly for any Nakamura graph, and to show that the collection of all such $C(\bar{\mathcal{G}})$ gives a cell decomposition of the moduli space $\mathcal{M}_{g,n}$.

3.1.3 Parameters of Nakamura graphs

Using the properties of Nakamura graphs listed in the previous subsection, we can find bounds on the number of strips (faces) and zeroes (internal vertices) of any Nakamura graph of a given genus g and number of poles n. We can also set up relations on the valencies of the zeroes and the number of internal lines of the graph, which aids in the computational cataloguing of the graphs.

A Nakamura graph is a ribbon graph that can be embedded in a surface, and so has V vertices, E edges, and F faces. The V vertices are separated into l zeroes and n poles. All edges connect to zeroes, and no edge connects two poles together. We use the parameter d for the number of faces of the graph, as we will show that a graph with d faces is described by permutations in the symmetric group of degree d. There are exactly two poles on the boundary of each of the d faces of the graph, one incoming and one outgoing. Hence, there are d external edges of the graph connecting incoming poles to zeroes, d external edges connecting outgoing poles to zeroes, and I internal edges that connect only to zeroes. We have

$$\begin{aligned} V &= l + n, \\ E &= 2d + I, \\ F &= d. \end{aligned}$$

The Euler characteristic of a surface with an embedded graph is $2 - 2g = V - E + F$, which gives the relation

$$d + I - l = 2g - 2 + n. \tag{3.1.6}$$

We next consider the valencies of the vertices. As all faces have on their boundary

exactly one incoming pole, the valencies of the incoming poles sum up to d, and similarly for the outgoing poles. As the zeroes always border an equal number of incoming and outgoing edges, the valencies of the zeroes are always even. The zeroes are points at which at least two real trajectories meet, so the valency of a zero is always greater than four. We define the **branching number** Δ to be

$$\Delta = \sum_{k=1}^{l} \left[\left(\frac{v_k}{2} \right) - 2 \right], \tag{3.1.7}$$

where the v_j are the valencies of each of the l zeroes. The branching number is a non-negative integer for every Nakamura graph. This sum rearranges to

$$2\Delta + 4l = \sum_{k=1}^{l} v_k. \tag{3.1.8}$$

Now, adding the sum of the valencies of the poles to this equation give us the sum over the valencies of all vertices, which must equal twice the number of edges. We thus have

$$2\Delta + 4l + 2d = 2E = 2(2d + I), \tag{3.1.9}$$

and hence we have the relation

$$\Delta = d + I - 2l. \tag{3.1.10}$$

We can use (3.1.6) and (3.1.10) to find a bound on the number of faces d for Nakamura graphs of any genus g and number of poles n. Using the equations to eliminate l, we write

$$2(2g - 2 + n) - d = (\Delta + I). \tag{3.1.11}$$

The constants Δ and I are always non-negative integers, so d is bounded from above by d_{max}, where

$$\boxed{d_{\max} := 2(2g - 2 + n) = -2\chi.} \tag{3.1.12}$$

This is the maximum number of faces of a Nakamura graph of genus g with n fixed points. To find Nakamura graphs computationally, it is helpful to first fix the Euler characteristic $|\chi|$ and then to find all the graphs of genus g with n poles such that

$|\chi| = (2g - 2 + n)$.

We can eliminate the number of internal edges I from (3.1.6) and (3.1.10) to find a relation between the branching number Δ, the number of zeros l, and the Euler characteristic $|\chi|$:

$$\boxed{\Delta = |\chi| - l.} \tag{3.1.13}$$

As $\Delta \geq 0$, this equation gives us a bound on the number of zeroes of a Nakamura graph. Since a Nakamura graph always has at least one zero, we have the bounds on the number of zeros of a Nakamura graph,

$$\boxed{1 \leq l \leq |\chi|.} \tag{3.1.14}$$

The set $C(\bar{\mathcal{G}})$ of Riemann surfaces that have the pole-labelled Nakamura graph $\bar{\mathcal{G}}$ is parametrised by the widths of the d strips and the interaction times of the l zeroes. The widths $b_j^{(i)}$ of the strips bordering a given pole P_i satisfy a relation $\sum_j b_j^{(i)} = |r_i|$. These residue relations specify $(n-1)$ independent constraints on the strip widths, due to the overall constraint $\sum_{i=1}^{n} r_i = 0$. There are $(l-1)$ real coordinates parametrising the positions of the l zeroes, due to the overall time translation symmetry. This means that the real dimension of the set $C(\bar{\mathcal{G}})$ is $(l-1)+d-(n-1)$. In terms of the branching and internal edges, this can be written

$$\dim_{\mathbb{R}}(C(\bar{\mathcal{G}})) = l + d - n = 6g - 6 + 2n - (2\Delta + I). \tag{3.1.15}$$

For a given genus g and number of poles n, the dimension of the moduli space is $6g - 6 + 2n$, and so the *codimension* of $C(\bar{\mathcal{G}})$ in moduli space is

$$\dim_{\mathbb{R}}(\mathcal{M}_{g,n}) - \dim_{\mathbb{R}}(C(\bar{\mathcal{G}})) = 2\Delta + I. \tag{3.1.16}$$

The structure of this set $C(\bar{\mathcal{G}})$ is discussed in more depth in Section 3.3.1.

3.1.4 Alternative definitions of moduli space

There are two distinct notions of the moduli space of Riemann surfaces discussed in [31], corresponding to the more conventional definition of moduli space $\mathcal{M}_{g,n}$, and a modified version of moduli space $\mathcal{M}_{g,1[n-1]}$. The former is the set of equivalence classes of Riemann surfaces of genus g with n labelled points under biholomorphisms which preserve the labelling of the points. The latter is the set of equivalence classes

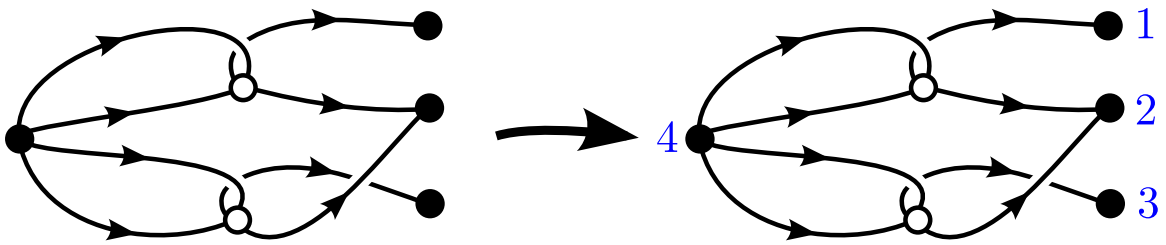

Figure 3.3: A Nakamura graph and a pole-labelled Nakamura graph.

under biholomorphisms which can permute the first $(n-1)$ labelled points. The more conventional moduli space $\mathcal{M}_{g,n}$ is more commonly-used in the literature, but the modified moduli space $\mathcal{M}_{g,1[n-1]}$ is simpler to work with computationally, as its cell decomposition is much coarser than that of $\mathcal{M}_{g,n}$.

We are free to choose any values for the residues r_i of the poles, so in the following we set exactly one of the residues r_n to be positive, and the remaining residues $r_1, \ldots, r_{n-1}$ to be negative. The corresponding Nakamura graphs will have one incoming pole and $(n-1)$ outgoing poles. When considering Nakamura graphs corresponding to cells in $\mathcal{M}_{g,1[n-1]}$, we must also set the negative residues to be equal: $r_1 = r_2 = \ldots = r_{n-1}$.

There are two notions of graph automorphisms given in [31]: the pole-permuting automorphisms, and the pole-fixing automorphisms. The automorphism group $\mathrm{Aut}(\mathcal{G})$ is the group of bijective mappings of the unlabelled graph $\mathcal{G}$ to itself which preserves the structure of the graph. Graph automorphisms preserve the orientation of the edges, and so map incoming poles to incoming poles and outgoing poles to outgoing poles, but may permute the poles in general. The automorphism group $\mathrm{Aut}_{\mathrm{fix}}(\mathcal{G})$ is the subgroup of $\mathrm{Aut}(\mathcal{G})$ consisting of the automorphisms which fix each pole separately.

Moduli spaces are orbifolds, and any cell in a cell decomposition of an orbifold is homeomorphic to a subset of $\mathbb{R}^k$ modulo a finite group. We will show explicitly in later sections that the automorphism group of a graph corresponds to the orbifold quotienting group of the cell in moduli space. The orbifold groups of the cells in $\mathcal{M}_{g,1[n-1]}$ correspond to the pole-permuting automorphism groups $\mathrm{Aut}(\mathcal{G})$, and the orbifold groups of the cells in $\mathcal{M}_{g,n}$ correspond to the pole-fixing automorphism groups $\mathrm{Aut}_{\mathrm{fix}}(\mathcal{G})$. Cells in $\mathcal{M}_{g,n}$ are naturally described by graphs with a labelling on the poles, and cells in $\mathcal{M}_{g,1[n-1]}$ are described by graphs with no labelling on the poles.

Let $\mathcal{G}$ be a graph with one incoming pole and $(n-1)$ outgoing poles, and let $\bar{\mathcal{G}}$ be the same graph with the labelling $\{1, 2, \ldots, n-1\}$ assigned to the outgoing poles, and

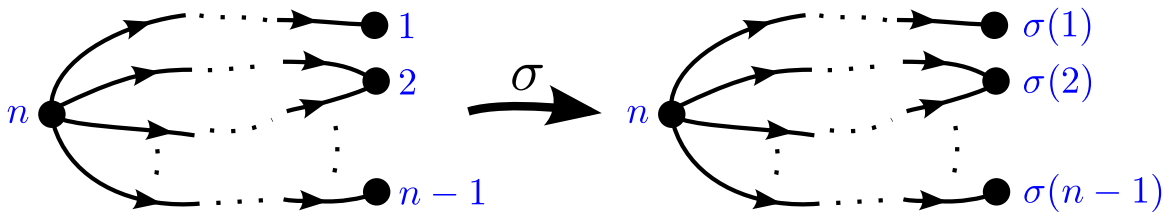

Figure 3.4: An element $\sigma \in S_{n-1}$ relabels the outgoing poles of a labelled graph $\bar{\mathcal{G}}$.

the label n assigned to the incoming pole. The automorphisms $\mathrm{Aut}(\mathcal{G})$ will permute these integer labels in general, while the automorphisms in $\mathrm{Aut}_{\mathrm{fix}}(\mathcal{G})$ will fix these labels. We define the automorphism group of a pole-labelled graph to be the pole-fixing automorphisms of the corresponding unlabelled graph $\mathrm{Aut}(\bar{\mathcal{G}}) = \mathrm{Aut}_{\mathrm{fix}}(\mathcal{G})$. An example of a pole-labelling of a graph is given in Figure 3.3.

The action of an automorphism $g \in \mathrm{Aut}(\mathcal{G})$ on a labelled graph $\bar{\mathcal{G}}$ permutes the poles of the graph, and so corresponds to a permutation in S_{n-1}. This gives a homomorphism

$$\begin{aligned} \phi : \mathrm{Aut}(\mathcal{G}) &\to S_{n-1} \\ g &\mapsto \kappa_g. \end{aligned} \tag{3.1.17}$$

The kernel of this homomorphism is the subgroup $\mathrm{Aut}_{\mathrm{fix}}(\mathcal{G})$. By the isomorphism theorem, the image of this homomorphism is isomorphic to the quotient group

$$H := \mathrm{Aut}(\mathcal{G})/\mathrm{Aut}_{\mathrm{fix}}(\mathcal{G}) \cong \mathrm{Im}(\phi) \subset S_{n-1}. \tag{3.1.18}$$

We can count the number of possible pole-labelled graphs $\{\bar{\mathcal{G}}\}$ corresponding to an unlabelled graph $\mathcal{G}$ as follows. An arbitrary element $\sigma \in S_{n-1}$ acts on a labelling $\bar{\mathcal{G}}$ of $\mathcal{G}$ by replacing the label i with $\sigma(i)$, as in Figure 3.4. The set of all such labelled graphs are all the possible labellings of the graph $\mathcal{G}$ with the label n assigned to the incoming pole. However, a pair of labellings $\bar{\mathcal{G}}$ and $\sigma(\bar{\mathcal{G}})$ are indistinguishable labellings of the same graph $\mathcal{G}$ if there is some (in general pole-permuting) graph automorphism $g \in \mathrm{Aut}(\mathcal{G})$ that acts on $\bar{\mathcal{G}}$ in such a way that $g(\bar{\mathcal{G}}) = \sigma(\bar{\mathcal{G}})$. This g is unique up to a pole-fixing automorphism $g_{\mathrm{fix}} \in \mathrm{Aut}_{\mathrm{fix}}(\mathcal{G})$, as $g \circ g_{\mathrm{fix}}(\bar{\mathcal{G}}) = g(\bar{\mathcal{G}})$. We see that $\sigma \in S_{n-1}$ does not generate a distinct labelling of $\bar{\mathcal{G}}$ if and only if σ is an element of $\mathrm{Aut}(\mathcal{G})/\mathrm{Aut}_{\mathrm{fix}}(\mathcal{G})$. This means that there is a one-to-one correspondence between the distinct labellings of $\mathcal{G}$ and the cosets S_{n-1}/H. The order of H is $|\mathrm{Aut}(\mathcal{G})|/|\mathrm{Aut}_{\mathrm{fix}}(\mathcal{G})|$,

so there are

$$(n-1)!\frac{|\mathrm{Aut}_{\mathrm{fix}}(\mathcal{G})|}{|\mathrm{Aut}(\mathcal{G})|} \tag{3.1.19}$$

distinct labelled graphs $\{\bar{\mathcal{G}}\}$ corresponding to a Nakamura graph $\mathcal{G}$.

In later sections, we will show that the unlabelled graphs give a cell decomposition of $\mathcal{M}_{g,1[n-1]}$, and the graphs with pole labellings give a cell decomposition of the moduli space $\mathcal{M}_{g,n}$. Each cell in $\mathcal{M}_{g,1[n-1]}$ corresponds to $(n-1)!|\mathrm{Aut}_{\mathrm{fix}}(\mathcal{G})|/|\mathrm{Aut}(\mathcal{G})|$ identified cells in $\mathcal{M}_{g,n}$.

3.2 Equivalence classes of permutation tuples

In the previous section we reviewed the fact that, for a given g and set of n real numbers $r_1, \ldots, r_n$ that sum to zero, each Riemann surface of genus g with n labelled points has a unique Giddings-Wolpert differential ω, which uniquely determines a pole-labelled Nakamura graph $\bar{\mathcal{G}}$. It was stated that the set of Riemann surfaces in moduli space with a given graph $\bar{\mathcal{G}}$ is a cell, and so the set of all admissible Nakamura graphs for a given g and n gives a cell decomposition of moduli space. Distinct points in a cell correspond to inequivalent Riemann surfaces with the same Nakamura graph but different Giddings-Wolpert differentials. The automorphism groups of the graphs correspond to the orbifold groups of their associated cells, and the automorphism groups of the graphs depends on the type of moduli space under consideration.

We can develop a useful description of Nakamura graphs by using equivalence classes of permutation tuples. Recall from Section 1.1.3 that holomorphic branched coverings from surfaces onto the sphere are described by Hurwitz equivalence classes of permutation tuples. Ribbon graphs and dessins d'enfants embedded on surfaces can be constructed from the preimages of Belyi maps, which are associated to Belyi triples (σ, τ, γ) with σ associated to the vertices of the graph, τ to the edges, and γ to the faces. While it is possible to describe Nakamura graphs with Belyi triples, this method requires large permutation groups to describe even the simplest graphs, and the set of conditions that a given Belyi triple must satisfy to give a Nakamura graph is quite cumbersome. In fact, the properties of Nakamura graphs allows for a cleaner description in terms of tuples of permutations of smaller degree than in Belyi triples.

For a Riemann surface with an embedded Nakamura graph, we can construct a branched covering of degree d onto the sphere with $(m+2)$ branch points, where d is the number of faces of the graph and m is the number of distinct time coordinates of the

zeroes. This map will not be holomorphic in general, but the approach of Section 1.1.3 generalises in a straightforward manner to topological branched coverings of surfaces. The tuple of permutations associated to this branched covering is a tuple of $(m+2)$ permutations in S_d, and such a tuple contains enough information to reconstruct the graph. We can find and count cells in the cell decomposition of moduli space by finding and counting the tuples of permutations that give distinct Nakamura graphs.

A pair of tuples which are conjugate by a permutation $\gamma \in S_d$ give the same Nakamura graph, but this action by conjugation may interchange the poles of the graph. As such, Hurwitz classes of tuples correspond to the unlabelled graphs discussed in the previous section, and the automorphism groups of the Hurwitz classes will correspond to the quotienting groups of cells in the modified moduli space $\mathcal{M}_{g,1[n-1]}$. Initially, we will set the residues r_i of the $(n-1)$ outgoing poles to be equal and consider only the cell decomposition of this modified moduli space via the Nakamura graphs without a pole labelling. We will extend our description to the moduli space $\mathcal{M}_{g,n}$ in the final part of this section by introducing a new type of permutation tuple, which we call a **split tuple**, that describes pole-labelled Nakamura graphs.

In general, there can be many distinct Hurwitz classes associated to the same Nakamura graph. This is because the zeroes of a graph, and their associated permutations in the Hurwitz tuple, can be ordered in many different ways without altering the graph at a topological level. To solve this redundancy, we introduce a new equivalence relation on the set of Hurwitz classes - which we call **slide-equivalence** - such that the equivalence classes of this relation are in one-to-one correspondence with the (unlabelled) Nakamura graphs. Also, the automorphism group of a Hurwitz tuple will not in general match the automorphism group of its graph. Within the slide-equivalence class of any Nakamura graph, we can make a canonical choice of a Hurwitz class - whose elements we call **reduced tuples** - with the property that the automorphism group of the graph is identical to the automorphism group of the reduced tuple. This description leads to a computationally powerful method of finding the Nakamura graphs and their automorphism groups by finding the reduced tuples.

3.2.1 Nakamura graphs from branched coverings

The Nakamura graph of a Riemann surface partitions the surface into d faces, each of which is holomorphic to an infinite complex strip, such as in Figure 3.1. The zeroes of the differential lie on the boundaries of the strips, and the poles are located at the negative and positive infinities of the strips. Given a graph and set of strip widths,

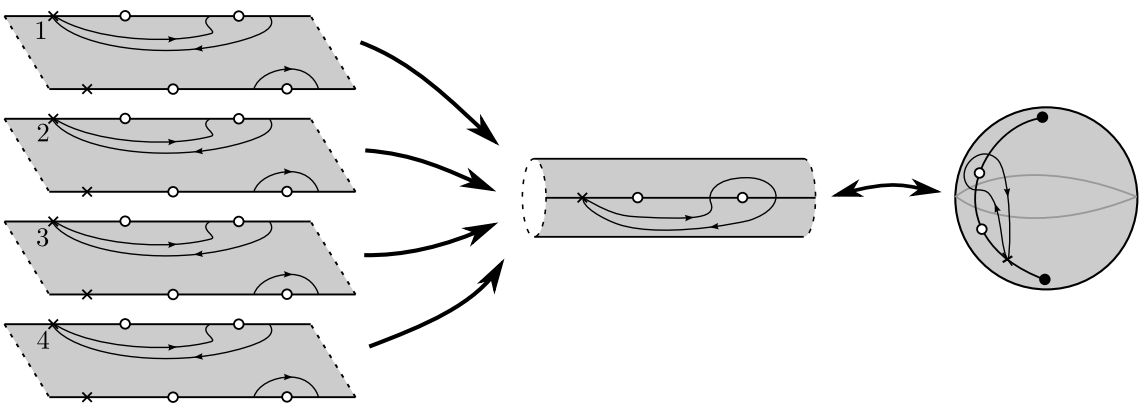

Figure 3.5: Nakamura graph strips naturally form a branched cover of the cylinder and the sphere.

the Riemann surface can be reconstructed by a gluing of the edges determined by the graph.

For a given Nakamura graph, consider a Riemann surface with a Giddings-Wolpert differential in which the d strips are of equal width 2π, and choose a consistent set of residues of the poles. The strips can then be viewed as copies of a single template strip of width 2π. There is a trivial map from each of the d worldsheet strips on to the target strip, in which all the preimages of a point on the target strip have the same time coordinate. On identifying the upper and lower edges of the target space strip, the map extends to a branched covering from the punctured Riemann surface onto the cylinder. All the real trajectories of the Nakamura graph are mapped on to a single infinite line on the cylinder, and all the zeroes are mapped on to this line. The positive (incoming) poles of the graph are mapped on to negative infinity, and the negative (outgoing) poles of the graph are mapped on to positive infinity. The map has $(m+2)$ branch points, where $m \leq l$ is the number of distinct time coordinates of the zeroes. If the time coordinates of all the zeroes are distinct, then $m = l$.

An infinite cylinder of circumference 2π can be mapped bijectively to the twice-punctured Riemann sphere with the exponential map $z \mapsto \exp z$. On restoring the removed points to the surface, the composition of the cylinder covering and the exponential map is a holomorphic branched covering f of the Riemann sphere with $(m+2)$ branch points. The positive poles of the Nakamura graph map on to 0, the negative poles of the graph map on to ∞, and the remaining l zeroes map on to m branch points along the real axis on the sphere. The Giddings-Wolpert differential on the worldsheet is $\frac{df}{f}$.

Now consider a more general Giddings-Wolpert differential where the strips are no longer of equal width. We can construct a bijective mapping from each strip onto a single template strip of width 2π in such a way that the preimages of a point on the template strip have the same time coordinate: however, this mapping will not be holomorphic in general. Applying the exponential map to this template strip gives a map f from a general Riemann surface onto the sphere. The differential cannot be written in the form $\frac{df}{f}$ in this more general case, but the map f is still a branched cover of the sphere, with ramification points at the poles and zeros of the differential.

The Hurwitz class description of branched covers discussed in Section 1.1.3 still holds for non-holomorphic maps in this case, but with the biholomorphism equivalence of maps replaced by homeomorphism equivalence. We mark an unbranched point on the sphere and label the preimages of this point with the integers $\{1, 2, \ldots, d\}$. The preimage of a small loop starting and ending on this marked point that encloses a branch point on the Riemann sphere is a collection of closed paths connecting the labelled preimages of the unbranched point. Each branch point determines a permutation $\sigma \in S_d$, and so the branched covering determines a tuple consisting of $(m+2)$ permutations

$$(\sigma_+, \sigma_1, \sigma_2, \ldots, \sigma_m, \sigma_-), \tag{3.2.1}$$

that describes the gluing of the different strips. The permutation σ_+ describes the branching about 0, the permutation σ_- describes the branching around ∞, and each σ_i describes the branching around the ith branch point on the real line. As this is a branched covering of the sphere, this tuple of permutations multiplies to one,

$$\sigma_+\sigma_1\sigma_2 \ldots \sigma_m\sigma_- = 1. \tag{3.2.2}$$

There is also an overall conjugacy equivalence of the tuple due to the arbitrary choice of labelling of the d inverse images of the marked point:

$$(\gamma\sigma_+\gamma^{-1}, \gamma\sigma_1\gamma^{-1}, \gamma\sigma_2\gamma^{-1}, \ldots, \gamma\sigma_m\gamma^{-1}, \gamma\sigma_-\gamma^{-1}) \sim (\sigma_+, \sigma_1, \sigma_2, \ldots, \sigma_m, \sigma_-), \tag{3.2.3}$$

where $\gamma \in S_d$. This construction is shown in Figure 3.5, where the marked point is chosen to lie on the real axis of the Riemann sphere, and the preimages of this point lie on the boundaries of the strips. The disjoint cycles of σ_+ and σ_- correspond to the poles of the Nakamura graph, and the non-trivial disjoint cycles of each σ_k with $k = 1, \ldots, m$ correspond to the zeroes of the graph. The Riemann-Hurwitz relation

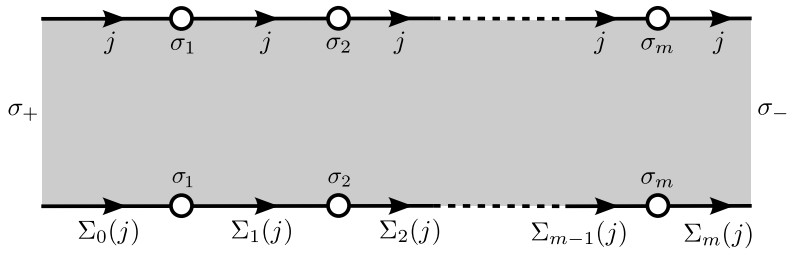

Figure 3.6: The gluing of the strips can be read off from the Hurwitz tuple.

on this branched covering of the sphere can be written

$$\begin{aligned}(2g-2) &= -2d + (d - C_{\sigma_+}) + (d - C_{\sigma_-}) + \sum_{k=1}^{m}(d - C_{\sigma_k}) \\ &= -n + \sum_{k=1}^{m}(d - C_{\sigma_k}). \end{aligned} \tag{3.2.4}$$

By considering the branching numbers $B_k = d - C_{\sigma_k}$ of the zeroes and relating these to the valencies of the vertices of the graph, it can be shown that the above relation is equivalent to the relation (3.1.13) given in the previous section.

The boundaries of the strips are the real trajectories of the differential, which form the Nakamura graph of the surface. We can choose to label the real trajectories bounding the upper edge of each strip with the same integer that was assigned to the marked point lying on the upper edge of this strip. This gives us an edge-labelling of the Nakamura graph associated to the surface, in which all the edges corresponding to the upper boundary of the same strip have the same label. We call this labelling of a Nakamura graph the **Hurwitz class description**, or the $\mathbf{S_d}$ **description**, as the Nakamura graph associated to this surface can be reconstructed from the S_d Hurwitz class of the branched covering.

The labelling of the edges glued to the lower boundary of a strip are determined by the Hurwitz tuple. On a strip in which the upper boundary is labelled by some integer $j \in \{1, 2, \ldots, d\}$, the edge preceding the preimage of the first branch point is labelled by $\Sigma_0(j)$, where $\Sigma_0 := \sigma_+$. The edge proceeding the next branch point is labelled $\Sigma_1(j)$, where $\Sigma_1 = \sigma_+\sigma_1$; the next edge is labelled $\Sigma_2(j)$, with $\Sigma_2 = \sigma_+\sigma_1\sigma_2$, and so on. This labelling for a general strip is shown in Figure 3.6.

Given a Nakamura graph associated to a surface, we can read off an associated Hurwitz tuple. Choose an ordering of the l zeroes of the graph that respects the

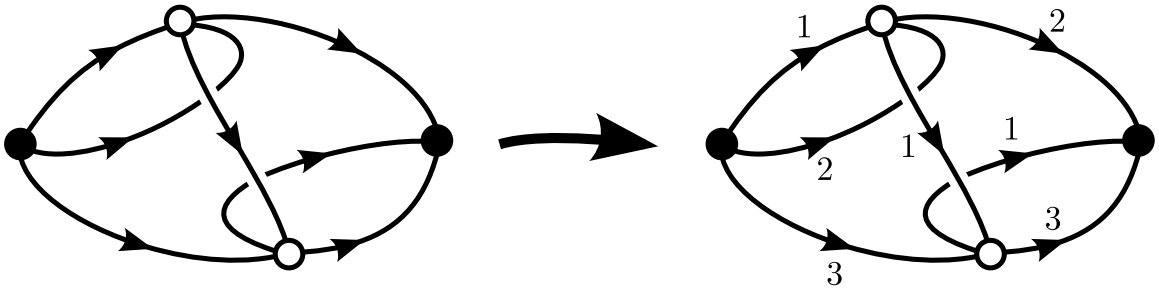

$$(\sigma_+, \sigma_1, \sigma_2, \sigma_-) = ((123), (12), (13), (123))$$

Figure 3.7: A labelling of the edges of a Nakamura graph and its associated S_d tuple.

orientations of the internal edges, and assign a labelling to the edges that lie on the upper boundary of a face. The cyclic ordering of the edges at the incoming and outgoing poles correspond to σ_+ and σ_- respectively, and the cyclic ordering of the incoming (or the outgoing) edges at the kth zero corresponds to σ_k. Each outgoing edge at a zero has the same label as the incoming edge located in the next clockwise position at the zero. An example of a Nakamura graph with Hurwitz class labellings is given in Figure 3.7 with its Hurwitz tuple description. Conversely, a Hurwitz tuple $(\sigma_+, \sigma_1, \ldots, \sigma_-)$ is enough to completely specify a Nakamura graph. Each Nakamura graph, and thus each Hurwitz class, determines a cell in the cell decomposition of moduli space. In general, extra data is required to specify a particular point within this cell, as the permutation tuple alone does not encode the continuous data of the strip widths and the time coordinates of the zeroes.

Not every possible Hurwitz class corresponds to a Nakamura graph. For a general S_d tuple of $(m+2)$ permutations to describe a Nakamura graph, it must satisfy three properties:

- The permutations corresponding to the zeroes $\{\sigma_1, \sigma_2, \ldots, \sigma_m\}$ are non-trivial. (This ensures that each permutation σ_k describes at least one interaction point.)
- Each integer in $\{1, 2, \ldots, d\}$ is permuted by at least one of the permutations describing the zeroes $\{\sigma_1, \sigma_2, \ldots, \sigma_m\}$. (This ensures that no trajectories connect poles directly to poles.)
- The tuple $(\sigma_+, \sigma_1, \ldots, \sigma_m, \sigma_-)$ acts transitively on $\{1, 2, \ldots, d\}$. (This ensures that the Riemann surfaces are connected.)

All the other conditions given in Section 3.1.2 that a Nakamura graph must satisfy are guaranteed by the construction of the permutation tuple.

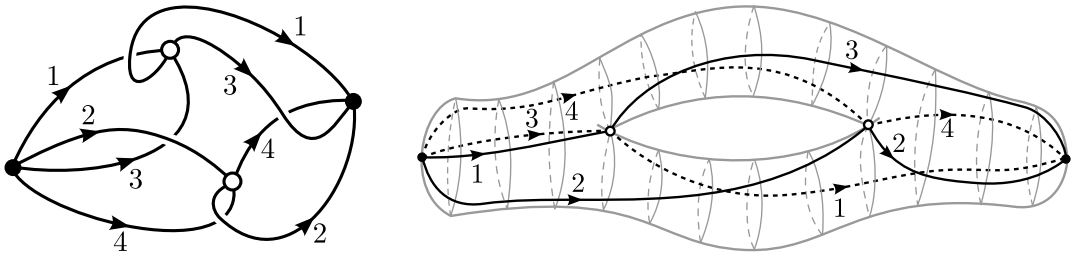

Figure 3.8: A Nakamura graph in the S_d picture, and an embedding of the graph on the torus with closed imaginary trajectories drawn in grey.

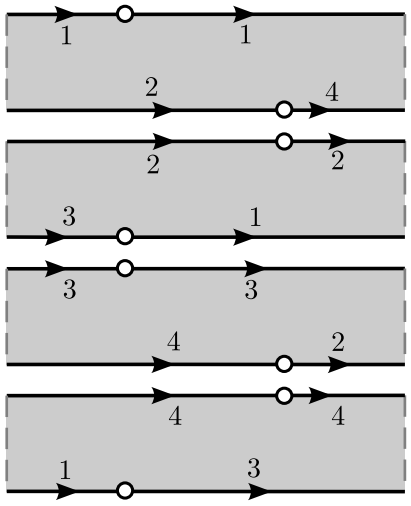

Figure 3.9: The strip decomposition of the above graph.

As an example of the strip decomposition of a surface via a Nakamura graph, and its description with an S_d tuple, we consider the example of a Nakamura graph with no internal edges and four faces, shown on the left of Figure 3.8. This graph corresponds to a genus one surface with two marked points, drawn with the embedded Nakamura graph on the right of Figure 3.8. With S_d labellings, this graph can be described by the Hurwitz class

$$(\sigma_+, \sigma_1, \sigma_2, \sigma_-) = ((1234), (13), (24), (1234)). \tag{3.2.5}$$

The strip decomposition of the surface is shown in Figure 3.9.

3.2.2 Slide-equivalence classes and reduced tuples

There is some redundancy in the Hurwitz class description of Nakamura graphs. Given a Riemann surface with a Giddings-Wolpert differential, then there exists a unique branched covering of the sphere as constructed above up to equivalence, and so there exists a unique Hurwitz class associated to the surface. The cycles of the permutations in the Hurwitz class correspond to the vertices of the Nakamura graph. However, there may be more than one Hurwitz class that can describe the same Nakamura graph. This is because a Hurwitz class has a well-defined total ordering of the branch points, derived from the time coordinates of the zeroes, but a Nakamura graph generally only has a partial ordering on its zeroes derived from the orientation of the edges.

This redundancy makes the automorphisms of a Nakamura graph harder to determine in the Hurwitz class description than for more general types of ribbon graphs. The set of permutations $\gamma \in S_d$ such that

$$(\gamma^{-1}\sigma_+\gamma,\ \gamma^{-1}\sigma_1\gamma,\ \ldots, \gamma^{-1}\sigma_m\gamma,\ \gamma^{-1}\sigma_-\gamma) = (\sigma_+, \sigma_1, \ldots, \sigma_m, \sigma_-) \tag{3.2.6}$$

are indeed automorphisms of the Nakamura graph, but they are not the only automorphisms. In some cases, there are permutations mapping the σ_i into each other upon conjugation which preserve the structure of the associated Nakamura graph.

To solve this redundancy in the Hurwitz class description, we introduce a new equivalence relation on the Hurwitz classes. For a general tuple of $(m+2)$ permutations $(\sigma_+, \sigma_1, \ldots, \sigma_m, \sigma_-)$ describing a Nakamura graph arising from a branched covering of the sphere, each permutation σ_k represents a set of zeroes with the same time coordinate. If there are two subsequent permutations σ_k and σ_{k+1} which are *disjoint* (the intersection of their moved-point sets is empty), then there are no internal edges directly connecting any of the zeroes which correspond to the cycles in the permutations. Any other branched covering with the $(m+1)$-permutation tuple

$$(\sigma_+, \sigma_1, \ldots, \sigma_k\sigma_{k+1}, \ldots, \sigma_m, \sigma_-), \tag{3.2.7}$$

would have an identical Nakamura graph. We therefore define a binary relation on the set of permutation tuples

$$(\sigma_+, \sigma_1, \ldots, \sigma_k, \sigma_{k+1}, \ldots, \sigma_m, \sigma_-) \sim (\sigma_+, \sigma_1, \ldots, \sigma_k\sigma_{k+1}, \ldots, \sigma_m, \sigma_-) \tag{3.2.8}$$

whenever σ_k and σ_{k+1}, $1 \leq k < m$ are disjoint. This relation extends to an equivalence

relation on the set of all tuples. The overall product of a tuple of permutations is unchanged by this relation, and the overall action of conjugacy on tuples commutes with this relation, which means that this relation is a well-defined equivalence relation on the set of Hurwitz classes describing Nakamura graphs. We call this relation **slide-equivalence**, as it represents the ability to 'slide' around the orderings of the zeroes of a Nakamura graph when there are no internal edges connecting the zeroes. Each slide-equivalence class of Hurwitz classes corresponds to a unique Nakamura graph.

Up to conjugacy equivalence, we can canonically choose a representative element for each slide-equivalence class, which we call the **reduced tuple** description of a Nakamura graph, and denote by $(\sigma_+, \tau_1, \ldots, \tau_m, \sigma_-)$. Each slide-equivalence class has exactly one Hurwitz class specified by a representative tuple $(\sigma_+, \tau_1, \ldots, \tau_m, \sigma_-)$ with the property that *every cycle in* τ_{k+1} *shares a moved point with* τ_k, for each $k = 1, 2, \ldots, (m-1)$. This is the S_d tuple constructed by taking a tuple and placing as many cycles as possible in the earliest possible permutation via slide-equivalence. Graphically, this can be thought of as 'sliding' the zeroes around so that as many zeroes as possible are vertically adjacent in the earliest position, and then subsequently as many zeroes as possible are arranged in the second earliest position, and so on.

The reduced tuple has the property that the graph automorphisms do not exchange cycles between different τ_k. Consequently, the automorphisms of a Nakamura graph described by a reduced tuple are precisely those $\gamma \in S_d$ such that

$$(\gamma^{-1}\sigma_+\gamma, \gamma^{-1}\tau_1\gamma, \ldots, \gamma^{-1}\tau_m\gamma, \sigma_-) = (\sigma_+, \tau_1, \ldots, \tau_m, \sigma_-). \tag{3.2.9}$$

Reduced tuples are a useful step in finding and cataloguing Nakamura graphs, as there is a one-to-one correspondence between Nakamura graphs and the Hurwitz equivalence classes of reduced tuples, and the automorphism group of a Nakamura graph is the automorphism group of its reduced tuple.

As an example, we consider the Nakamura graph from the previous subsection shown in Figure 3.8, and described by the S_d tuple

$$(\sigma_+, \sigma_1, \sigma_2, \sigma_-) = ((1234), (13), (24), (1234)). \tag{3.2.10}$$

The time coordinates of the zeroes associated to the permutations (13) and (24) satisfy $t_{(13)} < t_{(24)}$. If we were to consider a surface with a different Giddings-Wolpert differential in which the time coordinates of the zeroes were interchanged and $t_{(24)} < t_{(13)}$,

then the S_d description of the graph would be

$$(\sigma_+, \sigma_1, \sigma_2, \sigma_-) = ((1234), (24), (13), (1234)). \tag{3.2.11}$$

If we instead considered a surface where the time coordinates of the zeroes were identical, then the ramification of the branched cover of the sphere would no longer be simple, and the S_d description of the graph would be

$$(\sigma_+, \sigma_1, \sigma_-) = ((1234), (13)(24), (1234)). \tag{3.2.12}$$

In all three of these cases, the Nakamura graph corresponding to the surface is identical. These three tuples are in distinct Hurwitz classes, but lie in the same slide-equivalence class. This slide-equivalence can be thought of as 'sliding around' the time coordinate of the zero associated to the transposition (34). Of the three Hurwitz classes in the slide-equivalence class, the reduced tuple is

$$(\sigma_+, \tau, \sigma_-) \quad = \quad ((1234), (13)(24), (1234)), \tag{3.2.13}$$

as it is the only one of the three tuples above which (trivially) satisfies the property that every cycle in τ_{k+1} shares a moved point with τ_k for each k.

3.2.3 Split tuples

The slide-equivalence classes of tuples of permutations specify Nakamura graphs without pole labellings, corresponding to cells in $\mathcal{M}_{g,1[n-1]}$. We can extend this Hurwitz and slide-equivalence class description of Nakamura graphs to describe pole-labelled graphs by introducing *split tuples*, which assign an ordering to the distinct outgoing poles of a graph.

Let $\bar{\mathcal{G}}$ be a Nakamura graph with labelled poles and edges with an associated tuple $(\sigma_+, \sigma_1, \ldots, \sigma_m, \sigma_-)$. Each cycle of σ_- corresponds to an outgoing pole of the graph, labelled from 1 to $(n-1)$. We write $\sigma_-^{(i)}$ to denote the cycle corresponding to the ith pole of the labelled graph. A **split tuple** is a tuple arising from a Nakamura graph in which σ_- is replaced by $(n-1)$ disjoint ordered single cycles corresponding to the outgoing poles of the graph:

$$(\sigma_+, \sigma_1, \sigma_2, \ldots, \sigma_m;\ \sigma_-^{(1)}, \sigma_-^{(2)}, \ldots, \sigma_-^{(n-1)}). \tag{3.2.14}$$

If the Hurwitz class is a reduced tuple of a labelled graph $\bar{\mathcal{G}}$, then we call its split tuple

a **reduced split tuple**, and replace the σ_k with τ_k:

$$(\sigma_+, \tau_1, \tau_2, \ldots, \tau_m;\ \sigma_-^{(1)}, \sigma_-^{(2)}, \ldots, \sigma_-^{(n-1)}). \tag{3.2.15}$$

In this subsection, we will constrain ourselves to considering the reduced split tuples of labelled graphs.

The conjugacy equivalence classes of reduced split tuples correspond to distinct pole-labelled Nakamura graphs. We show this by matching the coset description of graph labellings given in Section 3.1.4 to the equivalence classes of reduced split tuples. A general element $\gamma \in S_d$ acts on a tuple by relabelling each individual cycle in the permutations

$$(j_1 j_2 \ldots j_p) \xrightarrow{\gamma} (\gamma(j_1)\gamma(j_2)\ldots\gamma(j_p)). \tag{3.2.16}$$

This relabelling corresponds to the action by conjugation on the permutations in the tuple $\sigma_+ \mapsto \gamma^{-1}\sigma_+\gamma$, $\tau_k \mapsto \gamma^{-1}\tau_k\gamma$, $\sigma_-^{(i)} \mapsto \gamma^{-1}\sigma_-^{(i)}\gamma$. (For a cycle (j) of length 1, the action of conjugation by γ is defined to be $(j) \mapsto (\gamma(j))$.) The group of permutations that preserve the reduced tuple $(\sigma_+, \tau_1, \ldots, \tau_m, \sigma_-)$ under this action are the automorphisms of the unlabelled graph $\mathrm{Aut}(\mathcal{G})$. An automorphism $a \in \mathrm{Aut}(\mathcal{G})$ will preserve σ_- under conjugation, but will not generally preserve each $\sigma_-^{(i)}$, and may interchange them. This means that the action of a on a given single-cycle $\sigma_-^{(i)}$ in σ_- will produce another single-cycle $\sigma_-^{(j)}$ in σ_-, and so we can read off an element $\kappa_a \in S_{n-1}$ such that the action of the automorphism is

$$\sigma_-^{(i)} \xrightarrow{a} \sigma_-^{(\kappa_a(i))}. \tag{3.2.17}$$

This is the homomorphism $\phi : \mathrm{Aut}(\mathcal{G}) \to S_{n-1}$ discussed in subsection 3.1.4. The kernel of this homomorphism is $\mathrm{Aut}_{\mathrm{fix}}(\mathcal{G})$, the group of automorphisms which fix each pole. By the isomorphism theorem, the group $H = \mathrm{Aut}(\mathcal{G})/\mathrm{Aut}_{\mathrm{fix}}(\mathcal{G})$ is isomorphic to a subgroup of S_{n-1}. This is the group of all $\kappa_a \in S_{n-1}$ arising from the automorphisms $a \in \mathrm{Aut}(\mathcal{G})$. Two permutations in this group κ_a, κ_b arising from the distinct automorphisms $a, b \in \mathrm{Aut}(\mathcal{G})$ are identical if there is some pole-fixing automorphism $a_{\mathrm{fix}} \in \mathrm{Aut}_{\mathrm{fix}}(\mathcal{G})$ with $a = b \circ a_{\mathrm{fix}}$.

A relabelling of the outgoing poles of a graph can be described by a general element

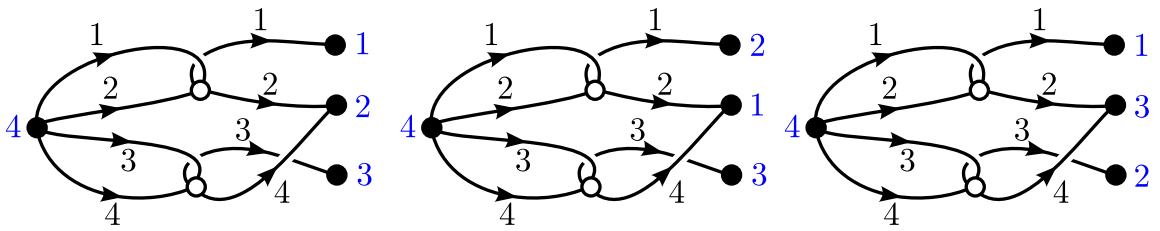

Figure 3.10: A Nakamura graph with edge labellings and three inequivalent pole labellings.

$\kappa \in S_{n-1}$ acting on the split tuple by rearranging the $(n-1)$ single cycles,

$$(\sigma_+, \tau_1, \tau_2, \ldots, \tau_m; \quad \sigma_-^{(1)}, \sigma_-^{(2)}, \ldots, \sigma_-^{(n-1)}) \tag{3.2.18}$$

$$\xrightarrow{\kappa} \quad (\sigma_+, \tau_1, \tau_2, \ldots, \tau_m; \quad \sigma_-^{(\kappa(1))}, \sigma_-^{(\kappa(2))}, \ldots, \sigma_-^{(\kappa(n-1))}). \tag{3.2.19}$$

The arrangements of the split cycles given in (3.2.18) and (3.2.19) correspond to the same graph if there is some relabelling of the graph edges $\gamma \in S_d$ that maps one to the other. Such a relabelling must preserve σ_+ and each τ_k separately, and hence must be an automorphism $\gamma \in \mathrm{Aut}(\mathcal{G}) \subset S_d$. The action of an automorphism γ on the $(n-1)$ split-cycles is described by some $\kappa_\gamma \in S_{n-1}$. We see that the tuples (3.2.18) and (3.2.19) describe the same graph if and only if κ corresponds to some automorphism, i.e. $\kappa = \kappa_\gamma$ for some $\gamma \in \mathrm{Aut}(\mathcal{G})$. This is precisely the statement that κ is in the image of $\mathrm{Aut}(\mathcal{G})$ under the homomorphism ϕ, i.e. $\kappa \in H$. We conclude that the distinct split tuples associated to a reduced tuple correspond to the distinct cosets of H in S_{n-1}.

As an example, we consider the graph from subsection 3.1.4, drawn in Figure 3.3. This has $n = 4$ poles, and is described by the unlabelled tuple

$$(\sigma_+, \tau, \sigma_-) = ((1234), (12)(34), (1)(24)(3)). \tag{3.2.20}$$

We can split σ_- into the constituent cycles $\sigma_-^{(1)}, \sigma_-^{(2)}, \sigma_-^{(3)}$:

$$(\sigma_-^{(1)}, \sigma_-^{(2)}, \sigma_-^{(3)}) = ((1), (24), (3)). \tag{3.2.21}$$

The distinct pole labellings correspond to the unique ways to order the permutations $\sigma_-^{(1)}, \sigma_-^{(2)}, \sigma_-^{(3)}$ in the tuple, up to edge-relabellings. We can derive the pole labellings from the cosets construction as follows. The automorphism group of the unlabelled tuple in Equation (3.2.20) is isomorphic to $\mathbb{Z}_2$, generated by the action by conjugation of the permutation $\gamma := (13)(24)$ on each element of the tuple. This automorphism

maps the split-cycles as follows:

$$\begin{aligned} \sigma_-^{(1)} &\xrightarrow{\gamma} \sigma_-^{(3)}, \\ \sigma_-^{(2)} &\xrightarrow{\gamma} \sigma_-^{(2)}, \\ \sigma_-^{(3)} &\xrightarrow{\gamma} \sigma_-^{(1)}, \end{aligned} \tag{3.2.22}$$

and so defines an element $\kappa_\gamma := (13) \in S_3 = S_{n-1}$. The cosets of $H := \langle (13) \rangle$ in S_3 correspond to the distinct ways to rearrange the outgoing poles of the tuple. The cosets are H, $(12)H$ and $(23)H$, and we can choose the representative elements of these cosets $\{(), (12), (23)\}$. Acting with these representative elements on the split-cycles in Equation (3.2.21) gives the three distinct pole-labelled graphs:

$$(\sigma_+, \tau;\ \sigma_-^{(1)}, \sigma_-^{(2)}, \sigma_-^{(3)}) = ((1234), (12)(34);\ (1), (24), (3)), \tag{3.2.23}$$

$$(\sigma_+, \tau;\ \sigma_-^{(2)}, \sigma_-^{(1)}, \sigma_-^{(3)}) = ((1234), (12)(34);\ (24), (1), (3)), \tag{3.2.24}$$

$$(\sigma_+, \tau;\ \sigma_-^{(1)}, \sigma_-^{(3)}, \sigma_-^{(2)}) = ((1234), (12)(34);\ (1), (3), (24)). \tag{3.2.25}$$

These split tuples describe all possible pole-labelled graphs associated to the unlabelled tuple (3.2.20). For example, we could see that the tuple created by acting on Equation (3.2.23) with (13), the generator of H, gives the tuple

$$(\sigma_+, \tau;\ \sigma_-^{(3)}, \sigma_-^{(2)}, \sigma_-^{(1)}) = ((1234), (12)(34);\ (3), (24), (1)), \tag{3.2.26}$$

which describes the same graph as the tuple in Equation (3.2.23) as the two tuples can be related by the relabelling automorphism $\gamma = (13)(24)$. The distinct pole-labelled graphs associated to these three tuples are shown in Figure (3.10).

3.3 The cell decomposition of moduli space

In the previous section, we showed that Nakamura graphs are related to equivalence classes of permutation tuples by constructing branched coverings from Riemann surfaces onto the sphere. Branched covers are described by Hurwitz classes which encode the same data as a Nakamura graph without pole labellings. Each slide-equivalence class of Hurwitz classes determines a distinct Nakamura graph. As every slide-equivalence class has a unique Hurwitz class of reduced tuples, there is a one-to-one correspondence between Hurwitz classes of reduced tuples and Nakamura graphs. Nakamura graphs with labelled poles are described by split tuples, and there

is a one-to-one correspondence between conjugacy classes of reduced split tuples and pole-labelled Nakamura graphs.

In this section, we explicitly show how to construct the set of points in moduli space associated to a pole-labelled graph $\bar{\mathcal{G}}$ by using its reduced split tuple. We find that the set is homeomorphic to $\mathbb{R}^{d+l-n}$ modulo the action of the pole-fixing graph automorphism group $\mathrm{Aut}(\bar{\mathcal{G}})$. We explain how to find the boundaries and incidences of these sets from the split tuples. This confirms the claim of [31] that the set of distinct Nakamura graphs give a valid cell decomposition of moduli space. We also discuss the generalisation to the moduli space $\mathcal{M}_{g,1[n-1]}$, and show that a cell $C(\mathcal{G})$ corresponding to a graph without pole labellings is described by a set homeomorphic to $\mathbb{R}^{d+l-n}$ modulo the pole-permuting automorphisms $\mathrm{Aut}(\mathcal{G})$.

As examples, we give the graph decompositions of the low-dimensional moduli spaces $\mathcal{M}_{0,4}$ and $\mathcal{M}_{1,2}$, and show that the cell decomposition of $\mathcal{M}_{0,4}$ matches the description of the space known by considering Möbius maps on the sphere. We briefly describe how to construct the moduli space $\mathcal{M}_{0,1[3]}$ from the quotienting of $\mathcal{M}_{0,4}$.

3.3.1 Cells

Recall that any cell in a cell decomposition of an orbifold is homeomorphic to a ball modulo a finite group. The aim of this section is to show that, from the reduced split tuple of any labelled Nakamura graph $\bar{\mathcal{G}}$, we can construct a convex real set $\mathcal{B}(\bar{\mathcal{G}})$ on which $\mathrm{Aut}(\bar{\mathcal{G}})$ acts naturally in such a way that $\mathcal{B}(\bar{\mathcal{G}})/\mathrm{Aut}(\bar{\mathcal{G}}) = C(\bar{\mathcal{G}})$.

Consider the moduli space of inequivalent Riemann surfaces of genus g with n labelled points $\mathcal{M}_{g,n}$, and choose a set of negative reals $r_1, \ldots, r_{n-1}$ and the positive real $r_n = -\sum_i r_i$. Let $C(\bar{\mathcal{G}})$ be the collection of points in $\mathcal{M}_{g,n}$ with the same labelled Nakamura graph $\bar{\mathcal{G}}$ associated to the tuple

$$(\sigma_+, \tau_1, \tau_2, \ldots, \tau_m;\ \sigma_-^{(1)}, \sigma_-^{(2)}, \ldots, \sigma_-^{(n-1)}). \tag{3.3.1}$$

A Riemann surface with this Nakamura graph is specified by a set of strip widths and interaction times. Label the widths of the d strips $b_1, b_2, \ldots, b_d$, and the interaction times of the zeroes $t_1, t_2, \ldots, t_l$. The cell $C(\bar{\mathcal{G}})$ is parametrised by a subspace of $\mathbb{R}^{d+l}$. The $(d+l)$ variables parametrising the cell are subject to some linear constraints determined by the structure of the graph and our choice of time-symmetry fixing:

- The strip widths must be consistent with the residues at the poles. Each single cycle $\sigma_-^{(i)} = (j_1 j_2 \ldots j_k)$ corresponds to the ith pole of the graph, which connects

to k strips with widths $b_{j_1}, b_{j_2}, \ldots, b_{j_k}$. This gives $(n-1)$ independent constraints of the form

$$b_{j_1} + b_{j_2} + \ldots + b_{j_k} = |r_i|. \tag{3.3.2}$$

(There is also a constraint that the total sum of the widths of all strips must correspond to $\sum |r_i|$, but this constraint is derived from the above $(n-1)$ constraints.)

- The time-translation symmetry of the zeroes is fixed by requiring that the sum over all the interaction times is zero,

$$t_1 + t_2 + \ldots + t_l = 0. \tag{3.3.3}$$

Each of these n constraints is of the form $\sum q_j = C$ for some continuous parameters q_j and some constant C, which are the equations of a set of hyperplanes in $\mathbb{R}^{d+l}$. As well as the above hyperplane constraints, there are some 'half-space' constraints on the variables, which are of the form $\sum q_j > C$. Each of these constraints partitions $\mathbb{R}^{d+l}$ into two subsets by a hyperplane, and so does not lower the dimension of the space. The independent half-space constraints are formulated from the reduced split tuple as follows:

- Each strip-width b_j must be positive. However, if a label $j \in \{1, \ldots d\}$ corresponds to some 1-cycle in σ_-, i.e. $\sigma_-^{(i)} = (j)$, then the constraint $b_j = |r_i|$ automatically implies that $b_j > 0$. (Geometrically, the hyperplanes $b_j = 0$ and $b_j = |r_i|$ are parallel.) The independent half-plane constraints on the strip widths are

$$b_j > 0, \qquad j \in \{1, 2, \ldots, d\} \text{ and } \sigma_-(j) \neq j. \tag{3.3.4}$$

- The interaction times of the zeroes must respect the ordering of the associated cycles of the reduced tuple. Recall that a given τ_k in the reduced tuple consists of multiple disjoint non-trivial single cycles of the form

$$\tau_k = \sigma_{p_1} \sigma_{p_2} \ldots \sigma_{p_a}, \tag{3.3.5}$$

where $\{p_1, p_2, \ldots, p_a\} \subset \{1, 2, \ldots, l\}$. Each σ_{p_j} corresponds to a zero of the Giddings-Wolpert differential on the surface with interaction time t_{p_j}. It follows

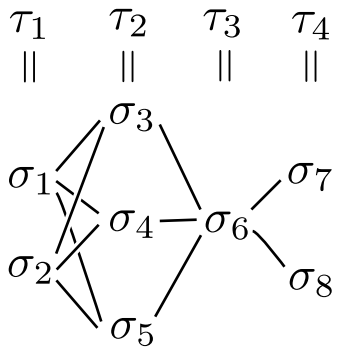

Figure 3.11: Each line corresponds to a time-ordering inequality.

explicitly from the construction of the reduced tuple that every cycle in τ_{k+1} must appear at a later interaction time than every cycle in τ_k. If τ_{k+1} has the decomposition

$$\tau_{k+1} = \sigma_{q_1}\sigma_{q_2}\ldots\sigma_{q_b}, \tag{3.3.6}$$

for some $\{q_1, q_2, \ldots, q_b\} \subset \{1, 2, \ldots, l\}\backslash\{p_1, p_2, \ldots, p_a\}$, then we have a half-plane constraint

$$t_{p_\alpha} < t_{q_\beta} \tag{3.3.7}$$

for each pair (p_α, q_β) with $p_\alpha \in \{p_1, p_2, \ldots, p_a\}$ and $q_\beta \in \{q_1, q_2, \ldots, q_b\}$. The collection of all such constraints are necessary and sufficient to guarantee that any configuration of the interaction times is consistent with the chosen Nakamura graph. If $\tau_1, \tau_2, \ldots, \tau_m$ each have $c_1, c_2, \ldots c_m$ constituent non-trivial cycles respectively, where $c_1 + c_2 + \ldots + c_m = l$, then there are

$$c_1c_2 + c_2c_3 + \ldots + c_{m-1}c_m \tag{3.3.8}$$

inequalities imposed on the interaction times.

A figure demonstrating the time-ordering inequalities associated to a permutation tuple is given in Figure 3.11. In this example, the single-cycle interaction permutations σ_k are collated into the reduced tuple permutations τ_k with $\tau_1 = \sigma_1\sigma_2$, $\tau_2 = \sigma_3\sigma_4\sigma_5$, $\tau_3 = \sigma_6$, and $\tau_4 = \sigma_7\sigma_8$. Each line connecting the consecutive σ_i corresponds to an inequality on the time coordinates of the respective interaction points.

Each of these hyperplane and half-space constraints defines a convex subspace of $\mathbb{R}^{d+l}$. The intersection of convex subspaces is convex, and so these constraints define a convex subspace of $\mathbb{R}^{d+l}$. The n hyperplane constraints define subspaces of $\mathbb{R}^{d+l}$ of codimension one, and the half-space constraints define subsets of codimension zero, hence these constraints define a convex $(d+l-n)$-dimensional subset of $\mathbb{R}^{d+l}$, which is homeomorphic to $\mathbb{R}^{d+l-n}$. We denote this subset by $\mathcal{B}(\bar{\mathcal{G}})$.

The group $\mathrm{Aut}(\bar{\mathcal{G}}) = \mathrm{Aut}_{\mathrm{fix}}(\mathcal{G})$ of pole-fixing automorphisms of the tuple (3.3.1) has a natural action on the parameters of $\mathcal{B}(\bar{\mathcal{G}})$. An element $a_{\mathrm{fix}} \in \mathrm{Aut}(\bar{\mathcal{G}}) \subset S_d$ acts on the strip widths by the relabelling

$$b_j \to b_{a_{\mathrm{fix}}(j)}. \tag{3.3.9}$$

It also acts on the interaction vertices by permutation: recall that the action by conjugation of an automorphism a_{fix} will fix any τ_k, but may permute around the constituent cycles $\sigma_{p_1}, \ldots, \sigma_{p_a}$ in τ_k. There is therefore some permutation κ acting on the integers $\{p_1, p_2, \ldots, p_a\}$ corresponding to the automorphism a_{fix}. The action of a_{fix} on the interaction times corresponds to this permutation:

$$t_{p_\alpha} \to t_{\kappa(p_\alpha)}. \tag{3.3.10}$$

We can see that the defining constraints of $\mathcal{B}(\bar{\mathcal{G}})$ are preserved under these actions. Pole-fixing automorphisms do not modify the split-cycles $\sigma_-^{(i)}$, so the strip-width equations (3.3.2) and inequalities (3.3.4) are all preserved. The interaction times are all permuted into each other, so the overall sum (3.3.3) is preserved. Also, the interaction vertices are only permuted within each τ_k separately: cycles within τ_k are mapped to cycles within τ_k. This means that the associated time-ordering inequalities of the form (3.3.7) are mapped into each other, and so these constraints are preserved. This is enough to conclude that pole-fixing automorphisms map $\bar{\mathcal{G}}$ into itself.

Finally, we can show that points in $\mathcal{B}(\bar{\mathcal{G}})$ related by a pole-fixing automorphism correspond to strip decompositions of Riemann surfaces related by a biholomorphism. Let X and $\tilde{X}$ be Riemann surfaces with the same labelled graph $\bar{\mathcal{G}}$ and the respective sets of strip parameters (b_j, t_k) and $(\tilde{b}_j, \tilde{t}_k)$. If there exists a biholomorphism $f : X \to \tilde{X}$, then the pull-back of the Giddings-Wolpert differential from the surface $\tilde{X}$ satisfies the required properties of a Giddings-Wolpert differential on the surface X, and so is the Giddings-Wolpert differential of X by uniqueness. This implies that the biholomorphism f preserves the strip decomposition of the surface, and so restricts to an automorphism of the graph $a_f \in \mathrm{Aut}(\bar{\mathcal{G}})$ on the strip boundaries, and the action of

this automorphism on the point in $\mathcal{B}(\bar{\mathcal{G}})$ is $a_f : (b_j, t_k) \mapsto (\tilde{b}_j, \tilde{t}_k)$. Conversely, if (b_j, t_k) and $(\tilde{b}_j, \tilde{t}_k)$ are points in $\mathcal{B}(\bar{\mathcal{G}})$ related by a graph automorphism $a \in \mathrm{Aut}(\bar{\mathcal{G}})$ which maps $b_j \mapsto \tilde{b}_j$ and $t_k \mapsto \tilde{t}_k$, then $\tilde{b}_j = b_{a(j)}$ and $\tilde{t}_k = t_{\alpha(k)}$ for some $\alpha \in S_l$. The strip decompositions of the Riemann surfaces constructed from the parameters (b_j, t_k) and $(\tilde{b}_j, \tilde{t}_k)$ are related by a biholomorphism mapping the strip with upper edges labelled j to the strip with upper edges labelled $a(j)$. This is enough to conclude the following:

Theorem: Given a Nakamura graph $\bar{\mathcal{G}}$ with genus g, d faces, l interaction points (zeroes), one ingoing pole, and $(n-1)$ outgoing poles labelled $1, 2, \ldots (n-1)$ respectively, then there is an open subset $\mathcal{B}(\bar{\mathcal{G}}) \subset \mathbb{R}^{d+l}$ of dimension $(d+l-n)$ which parametrises the possible strip widths and interaction times of the graph. The group $\mathrm{Aut}(\bar{\mathcal{G}})$ of pole-fixing automorphisms of $\bar{\mathcal{G}}$ is a subgroup of the isometries of $\mathcal{B}$, and there is a one-to-one correspondence between the quotient space $\mathcal{B}/\mathrm{Aut}(\bar{\mathcal{G}})$ and the set $C(\bar{\mathcal{G}})$ of Riemann surfaces with the Nakamura graph $\bar{\mathcal{G}}$.

We can extend the above description to cells in the modified moduli space $\mathcal{M}_{g,1[n-1]}$. We set the outgoing residues of the n poles to be equal, $r_1 = \ldots = r_{n-1} = r$, for some negative real r. For an unlabelled graph $\mathcal{G}$ with associated reduced tuple

$$(\sigma_+, \tau_1, \ldots, \tau_m, \sigma_-), \tag{3.3.11}$$

the parameter space $\mathcal{B}(\mathcal{G})$ is defined entirely similarly to that of a pole-labelled graph. Each cycle in $(j_1 \ldots j_k) \in \sigma_-$ determines a strip-width constraint

$$b_{j_1} + b_{j_2} + \ldots + b_{j_k} = |r|. \tag{3.3.12}$$

The pole-permuting automorphisms $\mathrm{Aut}(\mathcal{G})$ interchange the cycles of σ_-, and so permutes the set of $(n-1)$ constraints of the form (3.3.12) into each other: this is consistent when the outgoing pole residues are equal. The quotient space $\mathcal{B}(\mathcal{G})/\mathrm{Aut}(\mathcal{G})$ is therefore well-defined, and the arguments above for the one-to-one correspondence between strip decompositions of Riemann surfaces and the parameter space still hold for pole-permuting automorphisms. We deduce that $C(\mathcal{G}) = \mathcal{B}(\mathcal{G})/\mathrm{Aut}(\mathcal{G})$.

3.3.2 Boundaries

The boundaries of a cell $C(\bar{\mathcal{G}})$ correspond to the limits of the half-spaces of the form $t_p < t_q$ and $b > 0$. The first of these corresponds to the collapsing of an internal edge, which merges two interaction points together, and the second corresponds to the collapsing of one of the strips of the graph. In the following, we outline how to

determine the boundaries of the cells from both the strips description and the tuples description.

Recall that each pole-labelled Nakamura graph is described by an equivalence class of split tuples, in which tuples are equivalent when they are related by conjugacy or slide-equivalence. Every point in the cell of the graph has an associated conjugacy equivalence class of split tuples, generated from the branched covering of the surface onto the sphere and the labelling of the poles. Zeroes of the Nakamura graph with the same time coordinate will correspond to cycles in the same permutation. This conjugacy equivalence class will not be an equivalence class of reduced split tuples in general, but will be slide-equivalent to the reduced split tuple of the graph. The reduced tuple comes from tuning as many of the time-coordinates of the zeroes to be coincident and as early as possible. We can also generate an **expanded split tuple** by tuning the time-coordinates such that every zero of the graph has a distinct time coordinate.

We can encode the data given by a tuple $(\sigma_+, \sigma_1, \sigma_2, \ldots, \sigma_m; \sigma_-^{(1)}, \ldots \sigma_-^{(n-1)})$ in terms of the variables $\Sigma_0 := \sigma_+$, $\Sigma_k = \sigma_+\sigma_1 \ldots \sigma_k$. This alternative tuple

$$(\Sigma_0, \Sigma_1, \Sigma_2, \ldots, \Sigma_m; \sigma_-^{(1)}, \ldots \sigma_-^{(n-1)}) \tag{3.3.13}$$

directly encodes how the strips of a surface are glued, as was demonstrated in Section 3.2 in Figure 3.6. Each strip with upper edges all labelled i is glued to strips with lower edges labelled $\Sigma_k(i)$. Given a tuple Σ_i, we can recover the original tuple by inverting the above formulae: $\sigma_+ = \Sigma_0$, $\sigma_k = \Sigma_{k-1}^{-1}\Sigma_k$.

We consider the boundaries of the cell corresponding to the time-ordering constraints. These boundaries arise in the limit when two time coordinates merge together. Focusing on the (cell) codimension one boundaries of a cell, we first take a point in the bulk of the cell at which the l internal vertices have distinct time coordinates, and label the associated single-cycle permutations $\sigma_1, \ldots, \sigma_l$. For a pair of zeroes σ_k, σ_{k+1} which cannot be commuted past each other by slide-equivalence, there is an associated time-inequality $t_k < t_{k+1}$. As can be seen in Figure 3.12, taking the limit as $t_{k+1} \to t_k$ corresponds to removing the internal edges directly following the σ_k. The effect on the permutation is to replace the consecutive cycles σ_k, σ_{k+1} with the single permutation $\sigma_k\sigma_{k+1}$:

$$(\sigma_+, \ldots, \sigma_{k-1}, \sigma_k, \sigma_{k+1}, \ldots; \sigma_-^{(1)}, \ldots) \to (\sigma_+, \cdots, \sigma_{k-1}, \sigma_k\sigma_{k+1}, \ldots; \sigma_-^{(1)}, \ldots) \tag{3.3.14}$$

In terms of the Σ_i description, this type of cell incidence corresponds to dropping Σ_k

from the Σ-tuple:

$$(\Sigma_0, \ldots, \Sigma_{k-1}, \Sigma_k, \Sigma_{k+1}, \ldots;\ \sigma_-^{(1)}, \ldots) \to (\Sigma_0, \ldots, \Sigma_{k-1}, \Sigma_{k+1}, \ldots;\ \sigma_-^{(1)}, \ldots) \quad (3.3.15)$$

Such a contraction of the strip can in general change the genus of the strip-decomposed surface. In this case, the boundary of the cell is not a cell in $\mathcal{M}_{g,n}$. We can formulate a condition to ascertain if a contraction of permutations gives a surface of the same genus by using the Riemann-Hurwitz formula,

$$2g - 2 + n = \sum_{k=1}^{m} (d - C_{\sigma_k}) = \Delta + l. \quad (3.3.16)$$

The expression $(d - C_{\sigma_i})$ is the **branching number** of the permutation σ_i, and Δ is the (overall) branching number defined in Section 3.1.3 of a Nakamura graph with l zeroes. If each σ_i is a single non-trivial cycle, then a contraction of the subsequent non-disjoint cycles σ_k and σ_{k+1} will preserve the genus if the sum over the branching numbers is preserved:

$$(d - C_{\sigma_k}) + (d - C_{\sigma_{k+1}}) = (d - C_{\sigma_k \sigma_{k+1}}). \quad (3.3.17)$$

Equivalently, the genus is preserved if and only if $(\Delta + l)$ is unchanged in the merging. When this condition is satisfied, the permutation tuple resulting from the contraction defines a new slide equivalence class with one fewer time parameter, and so specifies a cell in $\mathcal{M}_{g,n}$ with one fewer dimension. For a given time-inequality $t_k < t_{k+1}$, there can be many different boundaries of the cell, which correspond to the different initial choices of the time-coordinates of the remaining interaction vertices.

As an example of when the genus-preserving condition is not satisfied, the contraction of a pair of permutations satisfying $\sigma_k \sigma_{k+1} = 1$ cannot preserve the genus, as the right-hand-side of (3.3.17) is zero and the left-hand-side is always positive. Another example of a genus-reducing contraction is when $\sigma_k = (123)$, $\sigma_{k+1} = (234)$, and $\sigma_k \sigma_{k+1} = (13)(24)$. Here, the branching numbers before contraction add up to four, but the product permutation has a branching number of two. We present some examples where genus is conserved in later sections.

Next, we consider the boundaries of the cell corresponding to the strip-width constraint $b_j > 0$. A strip can be collapsed to zero width if the label on the upper bound of the strip j is not fixed by σ_-. Look at the labels on the upper and lower edges of a strip, such as in the top half of Figure 3.12, we can see that the collapse of a strip

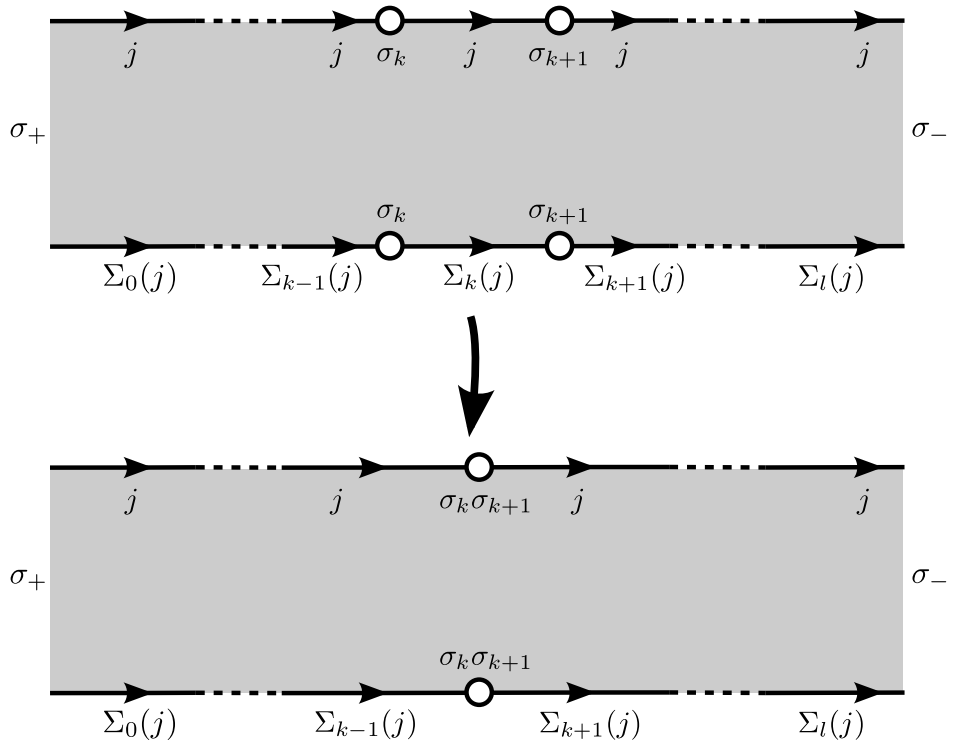

Figure 3.12: Taking the limit of a time inequality.

$b_j \to 0$ corresponds to replacing j in each permutation Σ_k with $\Sigma_k(j)$ when $\Sigma_k(j) \neq j$, or dropping the 1-cycle (j) from Σ_k when $\Sigma_k(j) = j$. In other words, we remove each occurrence of j from each permutation in the Σ-tuple

$$(\Sigma_0, \Sigma_1, \Sigma_2, \ldots, \Sigma_m; \sigma_-^{(1)}, \ldots \sigma_-^{(n-1)}). \tag{3.3.18}$$

To find a codimension one boundary of a cell from strip-collapse, we first take a point in the cell with distinct time coordinates for the l zeroes. We construct the associated Σ-tuple, remove each occurrence of j from the tuple, relabel the tuple with labels in $\{1, \ldots, d-1\}$, and rewrite the tuple back in terms of σ_k, dropping any identity permutations appearing within the σ_k, $k = 1, \ldots, l$.

As with the contraction of internal edges, the surface constructed from contracting a strip might not have the same genus as the original surface. In the case that strip contraction preserves the genus, then the slide-equivalence class of the new tuple specifies a new cell on the boundary of the original cell. The Riemann-Hurwitz formula (3.3.16) relates the sum of the branching numbers of the zeroes of a tuple to the genus and number of poles of the surface. We can deduce that a strip contraction of the

tuples $(\sigma_+, \sigma_1, \ldots, \sigma_-) \mapsto (\tilde{\sigma}_+, \tilde{\sigma}_1, \ldots, \tilde{\sigma}_-)$ preserves the genus of the surface if and only if the sum over branching numbers is conserved in the contraction:

$$\sum_{i=1}^{m}(d - C_{\sigma_i}) = \sum_{i=1}^{m}(d - 1 - C_{\tilde{\sigma}_i}). \tag{3.3.19}$$

Equivalently, strip contraction preserves the genus if and only if the sum $(\Delta + l)$ is conserved. We present some explicit examples of this collapsing in the following sections.

3.3.3 Example: $\mathcal{M}_{0,4}$ and $\mathcal{M}_{0,1[3]}$

We can explicitly derive the cell complex of $\mathcal{M}_{g,n}$ using this procedure for some examples of low genus and few punctures. One of the simplest non-trivial examples of a moduli space is $\mathcal{M}_{0,4}$, the space of inequivalent Riemann surfaces with four distinguishable labelled points. It is not hard to construct this space explicitly without reference to the Nakamura cell decomposition. Consider a base-space Riemann sphere with three labelled points, which we choose to be $(1, e^{2i\pi/3}, e^{4i\pi/3})$. The group of biholomorphic maps on the Riemann sphere are the Möbius maps, and given a Riemann sphere with four marked points q_1, q_2, q_3, q_4, then there exists a unique Möbius map which takes $q_1 \mapsto 1$, $q_2 \mapsto e^{2i\pi/3}$, $q_3 \mapsto e^{4i\pi/3}$. This biholomorphism maps q_4 to some point z, with $z^3 \neq 1$. The only biholomorphism fixing three points on the Riemann sphere is the identity, and so this map is unique; any two Riemann spheres with four labelled points are related by a biholomorphism if and only there are Möbius maps taking q_4 to the same point z with $q_1 \mapsto 1$, $q_2 \mapsto e^{2i\pi/3}$, $q_3 \mapsto e^{4i\pi/3}$. This z parametrises the equivalence classes of spheres with four labelled points, and so we deduce that the moduli space is the Riemann sphere with three punctures,

$$\mathcal{M}_{0,4} = \mathbb{C}_\infty \backslash \{1, e^{2i\pi/3}, e^{4i\pi/3}\}. \tag{3.3.20}$$

In this section, we show that the cell decomposition arising from Nakamura graphs reproduces this moduli space.

First, we choose an arbitrary set of residues r_1, r_2, r_3 to assign to the outgoing poles, where $r_i < 0$. There are three distinct Nakamura graphs of genus zero with four external points: these are shown in Figure 3.13. There are several distinct possible labellings of the outgoing poles for each graph. Each pole-labelled graph corresponds to a distinct cell in the cell decomposition of $\mathcal{M}_{0,4}$. The cells in moduli space corresponding to the same labelled graph are similar in structure, and differ only in their

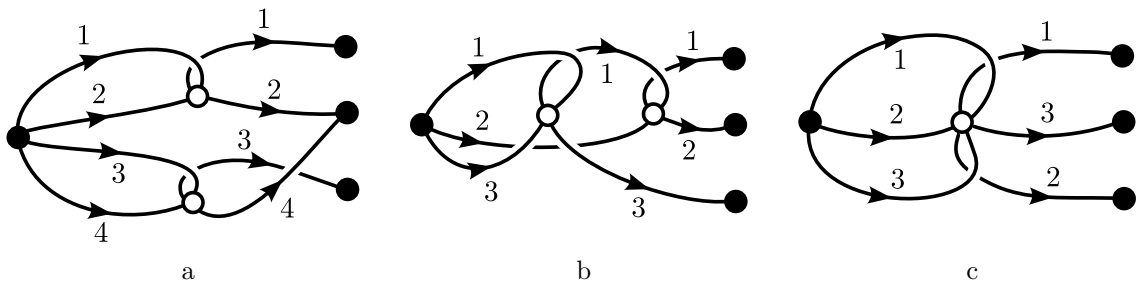

Figure 3.13: The Nakamura graphs of $\mathcal{M}_{0,4}$ (without pole labellings).

labellings and in the assignments of the r_i. In this example, all the boundaries of the cells in $\mathcal{M}_{0,4}$ will correspond to other cells in $\mathcal{M}_{0,4}$, as there are no genus-reducing cell boundaries.

The graph in Figure 3.13a was discussed in previous sections. There are three distinct pole-labelled Nakamura graphs corresponding to this unlabelled graph, and they are described by the split reduced tuples

$$A_1 : (\sigma_+, \tau;\ \sigma_-^{(1)}, \sigma_-^{(2)}, \sigma_-^{(3)}) = ((1234), (12)(34);\ (1), (24), (3)), \quad (3.3.21)$$

$$A_2 : (\sigma_+, \tau;\ \sigma_-^{(2)}, \sigma_-^{(1)}, \sigma_-^{(3)}) = ((1234), (12)(34);\ (24), (1), (3)), \quad (3.3.22)$$

$$A_3 : (\sigma_+, \tau;\ \sigma_-^{(1)}, \sigma_-^{(3)}, \sigma_-^{(2)}) = ((1234), (12)(34);\ (1), (3), (24)). \quad (3.3.23)$$

The pole-labelled graphs associated to these tuples were drawn in Figure 3.10. The cell A_1 associated to the first of these tuples is a subset of $\mathbb{R}^6$, with the coordinates $\{b_1, b_2, b_3, b_4; t_1, t_2\}$, subject to the constraints:

$$b_1 = |r_1|, \quad (3.3.24)$$

$$b_2 + b_4 = |r_2|, \quad (3.3.25)$$

$$b_3 = |r_3|, \quad (3.3.26)$$

$$t_1 + t_2 = 0, \quad (3.3.27)$$

$$b_2, b_4 > 0. \quad (3.3.28)$$

The other two cells A_2 and A_3 are defined similarly, but with the r_i interchanged. These equations define a two-dimensional subspace of $\mathbb{R}^6$, which we can parametrise by the two variables b_2 and t_2, subject to the relation

$$0 < b_2 < |r_2|. \quad (3.3.29)$$

The time coordinate t_2 is unconstrained and can take any real value. This means that the cell associated to this tuple is an infinite strip of width $|r_2|$. The upper and lower boundaries of the strip correspond to the limiting values of $b_2 = |r_2|$ (i.e. $b_4 = 0$) and $b_2 = 0$ respectively. The other two cells A_2 and A_3 are strips of width $|r_1|$ and $|r_3|$ respectively. The pole-fixing automorphism group of the graph is trivial, and so there is no orbifolding of the cells.

The graph in Figure 3.13b has six distinct pole labellings, given by the split tuples

$$\begin{aligned}
B_1 : (\sigma_+, \tau_1, \tau_2;\ \sigma_-^{(1)}, \sigma_-^{(2)}, \sigma_-^{(3)}) &= ((123), (13), (12);\ (1), (2), (3)), && (3.3.30)\\
B_2 : (\sigma_+, \tau_1, \tau_2;\ \sigma_-^{(2)}, \sigma_-^{(3)}, \sigma_-^{(1)}) &= ((123), (13), (12);\ (2), (3), (1)), && (3.3.31)\\
B_3 : (\sigma_+, \tau_1, \tau_2;\ \sigma_-^{(3)}, \sigma_-^{(1)}, \sigma_-^{(2)}) &= ((123), (13), (12);\ (3), (1), (2)), && (3.3.32)\\
B_4 : (\sigma_+, \tau_1, \tau_2;\ \sigma_-^{(1)}, \sigma_-^{(3)}, \sigma_-^{(2)}) &= ((123), (13), (12);\ (1), (3), (2)), && (3.3.33)\\
B_5 : (\sigma_+, \tau_1, \tau_2;\ \sigma_-^{(2)}, \sigma_-^{(1)}, \sigma_-^{(3)}) &= ((123), (13), (12);\ (2), (1), (3)), && (3.3.34)\\
B_6 : (\sigma_+, \tau_1, \tau_2;\ \sigma_-^{(3)}, \sigma_-^{(2)}, \sigma_-^{(1)}) &= ((123), (13), (12);\ (3), (2), (1)). && (3.3.35)
\end{aligned}$$

The cell B_1 associated to the first of these tuples is a subspace of $\mathbb{R}^5$ with coordinates $\{b_1, b_2, b_3; t_1, t_2\}$, defined by the constraints

$$\begin{aligned}
b_1 &= |r_1|, && (3.3.36)\\
b_2 &= |r_2|, && (3.3.37)\\
b_3 &= |r_3|, && (3.3.38)\\
t_1 + t_2 &= 0, && (3.3.39)\\
t_1 &< t_2. && (3.3.40)
\end{aligned}$$

There is only one free parameter in this cell, which we can take to be t_2, which satisfies

$$0 < t_2 < \infty. \tag{3.3.41}$$

The cell B_1 is a half-line, with a boundary at the point $t_2 = 0$. The automorphism group of the cell is trivial. The other cells $B_2, \ldots, B_6$ have similar descriptions.

Finally, the graph in Figure 3.13c has two associated pole-labellings, corresponding to the split tuples

$$\begin{aligned}
C_1 : (\sigma_+, \tau;\ \sigma_-^{(1)}, \sigma_-^{(2)}, \sigma_-^{(3)}) &= ((123), (132);\ (1), (2), (3)), && (3.3.42)\\
C_2 : (\sigma_+, \tau;\ \sigma_-^{(1)}, \sigma_-^{(3)}, \sigma_-^{(2)}) &= ((123), (132);\ (1), (3), (2)). && (3.3.43)
\end{aligned}$$

For the first cell C_1, the variables b_1, b_2, b_3, t satisfy the constraints

$$\begin{aligned} b_1 &= |r_1|, && (3.3.44)\\ b_2 &= |r_2|, && (3.3.45)\\ b_3 &= |r_3|, && (3.3.46)\\ t &= 0. && (3.3.47) \end{aligned}$$

All four variables are fixed, so this cell is zero-dimensional. The automorphism group is trivial, and so there is no orbifolding. Similarly, C_2 is a zero-dimensional cell.

Collating the above, the cell decomposition of $\mathcal{M}_{0,4}$ consists of three cells A_1, A_2, A_3 that are two-dimensional strips in parameter space, six cells $B_1, \ldots, B_6$ that are 1-dimensional half-lines, and a pair of 0-dimensional point cells C_1, C_2. The incidences of these cells can be found by looking at the tuples and applying the strip-collapsing or interaction point-collapsing algorithms. It can be shown that each of the two boundaries of a cell A_i contains a pair of half-line cells B_i, and that these half-lines share a boundary cell C_i. We will demonstrate the procedure for one of the boundaries of the strip cell A_1 and a boundary of the half-line cell B_1.

The cell A_1 is parametrised by the half-strip in (b_2, t_2)-space, where $0 < b_2 < |r_2|$, and t_2 can take any value. Consider the case of the strip width b_2 approaching $|r_2|$, with $t_2 < 0$. In this range of time coordinates, the zero corresponding to (34) appears at an earlier time than the zero corresponding to (12), and so the split tuple of points in the cell in this range is

$$(\sigma_+, \sigma_1, \sigma_2;\ \sigma_-^{(1)}, \sigma_-^{(2)}, \sigma_-^{(3)}) \quad = \quad ((1234), (34), (12);\ (1), (24), (3)). \qquad (3.3.48)$$

The limit $b_2 \to |r_2|$ corresponds to taking the strip width $b_4 \to 0$. Employing the procedure for strip collapse from the previous section, we convert the tuple into the Σ-notation:

$$(\Sigma_0, \Sigma_1, \Sigma_2;\ \sigma_-^{(1)}, \sigma_-^{(2)}, \sigma_-^{(3)}) = ((1234), (124)(3), (1)(24)(3); (1), (24), (3)). \qquad (3.3.49)$$

Here, we have written out the 1-cycles explicitly. Collapsing the strip with upper edges labelled 4 corresponds to removing the integer 4 from each cycle in the Σ-tuple:

$$(\Sigma_0, \Sigma_1, \Sigma_2;\ \sigma_-^{(1)}, \sigma_-^{(2)}, \sigma_-^{(3)}) = ((123), (12)(3), (1)(2)(3); (1), (2), (3)). \qquad (3.3.50)$$

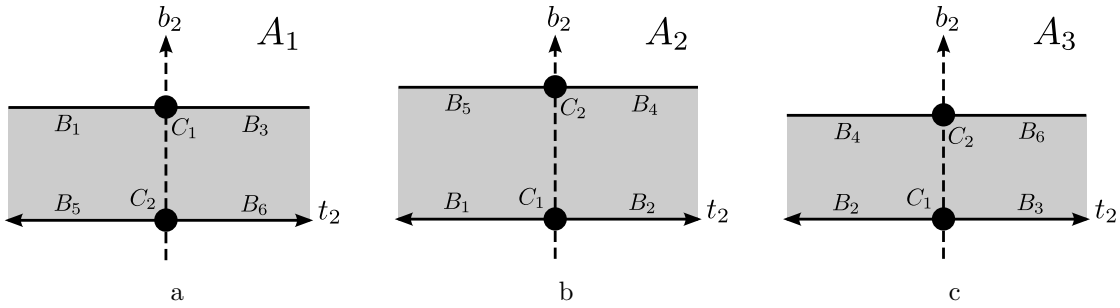

Figure 3.14: The 2-dimensional cells A_1, A_2, A_3, and their incidences with lower-dimensional cells.

Converting this back into the σ-notation, we find the split tuple

$$(\sigma_+, \sigma_1, \sigma_2;\ \sigma_-^{(1)}, \sigma_-^{(2)}, \sigma_-^{(3)}) = ((123), (13), (12); (1), (2), (3)). \tag{3.3.51}$$

This is the split tuple of the cell B_1, given in (3.3.30). We deduce that the $b_2 = |r_2|, t_2 < 0$ boundary of the cell A_1 is the cell B_1. A similar procedure can be applied to the $b_2 = |r_2|, t_2 > 0$ boundary, the $b_2 = 0, t_2 < 0$ boundary, and the $b_2 = 0, t_2 > 0$ boundary of the cell. We recover the split tuples of the half-line cells B_3, B_5, and B_6 respectively.

The cell B_1 is a half-line, corresponding to the split tuple (3.3.51), and parametrised by the time coordinate $\tilde{t}_2$ of the interaction point associated to the cycle (12), where $\tilde{t}_2 > 0$. (Note that this time coordinate is not the same as the time coordinate on the cell A_1 given above, as the ordering of the interaction vertices has been interchanged.) Taking the limit $\tilde{t}_2 \to 0$ while $\tilde{t}_1 + \tilde{t}_2 = 0$ is held fixed corresponds to merging the two interaction points together. The corresponding new interaction point is described by the product of the permutations of the original two points, as was shown in the previous subsection. The merging of the two points $\sigma_1 = (13)$ and $\sigma_2 = (12)$ generates the new split tuple

$$(\sigma_+, \tau;\ \sigma_-^{(1)}, \sigma_-^{(2)}, \sigma_-^{(3)}) = ((123), (132);\ (1), (2), (3)) \tag{3.3.52}$$

which is the split tuple (3.3.42) of the 0-dimensional cell C_1.

By performing a similar analysis on each cell A_1, A_2, A_3 in turn, we find that each cell borders four distinct 1-cells and two distinct 0-cells. A diagram showing the cells and their incidences is given in Figure 3.14. These cells glue together to form a sphere with three punctures, as shown in Figure 3.15, where the positive and negative infinities of the strips have been homeomorphically mapped to the white vertices of

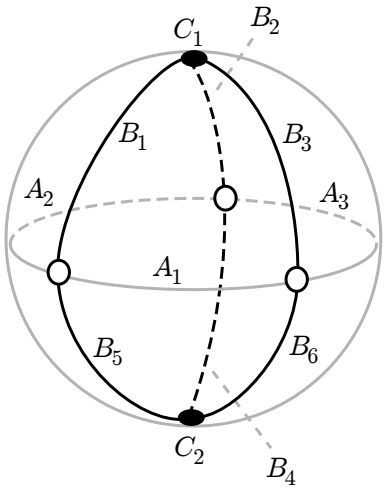

Figure 3.15: The cell decomposition of $\mathcal{M}_{0,4}$.

the diagram. This picture agrees with the description of $\mathcal{M}_{0,4}$ as a three-punctured sphere given at the beginning of this section.

We can also obtain the cell decomposition of $\mathcal{M}_{0,1[3]}$ by using this cell decomposition of $\mathcal{M}_{0,4}$. First, set $r_1 = r_2 = r_3 = r$ for some negative real r. The split tuples associated to the cells C_1, C_2 in $\mathcal{M}_{0,4}$ differ only by a rearrangement of the cycles representing the poles, and so these cells correspond to the same cell C in $\mathcal{M}_{0,1[3]}$, described by the tuple

$$(\sigma_+, \tau, \sigma_-) = ((123), (132), ()). \tag{3.3.53}$$

Similarly, there is a single 1-cell B in $\mathcal{M}_{0,1[3]}$ associated to the six 1-cells $B_1, \ldots, B_6$ of $\mathcal{M}_{0,4}$. There is also a single cell A in $\mathcal{M}_{0,1[3]}$, corresponding to the three cells A_1, A_2, A_3, with the reduced tuple

$$(\sigma_+, \tau, \sigma_-) = ((1234), (12)(34), (24)). \tag{3.3.54}$$

The covering space $\mathcal{B}(\mathcal{G})$ of the cell A is defined by the constraints

$$\begin{aligned} b_1 &= |r|, && (3.3.55)\\ b_2 + b_4 &= |r|, && (3.3.56)\\ b_3 &= |r|, && (3.3.57)\\ t_1 + t_2 &= 0, && (3.3.58)\\ b_2, b_4 &> 0. && (3.3.59) \end{aligned}$$

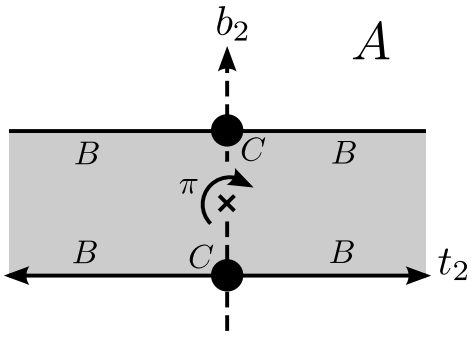

Figure 3.16: The 2-cell A in the cell decomposition of $\mathcal{M}_{0,1[3]}$.

The tuple has the non-trivial automorphism group $\mathbb{Z}_2$ generated by the permutation (13)(24). This acts on the parameter space by interchanging the time coordinates of the zeroes and strip widths $t_1 \leftrightarrow t_2$, $b_1 \leftrightarrow b_3$, $b_2 \leftrightarrow b_4$. This acts on the parametrising strip $-\infty < t_2 < \infty$, $0 < b_2 < |r|$ as a rotation by π about the point $t_2 = 0, b_2 = |r|/2$. The cell A in $\mathcal{M}_{0,1[3]}$ is the quotient space $\mathcal{B}(\mathcal{G})/\mathbb{Z}_2$. This is shown in Figure 3.16

The moduli space $\mathcal{M}_{0,1[3]}$ can be visualised as a quotienting of $\mathcal{M}_{0,4}$. In the Möbius maps description, a pair of points on the three-punctured sphere represent the same point in $\mathcal{M}_{0,1[3]}$ if they are related by a Möbius map which preserves the set of three punctures $\{1, e^{2\pi i/3}, e^{4\pi i/3}\}$. The set of Möbius maps which preserve these three points is the group S_3, and acts on the Riemann sphere 3.14 like a finite group of rotations. We deduce that

$$\mathcal{M}_{0,1[3]} = (\mathbb{C}_\infty \backslash \{1, e^{2i\pi/3}, e^{4i\pi/3}\})/S_3. \tag{3.3.60}$$

In terms of the cells decomposition of $\mathcal{M}_{0,4}$ shown in Figure 3.14, the quotienting by S_3 identifies the 2-cells labelled A_1, A_2, A_3, the 1-cells labelled $B_1, \ldots, B_6$, and the 0-cells labelled C_1, C_2. The 2-cell of $\mathcal{M}_{0,1[3]}$ acquires a non-trivial automorphism group $\mathbb{Z}_2$ in this quotienting.

3.3.4 Example: $\mathcal{M}_{1,2}$

In this subsection we present another example of an explicit low-dimensional cell decomposition of a moduli space. There are four Nakamura graphs with $g = 1$ and $n = 2$, which are shown in Figure 3.17. These graphs correspond to the cells of the four-dimensional moduli space $\mathcal{M}_{1,2}$. As there is one incoming and one outgoing pole for each graph, there is just one possible labelling of the outgoing pole for each graph, and so each graph corresponds to exactly one cell in the cell decomposition of moduli

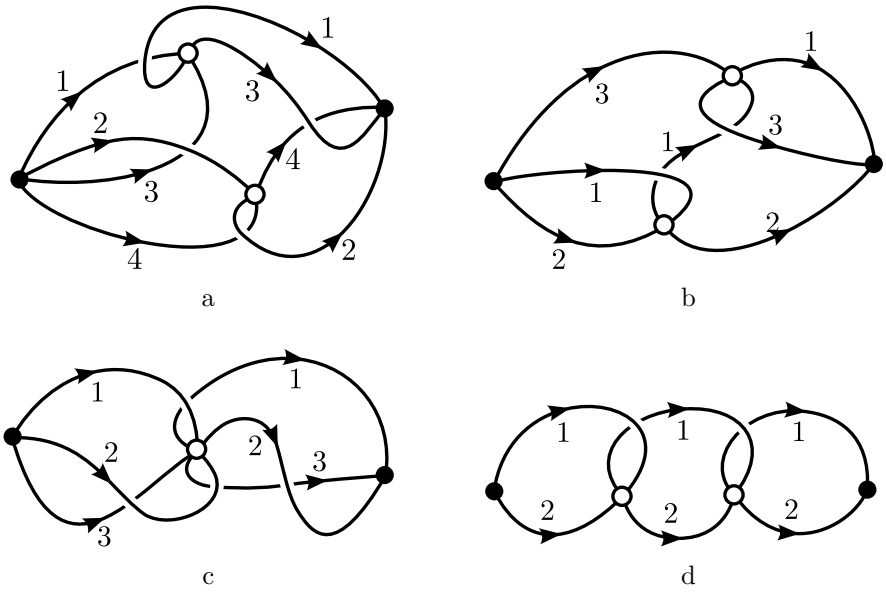

Figure 3.17: The Nakamura graphs of $\mathcal{M}^{\rm fix}_{1,2}$.

space. We refer to these cells as cell A, B, C, and D respectively. Unlike the previous example of $\mathcal{M}_{0,4}$, the automorphism groups $\mathrm{Aut}_{\rm fix}(\mathcal{G}) = \mathrm{Aut}(\mathcal{G})$ of these graphs are non-trivial, so $\mathcal{M}_{1,2}$ is not a manifold. Also, as this is a moduli space of Riemann surfaces with non-zero genus, there can be cell boundaries that correspond to surfaces of reduced genus, and so are not contained within the moduli space $\mathcal{M}_{1,2}$.

The four cells of $\mathcal{M}_{1,2}$ are described by the tuples

$$\begin{aligned} A : (\sigma_+, \tau;\ \sigma_-) &= ((1234), (13)(24);\ (1234)), && (3.3.61)\\ B : (\sigma_+, \tau_1, \tau_2; \sigma_-) &= ((123), (12), (13);\ (123)), && (3.3.62)\\ C : (\sigma_+, \tau;\ \sigma_-) &= ((123), (123);\ (123)), && (3.3.63)\\ D : (\sigma_+, \tau_1, \tau_2;\ \sigma_-) &= ((12), (12), (12);\ (12)). && (3.3.64) \end{aligned}$$

Cell A is constructed by quotienting a subspace of $\{(b_1, b_2, b_3, b_4; t_1, t_2)\}$ with $\mathbb{Z}_4$, the automorphism group of the graph. The strip widths and time coordinates of points in A satisfy the relations

$$\begin{aligned} b_1 + b_2 + b_3 + b_4 &= |r|, \\ b_i &> 0, \qquad i = 1, 2, 3, 4 \\ t_1 + t_2 &= 0. \end{aligned} \qquad (3.3.65)$$

The cell is four-dimensional, as b_4 and t_1 can be written in terms of the variables

$(b_1, b_2, b_3; t_2)$ which satisfy

$$\begin{aligned} b_i &> 0, \qquad i = 1, 2, 3, 4 \\ b_1 + b_2 + b_3 &< |r| \end{aligned} \tag{3.3.66}$$

with t_2 taking any real value. The generator a of the automorphism group $\mathrm{Aut}_{\mathrm{fix}}(\mathcal{G}) = \mathbb{Z}_4$ acts on the edge labels as the permutation (1234) and acts on the time coordinates as the permutation (12). Geometrically, this cell is the direct product of a 3-simplex (tetrahedron) and the real line, with a quotienting $\mathbb{Z}_4$ action on the tetrahedron and a $\mathbb{Z}_2$ action on the real line.

The automorphism group of cell A identifies the four boundaries of the parameter space at $b_j = 0$, so cell A has a single codimension one boundary. To determine the cell on this boundary, we first split up the time coordinates of the two vertices to generate the tuple

$$(\sigma_+, \sigma_1, \sigma_2;\ \sigma_-) = ((1234), (13), (24);\ (1234)), \tag{3.3.67}$$

and employ the procedure described in subsection 3.3.2 to take the strip width $b_4 \to 0$. The tuples generated at each step are:

$$\begin{aligned} \xrightarrow{\Sigma} (\Sigma_0, \Sigma_1, \Sigma_2;\ \sigma_-) &= ((1234), (12)(34), (1432);\ (1234)) && (3.3.68) \\ \xrightarrow{-4} (\Sigma_0, \Sigma_1, \Sigma_2;\ \sigma_-) &= ((123), (12)(3), (132);\ (123)) && (3.3.69) \\ \xrightarrow{\sigma} (\sigma_+, \sigma_1, \sigma_2;\ \sigma_-) &= ((123), (13), (23);\ (123)) && (3.3.70) \\ \xrightarrow{\text{relabel}} (\sigma_+, \sigma_1, \sigma_2;\ \sigma_-) &= ((123), (12), (13);\ (123)). && (3.3.71) \end{aligned}$$

In the last step, we have relabelled the tuple by acting on the tuple by conjugation with (123). We see that the cell B lies on the boundary of A.

Cell B is described by the variables $(b_1, b_2, b_3; t_1, t_2)$ which satisfy

$$\begin{aligned} b_1 + b_2 + b_3 &= |r| && (3.3.72) \\ b_1, b_2, b_3 &> 0, && (3.3.73) \\ t_1 + t_2 &= 0 && (3.3.74) \\ t_1 &< t_2 && (3.3.75) \end{aligned}$$

The cell is three-dimensional and can be parametrised by the variables $(b_1, b_2; t_2)$ sat-

isfying

$$b_1, b_2, t_2 > 0 \tag{3.3.76}$$
$$b_1 + b_2 < |r| \tag{3.3.77}$$
$$t_2 > 0. \tag{3.3.78}$$

The automorphism group $\mathrm{Aut}_{\mathrm{fix}}(\mathcal{G})$ of the graph is trivial. Geometrically, the cell is the direct product of a 2-simplex (triangle) and a half-line. The cell has four boundaries of the form $b_1 = 0$, $b_2 = 0$, $b_3 = 0$, and $t_2 = 0$.

The boundary $t_2 \to 0$ of cell B corresponds to the merging of the two interaction vertices; it can be seen that this gives the cell C of the graph with a single interior vertex. Collapsing either the strip width $b_3 \to 0$ or the strip width $b_2 \to 0$ leads to the tuple

$$(\sigma_+, \sigma_1, \sigma_2;\ \sigma_-) = ((12), (12), (12);\ (12)), \tag{3.3.79}$$

hence two of the boundaries of B are the cell D. However, collapsing the strip $b_1 \to 0$ leads to a different tuple: we have

$$\begin{aligned}
(\sigma_+, \sigma_1, \sigma_2; \sigma_-) &= ((123), (12), (13);\ (123)) && (3.3.80)\\
\xrightarrow{\Sigma} (\Sigma_0, \Sigma_1, \Sigma_2;\ \sigma_-) &= ((123), (1)(23), (132);\ (123)) && (3.3.81)\\
\xrightarrow{-1} (\Sigma_0, \Sigma_1, \Sigma_2;\ \sigma_-) &= ((23), (23), (23);\ (23)) && (3.3.82)\\
\xrightarrow{\text{relabel}} (\Sigma_0, \Sigma_1, \Sigma_2;\ \sigma_-) &= ((12), (12), (12);\ (12)) && (3.3.83)\\
\xrightarrow{\sigma} (\sigma_+, \sigma_1, \sigma_2;\ \sigma_-) &= ((12), (), ();\ (12)). && (3.3.84)\\
\xrightarrow{\text{remove ()}} (\sigma_+;\ \sigma_-) &= ((12);\ (12)). && (3.3.85)
\end{aligned}$$

This last tuple does not describe a cell in $\mathcal{M}_{1,2}$. We can interpret the tuple as describing a degenerate Nakamura graph, representing the single point in the trivial moduli space $\mathcal{M}_{0,2}$. This means that the boundary $b_1 = 0$ of cell B is not part of the decomposition of $\mathcal{M}_{1,2}$.

Cell C is a two-dimensional simplex, parametrised by b_1 and b_2 satisfying

$$b_1, b_2 > 0, \tag{3.3.86}$$
$$b_1 + b_2 < |r|, \tag{3.3.87}$$

under the quotienting group $\mathbb{Z}_3$ which acts like a $2\pi/3$ rotation on the simplex. The

boundary of this cell corresponds to the degenerate tuple $((12);(12))$, so is not a part of the moduli space. Cell D is also two-dimensional and is parametrised by b_1 and t_2 satisfying

$$0 < \quad b_1 \quad < |r| \tag{3.3.88}$$

$$t_2 \quad > \quad 0, \tag{3.3.89}$$

under a $\mathbb{Z}_2$ quotienting. Geometrically, this cell is a half-strip of width $|r|$ with a $\mathbb{Z}_2$ quotienting associated to a reflection in the line $b_2 = |r|/2$. The boundaries $b_1 = 0$ and $t_2 = 0$ again correspond to the degenerate tuple $((12);(12))$, and are not part of the moduli space.

3.4 The cell decomposition of Teichmüller space

Nakamura graphs can also be used to find a cell decomposition of Teichmüller space. Teichmüller space can be thought of as the set of equivalence classes of marked complex structures on a topological surface $\Sigma_{g,n}$ of genus g with n marked points. A marked complex structure on $\Sigma_{g,n}$ is a triple (X, P_i, ϕ) in which X is a Riemann surface with labelled points P_i and $\phi : \Sigma_{g,n} \to X$ is a homeomorphism which maps the labelled points of $\Sigma_{g,n}$ to the respective labelled points P_i of X. A pair of marked complex structures $(X_1, P_i^{(1)}, \phi_1)$ and $(X_2, P_i^{(2)}, \phi_2)$ are Teichmüller-equivalent if there exists a biholomorphism $f : X_1 \to X_2$ such that $f \circ \phi_1$ and ϕ_2 are isotopic through labelled point-preserving homeomorphisms. More discussion on Teichmüller space and its relation to moduli space and mapping class groups is given in Appendix E.

It was stated in [31] that the 'marked graphs' give a cell decomposition of Teichmüller space, and that the action of the mapping class group preserves these cells, giving a cell decomposition of moduli space. In this section, we confirm this claim, showing that each point in the Teichmüller space $\mathcal{T}_{g,n}$ corresponds to a Nakamura graph $\bar{\mathcal{G}}$, an embedding of this graph on a surface $\Sigma_{g,n}$, and some strip widths b_j and interaction times t_k. Each cell is specified by a pair $(\bar{\mathcal{G}}, \hat{\psi})$, where $\hat{\psi}$ is a graph embedding into $\Sigma_{g,n}$, and this cell is in one-to-one correspondence with the parameter space $\mathcal{B}(\bar{\mathcal{G}})$ of the graph.

On choosing a set of residues $r_1, r_2, \ldots r_n$, any Riemann surface X has a Nakamura strip decomposition $(\bar{\mathcal{G}}, b_j, t_k)$, which is unique up to relabellings of the parameters. Inverting the complex structure marking $\phi : \Sigma_{g,n} \to X$ gives a strip embedding $\psi : X \to \Sigma_{g,n}$, which restricts to a graph embedding on the boundaries of the strips

$\hat{\psi} : \mathcal{G} \to \Sigma_{g,n}$. A graph embedding $\hat{\psi}$ and a strip decomposition is enough to reconstruct a strip embedding ψ up to isotopy.

We can rephrase the above definition of Teichmüller space in terms of Nakamura graph embeddings and strip decompositions. Teichmüller space is the set of equivalence classes of tuples of the form $(\bar{\mathcal{G}}, \hat{\psi}, b_j, t_k)$ consisting of a pole-labelled graph, a graph embedding, a set of strip widths, and a set of time coordinates. A pair of tuples $(\bar{\mathcal{G}}^{(1)}, \hat{\psi}^{(1)}, b_j^{(1)}, t_k^{(1)})$ and $(\bar{\mathcal{G}}^{(2)}, \hat{\psi}^{(2)}, b_j^{(2)}, t_k^{(2)})$ are Teichmüller equivalent if and only if:

- The graphs are identical: $\bar{\mathcal{G}}^{(1)} = \bar{\mathcal{G}}^{(2)}$;
- There exists an automorphism $g \in \mathrm{Aut}(\bar{\mathcal{G}}^{(1)})$ which acts on the parameters of the graph as $b_j^{(1)} \mapsto b_j^{(2)}$, $t_k^{(1)} \mapsto t_k^{(2)}$;
- The graph embeddings $\hat{\psi}^{(1)}$ and $\hat{\psi}^{(2)} \circ g$ are isotopic.

In Section 3.3.1, we constructed the set $\mathcal{B}(\bar{\mathcal{G}})$ parametrising the possible strip decompositions $\{(b_j, t_k)\}$ of Riemann surfaces for a given graph. In general, there are distinct points in $\mathcal{B}(\bar{\mathcal{G}})$ that correspond to the same Riemann surface. The number of points in $\mathcal{B}(\bar{\mathcal{G}})$ that correspond to the same Riemann surface X is the order of the **biholomorphism group** $\mathrm{Bi}(X)$, which is the group of biholomorphisms from the surface X to itself.[1]

We show that for a given graph $\bar{\mathcal{G}}$ and graph embedding $\hat{\psi} : \bar{\mathcal{G}} \to \Sigma_{g,n}$, a pair of strip decompositions of the graph $(b_j^{(1)}, t_k^{(1)})$ and $(b_j^{(2)}, t_k^{(2)})$ in $\mathcal{B}(\bar{\mathcal{G}})$ can only correspond to Teichmüller-equivalent points when the parameters are identical. For Teichmüller-equivalence, these strip decompositions must correspond to the same Riemann surface X, and there must exist a graph automorphism g with the property that $\hat{\psi}$ and $\hat{\psi} \circ g$ are isotopic. This graph automorphism g acts on the parameters of the strips as a permutation, and so extends to a biholomorphism $f_g : X \to X$. The graph embedding $\hat{\psi}$ can be extended to a strip embedding $\psi : X \to \Sigma_{g,n}$, and so ψ and $\psi \circ f_g$ are isotopic embeddings of the strips into $\Sigma_{g,n}$, which implies that f_g is isotopic to the identity. However, it was shown by Hurwitz [96] that non-trivial biholomorphisms of hyperbolic Riemann surfaces are not isotopic to the identity. We deduce that f_g is trivial, the graph automorphism g is trivial, and so the parameters must satisfy $b_j^{(1)} = b_j^{(2)}$, $t_k^{(1)} = t_k^{(2)}$.

We write $\mathcal{B}(\bar{\mathcal{G}}, \hat{\psi}) := \mathcal{B}(\mathcal{G})$ for the set of points in Teichmüller space corresponding to a graph $\bar{\mathcal{G}}$ and a marking $\hat{\psi} : \bar{\mathcal{G}} \to \Sigma_{g,n}$. To construct a cell decomposition of

[1] This group is sometimes called the *automorphism group* $\mathrm{Aut}(X)$ of the Riemann surface in the literature.

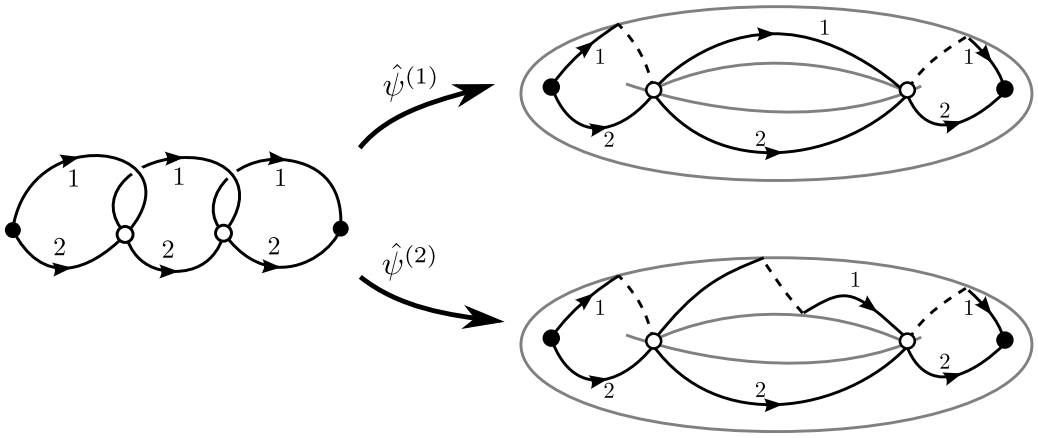

Figure 3.18: Two embeddings of a graph which cannot be identified by isotopy.

Teichmüller space $\mathcal{T}_{g,n}$, we find all the possible Nakamura graphs $\{\bar{\mathcal{G}}\}$ with genus g and n marked points, and the inequivalent graph embeddings $\hat{\psi}$ for each graph $\bar{\mathcal{G}}$. A pair of graph markings $\hat{\psi}^{(1)}$ and $\hat{\psi}^{(2)}$ are equivalent if there is a graph automorphism $g \in \mathrm{Aut}(\bar{\mathcal{G}})$ such that $\hat{\psi}^{(1)}$ and $\hat{\psi}^{(2)} \circ g$ are isotopic. The mapping class group $\Gamma_{g,n}$ acts on the set of graph embeddings in a well-defined way up to isotopy, and any two graph markings can be related by some element of the mapping class group. This confirms the claim that the marked graphs yield a cell decomposition of $\mathcal{T}_{g,n}$ which descends to a cell decomposition of $\mathcal{M}_{g,n}$.

We conclude this section with some examples of embeddings of a graph which was considered in the example in the previous section, determined by the tuple

$$(\sigma_+, \tau_1, \tau_2; \sigma_-) = ((12), (12), (12); (12)). \tag{3.4.1}$$

In Figure 3.18, we have shown two embeddings $\hat{\psi}^{(1)}$ and $\hat{\psi}^{(2)}$ of the graph into the two-punctured torus that cannot be isotopic. These two markings correspond to different cells $\mathcal{B}(\bar{\mathcal{G}}, \hat{\psi}^{(1)})$ and $\mathcal{B}(\bar{\mathcal{G}}, \hat{\psi}^{(2)})$ in Teichmüller space. In Figure 3.19, we have given two examples of strip embeddings $\psi^{(1)}$ and $\psi^{(3)}$ into the two-punctured torus. These embeddings of the strip decomposition correspond to the same point in Teichmüller space if and only if the strip widths are equal. The restriction of these strip embeddings to the graphs are $\hat{\psi}^{(1)}$ and $\hat{\psi}^{(3)}$, which are related by a graph automorphism, and so correspond to the same Teichmüller space cell $\mathcal{B}(\bar{\mathcal{G}}, \hat{\psi}^{(1)})$. This cell is parametrised by a strip width $b_1 \in (0, r)$ and an interaction time $t_2 > 0$, which is a semi-infinite strip.

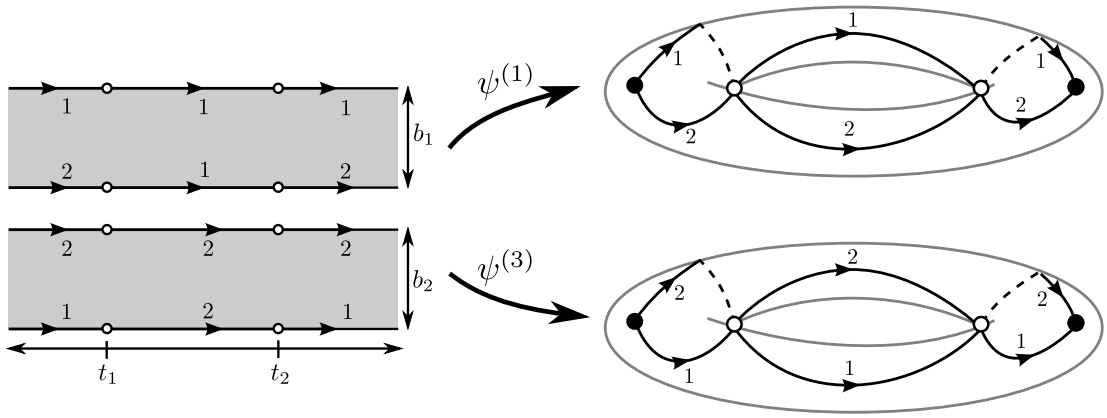

Figure 3.19: Two embeddings of the strips into the surface, which are Teichmüller-equivalent if and only if the strip widths are equal.

3.5 Verifying the cell decomposition with orbifold Euler characteristics

In [31], the orbifold Euler characteristic was used to verify at low genus that the Nakamura graphs give a cell decomposition of moduli space. All the graphs with graph Euler characteristic $|\chi| \leq 6$ were enumerated, along with their pole-permuting automorphism groups and dimensions. This enumeration matches the exact formula for the the orbifold Euler characteristic given in [34].

In the following subsections, we expand upon the idea of using the orbifold Euler characteristic as a check of the consistency of the Nakamura graph cell decomposition. The description of Nakamura graphs with equivalence classes of reduced tuples gives us some tractable methods to enumerate the graphs. The top-dimensional cells in $\mathcal{M}_{g,1[n-1]}$ correspond to Belyi triples of permutations, in which one of the permutations is a product of 2-cycles: these can be counted by using correlators of the Gaussian Hermitian matrix model. Similarly, the other high-dimensional cells of $\mathcal{M}_{g,1[n-1]}$ which correspond to graphs with no internal edges can be counted by using the correlators of the complex matrix model. We conclude this section with some discussion of how equivalence classes of reduced tuples were used to enumerate all the Nakamura graphs with graph Euler characteristic $|\chi| \leq 7$. The full details of the algorithmic approach that we used are presented in Appendix F.

3.5.1 The orbifold Euler characteristic

We review the construction of the orbifold Euler characteristic, following the definition of [97] for orbifolds with a cell decomposition. Let $\Gamma_{g,1[n-1]}$ to be the mapping class group of isotopy classes of homeomorphisms acting on a surface which fix one of the labelled points and permute the remaining $(n-1)$ labelled points. The quotienting of Teichmüller space $\mathcal{T}_{g,n}$ by this group gives the modified moduli space

$$\mathcal{M}_{g,1[n-1]} := \mathcal{T}_{g,n}/\Gamma_{g,1[n-1]}. \tag{3.5.1}$$

As discussed in previous sections, the cells of $\mathcal{M}_{g,n}$ correspond to unlabelled Nakamura graphs, the cells of the moduli space $\mathcal{M}_{g,1[n-1]}$ correspond to labelled Nakamura graphs, and the cells in the cell decomposition of $\mathcal{M}_{g,1[n-1]}$ can be constructed by quotienting the cells in $\mathcal{M}_{g,n}$. More discussion of the definitions of mapping class groups and Teichmüller space is given in Appendix E.

The orbifold Euler characteristic of a moduli space is equivalent to the *group Euler characteristic* of its associated mapping class group [98, 99]:

$$\chi(\mathcal{M}_{g,n}) = \chi(\Gamma_{g,n}). \tag{3.5.2}$$

A similar statement holds for the alternative definition of moduli space with permutable labelled points,

$$\chi(\mathcal{M}_{g,1[n-1]}) = \chi(\Gamma_{g,1[n-1]}). \tag{3.5.3}$$

This allows us to use some of the elementary properties of group Euler characteristics to find a relation between the orbifold Euler characteristics of $\mathcal{M}_{g,n}$ and $\mathcal{M}_{g,1[n-1]}$. We will not present a full definition of the group Euler characteristic in this section, but will instead quote the relevant properties, and refer to [100, 99] for a more complete treatment.

The Euler characteristic is defined for any discrete group G which is *virtually torsion-free*: that is, any group G with a torsion-free subgroup H of finite index. Mapping class groups are virtually torsion-free [101]. The group Euler characteristic respects quotienting: if H is a subgroup of G of finite index, then

$$\chi(G/H) = \frac{\chi(G)}{\chi(H)}. \tag{3.5.4}$$

In addition, the Euler characteristic of any finite group G is [98, 100]

$$\chi(G) = \frac{1}{|G|}. \tag{3.5.5}$$

These properties of group Euler characteristics give a means of relating the Euler characteristics of the two moduli spaces. An element of the mapping class group $\Gamma_{g,n}$ is also an element of $\Gamma_{g,1[n-1]}$, and the action of an element of $\Gamma_{g,1[n-1]}$ on the set of n distinguished points gives a permutation in $S_1 \times S_{n-1} \cong S_{n-1}$, so there is a short exact sequence

$$1 \to \Gamma_{g,n} \to \Gamma_{g,1[n-1]} \to S_{n-1} \to 1. \tag{3.5.6}$$

In other words, there is the group isomorphism

$$S_{n-1} \cong \Gamma_{g,1[n-1]}/\Gamma_{g,n}. \tag{3.5.7}$$

Noting that $|S_{n-1}| = (n-1)!$ and using the above properties of Euler characteristics, we have

$$\begin{aligned} \frac{1}{(n-1)!} &= \chi(S_{n-1}) \\ &= \chi(\Gamma_{g,1[n-1]}/\Gamma_{g,n}) \\ &= \chi(\Gamma_{g,1[n-1]})/\chi(\Gamma_{g,n}) \end{aligned} \tag{3.5.8}$$

and so the Euler characteristics of the moduli spaces satisfy the relation

$$\chi(\mathcal{M}_{g,n}) = (n-1)!\chi(\mathcal{M}_{g,1[n-1]}). \tag{3.5.9}$$

The relation (3.5.9) between the two types of moduli space can also be derived from the definition of the orbifold Euler characteristic. If $\{C\}$ is a cell decomposition of an orbifold such that the orbifold group at every point in a given cell is constant, then the orbifold Euler characteristic is [97]

$$\chi(\{C\}) = \sum_C (-)^{\dim(C)} \frac{1}{|A(C)|}, \tag{3.5.10}$$

where $A(C)$ is the orbifold group at any point in the cell C. The Nakamura graph cell decomposition of $\mathcal{M}_{g,1[n-1]}$ allows us to write this formula in terms of the graphs and

their parameters,

$$\chi(\mathcal{M}_{g,1[n-1]}) = \sum_{\mathcal{G}} (-)^{d+l-n} \frac{1}{|\mathrm{Aut}(\mathcal{G})|}. \tag{3.5.11}$$

The analogous formula for Euler characteristic of the moduli space $\mathcal{M}_{g,n}$ is

$$\chi(\mathcal{M}_{g,n}) = \sum_{\bar{\mathcal{G}}} (-)^{d+l-n} \frac{1}{|\mathrm{Aut}(\bar{\mathcal{G}})|}. \tag{3.5.12}$$

Recall from Section 3.1.4 that the possible labellings $\{\bar{\mathcal{G}}\}$ of an unlabelled graph $\mathcal{G}$ are given by the cosets of $H = \mathrm{Aut}(\mathcal{G})/\mathrm{Aut}_{\mathrm{fix}}(\mathcal{G})$ in S_{n-1}, and that there are $(n-1)!|\mathrm{Aut}_{\mathrm{fix}}(\mathcal{G})|/|\mathrm{Aut}(\mathcal{G})|$ cosets. The automorphism group $\mathrm{Aut}(\bar{\mathcal{G}})$ of any labelling of a graph $\mathcal{G}$ is isomorphic to $\mathrm{Aut}_{\mathrm{fix}}(\mathcal{G})$, and so we can see that

$$\begin{aligned} \sum_{\bar{\mathcal{G}}} (-)^{d+l-n} \frac{1}{|\mathrm{Aut}(\bar{\mathcal{G}})|} &= \sum_{\mathcal{G}} (-)^{d+l-n} \frac{(n-1)!}{|\mathrm{Aut}_{\mathrm{fix}}(\mathcal{G})|} \frac{|\mathrm{Aut}_{\mathrm{fix}}(\mathcal{G})|}{|\mathrm{Aut}(\mathcal{G})|} \\ &= (n-1)! \sum_{\mathcal{G}} (-)^{d+l-n} \frac{1}{|\mathrm{Aut}(\mathcal{G})|}, \end{aligned} \tag{3.5.13}$$

as required.

Explicit expressions for the Euler characteristic of $\mathcal{M}_{g,n}$ were derived in [34]. Using the relation (3.5.9), the Euler characteristics of $\mathcal{M}_{g,1[n-1]}$ are

$$\begin{aligned} \chi(\mathcal{M}_{0,1[n-1]}) &= \frac{(-)^{n-1}}{(n-1)(n-2)}, \qquad n \geq 3, \\ \chi(\mathcal{M}_{1,1[n-1]}) &= \frac{(-)^n}{12}, \qquad n \geq 2, \\ \chi(\mathcal{M}_{g,1[n-1]}) &= \frac{(-)^{2g}}{2g} \binom{2g+n-3}{n-1} B_{2g} \qquad g \geq 2, n \geq 2, \end{aligned} \tag{3.5.14}$$

where B_{2g} is a Bernoulli number. In [31], the primary method of confirming that the Nakamura graphs specified a cell decomposition of moduli space was by explicitly counting the unlabelled graphs of a given genus g with one incoming pole and $(n-1)$ outgoing poles, and comparing the sum (3.5.11) to these formulae. The results were found to match in all cases.

3.5.2 The Gaussian Hermitian matrix model

The moduli space $\mathcal{M}_{g,1[n-1]}$ has real dimension $(6g-6+2n)$. A cell $C(\mathcal{G})$ corresponding to a graph with branching number Δ and number of internal edges I has codimension $(2\Delta + I)$. The top-dimensional cells of moduli space are of codimension zero, and are associated to graphs with $\Delta = 0$ and $I = 0$. The zeroes of these graphs have valency four, and each zero can be described in the S_d description by a cycle permuting two labels (a transposition). There are no internal edges connecting the zeroes, so their associated cycles can all be collated into a single permutation τ by slide-equivalence. The triple $(\sigma_+, \tau, \sigma_-)$ is the reduced tuple of the graph; here, $\sigma_+ \in [d]$ is a single d-cycle, $\tau \in [2^l] = [2^{d/2}]$ is a product of 2-cycles, and σ_- consists of $(n-1)$ cycles. There are correlators in the Gaussian and complex matrix models that directly correspond to counting triples of permutations multiplying to one. This allows us to apply known explicit expressions for matrix model correlators to the counting of Nakamura graphs.

First, recall from Section 1.1 that a single-trace correlator in the Gaussian Hermitian matrix model can be written as

$$\mathrm{tr}X^d = X^{i_1}_{i_{\sigma_+(1)}} \cdots X^{i_d}_{i_{\sigma_+(d)}} \tag{3.5.15}$$

with $\sigma_+ = (12\ldots d)$. In other words, when we have a single trace, the lower indices are a cyclic permutation of the upper indices. Now when we perform the Wick contraction on the correlator, we are summing over the pairings of d objects, such as $(12)(34)\ldots(d-1,d)$. Each pairing corresponds to a permutation τ in the class $[2^l]$ where $l = d/2$. The matrix model correlator of a single trace $\mathrm{tr}X^d$ can be written in terms of these two permutations,

$$\langle \mathrm{tr}X^d \rangle = \sum_{\tau\in[2^l]} \sum_{\sigma_-\in S_d} \delta(\sigma_+\tau\sigma_-) N^{C_{\sigma_-}}, \tag{3.5.16}$$

where the delta function imposes the condition that the three permutations multiply to one, and C_{σ_-} is the number of cycles in the product $\sigma_- = (\sigma_+\tau)^{-1}$. We can also introduce a sum over the conjugacy class of single-cycles of length d accompanied by a factor of $|[d]| = (d-1)!$ without changing value of the correlator:

$$\langle \mathrm{tr}X^d \rangle = \frac{1}{(d-1)!} \sum_{\sigma_+\in[d]} \sum_{\tau\in[2^l]} \sum_{\sigma_-\in S_d} \delta(\sigma_+\tau\sigma_-) N^{C_{\sigma_-}}. \tag{3.5.17}$$

Now, consider the equivalence classes of triples $(\sigma_+, \tau, \sigma_-)$ under conjugacy by

$\gamma \in S_d$,

$$(\sigma'_+, \tau', \sigma'_-) \sim (\gamma\sigma_+\gamma^{-1}, \gamma\tau\gamma^{-1}, \gamma\sigma_-\gamma^{-1}). \tag{3.5.18}$$

These equivalence classes correspond precisely to the Nakamura graphs with a single incoming pole, no internal edges, and $\Delta = 0$. The number of poles in a Nakamura graph given by such a tuple is $C_{\sigma_+} + C_{\sigma_-}$, which is equal to n. As $C_{\sigma_+} = 1$, and we are interested in graphs with n poles, we can consider just the permutation tuples with $C_{\sigma_-} = n - 1$, and so consider the coefficient of N^{n-1} in the correlator:

$$\text{Coefficient}(\langle \text{tr} X^d \rangle, N^{n-1}) = \frac{1}{(d-1)!} \sum_{\sigma_+ \in [d]} \sum_{\tau \in [2^l]} \sum_{\substack{\sigma_- \in S_d \\ C_{\sigma_-} = (n-1)}} \delta(\sigma_+ \tau \sigma_-). \tag{3.5.19}$$

We can split the sum over σ_- into a sum over distinct conjugacy classes $\mathcal{T}_-$, each consisting of $(n-1)$ cycles, and a sum over each individual class $\sigma_- \in \mathcal{T}_-$:

$$\text{Coefficient}(\langle \text{tr} X^d \rangle, N^{n-1}) = \frac{1}{(d-1)!} \sum_{\mathcal{T}_-} \sum_{\sigma_+ \in [d]} \sum_{\tau \in [2^l]} \sum_{\sigma_- \in \mathcal{T}_-} \delta(\sigma_+ \tau \sigma_-). \tag{3.5.20}$$

Now the sum

$$\frac{1}{d!} \sum_{\sigma_+ \in [d]} \sum_{\tau \in [2^l]} \sum_{\sigma_- \in \mathcal{T}_-} \delta(\sigma_+ \tau \sigma_-) \tag{3.5.21}$$

can be written in terms of equivalence classes of permutation triples. By the orbit-stabiliser theorem, the number of times each equivalence class appears in the sum is

$$\frac{d!}{|\text{Aut}((\sigma_+, \tau, \sigma_-))|} \tag{3.5.22}$$

where $\text{Aut}(\{\sigma_+, \tau, \sigma_-\})$ is the order of the automorphism group of the triple. Each equivalence class corresponds to a distinct unlabelled graph $\mathcal{G}$. This means that

$$\begin{aligned} &\frac{1}{d!} \sum_{\mathcal{T}_-} \sum_{\sigma \in [d]} \sum_{\tau \in [2^l]} \sum_{\sigma_- \in \mathcal{T}_-} \delta(\sigma_+ \tau \sigma_-) \\ &= \sum_{\mathcal{T}_-} \sum_{\substack{\text{equiv. classes} \\ \text{of triples}}} \frac{1}{|\text{Aut}(\sigma_+, \tau, \sigma_-)|} \end{aligned}$$

$$= \sum_{\mathcal{G}} \frac{1}{|\mathrm{Aut}(\mathcal{G})|}. \tag{3.5.23}$$

This sum is taken over all the graphs specified by a permutation triple $(\sigma_+, \tau, \sigma_-)$ with one incoming pole and $(n-1)$ outgoing poles. This is exactly the sum (3.5.11), constrained to just the graphs corresponding to top-dimensional cells in $\mathcal{M}_{g,1[n-1]}$. We conclude that the contribution of the top dimensional cells of $\mathcal{M}_{g,n}$ to the orbifold Euler characteristic is

$$\chi_{\mathrm{top}}(\mathcal{M}_{g,1[n-1]}) = \frac{1}{d} \times \mathrm{Coefficient}(\langle \mathrm{tr} X^d \rangle, N^{n-1}). \tag{3.5.24}$$

There is a generating function for correlators of single traces in the Gaussian Hermitian matrix model, due to Harer and Zagier [34]:

$$\begin{aligned} Z(x,N) &= \sum_{l=1}^{\infty} \langle \mathrm{tr}(X^{2l}) \rangle \frac{x^{2l}}{(2l-1)!!} && (3.5.25) \\ &= \frac{1}{2x^2} \left(\left(\frac{1+x^2}{1-x^2} \right)^N - 1 \right). && (3.5.26) \end{aligned}$$

The contribution to the top-dimensional cell can be read off from this formula:

$$\chi_{\mathrm{top}}(\mathcal{M}_{g,1[n-1]}) = \frac{(d-1)!!}{d} \ \mathrm{Coefficient}(Z(x,N), x^d N^{n-1}). \tag{3.5.27}$$

We can calculate exactly the coefficient of N^{n-1} in this expression. Noting that

$$Z(x,N) = \frac{1}{2x^2} \left[\exp\left(N \log\left(\frac{1+x^2}{1-x^2} \right) \right) - 1 \right], \tag{3.5.28}$$

we differentiate this $(n-1)$ times with respect to N to see that

$$\mathrm{Coefficient}\ (Z(x,N), N^{n-1}) = \frac{1}{2x^2(n-1)!} \left[\log\left(\frac{1+x^2}{1-x^2} \right) \right]^{n-1}. \tag{3.5.29}$$

The contribution to the Euler characteristic is therefore

$$\begin{aligned} \chi_{\mathrm{top}}(\mathcal{M}_{g,1[n-1]}) &= \frac{(d-1)!!}{2d(n-1)!} \ \mathrm{Coefficient}\ \left(\frac{1}{x^2} \left[\log\left(\frac{1+x^2}{1-x^2} \right) \right]^{n-1}, \quad x^d \right) \\ &= \frac{(d-1)!!}{2d(n-1)!} \ \mathrm{Coefficient}\ \left(\left[\log\left(\frac{1+w}{1-w} \right) \right]^{n-1}, \quad w^{(n-1)+2g} \right), \end{aligned} \tag{3.5.30}$$

where $d = 2(2g-2+n)$, and we have substituted $w = x^2$ in the final equation. Written purely in terms of g and n, the expression for the Euler characteristic contribution is

$$\chi_{\rm top}(\mathcal{M}_{g,1[n-1]}) = \frac{(4g-5+2n)!}{2^{2g-3+n}(n-1)!(2g-2+n)!} \text{ Coefficient } \left(\log\left(\frac{1+w}{1-w}\right)^{n-1}, w^{(n-1)+2g} \right). \tag{3.5.31}$$

This expression matches the values found by counting graphs in Nakamura's paper.

In the case $n = 2$, the series expansion of the generating function can be found exactly. We have

$$\log\left(\frac{1+w}{1-w}\right) = 2\sum_{g=0}^{\infty} \frac{w^{2g+1}}{(2g+1)}, \tag{3.5.32}$$

so we deduce that

$$\chi_{\rm top}(\mathcal{M}_{g,2}) = \frac{(4g)!}{2^{2g}(2g)!}\frac{1}{4g}\frac{1}{2g+1} = \frac{(4g-1)!}{2^{2g}(2g+1)!}. \tag{3.5.33}$$

Starting at $g = 1$, the first few terms in this sequence are

$$\frac{1}{4}, \frac{21}{8}, \frac{495}{4}, \frac{225225}{16} \cdots \tag{3.5.34}$$

All four of these terms were verified by counting the top-dimensional graphs using GAP [102].

3.5.3 The complex matrix model

We can use the correlators of the complex matrix model to find expressions for the contributions to the orbifold Euler characteristic coming from the lower-dimensional cells with no internal edges. Let $\mathcal{T}$ be the S_d conjugacy class $[2^{k_2}3^{k_3}\dots d^{k_d}]$. Choose a representative element $\hat{\sigma}_+ \in [d]$ and $\hat{\tau} \in \mathcal{T}$. The complex matrix model correlator of a holomorphic trace and an antiholomorphic product of traces corresponding to these classes is

$$\begin{aligned} \langle \mathrm{tr}(\hat{\sigma}_+ Z^{\otimes d})\mathrm{tr}(\hat{\tau} Z^{\dagger\otimes d})\rangle &:= \langle \mathrm{tr}Z^d (\mathrm{tr}Z^{\dagger 2})^{k_2}(\mathrm{tr}Z^{\dagger 3})^{k_3}\dots(\mathrm{tr}Z^{\dagger d})^{k_d}\rangle \\ &= \frac{d}{|\mathcal{T}|}\sum_{\sigma_+\in[d]}\sum_{\tau\in\mathcal{T}}\sum_{\sigma_-\in S_d} N^{C_{\sigma_-}}\delta(\sigma_+\tau\sigma_-). \end{aligned} \tag{3.5.35}$$

As in the Hermitian matrix model, this correlator is a sum over conjugacy classes of permutation triples that multiply to one. Splitting up the sum over $\sigma_- \in S_d$, we can write

$$\langle \mathrm{tr}(\hat{\sigma}_+ Z^{\otimes d}) \mathrm{tr}(\hat{\tau} Z^{\dagger \otimes d}) \rangle = \frac{d}{|\mathcal{T}|} \sum_{n=2}^{d-1} N^{n-1} \sum_{\sigma_+ \in [d]} \sum_{\tau \in \mathcal{T}} \sum_{\substack{\sigma_- \in S_d \\ C_{\sigma_-}=n-1}} \delta(\sigma_+ \tau \sigma_-). \tag{3.5.36}$$

This expression is a sum over the Nakamura graphs with $(n-1)$ outgoing poles, no internal edges, and the internal vertex structure given by $\mathcal{T}$:

$$\langle \mathrm{tr}(\hat{\sigma}_+ Z^{\otimes d}) \mathrm{tr}(\hat{\tau} Z^{\dagger \otimes d}) \rangle = \frac{d! d}{|\mathcal{T}|} \sum_{n=2}^{d-1} N^{n-1} \sum_{\mathcal{G}} \frac{1}{|\mathrm{Aut}(\mathcal{G})|}. \tag{3.5.37}$$

This sum appears in the orbifold Euler characteristic of moduli space of genus g with n marked points. Defining the contribution to the orbifold Euler characteristic coming from a class $\mathcal{T}$ by the formula

$$\chi_{\mathcal{T}}(g,n) = \sum_{\mathcal{G}} \frac{1}{\mathrm{Aut}(\mathcal{G})}, \tag{3.5.38}$$

we can state that the contribution to the Euler characteristic coming from graphs with class $\mathcal{T}$ is

$$\chi_{\mathcal{T}}(g,n) = \frac{|\mathcal{T}|}{d! d} \,\mathrm{Coefficient}(\langle \mathrm{tr}(\hat{\sigma}_+ Z^{\otimes d}) \mathrm{tr}(\hat{\tau} Z^{\dagger \otimes d}) \rangle, N^{n-1}). \tag{3.5.39}$$

The parameters k_i defining $\mathcal{T}$ are related to the branching constant Δ and number of zeroes l of the graphs by the formulae

$$l = \sum_{i=2}^{d} k_i, \qquad \Delta = \sum_{i=2}^{d} (i-2) k_i = d - 2l. \tag{3.5.40}$$

The complex matrix model correlator can be calculated by using character sums.

In Appendix D, it is shown that

$$\langle \mathrm{tr}Z^d(\mathrm{tr}Z^{\dagger 2})^{k_2}(\mathrm{tr}Z^{\dagger 3})^{k_3}\dots(\mathrm{tr}Z^{\dagger d})^{k_d}\rangle = d!\sum_{t=0}^{d}\sum_{\substack{S\subset\{1,2,\dots l\}\\|S|=t}}(-)^{l-t}\binom{N+\sum_{i\in S}k_i}{d+1}$$
$$= d!\sum_{r_1=0}^{k_1}\sum_{r_2=0}^{k_2}\dots\sum_{r_d=0}^{k_d}(-)^{k_1+\dots+k_d-r_1-\dots-r_d}\binom{k_1}{r_1}\dots\binom{k_d}{r_d}\binom{N+\sum_{j=1}^{d}jr_j}{d+1}. \quad (3.5.41)$$

The size of the conjugacy class $\mathcal{T}$ is

$$|\mathcal{T}| = \frac{d!}{k_2!2^{k_2}k_3!3^{k_3}\dots k_d!d^{k_d}}. \quad (3.5.42)$$

This gives us an explicit expression for the orbifold Euler characteristic contribution from the class $\mathcal{T} = [2^{k_2}3^{k_3}\dots d^{k_d}]$:

$$\chi_{\mathcal{T}}(g,n) = \frac{(d-1)!}{k_2!2^{k_2}k_3!3^{k_3}\dots k_d!d^{k_d}}\sum_{r_1=0}^{k_1}\dots\sum_{r_d=0}^{k_d}(-)^{k_1+\dots+k_d-r_1-\dots-r_d}\binom{k_1}{r_1}\dots\binom{k_d}{r_d}\times$$
$$\times\,\text{Coefficient}\left[\binom{N+\sum_{j=1}^{d}jr_j}{d+1},N^{n-1}\right]. \quad (3.5.43)$$

This formula can reproduce the Euler characteristic contributions for cells of codimension zero from the previous subsection. For fixed g and n with $\Delta = 0$, then the degree d is $2(2g-2+n)$, the number of zeroes is $l = d/2 = 2g+n-2$, and the contribution to the Euler characteristic is

$$\chi_{[2^l]}(g,n) = \frac{(2l-1)!}{l!2^l}\sum_{r_2=0}^{l}(-)^{l-r_2}\binom{l}{r_2}\text{Coefficient}\left[\binom{N+2r_2}{2l+1},N^{n-1}\right]$$
$$= \frac{(4g+2n-5)!}{(2g+n-2)!2^{2g+n-2}}\sum_{r_2=0}^{2g+n-2}(-)^{2g+n-2-r_2}\binom{2g+n-2}{r_2}\text{Coefficient}\left[\binom{N+2r_2}{4g+2n-3},N^{n-1}\right]. \quad (3.5.44)$$

This formula has been checked computationally for all graphs with degree $d \le 9$. We have written the relevant top-cell graphs in Table 3.1, using the notation $[a]\times n$ to denote n graphs with cyclic automorphism groups of order a. The contribution to the Euler character calculated by counting the graphs and using the formula (3.5.23) exactly matches the results derived from the complex matrix model formula (3.5.44) and the Hermitian matrix model formula (3.5.31).

(g,n)	$\chi_{[2^l]}(g,n)$	$\Delta=0$ Graphs
$(0,5)$	$\frac{5}{6}$	$[2]\times 1,[3]\times 1$
$(0,6)$	$\frac{7}{4}$	$[1]\times 1,[2]\times 1,[4]\times 1$
$(0,7)$	$\frac{21}{5}$	$[1]\times 3,[2]\times 2,[5]\times 1$
$(1,3)$	$\frac{5}{3}$	$[1]\times 1,[2]\times 1,[6]\times 1$
$(1,4)$	$\frac{35}{4}$	$[1]\times 7,[2]\times 3,[4]\times 1$
$(1,5)$	42	$[1]\times 38,[2]\times 8$
$(2,2)$	$\frac{21}{8}$	$[1]\times 2,[2]\times 1,[8]\times 1$

(g,n)	$\chi_{[2^{l-1}3]}(g,n)$	$\Delta=1$ Graphs
$(0,5)$	1	$[1]\times 1$
$(0,6)$	3	$[1]\times 3$
$(0,7)$	$\frac{28}{3}$	$[1]\times 9,[3]\times 1$
$(1,3)$	3	$[1]\times 3$
$(1,4)$	20	$[1]\times 20$
$(1,5)$	$\frac{350}{3}$	$[1]\times 116,[3]\times 2$
$(2,2)$	7	$[1]\times 7$

Table 3.1: The number of graphs and their automorphism group sizes against $\chi_{[2^l]}(g,n)$ and $\chi_{[2^{l-1}3]}(g,n)$ for different values of g and n. The notation $[a]\times n$ denotes n graphs with cyclic automorphism group of order a.

For graphs with $\Delta=1$, the conjugacy class $\mathcal{T}$ is of the form $\mathcal{T}=[2^{l-1},3]$ for some l. We have $d=3+2(l-1)=2(2g-2+n)-1$, so $l=2g+n-3$. The Euler characteristic sum is

$$\begin{aligned}\chi_{[2^l]}(g,n) &= \frac{2l!}{(l-1)!2^{l-1}3}\sum_{r_2=0}^{l-1}\sum_{r_3=0}^{1}(-)^{l-r_2-r_3}\binom{l-1}{r_2}\binom{1}{r_3}\text{Coefficient}\left[\binom{N+2r_2+3r_3}{2l+2},N^{n-1}\right]\\ &= \frac{(4g+2n-6)!}{(2g+n-4)!2^{2g+n-4}3}\sum_{r_2=0}^{2g+n-4}\sum_{r_3=0}^{1}(-)^{2g+n-3-r_2-r_3}\binom{2g+n-4}{r_2}\binom{1}{r_3}\\ &\qquad\text{Coefficient}\left[\binom{N+2r_2+3r_3}{4g+2n-4},N^{n-1}\right]. \quad (3.5.45)\end{aligned}$$

A program was written in GAP to count all the graphs with $I=0$ and $\Delta=1$ for a given genus g and number of external points n; the results are tallied in Table 3.1. The formula (3.5.45) precisely matches the calculation of the contribution to the Euler character produced by using the explicit graph counting and (3.5.38).

3.5.4 Counting graphs using GAP

We used the software package GAP to find all the equivalence classes of reduced tuples corresponding to Nakamura graphs of a given genus g and number of poles n, along with the dimensions of their cells and their pole-permuting automorphism groups $\mathrm{Aut}(\mathcal{G})$. A pair of reduced tuples with the same incoming pole permutation $\sigma_+=(12\dots d)$ are in the same Hurwitz equivalence class if and only if they are conjugate by an element in $\langle\sigma_+\rangle\cong\mathbb{Z}_d$. We used this to find all the distinct Nakamura

graphs by finding the $\mathbb{Z}_d$-equivalence classes of the **reduced τ-tuples** $(\tau_1, \tau_2, \ldots, \tau_m)$.

The program we used takes a graph Euler characteristic $|\chi|$ as input, uses the relations from Section 3.1.3 to find constraints on the number of zeroes l and the branching number Δ, and constructs all the consistent cycle-types (S_d-conjugacy classes) that the τ_i can have, for each value of l and Δ. At this stage, we found two different methods for finding the reduced τ-tuples from the cycle-types. The first method is to consider each potential τ-tuple in turn and test to see if such a tuple gave a Nakamura graph. This method is feasible for $|\chi| \leq 6$, but is not powerful enough to find graphs with Euler characteristic $|\chi| = 7$, as there is a large number of tuples generated by the program that do not correspond to graphs. The second method involves introducing a new type of diagram called an *I-structure*, which describes the internal edges of a Nakamura graph. Each equivalence class of τ-tuples has a unique I-structure, but there can be many inequivalent τ-tuples with the same I-structure. By determining all the possible I-structures consistent with a given cycle-type of the τ_i, and then determining all the possible τ-tuples consistent with this I-structure, we were able to circumvent a large amount of the degeneracy of the first method. By using I-structures, the program was able to find all the Nakamura graphs for $|\chi| \leq 7$.

From the generated consistent τ-tuples, the program finds all the $\mathbb{Z}_d$-equivalence classes, adds the permutation $\sigma_+ = (12\ldots d)$ to each tuple, and calculates $\sigma_- = (\sigma_+\tau_1 \ldots \tau_m)^{-1}$. Each $\mathbb{Z}_d$-equivalence class corresponds to a graph, and the number of poles n, genus g, and size of the automorphism group $\mathrm{Aut}(\mathcal{G})$ can be read off from a tuple in this class. The details of these algorithms and I-structures are given in more depth in Appendix F.

The resulting output generated by the program matched the data given in [31], and also found the graphs with graph Euler characteristic $|\chi| = 7$, corresponding to the moduli spaces $\mathcal{M}_{0,1[8]}$, $\mathcal{M}_{1,1[6]}$, $\mathcal{M}_{2,1[4]}$, and $\mathcal{M}_{3,1[2]}$. This data is listed in Appendix F.3. From the orbifold Euler characteristic formula

$$\sum_{\mathcal{G}} (-1)^{\dim(C(\mathcal{G}))} \frac{1}{|\mathrm{Aut}(\mathcal{G})|}, \tag{3.5.46}$$

we can read off the orbifold Euler characteristics associated to these moduli spaces,

$$\begin{aligned}\chi(\mathcal{M}_{0,1[8]}) &= \frac{1}{56},\\ \chi(\mathcal{M}_{1,1[6]}) &= -\frac{1}{12},\\ \chi(\mathcal{M}_{2,1[4]}) &= \frac{1}{8},\\ \chi(\mathcal{M}_{3,1[2]}) &= -\frac{5}{84}.\end{aligned}$$

This is consistent with the formulae (3.5.14) from Harer and Zagier.

3.6 Discussion

In this chapter we have developed the Nakamura graphs description of the light-cone cell decomposition of moduli space. By associating branched coverings of the sphere to Riemann surfaces with Giddings-Wolpert differentials, we have linked Nakamura graphs of surfaces to Hurwitz classes of permutation tuples. We introduced an equivalence relation on the Hurwitz classes called slide-equivalence, with the property that each slide-equivalence class corresponds to a single Nakamura graph. Two definitions of moduli space were considered: the space $\mathcal{M}_{g,n}$ of equivalence classes of genus g Riemann surfaces with n labelled distinguishable points, and the space $\mathcal{M}_{g,1[n-1]}$ in which $(n-1)$ of the labelled points on the Riemann surfaces are indistinguishable. The moduli space $\mathcal{M}_{g,n}$ is more commonly used in mathematics and string theory literature, while the moduli space $\mathcal{M}_{g,1[n-1]}$ is simpler space to work with as there are fewer cells in its cell decomposition. We introduced split tuples to describe graphs with labelled poles, corresponding to cells in $\mathcal{M}_{g,n}$.

The orbifold Euler characteristic is a topological invariant of moduli space with an explicit exact formula (3.5.14), and a formula related to its cell-decomposition (3.5.46). The matching of these two formulae was used as a check of the validity of the cell decomposition. We developed links between Hermitian and complex matrix model correlators and graphs with $I = 0$ (no internal edges). We used known exact results for Hermitian matrix model correlators to give analytic results for the contribution of the top-dimensional cells to the orbifold Euler character in the light-cone decomposition. Beyond the top-dimensional cells, we related the contributions to the orbifold Euler characteristic from lower-dimensional cells with $\Delta > 0$ and $I = 0$ to analytic expressions in complex matrix models.

The light-cone cell decomposition via Nakamura graphs associates a ribbon graph,

set of strip widths and interaction times to each point in moduli space. In the original light-cone picture, each point in moduli space is specified by a light-cone diagram with internal string momenta (cylinder widths) and twist angles [32, 33, 103, 95]. It is an interesting open problem how to relate these two approaches. In particular, the graph automorphism groups and surface biholomorphism groups should have an interpretation in terms of the more traditional light-cone diagrams.

The light-cone cell decomposition of moduli space is used in a new foundational approach to the geometry of string theory called the *metastring* [104, 105]. This formulation requires a parametrisation of the moduli space of Riemann surface that includes a notion of worldsheet time while preserving invariance under the mapping class group. Our description of Teichmüller space in terms of the Nakamura graphs explicitly shows that the cell decomposition is invariant under the mapping class group, which is necessary for the consistency of the metastring theory.

As observed in [31], the numbers of cells in the light-cone cell decomposition for given g and n is smaller than the corresponding number in the Kontsevich-Penner cell decomposition [35, 36]. This is because the Nakamura graphs corresponding to cells have tight restrictions dictated by the form of the Giddings-Wolpert differential. The quadratic differential formed by taking the square of a Giddings-Wolpert differential satisfies all the properties of a Strebel differential; however, not all Strebel differentials have a Giddings-Wolpert differential as a square root. This is because Strebel differentials are defined for any punctured Riemann surface with any choice of residues at the punctures, while Giddings-Wolpert differentials need the residues to sum to zero. It is an open problem as to how the parameters of a Nakamura strip decomposition and the edge lengths of a Strebel differential metric ribbon graph are related.

The fact that there is a well-defined global time coordinate imposes restrictions on which connected ribbon graphs can be Nakamura graphs. These restrictions are detailed in the language of permutations in Section 3.2. This suggests that it would be worthwhile to revisit mathematical questions on the topology of $\mathcal{M}_{g,n}$ using the light-cone cell decomposition. The computation of all the homology groups is still an open question [106]. From a physics perspective, an immediate goal would be to use the improved understanding of the light-cone cell decomposition in the computation of string amplitudes in the light-cone gauge, either in the first-quantised or second-quantised string field formalism.

Chapter 4

Conclusion

The mathematical theories of permutation groups, ribbon graphs and cell decompositions are invaluable tools within theoretical physics, string theory, and the AdS/CFT correspondence. In the first chapter of this thesis, we found two holographically-related spacetime theories of the Belyi string via the Hermitian matrix model. By expanding the matrix fields in terms of the $su(2)$-covariant fuzzy spherical harmonics, we showed that there exists a cut-off topological scalar theory on the target sphere which matches the Hermitian matrix model. We expressed the ribbon graphs of the matrix model in terms of $su(2)$ representation labels and their couplings. This showed that the trivalent ribbon graphs are equivalent to spin networks with extra $6j$ weights and representation label sums. An algorithm involving trivalent graph moves was exhibited that allows any spin network sum to be expressed in terms of $6j$ symbols and representation dimensions. By manipulating the ribbon graph evaluations into this form, we were able to find labelled triangulated 3-manifolds, which we called complete Belyi 3-complexes, with Ponzano-Regge partition functions matching the $6j$ sum. In the planar case, we showed this matching by directly constructing triangulations of the solid ball with matching ribbon graph and Ponzano-Regge state sums. For the non-planar case, we exhibited an algorithm that shows that the partition function of any complete Belyi 3-complex matches its ribbon graph evaluation. As these 3-complexes contain embeddings of the trivalent ribbon graphs on their boundaries, and Ponzano-Regge is equivalent to three-dimensional Euclidean gravity, this gives a holographic interpretation of the Belyi string matrix model.

In the second chapter of this thesis, we studied the limits of large N factorisation within the $\mathrm{AdS}_5/\mathrm{CFT}_4$ duality. The three-point correlators of single-trace operators in the half-BPS sector of $\mathcal{N} = 4$ super Yang-Mills theory have known finite N evaluations. Taking these expressions as our starting point, we undertook a careful asymptotic analysis of the three-point functions in the limits when N and the operator dimensions J_i are both large by using Stirling's formula. We found that correlators become of order

one when the product of the single-trace operator dimensions are of order $N \log N$. From the bulk perspective, we interpreted this as a sign that some new non-local gravitational theory is emerging in the bulk at this energy scale. By considering the normalised correlators of multiple gravitons, near-extremal correlators, and correlators in non-trivial backgrounds, we found many cases where factorisation fails when a pair of operator dimensions are of the order $J_i J_j \sim N \log N$, suggesting a universality of this threshold. We also found that increasing the number of gravitons, decreasing the separation in the energies of the gravitons, or decreasing the separation in the boundary directions of the gravitons, can lead to factorisation breakdown. These results suggest that information about a possible modification to the bulk theory at finite string coupling can be found by studying the gauge theory at finite N.

In the third chapter of this thesis, we developed the light-cone cell decomposition of moduli space via Nakamura graphs. By constructing a branched covering of the sphere for each Riemann surface with a Giddings-Wolpert differential, we were able to read off a Hurwitz tuple that describes the Nakamura graph of the surface. Each cell in the light-cone cell decomposition corresponds to a distinct Nakamura graph. Some of the cycles in the Hurwitz tuples can be rearranged without altering the structure of the graph, so we introduced slide-equivalence on Hurwitz tuples to solve this degeneracy. Each slide-equivalence class corresponds to a unique Nakamura graph. Within each slide-equivalence class, we found a canonical choice of tuple which we called the reduced tuple. The counting of Nakamura graphs is equivalent to the counting of Hurwitz classes of reduced tuples. This gave us the means to construct links between the Hermitian and complex matrix model correlators and the counting of Nakamura graphs, and to create a program which catalogued the graphs and their automorphism groups. The structure of the reduced tuples associated to Nakamura graphs also allows us to explicitly read off a parametrisation of the cells in moduli space, their boundaries, and their orbifold automorphism groups. We were able to use this to give some explicit low-genus examples of the light-cone cell decomposition of moduli space.

We have found many applications for discrete mathematical techniques to physical theories within this thesis. Hurwitz classes of permutation tuples can describe Belyi maps and cells in the light-cone cell decomposition. Matrix models can link the topological A-string on a 2-sphere target and Ponzano-Regge state sums in three-dimensional gravity. Schur polynomials and character sums can be used to evaluate non-extremal and many-graviton correlators in the half-BPS sector of $\mathcal{N} = 4$ super Yang-mills theory. These diverse applications within string theory and gauge-string duality indicate that combinatoric and graphical methods will remain important tools

within mathematics and physics in the foreseeable future.

Appendix A

The coupling coefficients of $su(2)$ representations

In this appendix we summarise the representation theory of $su(2)$ that we have used in this thesis, taking definitions, expressions and identities from [61, 57, 58]. The finite dimensional irreducible representations of the Lie algebra $su(2)$ are labelled by a half-integer $j \in \{0, \frac{1}{2}, 1, \frac{3}{2}, \ldots\}$, where the dimension of each representation is $(2j+1)$. Each representation labelled by j has a basis $\{|jm\rangle\}$, where m runs over the half-integers in $\{-j, -j+1, \ldots, j-1, j\}$. The labels j associated to a representation are commonly called the **spin labels**, and the integer m labelling the vector in the representation is called the **state label**. The tensor product of two representations of $su(2)$ can be decomposed into a direct sum of irreducible representations of $su(2)$. Individual product states in the tensor product representation are linearly related to sums over states within other irreducible representations of $su(2)$; the linear coefficients relating these decompositions are the Clebsch-Gordan coefficients. The Wigner $3j$ symbols are more symmetric versions of these coefficients, and the Wigner $6j$ symbols are a generalisation to describe the coupling of three representations. The $3j$ and $6j$ symbols enjoy many orthogonality properties and coupling relations, allowing for the simplification of many expressions in the spin network calculus and the Ponzano-Regge model.

A.1 Clebsch-Gordan coefficients

For two representations of $su(2)$ labelled by the half-integers j_1 and j_2, a state in the product representation $|JM\rangle$ can be written

$$|J, M\rangle = \sum_{m_1, m_2} \langle j_1, m_1; j_2, m_2 | J, M\rangle |j_1, m_1\rangle \otimes |j_2, m_2\rangle, \tag{A.1.1}$$

where $\langle j_1, m_1; j_2, m_2 | J, M\rangle$ are the Clebsch-Gordan coefficients of this coupling. The inverse equation is

$$|j_1, m_1\rangle \otimes |j_2, m_2\rangle = \sum_{J,M} \langle J, M | j_1, m_1; j_2, m_2\rangle |J, M\rangle. \tag{A.1.2}$$

The Clebsch-Gordan coefficients can be chosen to be real:

$$\langle j_1, m_1; j_2, m_2 | J, M\rangle = \langle J, M | j_1, m_1; j_2, m_2\rangle. \tag{A.1.3}$$

For this Clebsch-Gordan coefficient to be non-zero, the values of J and M in the coupled representation must satisfy

$$M = m_1 + m_2, \qquad J \in \{|j_1 - j_2|, |j_1 - j_2| + 1, \ldots, j_1 + j_2\}. \tag{A.1.4}$$

Note that the conditions

$$j_3 \in \{|j_1 - j_2|, |j_1 - j_2| + 1, \ldots, j_1 + j_2\}, \qquad j_1 + j_2 + j_3 \text{ is an integer} \tag{A.1.5}$$

are invariant under any permutation of the labels $\{j_1, j_2, j_3\}$. These conditions are called the **triangle constraints** on the labels $\{j_1, j_2, j_3\}$. We introduce the function $\Delta(j_1, j_2, j_3)$ that is defined to be equal to 1 if the labels $\{j_1, j_2, j_3\}$ satisfy the triangle constraints, and zero otherwise. The Clebsch-Gordan coefficient $\langle j_3, m_3 | j_1, m_1; j_2, m_2\rangle$ is non-vanishing if and only if $\Delta(j_1, j_2, j_3) = 1$. The coefficients satisfy the two orthogonality relations

$$\sum_{m_1, m_2} \langle J', M' | j_1, m_1; j_2, m_2\rangle \langle j_1, m_1; j_2, m_2 | J, M\rangle = \delta_{J,J'} \delta_{M,M'} \Delta(j_1, j_2, J), \tag{A.1.6}$$

$$\sum_{J,M} \langle j_1, m_1'; j_2, m_2' | J, M\rangle \langle J, M | j_1, m_1; j_2, m_2\rangle = \delta_{m_1, m_1'} \delta_{m_2, m_2'}. \tag{A.1.7}$$

An explicit closed form of a Clebsch-Gordan coefficient is given in [107, 58]:

$$\begin{aligned}\langle j_3, m_3 | j_1, m_1; j_2, m_2\rangle = {} & \left[(2j_3+1)\frac{(j_3+j_1-j_2)!(j_3-j_1+j_2)!(j_1+j_2-j_3)!(j_3+m_3)!(j_3-m_3)!}{(j_1+j_2+j_3+1)!(j_1-m_1)!(j_1+m_1)!(j_2-m_2)!(j_2+m_2)!}\right]^{\frac{1}{2}} \\ & \times \delta_{m_3, m_1+m_2} \sum_{\nu} \frac{(-)^{\nu+j_2-m_2}}{\nu!} \frac{(j_2+j_3+m_1-\nu)!(j_1-m_1+\nu)!}{(j_3-j_1+j_2-\nu)!(j_3+m_3-\nu)!(\nu+j_1-j_2-m_3)!}.\end{aligned} \tag{A.1.8}$$

The sum over ν runs over the integer values where the factorial expressions are non-negative. This is a somewhat cumbersome expression, but it is possible to use it to derive some relations of the coefficients under switching and reversing of their labels. For example, it can be shown that

$$\begin{aligned}\langle j_3, m_3 | j_1, m_1; j_2, m_2\rangle &= (-)^{j_1+j_2-j_3}\langle j_3, -m_3 | j_1, -m_1; j_2, -m_2\rangle \\ &= (-)^{j_1+j_2-j_3}\langle j_3, m_3 | j_2, m_2; j_1, m_1\rangle \\ &= (-)^{j_1-m_1}\left(\frac{2j_3+1}{2j_2+1}\right)^{\frac{1}{2}}\langle j_2, -m_2 | j_1 m_1; j_3, -m_3\rangle \quad \text{(A.1.9)}\end{aligned}$$

A.2 Wigner $3j$ symbols

The Wigner $3j$ symbols are a much more symmetric version of the Clebsch-Gordan coupling coefficients. We define

$$\begin{pmatrix} j_1 & j_2 & j_3 \\ m_1 & m_2 & m_3 \end{pmatrix} = (-)^{j_1-j_2-m_3}(2j_3+1)^{-\frac{1}{2}}\langle j_3, -m_3 | j_1, m_1; j_2, m_2\rangle. \quad \text{(A.2.1)}$$

This symbol is non-zero when the triangle constraint (A.1.5) and the state label relation $m_1 + m_2 + m_3 = 0$ are satisfied. As the Clebsch-Gordan coefficients are real and $j_1 - j_2 - m_3$ is an integer when the triangle constraints are satisfied, the $3j$ symbols are real. From (A.1.9), the symmetry under permutation of the labels is simply

$$\begin{aligned}\begin{pmatrix} j_1 & j_2 & j_3 \\ m_1 & m_2 & m_3 \end{pmatrix} &= \begin{pmatrix} j_2 & j_3 & j_1 \\ m_2 & m_3 & m_1 \end{pmatrix} = \begin{pmatrix} j_3 & j_1 & j_2 \\ m_3 & m_1 & m_2 \end{pmatrix} \\ = (-)^{j_1+j_2+j_3}\begin{pmatrix} j_1 & j_3 & j_2 \\ m_1 & m_3 & m_2 \end{pmatrix} &= (-)^{j_1+j_2+j_3}\begin{pmatrix} j_2 & j_1 & j_3 \\ m_2 & m_1 & m_3 \end{pmatrix} = (-)^{j_1+j_2+j_3}\begin{pmatrix} j_3 & j_2 & j_1 \\ m_3 & m_2 & m_1 \end{pmatrix} \\ &= (-)^{j_1+j_2+j_3}\begin{pmatrix} j_1 & j_2 & j_3 \\ -m_1 & -m_2 & -m_3 \end{pmatrix}. \quad \text{(A.2.2)}\end{aligned}$$

A phase of $(-)^{j_1+j_2+j_3}$ is introduced when two sets of labels in a $3j$ symbol are transposed, or when the state labels m_i are inverted. They now satisfy the two orthogonality relations

$$\sum_{m_1,m_2}(2j_3+1)\begin{pmatrix} j_1 & j_2 & j_3 \\ m_1 & m_2 & m_3 \end{pmatrix}\begin{pmatrix} j_1 & j_2 & j_3' \\ m_1 & m_2 & m_3' \end{pmatrix} = \delta_{j_3,j_3'}\delta_{m_3,m_3'}\Delta(j_1,j_2,j_3), \quad \text{(A.2.3)}$$

$$\sum_{j_3,m_3}(2j_3 + 1)\begin{pmatrix} j_1 & j_2 & j_3 \\ m_1 & m_2 & m_3 \end{pmatrix}\begin{pmatrix} j_1 & j_2 & j_3 \\ m_1' & m_2' & m_3 \end{pmatrix} = \delta_{m_1,m_1'}\delta_{m_2,m_2'}. \quad \text{(A.2.4)}$$

A.3 Wigner $6j$ symbols

The Wigner $3j$ symbols describe the tensor product of two representations with labels j_1 and j_2. We now consider the tensor product of three representations labelled j_1, j_2, and j_3. We could first take the tensor product of the representations j_1 and j_2, which gives a direct sum over representations that we label j_{12}, and then couple these representations to j_3, generating a direct sum of triply-coupled representations J. Alternatively, we could start by coupling j_2 and j_3 to a direct sum of representations j_{23}, and then couple these representations to j_1 to generate a direct sum of triply-coupled representations $\tilde{J}$. The Wigner $6j$ symbol is the coupling coefficient describing how a single triply-coupled representation $J = \tilde{J}$ is generated via the intermediate representations j_{12} and j_{23}.

Consider a state in the representation $|JM\rangle_{12}$ arising from the coupling of j_{12} to j_3. This can be written in terms of the Clebsch-Gordan coefficients

$$\begin{aligned} |JM\rangle_{12} &= \sum_{m_{12},m_3}\langle JM|j_{12},m_{12};j_3,m_3\rangle|j_{12},m_{12}\rangle\otimes|j_3,m_3\rangle \\ &= \sum_{m_1m_2m_3m_{12}}\langle JM|j_{12},m_{12};j_3,m_3\rangle\langle j_{12},m_{12}|j_1,m_1;j_2,m_2\rangle|j_1m_1\rangle|j_2m_2\rangle|j_3m_3\rangle. \quad \text{(A.3.1)} \end{aligned}$$

The state corresponding to the coupling of j_{23} to j_1 is similarly written

$$|JM\rangle_{23} = \sum_{m_1m_2m_3m_{23}}\langle JM|j_1,m_1;j_{23},m_{23}\rangle\langle j_{23},m_{23}|j_2,m_2;j_3,m_3\rangle|j_1m_1\rangle|j_2m_2\rangle|j_3m_3\rangle.$$

We can consider the difference between the two methods of coupling by considering their inner product,

$$\begin{aligned} \langle JM|_{12}JM\rangle_{23} = \sum_{\substack{m_1m_2m_3\\ m_{12}m_{23}}}&\langle j_{12},m_{12}|j_1,m_1;j_2,m_2\rangle\langle JM|j_{12},m_{12};j_3,m_3\rangle \\ &\times\langle j_{23},m_{23}|j_2,m_2;j_3,m_3\rangle\langle JM|j_1,m_1;j_{23},m_{23}\rangle. \quad \text{(A.3.2)} \end{aligned}$$

It can be shown that this expression is independent of the choice of state label M [57]. This inner product is therefore a function purely of the six spin labels j. The **Wigner**

$6j$ **symbol** is defined to be a symmetrised version of this inner product,

$$\left|\begin{array}{ccc} j_1 & j_2 & j_{12} \\ j_3 & J & j_{23} \end{array}\right| = [(2j_{12}+1)(2j_{23}+1)]^{-\frac{1}{2}}(-)^{j_{12}+j_{23}}\langle JM|_{12}JM\rangle_{23}$$
$$= [(2j_{12}+1)(2j_{23}+1)]^{-\frac{1}{2}}(-)^{j_{12}+j_{23}} \sum_{\substack{m_1 m_2 m_3 \\ m_{12} m_{23}}} \langle j_{12}, m_{12}|j_1, m_1; j_2, m_2\rangle\langle JM|j_{12}, m_{12}; j_3, m_3\rangle$$
$$\times \langle j_{23}, m_{23}|j_2, m_2; j_3, m_3\rangle\langle JM|j_1, m_1; j_{23}, m_{23}\rangle. \quad \text{(A.3.3)}$$

With this definition, a $6j$ symbol is not always real, as the power in the phase factor is not always an integer. A $6j$ will be either real or pure imaginary, depending on whether $j_{12} + j_{23}$ is an integer or a half-integer. (Some authors use the convention where the $6j$s are taken to be real.)

The $6j$ symbol can be expressed in a more symmetric form by using Wigner $3j$ symbols, introducing a summation over the states in the triply-coupled representation, and choosing a more symmetric spin labelling:

$$\left|\begin{array}{ccc} j_1 & j_2 & j_3 \\ j_4 & j_5 & j_6 \end{array}\right| = \sum_{\substack{m_1,\ m_2,\ m_3 \\ m_4,\ m_5,\ m_6}} (-)^{m_1+m_2+m_3+m_4+m_5+m_6} \begin{pmatrix} j_1 & j_2 & j_3 \\ m_1 & m_2 & m_3 \end{pmatrix} \times$$
$$\times \begin{pmatrix} j_1 & j_5 & j_6 \\ -m_1 & m_5 & -m_6 \end{pmatrix} \begin{pmatrix} j_3 & j_4 & j_5 \\ -m_3 & m_4 & -m_5 \end{pmatrix} \begin{pmatrix} j_2 & j_6 & j_4 \\ -m_2 & m_6 & -m_4 \end{pmatrix}. \quad \text{(A.3.4)}$$

The $6j$ symbol is real when the sum of the spin labels in any column is an integer, and is pure imaginary when the sum of the spin labels in any column is not an integer. The $6j$ is invariant under any permutation of its columns,

$$\left|\begin{array}{ccc} j_1 & j_2 & j_3 \\ j_4 & j_5 & j_6 \end{array}\right| = \left|\begin{array}{ccc} j_3 & j_1 & j_2 \\ j_6 & j_4 & j_5 \end{array}\right| = \left|\begin{array}{ccc} j_2 & j_3 & j_1 \\ j_5 & j_6 & j_4 \end{array}\right|$$
$$= \left|\begin{array}{ccc} j_1 & j_3 & j_2 \\ j_4 & j_6 & j_5 \end{array}\right| = \left|\begin{array}{ccc} j_3 & j_2 & j_1 \\ j_6 & j_5 & j_4 \end{array}\right| = \left|\begin{array}{ccc} j_2 & j_1 & j_3 \\ j_5 & j_4 & j_6 \end{array}\right|, \quad \text{(A.3.5)}$$

and also under the interchange of the upper and lower arguments in any two of their columns,

$$\left|\begin{array}{ccc} j_1 & j_2 & j_3 \\ j_4 & j_5 & j_6 \end{array}\right| = \left|\begin{array}{ccc} j_4 & j_5 & j_3 \\ j_1 & j_2 & j_6 \end{array}\right| = \left|\begin{array}{ccc} j_4 & j_2 & j_6 \\ j_1 & j_5 & j_3 \end{array}\right| = \left|\begin{array}{ccc} j_1 & j_5 & j_6 \\ j_4 & j_2 & j_3 \end{array}\right|. \quad \text{(A.3.6)}$$

As the $6j$s are composed of Clebsch-Gordan coefficients which obey the triangular

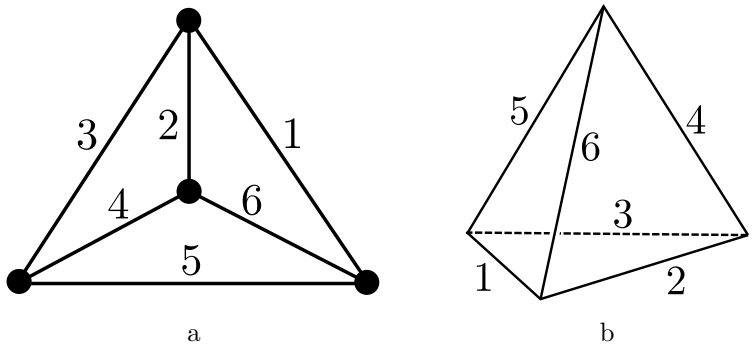

Figure A.1: The $6j$ symbol as a planar spin network and as a tetrahedron.

constraints, the above $6j$ is only non-zero when the sets of variables

$$\{j_1, j_2, j_3\}, \quad \{j_1, j_5, j_6\}, \quad \{j_2, j_4, j_6\}, \quad \{j_3, j_4, j_5\} \tag{A.3.7}$$

all obey the triangle constraint (A.1.5). These triples are mapped into each other by the action of the symmetries (A.3.5) and (A.3.6).

A $6j$ symbol can be viewed as a weight associated with a planar spin network (a ribbon graph embedded on a plane, with edges labelled by spins) or as a tetrahedron with edges labelled by spins. The 24 symmetries of the $6j$ generated by (A.3.5) and (A.3.6) correspond to the symmetry group of the tetrahedron S_4. The spin network can be obtained by a 2D duality on the surface of the tetrahedron. In Figure A.1a, the trivalent vertices of the graph represent the couplings of the triples of representations, and the triangle constraints are satisfied by the labels meeting at a vertex. The interpretation of a $6j$ symbol as a spin network is used in Section 1.3 in describing the $3j$ sums arising from ribbon graphs. Alternatively, as in Figure A.1b, the couplings of representations can be interpreted as the triangular faces of the tetrahedron. This interpretation of the $6j$ as a tetrahedron is used in the Ponzano-Regge model in Section 1.4.

There are many relations and identities regarding sums of $3j$s and $6j$s, many of which are listed in [61]. Perhaps the most useful $6j$ relations in this thesis are the orthogonality relation

$$\sum_{j_3} (-)^{2j_3+2j_6}(2j_3+1)(2j_6+1) \begin{vmatrix} j_1 & j_2 & j_3 \\ j_4 & j_5 & j_6 \end{vmatrix} \begin{vmatrix} j_1 & j_2 & j_3 \\ j_4 & j_5 & j_7 \end{vmatrix} = \Delta(l_1, l_5, l_6)\Delta(l_2, l_4, l_6)\delta_{j_6, j_7}, \tag{A.3.8}$$

and the Biedenharn-Elliot identity,

$$\sum_{j_a}(-)^{2j_a(2j_a+1)}\left|\begin{array}{ccc} j_1 & j_5 & j_6 \\ j_a & j_9 & j_8 \end{array}\right|\left|\begin{array}{ccc} j_2 & j_4 & j_6 \\ j_a & j_9 & j_7 \end{array}\right|\left|\begin{array}{ccc} j_3 & j_4 & j_5 \\ j_a & j_8 & j_7 \end{array}\right| = \left|\begin{array}{ccc} j_1 & j_2 & j_3 \\ j_4 & j_5 & j_6 \end{array}\right|\left|\begin{array}{ccc} j_1 & j_2 & j_3 \\ j_7 & j_8 & j_9 \end{array}\right|. \tag{A.3.9}$$

The Biedenharn-Elliot identity has an interpretation as the equivalence of the Ponzano-Regge state sum model under the 3-2 Pachner Move on tetrahedra given in Figure 1.12. The $3j$ and $6j$ symbols also satisfy the 2-2 identity

$$\begin{aligned}\sum_{m_3}(-)^{m_3}\left(\begin{array}{ccc} j_1 & j_2 & j_3 \\ m_1 & m_2 & -m_3 \end{array}\right)\left(\begin{array}{ccc} j_4 & j_5 & j_3 \\ m_4 & m_5 & m_3 \end{array}\right) = \\ = (-)^{2j_5}\sum_{j_6,m_6}(-)^{m_6}(2j_6+1)\left(\begin{array}{ccc} j_5 & j_1 & j_6 \\ m_5 & m_1 & m_6 \end{array}\right)\left(\begin{array}{ccc} j_2 & j_4 & j_6 \\ m_2 & m_4 & -m_6 \end{array}\right)\left|\begin{array}{ccc} j_1 & j_2 & j_3 \\ j_4 & j_5 & j_6 \end{array}\right|\end{aligned} \tag{A.3.10}$$

and the 3-1 identity

$$\begin{aligned}\sum_{m_4,m_5,m_6}(-)^{m_4+m_5+m_6}\left(\begin{array}{ccc} j_5 & j_1 & j_6 \\ m_5 & m_1 & -m_6 \end{array}\right)\left(\begin{array}{ccc} j_4 & j_3 & j_5 \\ m_4 & m_3 & -m_5 \end{array}\right)\left(\begin{array}{ccc} j_6 & j_2 & j_4 \\ m_6 & m_2 & -m_4 \end{array}\right) \\ = \left(\begin{array}{ccc} j_1 & j_2 & j_3 \\ m_1 & m_2 & m_3 \end{array}\right)\left|\begin{array}{ccc} j_1 & j_2 & j_3 \\ j_4 & j_5 & j_6 \end{array}\right|\end{aligned} \tag{A.3.11}$$

which are used to relate different spin network graphs in section 1.3.

These following relations are used in various parts in section 1.4 to calculate state sums in the Ponzano-Regge model:

$$\sum_{l}(2l+1)\Delta(l,j,j) = (2j+1)^2, \tag{A.3.12}$$

$$\sum_{l_1}(2l_1+1)\left|\begin{array}{ccc} l_1 & l_2 & l_3 \\ j & j & j \end{array}\right|\left|\begin{array}{ccc} l_1 & l_2 & l_3 \\ j & j & j \end{array}\right| = \frac{(-)^{2j}}{(2j+1)}\Delta(l_2,j,j)\Delta(l_3,j,j), \tag{A.3.13}$$

$$\sum_{l_1,l_2}(2l_1+1)(2l_2+1)\left|\begin{array}{ccc} l_1 & l_2 & l_3 \\ j & j & j \end{array}\right|\left|\begin{array}{ccc} l_1 & l_2 & l_3 \\ j & j & j \end{array}\right| = (-)^{2j}(2j+1)\Delta(l_3,j,j), \tag{A.3.14}$$

$$\sum_{l_1,l_2}(-)^{l_1+l_2}(2l_1+1)(2l_2+1)\begin{vmatrix} l_1 & l_2 & l_3 \\ j & j & j \end{vmatrix}\begin{vmatrix} l_1 & l_2 & l_3 \\ j & j & j \end{vmatrix} = (2j+1)\delta_{l_3,0}, \quad \text{(A.3.15)}$$

$$\sum_{l_1}(-)^{3j+l_1}(2l_1+1)^{\frac{3}{2}}\begin{vmatrix} l_1 & l_1 & 0 \\ j & j & j \end{vmatrix} = (2j+1)^{\frac{3}{2}}. \quad \text{(A.3.16)}$$

A.4 Quantum $6j$ symbols

The Lie algebra of $su(2)$ can be deformed to the quantum algebra $U_q(su(2))$. Representations of $U_q(su(2))$ are labelled by integers and half-integers j each containing $(2j+1)$ states. When q is an r^{th} root of unity $q = e^{2\pi i/r}$, then $U_q(su(2))$ has a finite number of finite-dimensional representations. The conventional representation theory of $su(2)$ is recovered in the limit $r \to \infty$, $q \to 1$.

A *quantum integer* $[n]$ is defined to be

$$[n] := \frac{q^{n/2} - q^{-n/2}}{q^{1/2} - q^{-1/2}}, \quad \text{(A.4.1)}$$

which has the property that $[n] \to n$ as $r \to \infty$ and $q \to 1$. A *quantum factorial* $[n]!$ is defined to be

$$[n]! := [n][n-1]\dots[2][1]. \quad \text{(A.4.2)}$$

We say that a triple of spin labels $\{j_1, j_2, j_3\}$ satisfy the *quantum triangle constraints* if they satisfy the classical triangle constraints with the extra conditions

$$j_p \le (r-2)/2, \qquad j_1 + j_2 + j_3 \le r - 2. \quad \text{(A.4.3)}$$

The function $\Delta_q(j_1, j_2, j_3)$ is defined to be one when the quantum triangle constraints are satisfied by the spin labels $\{j_1, j_2, j_3\}$, and zero otherwise. The quantum integers satisfy the identity

$$\sum_{a,b}(-)^{2a+2b}[2a+1][2b+1]\Delta_q(a,b,c) = w^2(-)^{2c}[2c+1], \quad \text{(A.4.4)}$$

where w^2 is the *quantum weight factor*

$$w^2 = -\frac{2r}{(q^{1/2} - q^{-1/2})^2}. \tag{A.4.5}$$

This factor is divergent in the $q \to 1$ limit.

The quantum analogues of the Clebsch-Gordan coefficients can be derived from the explicit expression (A.1.8) by replacing the factorials with quantum factorials. This leads to a definition of the quantum $3j$ symbol and the quantum $6j$ symbol by replacing the factors in (A.2.1) and (A.3.4) with their quantum analogues. All the identities stated in the previous subsection still hold when the $6j$s and representation dimension factors are replaced by their quantum analogues. They also satisfy the identity corresponding to the '4-1' Pachner move (shown in Figure 1.11),

$$w^{-2} \sum_{a,b,c,d} (-)^{2a+2b+2c+2d} [2a+1][2b+1][2c+1][2d+1] \times \\ \left| \begin{array}{ccc} j_1 & j_2 & j_3 \\ a & b & c \end{array} \right|_q \left| \begin{array}{ccc} j_1 & j_5 & j_6 \\ d & c & b \end{array} \right|_q \left| \begin{array}{ccc} j_2 & j_4 & j_6 \\ d & c & a \end{array} \right|_q \left| \begin{array}{ccc} j_3 & j_4 & j_5 \\ d & b & a \end{array} \right|_q = \left| \begin{array}{ccc} j_1 & j_2 & j_3 \\ j_4 & j_5 & j_6 \end{array} \right|_q . \tag{A.4.6}$$

Appendix B

Summary of the trivalent graph and Pachner moves

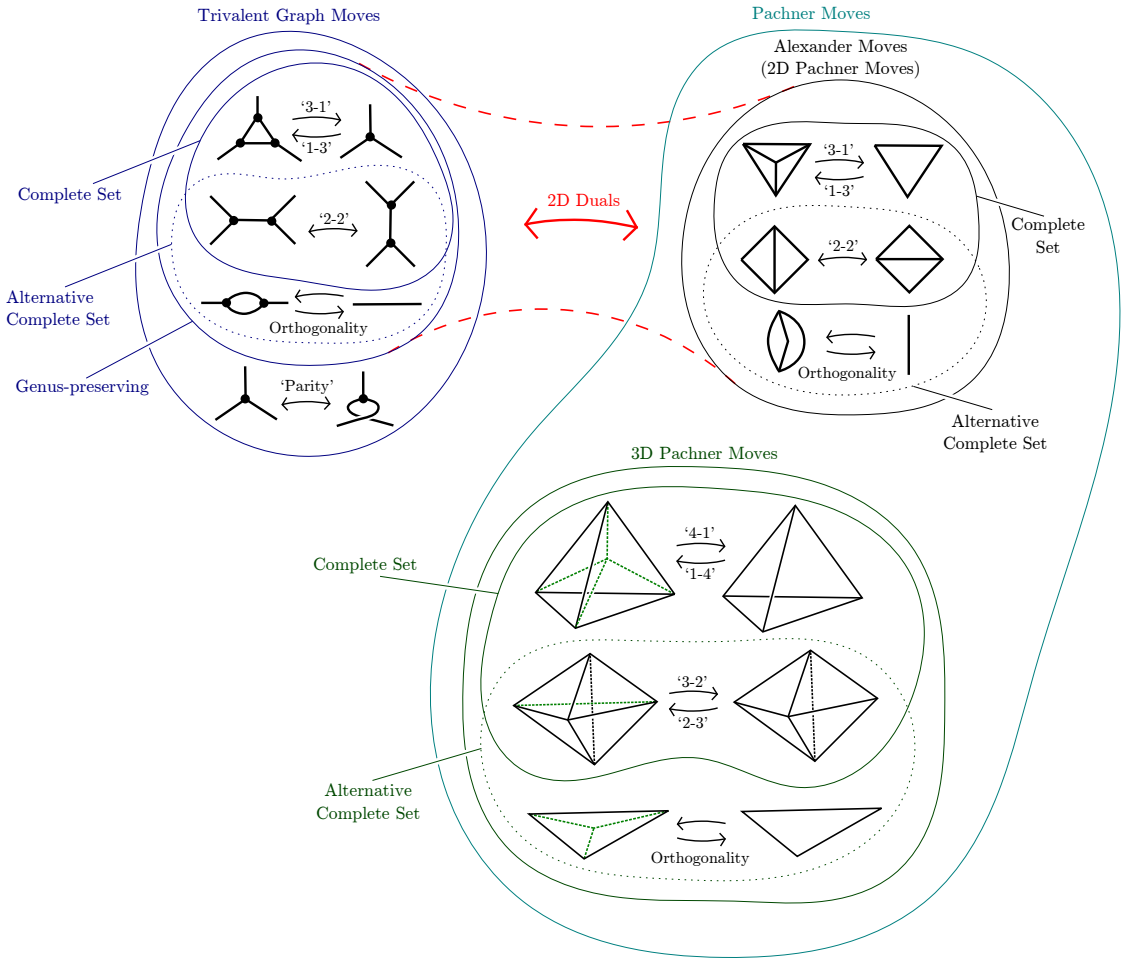

We have used several operations on embedded trivalent graphs and triangulations of manifolds in this thesis, which we referred to as 'moves'.

The **trivalent graph moves** are operations that relate trivalent ribbon graphs embedded on 2D surfaces. The **genus-preserving trivalent graph moves** are the moves which do not change the genus of the graph. A **complete set** of genus-preserving trivalent graph moves are sufficient to relate any two trivalent graphs of the same genus by a sequence of moves.

The **Pachner moves** are operations that relate triangulations of manifolds. Any two triangulations of a compact manifold can be related to each other by a sequence of Pachner moves. The **2D Pachner moves** are sometimes called **Alexander moves**, and can relate any two triangulations of a compact surface. The genus-preserving moves on ribbon graphs are **dual** to the Alexander moves. A **complete set** of Alexander moves is sufficient to relate any two triangulations of a surface of the same genus. The **3D Pachner moves** can relate any two triangulations of a compact 3-manifold with boundary, provided that the boundary triangulations are identical. A **complete set** of 3D Pachner moves are sufficient to relate any two triangulations of the same 3-manifold. (The orthogonality 3D Pachner move reduces a 'pillow' pair of tetrahedra, glued together on three faces, to a single triangle.)

Appendix C

The Lambert W-function

The Lambert W-function is, by definition, the solution to the equation

$$W(z)e^{W(z)} = z. \tag{C.0.1}$$

This equation cannot be solved in a closed form in terms of elementary functions, but a Taylor series can be found near $z = 0$, and its asymptotic series can be derived for large positive z.

There are many solutions $W(z)$ to the equation (C.0.1), which means that the Lambert W-function is multivalued. However, only two solutions take real values when z is real, and these are the only relevant solutions in this thesis. One of these solutions is the principal branch $W_0(z)$, which is real and satisfies $W_0(z) \geq -1$ on its domain $z \in [-e^{-1}, \infty)$. The other is the $W_{-1}(z)$ branch, which takes values in the range $W_{-1}(z) \leq -1$ and is defined on the domain $z \in [-e^{-1}, 0)$. The two real branches of the W-function are shown in figure C.1.

The large z expansion of the principal branch of the W-function is

$$W(z) \simeq \log z - \log\log z + \sum_{n=1}^{\infty} \left(\frac{-1}{\log z}\right)^n \sum_{k=1}^{n} \begin{bmatrix} n \\ n-k+1 \end{bmatrix} \frac{(-\log\log z)^k}{k!}, \tag{C.0.2}$$

where the coefficients in the square brackets are the (unsigned) Stirling cycle numbers of the first kind. The notation $\begin{bmatrix} n \\ k \end{bmatrix}$ denotes the number of permutations of n elements composed of k disjoint cycles. (For example, $\begin{bmatrix} 4 \\ 2 \end{bmatrix}$ refers to the number of permutations in the symmetric group S_4 composed of two disjoint cycles. There are six permutations in S_4 composed of a 3-cycle and a 1-cycle, and three permutations composed of a pair of disjoint 2-cycles, and these are the only permutations composed of two disjoint cycles in S_4. Hence, $\begin{bmatrix} 4 \\ 2 \end{bmatrix} = 6 + 3 = 9$.)

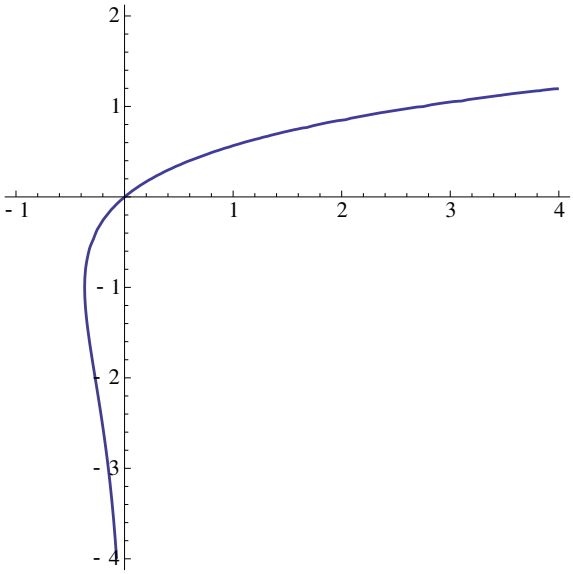

Figure C.1: The Lambert W-function $W(x)$ for real x is multivalued: the principal branch W_0 takes values greater than -1, and the other branch W_{-1} is defined for $W < -1$.

Appendix D

Combinatoric calculations using character sums

In this appendix we present some finite N calculations of correlators using matrix model techniques. The extremal correlator $\langle \mathrm{tr}Z^{J_1}\mathrm{tr}Z^{J_2}\mathrm{tr}Z^{\dagger J_1+J_2}\rangle$ was calculated in [27], and using character sums in [28]. We use the methods of [28] to calculate the norm of the operator $\mathrm{Str}(Z^{J_1}Y^{J_2})$, and to calculate the $k \to 1$ correlator

$$\langle \mathrm{tr}Z^{J_1}\mathrm{tr}Z^{J_2}\ldots\mathrm{tr}Z^{J_k}\mathrm{tr}Z^{\dagger \sum_i J_i}\rangle. \tag{D.0.1}$$

We then find an expression for the normalised $(k+1)$-point correlator at large N.

D.1 The non-extremal operator norm

Consider the non-extremal two-point function which is the norm of a mixed operator consisting of two types of adjoint fields,

$$\| \mathrm{Str}(Z^{J_1}Y^{J_2}) \|^2 \;=\; \langle \mathrm{Str}(Z^{J_1}Y^{J_2})\mathrm{Str}(Z^{\dagger J_1}Y^{\dagger J_2})\rangle. \tag{D.1.1}$$

The symmetrised trace of a string of matrices in the adjoint representation of the gauge group $U(N)$ is

$$\mathrm{Str}(Z^{J_1}Y^{J_3}) = \frac{1}{(J_1+J_3-1)!}\sum_{\sigma\in[J_1+J_3]} X^{i_1}_{i_{\sigma(1)}}X^{i_2}_{i_{\sigma(2)}}\ldots X^{i_{J_1}}_{i_{\sigma(J_1)}}Y^{i_{J_1+1}}_{i_{\sigma(J_1+1)}}\ldots Y^{i_{J_1+J_3}}_{i_{\sigma(J_1+J_3)}}. \tag{D.1.2}$$

The sum is performed over all permutations in $[J_1+J_3]$, the conjugacy class in $S_{J_1+J_3}$ consisting of all the cyclic permutations with a single cycle of length (J_1+J_3). All matching pairs of adjoint matrix indices i_l are implicitly summed. This expression can

be written more concisely in tensor space notation [28] as

$$\mathrm{Str}(Z^{J_1}Y^{J_3}) = \frac{1}{(J_1+J_3-1)!}\sum_{\sigma\in[J_1+J_3]}\mathrm{tr}(\sigma X^{\otimes J_1}\otimes Y^{\otimes J_3}). \tag{D.1.3}$$

This two-point function can be calculated by using diagrammatic tensor space techniques [28]:

$$\| \mathrm{Str}(Z^{J_1}Y^{J_2}) \|^2 = \frac{1}{(J_1+J_2-1)!^2}\sum_{\sigma_1,\sigma_2\in[J_1+J_2]} \tag{D.1.4}$$

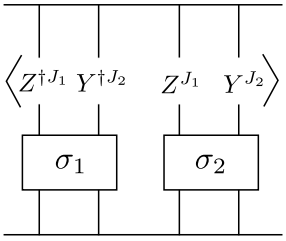

$$= \frac{1}{(J_1+J_2-1)!^2}\sum_{\substack{\sigma_1,\sigma_2\in[J_1+J_2]\\ \gamma_1\in S_{J_1}\\ \gamma_2\in S_{J_2}}} \tag{D.1.5}$$

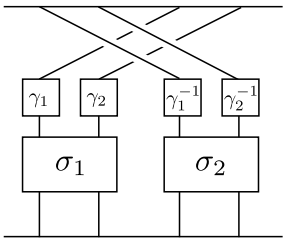

$$\frac{J_1!J_2!}{(J_1+J_2-1)!^2}\sum_{\sigma_1,\sigma_2\in[J_1+J_2]} \tag{D.1.6}$$

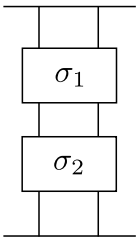

We can replace the permutation sums with sums over representations with projectors on the group algebra,

$$\| \mathrm{Str}(Z^{J_1}Y^{J_2}) \|^2 = J_1!J_2!\sum_{R_1,R_2\vdash(J_1+J_2)} \frac{\chi_{R_1}([J_1+J_2])\chi_{R_2}([J_1+J_2])}{d_{R_1}d_{R_2}} \tag{D.1.7}$$

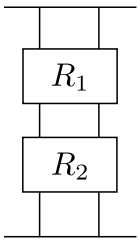

where $\chi_{R_1}([J_1+J_2])$ is the character in R_1 of a permutation in the conjugacy class $[J_1+J_2]$. Representation projectors satisfy the identity $P_{R_1}P_{R_2} = \delta_{R_1R_2}P_{R_1}$, and

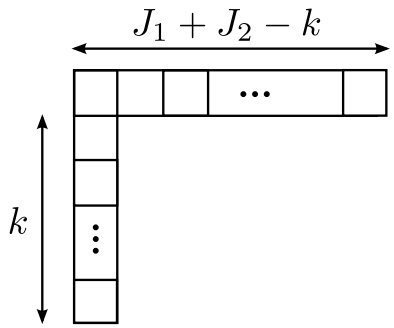

Figure D.1: A Young diagram with $J_1 + J_2$ boxes corresponding to a hook rep with hook length k.

$\mathrm{tr} P_R = \dim_N(R) d_R$, where $\dim_N(R)$ and d_R are the respective dimensions of the $U(N)$ and $S_{J_1+J_2}$ representations associated to the Young diagram R. From the Murnaghan-Nakayama lemma [109], the character of a (J_1+J_2)-cycle in $S_{J_1+J_2}$ is ± 1 if the diagram is a *hook*, and zero otherwise. A hook representation corresponds to a Young tableau where all the boxes are in the first row or the first column, as in Figure D.1. We find

$$\| \mathrm{Str}(Z^{J_1} Y^{J_2}) \|^2 = J_1! J_2! \sum_{R \vdash (J_1+J_2)} \frac{\chi_R([J_1+J_2])^2}{d_R^2} \mathrm{tr}(P_R) \tag{D.1.8}$$

$$= J_1! J_2! \sum_{R \text{ a hook rep}} \frac{\dim_N(R)}{d_R}. \tag{D.1.9}$$

This sum is weighted by the dimension of a hook rep of $U(N)$ divided by the dimension of the corresponding hook rep in $S_{J_1+J_2}$. Parametrizing the hook lengths by the hook length k, where $k = 0, 1, \ldots (J_1 + J_2 - 1)$, we find that the ratio of the dimensions is

$$\frac{\dim_N(R)}{d_R} = \binom{N + J_1 + J_2 - k - 1}{J_1 + J_2}, \tag{D.1.10}$$

and hence the correlator is

$$\| \mathrm{Str}(Z^{J_1} Y^{J_2}) \|^2 = J_1! J_2! \sum_{k=0}^{J_1+J_2-1} \binom{N + J_1 + J_2 - k - 1}{J_1 + J_2} \tag{D.1.11}$$

$$= J_1! J_2! \sum_{k=0}^{J_1+J_2-1} \binom{N+k}{J_1+J_2}. \tag{D.1.12}$$

Finally, we employ the general identity

$$\sum_{k=0}^{n-1}\binom{N+k}{m}=\binom{N+n}{m+1}-\binom{N}{m+1} \tag{D.1.13}$$

to deduce the final exact answer,

$$\| \operatorname{Str}(Z^{J_1}Y^{J_2}) \|^2 = J_1!J_2!\left[\binom{N+J_1+J_2}{J_1+J_2+1}-\binom{N}{J_1+J_2+1}\right]. \tag{D.1.14}$$

D.2 The $(k+1)$-graviton correlator character sum

In this section we present a calculation of the $(k+1)$-graviton correlator in the gauge theory. A similar calculation was done previously in [110]. The representation sum of the general extremal correlator was stated in [28] as being

$$\langle\prod_{i=1}^{k}(\mathrm{tr}Z^{J_i})\mathrm{tr}Z^{\dagger J}\rangle=\sum_{R\vdash J} f_R\chi_R([J_1\dots J_k])\chi_R([J]). \tag{D.2.1}$$

We adopt the notation $J=\sum_i J_i$ throughout this subsection. Using the Murnaghan-Nakayama lemma [109], we find that $\chi_R([J])$ is non-zero only if R is a hook rep, and equal to $(-)^k$ for a hook of length k. This constrains the sum to run only over hook representations, and so

$$\langle\prod_{i=1}^{k}(\mathrm{tr}Z^{J_i})\mathrm{tr}Z^{\dagger J}\rangle \;=\; J!\sum_{l=0}^{J-1}\binom{N+l}{J}(-)^{J-1-l}\chi_{H_l}([J_1\dots J_k]), \tag{D.2.2}$$

where H_l denotes the hook representation $[l+1,1^{J-1-l}]$. The Murnaghan-Nakayama lemma states that we can knock J_k boxes off this J-box hook rep to get

$$\chi_{H_l}[J_1\dots J_k]=\delta(l\geq J_k)\chi_{H_{l-J_k}}([J_1\dots J_{k-1}])+(-)^{J_k+1}\delta(J-l>J_k)\chi_{H_l}([J_1\dots J_{k-1}])$$

If we replace the expressions in the binomial coefficient by the general terms M, m, we have

$$\sum_{l=0}^{J-1}(-)^l\binom{M+l}{m}\chi_{H_l}([J_1\dots J_k])=\sum_{l=0}^{J-J_k-1}(-)^{J_k}\chi_{H_l}([J_1\dots J_{k-1}])\left[\binom{M+J_k+l}{m}-\binom{M+l}{m}\right]$$

We can plug this formula in to (D.2.2) for different values of M and m. We get

$$\langle\prod_{i=1}^{k}(\mathrm{tr}Z^{J_i})\mathrm{tr}Z^{\dagger J}\rangle = J!(-)^{J-1}\sum_{l=0}^{J-1}(-)^l\chi_{H_l}([J_1\dots J_k])\binom{N+l}{J}$$
$$= J!(-)^{J-J_k-1}\sum_{l=0}^{J-J_k-1}(-)^l\chi_{H_l}([J_1\dots J_{k-1}])\left[\binom{N+J_k+l}{J}-\binom{N+l}{J}\right]$$

$$= J!(-)^{J-J_k-J_{k-1}-1}\sum_{l=0}^{J-J_k-J_{k-1}-1}(-)^l\chi_{H_l}([J_1\dots J_{k-2}])\left[\binom{N+J_k+J_{k-1}+l}{J}-\right.$$
$$\left.\binom{N+J_k+l}{J}-\binom{N+J_{k-1}+l}{J}+\binom{N+l}{J}\right]$$

$$= J!(-)^{J_1-1}\sum_{l=0}^{J_1-1}(-)^l\chi_{H_l}([J_1])\left[\binom{N+J-J_1+l}{J}-\ldots+(-)^{k-1}\binom{N+l}{J}\right], \quad \text{(D.2.3)}$$

where we have omitted the intermediate binomials with arguments containing all sums of elements in $\{J_2, J_3\dots, J_k\}$. Using $\chi_{H_l}([J_1]) = (-)^{J_1-1-l}$ and

$$\sum_{l=0}^{J_1-1}\binom{M+l}{J} = \binom{M+J_1}{J+1}-\binom{M}{J+1}, \quad \text{(D.2.4)}$$

we can now evaluate the sums to find that

$$\langle\prod_{i=1}^{k}(\mathrm{tr}Z^{J_i})\mathrm{tr}Z^{\dagger J}\rangle = J!\left[\binom{N+J}{J+1}-\ldots+(-)^k\binom{N}{J+1}\right] \quad \text{(D.2.5)}$$

and restoring the omitted terms, we deduce that

$$\langle\prod_{i=1}^{k}(\mathrm{tr}Z^{J_i})\mathrm{tr}Z^{\dagger J}\rangle = J!\sum_{t=0}^{k}\sum_{\substack{S\subseteq\{1,\dots,k\}\\|S|=t}}(-)^{k-t}\binom{N+\sum_{i\in S}J_i}{J+1}. \quad \text{(D.2.6)}$$

The sum over S is a sum over all the subsets of the k-element set.

Appendix E

Moduli space, the mapping class group, and Teichmüller space

In this chapter, we consider compact Riemann surfaces of some genus g with sets of n distinguished labelled points $(P_1, P_2, \ldots, P_n)$. A pair of Riemann surfaces $X^{(1)}$ and $X^{(2)}$ with respective sets of labelled points $P_i^{(1)}$ and $P_i^{(2)}$ are equivalent if there exists a map $f : X^{(1)} \to X^{(2)}$ between the surfaces which is bijective and holomorphic (a **biholomorphism**) which preserves each labelled point: $f(P_i^{(1)}) = P_i^{(2)}$. The space of equivalence classes of Riemann surfaces with a given genus g and number of labelled points n is the **moduli space** $\mathcal{M}_{g,n}$.

We can also consider Riemann surfaces of genus g with sets of n distinguished points $\{P_1, \ldots, P_n\}$, but with a different equivalence relation, leading to an alternative definition of moduli space. We say that two surfaces $X^{(1)}$ and $X^{(2)}$ with respective sets of labelled points $P_i^{(1)}$ and $P_i^{(2)}$ are equivalent if there is a biholomorphism f between the two surfaces which maps the sets of labelled points to each other, and maps the point $P_n^{(1)}$ to $P_n^{(2)}$. This f will permute the remaining $(n-1)$ points n general, so $f(P_i^{(1)}) = P_{\sigma(i)}^{(2)}$ for some $\sigma \in S_{n-1} \times S_1 \cong S_{n-1}$. The set of equivalence classes under this equivalence relation is the modified moduli space of Riemann surfaces $\mathcal{M}_{g,1[n-1]}$.

A compact Riemann surface X with n distinguished labelled points can also be thought of as a non-compact surface $\hat{X}$, constructed by removing the n distinguished points from X. A biholomorphism between two surfaces $X^{(1)}$ and $X^{(2)}$ preserving the labelled points restricts to a biholomorphism between the two surfaces $\hat{X}^{(1)}$ and $\hat{X}^{(2)}$ preserving the n labelled punctures. The moduli space of punctured surfaces is the same as the moduli space of surfaces with distinguished points, $\mathcal{M}_{g,n}$. Similarly, if we consider surfaces to be equivalent if they are related by puncture-permuting biholomorphisms that fix a single puncture, then the associated moduli space is $\mathcal{M}_{g,1[n-1]}$. We can switch between these two descriptions of Riemann surfaces by adding and

removing the labelled points from the surfaces.

In general, moduli spaces are not manifolds; they are orbifolds. An **orbifold** is a topological space in which the neighbourhood of every point is homeomorphic to $\mathbb{R}^n$ modulo a finite group (see [97] for a more thorough definition). A manifold can then be viewed as a particular type of orbifold, where the quotienting group at every point is trivial.

The mapping class group $\Gamma_{g,n}$ is a discrete group that describes the large homeomorphisms of a surface $\Sigma_{g,n}$ of genus g with n labelled points. (In this thesis, we will use X to denote Riemann surfaces with a complex structure, and Σ to denote topological surfaces without an intrinsic complex structure.) Let $\text{Homeo}^+(\Sigma_{g,n})$ be the group of orientation-preserving homeomorphisms of a surface $\Sigma_{g,n}$ that preserve the n labelled points. A pair of homeomorphisms ϕ_1, ϕ_2 are **isotopic** if there exists a continuous function $F : [0,1] \times \Sigma_{g,n} \to \Sigma_{g,n}$ such that $F(0,p) = \phi_1(p)$ and $F(1,p) = \phi_2(p)$ for any point p on $\Sigma_{g,n}$. Let $\text{Homeo}_0(\Sigma_{g,n})$ be the set of homeomorphisms of a surface that are isotopic to the identity. This is a normal subgroup of $\text{Homeo}^+(\Sigma_{g,n})$. The group of orientation-preserving homeomorphisms, up to homeomorphisms isotopic to the identity, is the **mapping class group** of the surface:

$$\Gamma_{g,n} = \text{Homeo}^+(\Sigma_{g,n})/\text{Homeo}_0(\Sigma_{g,n}). \tag{E.0.1}$$

Similarly, we can define the mapping class group $\Gamma_{g,1[n-1]}$ by considering the group of orientation-preserving homeomorphisms that can interchange $(n-1)$ of the labelled points, $\text{Homeo}^+(\Sigma_{g,1[n-1]})$. The group $\text{Homeo}^+(\Sigma_{g,n})$ is a subgroup of $\text{Homeo}^+(\Sigma_{g,1[n-1]})$ and $\text{Homeo}_0(\Sigma_{g,n})$ is isomorphic to $\text{Homeo}_0(\Sigma_{g,1[n-1]})$, so $\Gamma_{g,n}$ is a subgroup of $\Gamma_{g,1[n-1]}$. The permutation of the first $(n-1)$ labelled points associated to each element of $\Gamma_{g,1[n-1]}$ gives us a mapping into S_{n-1}, and so there is a **short exact sequence**

$$1 \to \Gamma_{g,n} \to \Gamma_{g,1[n-1]} \to S_{n-1} \to 1. \tag{E.0.2}$$

The Teichmüller space $\mathcal{T}_{g,n}$ of genus g surfaces with n labelled points can be defined in several equivalent ways. We use the definition given in [108] that classifies the possible marked complex structures that can be placed on a topological surface. Consider a topological surface $\Sigma_{g,n}$ of genus g with n distinguished labelled points $\tilde{P}_i$. A **marked complex structure** on $\Sigma_{g,n}$ is a triple (X, P_i, ϕ) in which X is a Riemann surface (i.e. a complex structure on $\Sigma_{g,n}$) with distinguished points P_i and $\phi : \Sigma_{g,n} \to X$ is a homeomorphism mapping $\tilde{P}_i$ to P_i. A pair of marked complex structures $(X_1, P_i^{(1)}, \phi_1)$ and $(X_2, P_i^{(2)}, \phi_2)$ are **Teichmüller equivalent** if there exists a

bijective holomorphism $f : X_1 \to X_2$ such that $f \circ \phi_1$ and ϕ_2 are isotopic through labelled point-preserving homeomorphisms. (This means that there exists a continuous function $F : [0,1] \times \Sigma_{g,n} \to X_2$ with $F(0,p) = f \circ \phi_1(p)$ and $F(1,p) = \phi_2(p)$ for all p on $\Sigma_{g,n}$, and $F(t, \tilde{P}_i) = P_i^{(2)}$ for all $t \in [0,1]$.) The set of Teichmüller-equivalence classes of marked complex structures is the **Teichmüller space**

$$\mathcal{T}_{g,n} = \{(X, P_i, \phi)\}/\sim . \tag{E.0.3}$$

The mapping class group acts on Teichmüller space as follows. Given an element $g \in \Gamma_{g,n}$, we can pick a representative element of the isotopy equivalence class $\phi_g : \Sigma_{g,n} \to \Sigma_{g,n}$ which is an orientation and labelled point-preserving homeomorphism. The action of ϕ_g on a marked complex structure is then

$$g : (X, P_i, \phi) \mapsto (X, P_i, \phi \circ \phi_g). \tag{E.0.4}$$

This action is well-defined on Teichmüller equivalence classes: any other choice of homeomorphism $\tilde{\phi}_g$ for this $g \in \Gamma_{g,n}$ will give a pair $(X, P_i, \phi \circ \tilde{\phi}_g)$ which is Teichmüller-equivalent to $(X, P_i, \phi \circ \phi_g)$, and if $(X_1, P_i^{(1)}, \phi_1)$ and $(X_2, P_i^{(2)}, \phi_2)$ are Teichmüller-equivalent marked complex structures, then $(X_1, P_i^{(1)}, \phi_1 \circ \phi_g)$ and $(X_2, P_i^{(2)}, \phi_2 \circ \phi_g)$ are also Teichmüller-equivalent. Given any pair of markings ϕ_1, ϕ_2 of the same Riemann surface X, then the isotopy class of the mapping $\phi_1^{-1} \circ \phi_2$ from $\Sigma_{g,n}$ to itself is an element of the mapping class group $g \in \Gamma$, and the action of g on $(X, P_i, \phi_1) \in \mathcal{T}_{g,n}$ is

$$g : (X, P_i, \phi_1) \mapsto (X, P_i, \phi_2). \tag{E.0.5}$$

This shows that any two markings (X, P_i, ϕ_1) and (X, P_i, ϕ_2) of the same labelled Riemann surface can be related by an element of the mapping class group. The quotienting of Teichmüller space by the mapping class group can be thought of as dropping the last argument of each triple (X, P_i, ϕ): distinct points in the quotient space correspond to distinct Riemann surfaces with labelled points. This shows that the moduli space of Riemann surfaces is the quotient space

$$\mathcal{M}_{g,n} = \mathcal{T}_{g,n}/\Gamma_{g,n}. \tag{E.0.6}$$

The action of $\Gamma_{g,n}$ on Teichmüller space can be extended to an action of $\Gamma_{g,1[n-1]}$, the mapping class group that permutes $(n-1)$ of the labelled points. Consider a marked complex structure (X, P_i, ϕ) representing a point in $\mathcal{T}_{g,n}$. For an element

$g \in \Gamma_{g,1[n-1]}$, we can choose a distinguished point-permuting homeomorphism of the surface $\phi_g : \Sigma_{g,n} \to \Sigma_{g,n}$ such that $\phi_g(\tilde{P}_i) = \tilde{P}_{\sigma(i)}$ for some $\sigma \in S_{n-1} \times S_1$. The action of the element g on the triple preserves the complex structure of X but relabels the distinguished points:

$$g : (X, P_i, \phi) \mapsto (X, P_{\sigma(i)}, \phi \circ \phi_g). \tag{E.0.7}$$

As $\Gamma_{g,n}$ is a subgroup of $\Gamma_{g,1[n-1]}$, the quotienting of Teichmüller space by this group not only identifies all marked complex structures of the same Riemann surface X, but also identifies marked complex structures that differ by a relabelling of $(n-1)$ of the distinguished points. This results in the coarser version of moduli space,

$$\mathcal{M}_{g,1[n-1]} = \mathcal{T}_{g,n}/\Gamma_{g,1[n-1]}. \tag{E.0.8}$$

The definition of Teichmüller space in terms of marked complex structures makes it explicit how moduli space arises from the quotienting of the mapping class group. However, some other fundamental properties of Teichmüller space are obscured in this approach. It can be shown that Teichmüller space $\mathcal{T}_{g,n}$ is actually the universal covering orbifold of $\mathcal{M}_{g,n}$, and so is a simply-connected space. Also, the orbifolding at each point in $\mathcal{T}_{g,n}$ is trivial, which makes Teichmüller space a manifold. When $3g-3+n > 0$, the Teichmüller space $\mathcal{T}_{g,n}$ is homeomorphic to $\mathbb{R}^{6g-6+2n}$. These properties are proved in several texts on the subject, such as in [108].

Appendix F

Counting Nakamura graphs in the S_d picture using GAP

In this appendix, we outline a method for finding Nakamura graphs (without pole labellings) computationally, which we were able to implement with the software package GAP [102]. Each Nakamura graph corresponds to a slide-equivalence class of Hurwitz classes, in each of which there is a unique Hurwitz class of reduced tuples. Each graph with d faces has a single incoming pole, so we can use the S_d equivalence to consider only the reduced tuples with $\sigma_+ = (1, 2, \ldots, d)$. Reduced tuples of these form are equivalent if their associated **τ-tuples** $(\tau_1, \tau_2, \ldots, \tau_m)$ are conjugate by an element of S_d which fixes σ_+ under conjugation. We can therefore count all the Nakamura graphs of a given genus g and number of poles n by counting the equivalence classes of reduced τ-tuples $(\tau_1, \ldots, \tau_m)$ under the action of $\mathbb{Z}_d = \langle (1, 2, \ldots, d) \rangle$.

The algorithm proceeds as follows:

- First, fix a value of the (graph) Euler characteristic $\chi = 2-2g-n$. From (3.1.12), this gives the maximum number of faces d of the associated Nakamura graphs, $d_{\max} = 2|\chi|$. This corresponds to the maximum degree of the permutation groups S_d used in the tuples.

- Allow the number of zeroes (internal vertices) l to scroll over the range (3.1.14), $1 \leq l \leq |\chi|$. For each l, (3.1.13) gives us the branching number $\Delta = |\chi| - l$.

- Given l and Δ, find all the possible valencies of the zeroes. A zero of a Nakamura graph with valency $2k$ is described by a k-cycle in its permutation tuple, where $k > 2$. The branching number Δ is defined in (3.1.7) in terms of the valencies. Writing this expression in terms of the l cycle lengths $k_1, \ldots, k_l$, the branching

number is

$$\Delta = |\chi| - l = \sum_{i=1}^{l} (k_i - 2). \tag{F.0.1}$$

The possible valencies of the zeroes correspond to the partitions of $(|\chi| - l)$ into l parts: we write these as **valency partitions** $[k_1, k_2, \ldots, k_l]$, with $k_i \geq 2$ and $k_i \leq k_{i+1}$ for each i. For example, if we had $|\chi| = 5$ and $l = 3$, then the possible valency partitions are $[2, 3, 3]$ and $[2, 2, 4]$.

- For each valency partition $[k_1, \ldots, k_l]$ determining the valencies of the zeroes, construct all the 'reduced class tuples' which specify where the cycles appear within the reduced tuples. A **reduced class tuple** is an ordered list of $S_{d_{\max}}$ conjugacy classes $(\mathcal{T}_1, \mathcal{T}_2, \ldots, \mathcal{T}_m)$ for some $m \leq l$, where the conjugacy classes are specified by partitioning $(k_1, \ldots, k_l)$ into m parts. Each conjugacy class $\mathcal{T}_i$ is of the form $[k_{a_1}, k_{a_2}, \ldots, k_{a_p}]$, where $a_1, \ldots, a_p$ are distinct integers from 1 to l. In a given reduced class tuple, each cycle length from the valency partition appears in exactly one $\mathcal{T}_i$. For example, the valency partition $[2, 3, 3]$ can be combined as $\mathcal{T}_1 = [2, 3, 3]$ with $m = 1$, or as $(\mathcal{T}_1, \mathcal{T}_2) \in \{([3, 3], [2]), ([2], [3, 3]), ([2, 3], [3]), ([3], [2, 3])\}$ for $m = 2$, or as $(\mathcal{T}_1, \mathcal{T}_2, \mathcal{T}_3) \in \{([3], [3], [2]), ([3], [2], [3]), ([2], [3], [3])\}$ for $m = 3$.

  We are only interested in the reduced class tuples which can give valid Nakamura graphs in the reduced tuple picture. This means we should discard any sequence of class tuples in which there is some $i \in \{1, \ldots m-1\}$ such that $\tau_i \in \mathcal{T}_i$ permutes fewer integers than the number of disjoint cycles in $\tau_{i+1} \in \mathcal{T}_{i+1}$. For example, if we were to partition the valency partition $[2, 2, 2, 2]$ into reduced class tuples, then we would discard $(\mathcal{T}_1, \mathcal{T}_2) = ([2], [2, 2, 2])$, as any a permutation $\tau_1 \in \mathcal{T}_1$ moves two points while all permutations in $\mathcal{T}_2$ have three non-trivial cycles, so no elements in these classes can give a valid Nakamura graph in the reduced tuple description.

- For each reduced class tuple, scroll over all the tuples $(\tau_1, \ldots, \tau_m)$ in the conjugacy classes $(\mathcal{T}_1, \ldots, \mathcal{T}_m)$, and keep the tuples with the following two properties:
  - For all $i \in \{1, \ldots m - 1\}$, there is no cycle in τ_{i+1} that is disjoint from all cycles in τ_i.
  - The set of points moved by at least one of the τ_i is exactly $\{1, 2, \ldots, d\}$ for some d.

The number of points moved by the τ_i tuple is d, the degree of the permutation group S_d associated to the tuple.

- Act on the set of τ-tuples of the same degree and same reduced class tuple with the cyclic group $\langle(1, 2 \ldots, d)\rangle$. Each conjugacy class, together with $\sigma_+ = (1, 2, \ldots d)$ and $\sigma_- := (\sigma_+\tau_1 \ldots \tau_m)^{-1}$, gives a Hurwitz class of a reduced tuple, and so is associated to a distinct Nakamura graph. Each graph has an automorphism group $\mathbb{Z}_{(d/k)}$ generated by $(1, 2, \ldots, d)^k$, where k is the size of the conjugacy class of the τ-tuple.

- Collate the graphs by genus g, the number of poles n, and the dimension of its cell in moduli space. The number of disjoint cycles in $\sigma_- = (\sigma_+\tau_1 \ldots \tau_m)^{-1}$ is equal to $(n-1)$, the number of outgoing poles of the graph. The graph has genus g, where

$$g = -\frac{1}{2}\chi - \frac{n}{2} + 1. \tag{F.0.2}$$

The dimension of the cell in moduli space associated to the graph is $l + d - n$.

This procedure can quickly generate all Nakamura graphs for $d_{max} \leq 10$ or so, and is capable of generating all Nakamura graphs for $d_{max} = 12$, given sufficient time. However, the step of scrolling over all tuples in $(\mathcal{T}_1, \ldots, \mathcal{T}_m)$ is very resource-intense, as a relatively small percentage of the trial tuples give a valid Nakamura graph. (For $d = 10$, about 6% of trial tuples satisfy the two properties given above.) In addition, the vast majority of Nakamura graphs have trivial automorphism group, so there is virtually a d-fold degeneracy in the graphs counted. For these reasons, we introduce in the next section a new structure within the reduced S_d tuple description that circumvents both these issues and results in a much more powerful method of counting Nakamura graphs.

F.1 I-structures

A Nakamura graph has I internal edges that connect zeroes to zeroes. In terms of its reduced tuple description, these edges are labelled by precisely those integers in $\{1, 2, \ldots d\}$ which are permuted by more than one of the τ_i in the tuple $(\tau_1, \tau_2, \ldots \tau_m)$. The integers which are permuted by exactly one τ_i correspond to the external edges, which connect zeroes only to poles. We can describe the structure of the internal

edges of the graph by creating a diagram that shows which permuted points are shared between the different τ_i, which we call an *I-structure.*

An **I-structure** is a diagram consisting of m parallel vertical edges, which we call 'columns', and several rows of horizontal edges, which we call 'I-rows'. Each I-row is a connected line of horizontal edges and vertices, with the vertices connecting columns and horizontal edges. An I-structure may contain the same I-row multiple times, and the I-rows of an I-structure are taken to be interchangeable. All pairs of adjacent columns are connected by at least one edge of an I-row. An example of an I-structure is given in Figure F.1.

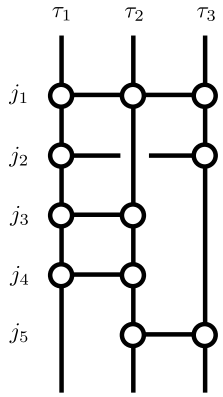

Figure F.1: An I-structure with five I-rows and three columns.

There is a unique I-structure corresponding to each reduced tuple of permutations τ_i, which represents the internal edges of the associated Nakamura graph. The m columns correspond to the m permutations in the tuple $(\tau_1, \ldots, \tau_m)$. From the definition of a Nakamura graph, each integer in the set $\{1, 2, \ldots d\}$ is permuted by at least one of the τ_i. If an integer j is permuted by two or more of the τ_i, then there is an I-row associated to this integer. The vertices of this I-row are drawn on the columns corresponding to the τ_i which permute the integer j. There is a horizontal edge associated to every consecutive pair of vertices along the I-row; these edges correspond to the internal edges of the Nakamura graph. Each vertex of the I-structure corresponds to a zero (internal vertex) of the Nakamura graph, but there will in general be zeroes which do not correspond to vertices of the I-structure, and there can be many vertices of an I-structure representing the same zero of the graph.

The I-structure constructed from a permutation tuple is unique, but there will be many different permutation tuples that have the same I-structure. For example, the

I-structure given in Figure F.1 could be generated by the tuple of S_6 permutations

$$\tau_1 = (1,2)(3,4), \qquad \tau_2 = (1,3)(4,5), \qquad \tau_3 = (1,2)(5,6). \tag{F.1.1}$$

The integers $\{1,2,3,4,5\}$ correspond to internal edges, and the integer '6' corresponds to an external edge. If we conjugate the above tuple by some $\gamma \in S_6$, then we have the new tuple

$$(\tilde{\tau_1}, \tilde{\tau_2}, \tilde{\tau_3}) = (\gamma\tau_1\gamma^{-1}, \gamma\tau_2\gamma^{-1}, \gamma\tau_3\gamma^{-1}), \tag{F.1.2}$$

which is just a relabelling of the τ_i and so has the same I-structure. In general, conjugate permutation tuples have the same I-structure, but there can also be distinct tuples which are not conjugate which have the same I-structure. An example of a permutation tuple that also generates the I-structure in Figure F.1 and is not conjugate to the above tuple is

$$\tau_1 = (1,2,3,4), \qquad \tau_2 = (1,3,4,5), \qquad \tau_3 = (1,2,5). \tag{F.1.3}$$

For small values of I, we can explicitly list all the possible I-structures that can be generated from Nakamura graphs. We start by considering $I = 0$. Any graph with no internal edges must have $m = 1$ in the reduced tuple description, and so the tuples of these graphs take the form

$$\sigma_+\tau\sigma_- = 1. \tag{F.1.4}$$

The Nakamura graphs with $I = 0$ have no I-structure. These graphs were counted using matrix models in Section 3.5.2.

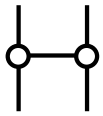

Figure F.2: The only possible I-structure for $I = 1$.

Now consider the graphs where $I = 1$, which have exactly one internal edge. From the definition of a reduced tuple, the zeroes of an $I = 1$ graph must be described by

a pair of permutations τ_1 and τ_2, and there exists a unique $j \in \{1, 2, \ldots d\}$ such that

$$\begin{aligned} \tau_1(j) &\neq j \\ \tau_2(j) &\neq j. \end{aligned} \tag{F.1.5}$$

In other words, j belongs to the moved-point sets of both τ_1 and τ_2. The associated I-structure consists of two columns and a single I-row with two vertices. This is given in Figure F.2.

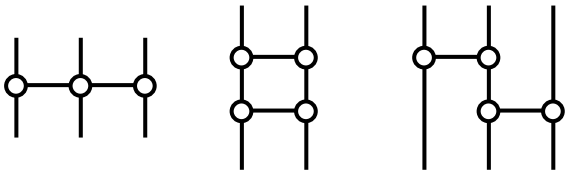

Figure F.3: The I-structures for $I = 2$.

In the case that $I = 2$, there are three distinct I-structures, as drawn in Figure F.3. The first I-structure has three columns and one I-row with three vertices. This corresponds to tuples in which there is a single integer $j \in \{1, 2, \ldots, d\}$ that is permuted by all three permutations τ_1, τ_2, τ_3, and no other integer in the set $\{1, 2, \ldots, d\}$ is permuted by any two of the τ_i. The second I-structure has two columns and two identical I-rows, each with two vertices. This structure corresponds to graphs for which there are exactly two integers $j_1, j_2 \in \{1, 2, \ldots, d\}$ that are mutually permuted by the pair of permutations τ_1 and τ_2. The third I-structure has three columns and two distinct I-rows with two vertices. This corresponds to a triple τ_1, τ_2, τ_3, with the property that there is some pair $j_1, j_2 \in \{1, 2, \ldots, d\}$ such that

$$\begin{aligned} \tau_1(j_1) &\neq j_1, & \tau_2(j_1) &\neq j_1, & \tau_3(j_1) &= j_1 \\ \tau_1(j_2) &= j_2, & \tau_2(j_2) &\neq j_2, & \tau_3(j_2) &\neq j_2 \end{aligned} \tag{F.1.6}$$

For $I = 3$, there are eleven I-structures that can be drawn that correspond to tuples in the reduced S_d description. These are shown in Figure F.4.

F.2 An algorithm utilising I-structures

There is an efficient algorithm that counts Nakamura graphs by using I-structures. As in the original algorithm outlined above, the I-structures algorithm takes the graph

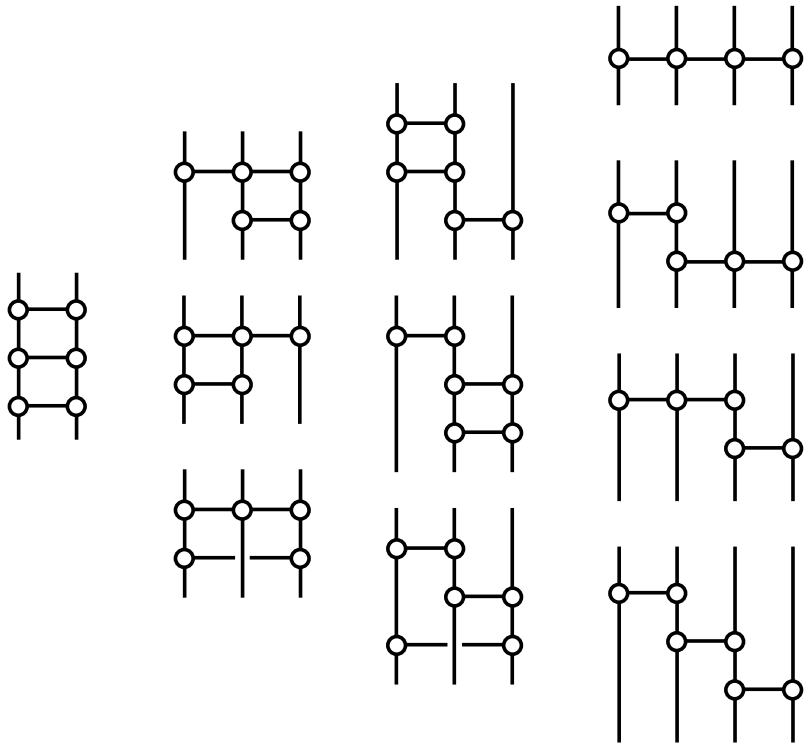

Figure F.4: The I-structures for $I = 3$.

Euler characteristic $|\chi|$ as input, and starts by finding all the valency partitions and reduced class tuples. For each reduced class tuple $(\mathcal{T}_1, \ldots, \mathcal{T}_m)$, the algorithm finds all possible I-structures that are consistent with this class tuple. Each I-structure must have one edge connecting columns $(i-1)$ and i for each cycle in $\tau_i \in \mathcal{T}_i$, where $i = 2, \ldots, m$. Also, there must be no more edges connecting each column $i = 1, 2, \ldots m$ in an I-structure than the total number of labels permuted by any $\tau_i \in \mathcal{T}_i$.

The algorithm considers each reduced class tuple and I-structure in turn. All Nakamura graphs with this reduced class tuple have the same values of Δ and I, and all Nakamura graphs with this chosen I-structure have the same value of I, and so all graphs with this I-structure and class tuple have the same degree,

$$d = \Delta + 2l - I. \tag{F.2.1}$$

Let $\Omega_{\mathcal{I},\mathcal{T}}$ be the set of tuples $(\tau_1, \ldots, \tau_m)$ with a given I-structure $\mathcal{I}$ and reduced class tuple $(\mathcal{T}_1, \ldots, \mathcal{T}_m)$. The Nakamura graphs with the specified I-structure and reduced

class tuple are the equivalence classes of this set under the conjugation action

$$(\tau_1, \ldots, \tau_m) \sim (\gamma^{-1}\tau_1\gamma, \ldots, \gamma^{-1}\tau_m\gamma), \tag{F.2.2}$$

for $\gamma \in \langle(1, 2, \ldots, d)\rangle = \mathbb{Z}_d$. However, the set $\Omega_{\mathcal{I},\mathcal{T}}$ can be very large in general, so it is computationally very expensive to split this set into $\mathbb{Z}_d$ conjugacy classes directly. We circumvent this difficulty by breaking the problem into stages: first, we split $\Omega_{\mathcal{I},\mathcal{T}}$ into conjugacy classes under the equivalence relation

$$(\tau_1, \tau_2, \ldots, \tau_m) \sim (\alpha^{-1}\tau_1\alpha, \alpha^{-1}\tau_2\alpha, \ldots, \alpha^{-1}\tau_m\alpha), \tag{F.2.3}$$

where $\alpha \in S_d$. Once we have found the S_d-equivalence classes of $\Omega_{\mathcal{I},\mathcal{T}}$, we then split these classes down into Z_d-equivalence classes, which correspond to distinct Nakamura graphs. Rather than directly constructing the very large set $\Omega_{\mathcal{I},\mathcal{T}}$ and then splitting this set into S_d equivalence classes, it is more efficient to construct the S_d-equivalence classes directly by finding a representative element of each class.

We find the representative elements of the S_d-classes by using the I-structure and breaking the S_d symmetry. Let k be the number of rows in the I-structure $\mathcal{I}$, where $k \in \{0, 1, \ldots, d\}$. For any tuple $(\tau_1, \ldots, \tau_m) \in \Omega_{\mathcal{I},\mathcal{T}}$, there are exactly k integers in $\{1, 2, \ldots, d\}$ that are permuted by more than one τ_i. These integers correspond to the internal edges of the Nakamura graph. By adding the length of the cycles in the class $\mathcal{T}_i$ for some $i \in \{1, 2, \ldots, m\}$ and subtracting the number of vertices in the ith column of the I-structure, we have the number of integers e_i that are permuted by only the permutation τ_i within the tuple $(\tau_1, \ldots, \tau_m)$. These integers correspond to the external edges of the graph. Consider the set of 'canonically-labelled' τ_i-tuples $\tilde{\Omega}_{\mathcal{I},\mathcal{T}} \subset \Omega_{\mathcal{I},\mathcal{T}}$ which consists of those tuples in which the permuted integers 1 to k correspond to the rows of the I-structure, the integers $k+1, \ldots, k+e_1$ are permuted only by τ_1, the labels $k+e_1+1, \ldots, k+e_1+e_2$ are permuted only by τ_2, and so on. Each S_d-equivalence class of $\Omega_{\mathcal{I},\mathcal{T}}$ contains at least one such canonically labelled τ_i-tuple. A pair of canonically-labelled tuples are in the same S_d-equivalence class if and only if they are conjugate to each other by an element of the group $S_k \times S_{e_1} \times \ldots S_{e_m}$. This means that the orbits of the canonically-labelled tuples under the action by conjugation of the group $S_k \times S_{e_1} \times \ldots S_{e_m}$ are in direct correspondence with the equivalence classes of $\Omega_{\mathcal{I},\mathcal{T}}$ under conjugation by S_d. As the set $\tilde{\Omega}_{\mathcal{I},\mathcal{T}}$ is usually much smaller than $\Omega_{\mathcal{I},\mathcal{T}}$, it is relatively cheap computationally to construct the set of canonically-labelled tuples, find their orbits under $S_k \times S_{e_1} \times \ldots S_{e_m}$, and choose a representative element from each orbit. In this way, we can construct a set of representative elements of the S_d

classes of $\Omega_{\mathcal{I},\mathcal{T}}$.

Consider each S_d-equivalence class of $\Omega_{\mathcal{I},\mathcal{T}}$ in turn, specified by a representative τ-tuple $(\tau_1,\ldots,\tau_m)$. All the elements of this S_d equivalence class are of the form $(\alpha^{-1}\tau_1\alpha,\ldots,\alpha^{-1}\tau_m\alpha)$, where $\alpha\in S_d$. Let $\mathrm{Aut}(\tau)$ be the automorphism group of the representative τ-tuple $(\tau_1,\ldots,\tau_m)$; that is, the set of elements $\gamma\in S_d$ that satisfy $\gamma^{-1}\tau_i\gamma=\tau_i$ for all $i=1,2,\ldots,m$. If two permutations $\alpha,\tilde{\alpha}$ satisfy $\tilde{\alpha}=\gamma\alpha$ for some $\gamma\in\mathrm{Aut}(\tau)$, then

$$(\alpha^{-1}\tau_1\alpha,\ldots,\alpha^{-1}\tau_m\alpha)=(\tilde{\alpha}^{-1}\tau_1\tilde{\alpha},\ldots,\tilde{\alpha}^{-1}\tau_m\tilde{\alpha}). \tag{F.2.4}$$

We can therefore see that each *right coset* $\mathrm{Aut}(\tau)\alpha\in\mathrm{Aut}(\tau)\backslash S_d$ specifies a unique element in the S_d-equivalence class of the τ-tuple.

We wish to split this S_d equivalence class into $\mathbb{Z}_d$ equivalence classes. A pair of elements of the S_d equivalence class $(\alpha^{-1}\tau_1\alpha,\ldots,\alpha^{-1}\tau_m\alpha)$ and $(\tilde{\alpha}^{-1}\tau_i\tilde{\alpha},\ldots,\tilde{\alpha}^{-1}\tau_m\tilde{\alpha})$ are in the same $\mathbb{Z}_d$ equivalence class if and only if

$$(\tilde{\alpha}^{-1}\tau_i\tilde{\alpha},\ldots,\tilde{\alpha}^{-1}\tau_m\tilde{\alpha})=(z^{-1}\alpha^{-1}\tau_1\alpha z,\ldots,z^{-1}\alpha^{-1}\tau_m\alpha z) \tag{F.2.5}$$

for some $z\in\mathbb{Z}_d=\langle(1,2,\ldots,d)\rangle$. This means that two right cosets $\mathrm{Aut}(\tau)\alpha$ and $\mathrm{Aut}(\tau)\tilde{\alpha}$ are in the same $\mathbb{Z}_d$-equivalence class if $\mathrm{Aut}(\tau)\tilde{\alpha}=(\mathrm{Aut}(\tau)\alpha)z$ for some $z\in\mathbb{Z}_d$. We deduce that the **double cosets**

$$\mathrm{Aut}(\tau)\alpha\mathbb{Z}_d \quad\in\quad \mathrm{Aut}(\tau)\backslash S_d/\mathbb{Z}_d \tag{F.2.6}$$

parametrise the $\mathbb{Z}_d$-equivalence classes of a given S_d-equivalence class of $\Omega_{\mathcal{I},\mathcal{T}}$, and so give the Nakamura graphs associated to a given S_d-equivalence class of $\Omega_{\mathcal{I},\mathcal{T}}$.

We can read off the size of the automorphism group of each graph by looking at the size of its associated double coset. The product group $\mathrm{Aut}(\tau)\times\mathbb{Z}_d$ acts on the elements in S_d by left and right multiplication. The orbits of this action are the double cosets $\mathrm{Aut}(\tau)\backslash S_d/\mathbb{Z}_d$. The stabiliser group of an element $\alpha\in S_d$ under this action consists of the pairs of elements (γ,z) which satisfy $\gamma\alpha z=\alpha$, or equivalently $\alpha^{-1}\gamma\alpha=z^{-1}$. As γ and z can be any elements of the groups $\mathrm{Aut}(\tau)$ and $\mathbb{Z}_d$ respectively, the stabiliser of α is precisely the intersection of the groups $\alpha^{-1}\mathrm{Aut}(\tau)\alpha$ and $\mathbb{Z}_d$. These are exactly the elements which fix under conjugation every element in the tuple $(\sigma_+,\alpha^{-1}\tau_1\alpha,\ldots,\alpha^{-1}\tau_m\alpha,\sigma_-)$, and so the stabiliser of α is the automorphism group of the graph. By the orbit-stabiliser theorem, we therefore deduce that the size of the

automorphism group of a Nakamura graph given by the double coset $\mathrm{Aut}(\tau)\alpha\mathbb{Z}_d$ is

$$\frac{d|A|}{|\mathrm{Aut}(\tau)\alpha\mathbb{Z}_d|}. \tag{F.2.7}$$

GAP can efficiently count double cosets and find their representative elements and sizes. The algorithm we have devised is therefore able to quickly find all the Nakamura graphs that arise from a given representative τ-tuple in the S_d-equivalence classes of $\Omega_{\mathcal{I},\mathcal{T}}$, and to read off their automorphism group sizes.

As an example of this procedure, we consider the reduced class tuple $(\mathcal{T}_1, \mathcal{T}_2, \mathcal{T}_3) = ([2,2],[3],[2])$ with $|\chi| = 5$. This class tuple contains only one cycle with cycle size greater than 2, so its branching number is $\Delta = 1$. From the relation

$$2|\chi| - d = \Delta + I, \tag{F.2.8}$$

we know that the degree and the number of internal edges are related by $d + I = 9$. Permutations in the class $\mathcal{T}_1$ permute four integers, so the degree is bounded from below by 4. There are three classes in this reduced class tuple, so there are at least two internal edges. This means that the number of internal edges I lies in the range $\{2,3,4,5\}$.

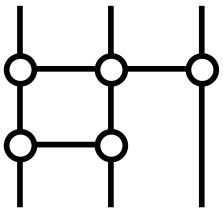

Figure F.5: An example of an I-structure of the reduced class tuple $(\mathcal{T}_1, \mathcal{T}_2, \mathcal{T}_3) = ([2,2],[3],[2])$.

One of the I-structures found by the algorithm is given in Figure F.5. This structure has $I = 3$ internal edges, and degree $d = 6$. Let $\Omega_{\mathcal{I},\mathcal{T}}$ be the set of tuples corresponding to this I-structure and reduced class structure. This I-structure has two rows, so there are $k = 2$ integers corresponding to internal edges in each tuple. The first column has two vertices, and corresponds to the class $\mathcal{T}_1 = [2,2]$ of permutations which permute four integers. This means that there are $e_1 = 2$ integers permuted by the first permutation in each tuple which correspond to external edges. Similarly,

there are $e_2 = 1$ integers permuted only by the permutation τ_2 within each tuple and $e_3 = 1$ integers permuted by the permutation τ_3.

To find the S_d-equivalence classes of $\Omega_{\mathcal{I},\mathcal{T}}$, we first find the 'canonically-labelled' tuples (τ_1, τ_2, τ_3) in which τ_1 permutes the integers $\{1, 2, 3, 4\}$, τ_2 permutes $\{1, 2, 5\}$, and τ_3 permutes $\{1, 6\}$. There are six such elements, and the set of canonically-labelled tuples is

$$\tilde{\Omega}_{\mathcal{I},\mathcal{T}} = \{(1,2)(3,4), (1,3)(2,4), (1,4)(2,3)\} \times \{(1,2,5), (1,5,2)\} \times \{(1,6)\}. \quad \text{(F.2.9)}$$

Next, we consider the orbits in $\Omega_{\mathcal{I},\mathcal{T}}$ generated by this set under the action of the group $S_k \times S_{e_1} \times S_{e_2} \times S_{e_3} = \langle (1,2), (3,4) \rangle$. Note that the set $\tilde{\Omega}_{\mathcal{I},\mathcal{T}}$ is not closed under this group action. The tuples $((1,3)(2,4), (1,2,5), (1,6))$ and $((1,4)(2,3), (1,2,5), (1,6))$ are conjugate, as are the tuples $((1,3)(2,4), (1,5,2), (1,6))$ and $((1,4)(2,3), (1,5,2), (1,6))$, and so a set of representatives for the orbits of the canonically-labelled tuples (τ_1, τ_2, τ_3) is

$$\begin{aligned} &((1,2)(3,4), (1,2,5), (1,6)), \\ &((1,2)(3,4), (1,5,2), (1,6)), \\ &((1,3)(2,4), (1,2,5), (1,6)), \\ &((1,3)(2,4), (1,5,2), (1,6)). \end{aligned} \quad \text{(F.2.10)}$$

These are representative elements of the S_d-equivalence classes of $\Omega_{\mathcal{I},\mathcal{T}}$.

For each representative tuple, the Nakamura graphs are given by the double cosets $\mathrm{Aut}(\tau) \backslash S_d / \mathbb{Z}_d$. The representative tuple $(\tau_1, \tau_2, \tau_3) = ((1,2)(3,4), (1,2,5), (1,6))$ has the automorphism group $\mathrm{Aut}(\tau) = \langle (3,4) \rangle$, and so the Nakamura graphs correspond to the double cosets $\langle (3,4) \rangle \backslash S_6 / \langle (1,2,\ldots,6) \rangle$. There are 60 distinct double cosets, all consisting of 12 elements, and so there are 60 Nakamura graphs in this S_d-class. All these graphs have trivial automorphism group. For the representative tuple $(\tau_1, \tau_2, \tau_3) = ((1,3)(2,4), (1,2,5), (1,6))$, the automorphism group $\mathrm{Aut}(\tau)$ is trivial, and so the double cosets are $\{()\} \backslash S_6 / \langle (1,2,\ldots,6) \rangle$. There are 120 distinct double cosets in this case, and so there are 120 Nakamura graphs in this S_d-equivalence class.

F.3 Tables of Nakamura graphs with $|\chi| = 7$

Table F.1: (g, n)=(0,9)

dimension	12	11	10	9	8	7
Graphs ([Aut] × Number)	[1] 28 [2] 5 [7] 1	[1] 297	[1] 1324 [2] 25	[1] 3675	[1] 6795 [2] 52 [4] 1	[1] 8892

	6	5	4	3	2	1	0
⋯	[1] 8169 [2] 57	[1] 5250	[1] 2226 [2] 29 [4] 2	[1] 595	[1] 85 [2] 6	[1] 6	[8] 1

Table F.2: (g, n)=(1,7)

dimension	14	13	12	11	10	9	
Graphs ([Aut] × #)	[1] 838 [2] 40	[1] 9702	[1] 51870 [2] 210	[1] 174090	[1] 404059 [2] 471 [3] 1 [4] 2 [6] 1	[1] 680960	⋯

	8	7	6	5	4	3	2	1
⋯	[1] 843976 [2] 574	[1] 766000 [3] 5	[1] 497046 [2] 378 [4] 4	[1] 222057	[1] 64087 [2] 124 [3] 5 [6] 2	[1] 10820	[1] 863 [2] 15 [4] 1	[1] 18 [3] 2

Table F.3: (g, n)=(2,5)

dimension	16	15	14	13	12	⋯
Graphs ([Aut] × #)	[1] 4680 [2] 78	[1] 59598	[1] 359771 [2] 485	[1] 1374975	[1] 3688668 [2] 1322 [3] 9 [4] 2	

⋯	11	10	9	8	7	6	⋯
	[1] 7291788	[1] 10799810 [2] 1995	[1] 11954262 [3] 30	[1] 9708622 [2] 1671 [4] 5	[1] 5611630	[1] 2204212 [2] 695 [3] 36	

⋯	5	4	3	2
	[1] 548779	[1] 76822 [2] 101 [4] 3 [8] 1	[1] 4814 [3] 12	[1] 84

Table F.4: (g, n)=(3,3)

dimension	18	17	16	15	14	⋯
Graphs ([Aut] × #)	[1] 4013 [2] 63 [7] 2 [14] 1	[1] 55143	[1] 360892 [2] 421	[1] 1502760	[1] 4420204 [2] 1236 [3] 7 [4] 5 [6] 1	

⋯	13	12	11	10	9	8	⋯
	[1] 9649120	[1] 15910334 [2] 2031	[1] 19771176 [3] 25	[1] 18191095 [2] 1891 [4] 11	[1] 12042490	[1] 5502643 [2] 940 [3] 29 [6] 2	

⋯	7	6	5	4
	[1] 1632983	[1] 284718 [2] 203 [4] 4 [8] 2	[1] 24312 [3] 10	[1] 680 [2] 12

Bibliography

[1] M. Bauer and C. Itzykson, "Triangulations", Discrete Mathematics **156**, 1996, pp. 29-81.

[2] E. Looijenga, "Intersection theory on Deligne-Mumford compactifications", Seminaire Bourbaki **35**, 1992-1993, pp. 187-212.

[3] R. d. M. Koch and S. Ramgoolam, "From Matrix Models and Quantum Fields to Hurwitz Space and the absolute Galois Group," arXiv:1002.1634 [hep-th].

[4] R. Gopakumar, "What is the Simplest Gauge-String Duality?," arXiv:1104.2386 [hep-th].

[5] R. Gopakumar and R. Pius, "Correlators in the Simplest Gauge-String Duality," JHEP **1303**, 175 (2013) [arXiv:1212.1236].

[6] R. de Mello Koch and L. Nkumane, "Topological String Correlators from Matrix Models," JHEP **1503**, 004 (2015) [arXiv:1411.5226 [hep-th]].

[7] J. Madore, "The fuzzy sphere," Class. Quant. Grav. **9** (1992) 69.

[8] J. P. Moussouris, "Quantum Models of Space-Time Based on Recoupling Theory" (D. Phil. thesis, Oxford, 1983)

[9] R. J. Dowdall, "Spin foam models for 3D quantum geometry", PhD thesis, University of Nottingham (2011).

[10] E. Witten, "(2+1)-Dimensional Gravity as an Exactly Soluble System," Nucl. Phys. B **311** (1988) 46.

[11] G. Ponzano and T. Regge, "Semiclassical limit of Racah coefficients", Spectroscopic and Group Theoretical Methods in Physics, North-Holland, Amsterdam (1968) pp. 1-58

[12] H. Ooguri and N. Sasakura, "Discrete and continuum approaches to three-dimensional quantum gravity," Mod. Phys. Lett. A **6**, 3591 (1991) [hep-th/9108006].

[13] H. Ooguri, "Partition functions and topology changing amplitudes in the 3-D lattice gravity of Ponzano and Regge," Nucl. Phys. B **382**, 276 (1992) [hep-th/9112072].

[14] J. M. Maldacena, "The Large N limit of superconformal field theories and supergravity," Adv. Theor. Math. Phys. **2** (1998) 231 [hep-th/9711200].

[15] S. S. Gubser, I. R. Klebanov and A. M. Polyakov, "Gauge theory correlators from noncritical string theory," Phys. Lett. B **428** (1998) 105 [hep-th/9802109].

[16] E. Witten, "Anti-de Sitter space and holography," Adv. Theor. Math. Phys. **2** (1998) 253 [hep-th/9802150].

[17] S. Lee, S. Minwalla, M. Rangamani and N. Seiberg, "Three point functions of chiral operators in D = 4, N=4 SYM at large N," Adv. Theor. Math. Phys. **2** (1998) 697 [hep-th/9806074].

[18] K. A. Intriligator, "Bonus symmetries of N=4 superYang-Mills correlation functions via AdS duality," Nucl. Phys. B **551**, 575 (1999) [hep-th/9811047].

[19] K. A. Intriligator and W. Skiba, "Bonus symmetry and the operator product expansion of N=4 super Yang-Mills," Nucl. Phys. B **559**, 165 (1999) [hep-th/9905020].

[20] B. Eden, P. S. Howe and P. C. West, "Nilpotent invariants in N=4 SYM," Phys. Lett. B **463**, 19 (1999) [hep-th/9905085].

[21] A. Petkou and K. Skenderis, "A non-renormalization theorem for conformal anomalies," Nucl. Phys. B **561**, 100 (1999) [hep-th/9906030].

[22] P. S. Howe, C. Schubert, E. Sokatchev and P. C. West, "Explicit construction of nilpotent covariants in N=4 SYM," Nucl. Phys. B **571**, 71 (2000) [hep-th/9910011].

[23] P. J. Heslop and P. S. Howe, "OPEs and three-point correlators of protected operators in N=4 SYM," Nucl. Phys. B **626**, 265 (2002) [hep-th/0107212].

[24] V. Balasubramanian, M. Berkooz, A. Naqvi and M. J. Strassler, "Giant gravitons in conformal field theory," JHEP **0204** (2002) 034 [hep-th/0107119].

[25] S. Corley, A. Jevicki and S. Ramgoolam, "Exact correlators of giant gravitons from dual N=4 SYM theory," Adv. Theor. Math. Phys. **5** (2002) 809 [hep-th/0111222].

[26] D. Berenstein, "A Toy model for the AdS / CFT correspondence," JHEP **0407**, 018 (2004) [hep-th/0403110].

[27] C. Kristjansen, J. Plefka, G. W. Semenoff, M. Staudacher, "A New Double-Scaling Limit of N=4 Super Yang-Mills Theory and pp-Wave Strings", [hep-th/0205033].

[28] S. Corley and S. Ramgoolam, "Finite factorization equations and sum rules for BPS correlators in N=4 SYM theory," Nucl. Phys. B **641**, 131 (2002) [hep-th/0205221].

[29] A. B. Zamolodchikov, "Irreversibility of the Flux of the Renormalization Group in a 2D Field Theory," JETP Lett. **43**, 730 (1986) [Pisma Zh. Eksp. Teor. Fiz. **43**, 565 (1986)].

[30] S. Giddings and S. Wolpert, "A Triangulation of Moduli Space from Light-cone String Theory," Comm. Math. Phys. Volume 109, Number 2 (1987), 177-190.

[31] S. Nakamura, "A Calculation of the Orbifold Euler Number of the Moduli Space of Curves by a New Cell Decomposition of the Teichmüller Space," Tokyo J. of Math. Volume 23, Number 1 (2000), 87-100.

[32] S. Mandelstam, "Interacting String Picture of Dual Resonance Models," Nucl. Phys. B64 (1973) 205235.

[33] S. Mandelstam, "The Interacting String Picture and Functional Integration," Lectures given at Workshop on Unified String Theories, Santa Barbara, CA, Jul 29 - Aug 16, 1985.

[34] J. Harer and D. Zagier, "The Euler characteristic of the moduli space of curves," Inventiones mathematicae 1986, Volume 85, Issue 3, pp 457-485

[35] R. C. Penner, "Perturbative series and the moduli space of Riemann surfaces," J. Diff. Geom., 27, 35 (1988).

[36] M. Kontsevich, "Intersection theory on the moduli space of curves and the matrix Airy function," Commun. Math. Phys. 147, 1 (1992).

[37] P. Tourkine, "Tropical Amplitudes," arXiv:1309.3551 [hep-th].

[38] A. Grothendieck, "Esquisse d'un programme," (1984)

[39] G. V. Belyi, "On Galois Extensions of a Maximal Cyclotomic Field", Mathematics of the USSR-Izvestiya (1980), 14(2):247

[40] E. Witten, "On The Structure Of The Topological Phase Of Two-dimensional Gravity," Nucl. Phys. B340, 281-332 (1990).

[41] R. Dijkgraaf, E. Witten, "Mean Field Theory, Topological Field Theory, And Multimatrix Models," Nucl. Phys. B342, 486-522 (1990).

[42] T. Tao, "Topics in random matrix theory," Graduate Studies in Mathematics, 132. American Mathematical Society, Providence, 2012.

[43] G. 't Hooft, "A Planar Diagram Theory for Strong Interactions," Nucl. Phys. B **72** (1974) 461.

[44] B. Riemann, "Collected Papers," (translated by R. Basker and C. Christenson and H. Orde) Kendrick Press, Heber City, 2004.

[45] S. K. Donaldson, "Riemann surfaces", Oxford Graduate Texts in Mathematics, Vol. 22, Oxford University Press, Oxford, 2011.

[46] T. Eguchi, S. -K. Yang, "The Topological CP^1 model and the large N matrix integral," Mod. Phys. Lett. A9, 2893-2902 (1994) [hep-th/9407134].

[47] S. Kryszewski and M. Zachciał, "Alternative representation of $N \times N$ density matrix", arXiv:0602065v1 [quant-ph].

[48] C. -S. Chu, J. Madore and H. Steinacker, "Scaling limits of the fuzzy sphere at one loop," JHEP **0108**, 038 (2001) arXiv:0106205v2 [hep-th].

[49] S. Vaidya, "Perturbative dynamics on the fuzzy S^2 and $\mathbb{R}P^2$," Phys. Lett. B **512**, 403 (2001) arXiv:0102212v1 [hep-th].

[50] S. Iso, Y. Kimura, K. Tanaka and K. Wakatsuki, "Noncommutative gauge theory on fuzzy sphere from matrix model," Nucl. Phys. B **604**, 121 (2001) arXiv:0101102v4 [hep-th].

[51] R. Penrose, "Angular momentum: An approach to combinatorial space-time," in "Quantum Theory and Beyond," ed. T. Bastin, Cambridge University Press, Cambridge, 1971.

[52] J. C. Baez, "An Introduction to spin foam models of quantum gravity and BF theory," Lect. Notes Phys. **543**, 25 (2000) [gr-qc/9905087].

[53] S. A. Major, "A Spin network primer," Am. J. Phys. **67**, 972 (1999) [gr-qc/9905020].

[54] J. W. Barrett and I. Naish-Guzman, "The Ponzano-Regge model," Class. Quant. Grav. **26** (2009) 155014 [arXiv:0803.3319 [gr-qc]].

[55] H. Ruegg, "A Simple Derivation Of The Quantum Clebsch Gordan Coefficients For $SU(2)_q$," J. Math. Phys. **31**, 1085 (1990).

[56] V. G. Turaev and O. Y. Viro, "State Sum Invariants of 3-manifolds and Quantum $6j$-symbols", Topology **31** (1992) pp. 865-902.

[57] A. R. Edmonds, "Angular Momentum in Quantum Mechanics", Princeton University Press, Princeton, 1960.

[58] M. E. Rose, "Elementary Theory of Angular Momentum", Wiley and Sons, New York, 1957.

[59] A. N. Kirillov and N. Y. Reshetikhin, "Representations of the Algebra $U_q(sl(2))$, q-Orthogonal Polynomials and Invariants of Links", Advanced Series in Mathematical Physics **7** (1989).

[60] U. Pachner, "P.L. homeomorphic manifolds are equivalent by elementary shellings", European Journal of Combinatorics **12** (1991).

[61] D.A. Varshalovich, A.N. Moskalev, and V.K. Khernsonsky, "Quantum Theory Of Angular Momentum: Irreducible Tensors, Spherical Harmonics, Vector Coupling Coefficients, 3nj Symbols," World Scientific (1989).

[62] J. W. Alexander, "The combinatorial theory of complexes", Ann. of Math. **31** (1930)

[63] W. Jaco, J. H. Rubinstein, "Layered-triangulations of 3-manifolds", arXiv:0603601 [math-gt]

[64] H. -C. Ruiz, "Toroidal Spin Networks: Towards a Generalization of the Decomposition Theorem", arXiv:1210.0865v1 [math-ph]

[65] O. Aharony, O. Bergman, D. L. Jafferis and J. Maldacena, "N=6 superconformal Chern-Simons-matter theories, M2-branes and their gravity duals," JHEP **0810** (2008) 091 arXiv:0806.1218 [hep-th].

[66] J. McGreevy, L. Susskind and N. Toumbas, "Invasion of the giant gravitons from Anti-de Sitter space," JHEP **0006**, 008 (2000) [hep-th/0003075].

[67] H. Lin, O. Lunin and J. M. Maldacena, "Bubbling AdS space and 1/2 BPS geometries," JHEP **0410**, 025 (2004) [hep-th/0409174].

[68] Avinash Dhar, Gautam Mandal, Mikael Smedbäck, "From Gravitons to Giants", [hep-th/0512312].

[69] J. M. Maldacena and A. Strominger, "AdS(3) black holes and a stringy exclusion principle," JHEP **9812** (1998) 005 [hep-th/9804085].

[70] A. Jevicki and S. Ramgoolam, "Noncommutative gravity from the AdS / CFT correspondence," JHEP **9904** (1999) 032 [hep-th/9902059].

[71] L. Susskind and E. Witten, "The Holographic bound in anti-de Sitter space," hep-th/9805114.

[72] A. W. Peet and J. Polchinski, "UV / IR relations in AdS dynamics," Phys. Rev. D **59** (1999) 065011 [hep-th/9809022].

[73] J. Maldacena, "The Gauge/gravity duality," arXiv:1106.6073 [hep-th].

[74] K. Papadodimas and S. Raju, "An Infalling Observer in AdS/CFT," arXiv:1211.6767 [hep-th].

[75] R. de Mello Koch, T. K. Dey, N. Ives and M. Stephanou, "Correlators Of Operators with a Large R-charge," JHEP **0908** (2009) 083 [arXiv:0905.2273 [hep-th]].

[76] R. M. Corless , G. H. Gonnet , D. E. G. Hare , D. J. Jeffrey , D. E. Knuth, "On the Lambert W Function" (1996), http://www.apmaths.uwo.ca/ djeffrey/Offprints/W-adv-cm.pdf

[77] Robert M. Corless, David J. Jeffrey, and Donald E. Knuth, "A Sequence of Series for the Lambert W Function" (1997), http://www.apmaths.uwo.ca/ rcorless/frames/PAPERS/LambertW/CorlessJeffreyKnuth.ps.gz

[78] M. Czakon, "The Four-loop QCD beta-function and anomalous dimensions," Nucl. Phys. B **710** (2005) 485 [hep-ph/0411261].

[79] A. I. Alekseev, "Strong coupling constant to four loops in the analytic approach to QCD," Few Body Syst. **32** (2003) 193 [hep-ph/0211339].

[80] M. Mariño, "Lectures on non-perturbative effects in large N gauge theories, matrix models and strings," arXiv:1206.6272 [hep-th].

[81] V. Balasubramanian, J. de Boer, V. Jejjala and J. Simon, "The Library of Babel: On the origin of gravitational thermodynamics," JHEP **0512** (2005) 006 [hep-th/0508023].

[82] T. W. Brown, R. de Mello Koch, S. Ramgoolam and N. Toumbas, "Correlators, Probabilities and Topologies in N=4 SYM," JHEP **0703**, 072 (2007) [hep-th/0611290].

[83] D. A. Lowe, J. Polchinski, L. Susskind, L. Thorlacius and J. Uglum, "Black hole complementarity versus locality," Phys. Rev. D **52** (1995) 6997 [hep-th/9506138].

[84] A. Almheiri, D. Marolf, J. Polchinski and J. Sully, "Black Holes: Complementarity or Firewalls?," JHEP **1302** (2013) 062 [arXiv:1207.3123 [hep-th]].

[85] V. Balasubramanian, S. B. Giddings and A. E. Lawrence, "What do CFTs tell us about Anti-de Sitter space-times?," JHEP **9903** (1999) 001 [hep-th/9902052].

[86] A. Hamilton, D. N. Kabat, G. Lifschytz and D. A. Lowe, "Local bulk operators in AdS/CFT: A Holographic description of the black hole interior," Phys. Rev. D **75** (2007) 106001 [Erratum-ibid. D **75** (2007) 129902] [hep-th/0612053].

[87] S. R. Das and A. Jevicki, "String Field Theory and Physical Interpretation of $D = 1$ Strings," Mod. Phys. Lett. A **5** (1990) 1639.

[88] G. D'Appollonio, P. Di Vecchia, R. Russo and G. Veneziano, "High-energy string-brane scattering: Leading eikonal and beyond," JHEP **1011** (2010) 100 [arXiv:1008.4773 [hep-th]].

[89] P. Arnold, P. Szepietowski, D. Vaman and G. Wong, "Tidal stretching of gravitons into classical strings: application to jet quenching with AdS/CFT," JHEP **1302** (2013) 130 [arXiv:1212.3321 [hep-th]].

[90] R. d. M. Koch, M. Dessein, D. Giataganas and C. Mathwin, "Giant Graviton Oscillators," JHEP **1110** (2011) 009 [arXiv:1108.2761 [hep-th]].

[91] R. de Mello Koch and S. Ramgoolam, "A double coset ansatz for integrability in AdS/CFT," JHEP **1206** (2012) 083 [arXiv:1204.2153 [hep-th]].

[92] R. d. M. Koch, S. Graham and I. Messamah, "Higher Loop Nonplanar Anomalous Dimensions from Symmetry," arXiv:1312.6227 [hep-th].

[93] R. Akhoury, R. Saotome and G. Sterman, "Collinear and Soft Divergences in Perturbative Quantum Gravity," Phys. Rev. D **84** (2011) 104040 [arXiv:1109.0270 [hep-th]].

[94] S. B. Giddings, "Flat space scattering and bulk locality in the AdS / CFT correspondence," Phys. Rev. D **61** (2000) 106008 [hep-th/9907129].

[95] N. Ishibashi and K. Murakami, "Multiloop Amplitudes of Light-cone Gauge Bosonic String Field Theory in Noncritical Dimensions," JHEP **1309** (2013) 053 [arXiv:1307.6001 [hep-th]].

[96] A. Hurwitz, "Uber Riemann'sche Flächen mit gegebenen Veizweigungspunkten", Math. Ann., 39, (1891), 161.

[97] W. Thurston, "The geometry and topology of three-manifolds," Princeton lecture notes (1980).

[98] G. Mislin, "Mapping class groups, characteristic classes, and Bernouilli numbers," CRM Proc. Lect. Notes 6 (1994), 103131.

[99] P. Etingof, "Geometry and Quantum Field Theory", Massachusetts Institute of Technology lecture notes (2002).

[100] Micheal N. Dyer, "Euler Characteristics of Groups", Quart. J. Math. Oxford Ser. (2) 38 (1987), 35-44.

[101] N. V. Ivanov, "Mapping class groups", in Handbook of geometric topology, North-Holland, Amsterdam (2002), 523633.

[102] The GAP Group, *GAP – Groups, Algorithms, and Programming, Version 4.7.7*; 2015, (`http://www.gap-system.org`).

[103] E. D'Hoker and D. H. Phong, "The Geometry of String Perturbation Theory," Rev. Mod. Phys. **60** (1988) 917.

[104] L. Freidel, R. G. Leigh and D. Minic, "Born Reciprocity in String Theory and the Nature of Spacetime," Phys. Lett. B **730** (2014) 302 [arXiv:1307.7080].

[105] L. Freidel, R. G. Leigh and D. Minic, "Metastring Theory: The classical structure," to appear.

[106] Riccardo Murri, "Fatgraph Algorithms and the Homology of the Kontsevich Complex," http://arxiv.org/abs/1202.1820

[107] E. P. Wigner, "Group Theory and its Application to the Quantum Mechanics of Atomic Spectra," translation from German by J. J. Griffin. New York: Academic Press (1959).

[108] B. Farb and D. Margalit, "A Primer on Mapping Class Groups," (PMS-49) Princeton University Press, 2011.

[109] W. Fulton and J. Harris, "Representation Theory: A First Course," Springer-Verlag, 1991.

[110] P. Caputa and B. A. E. Mohammed, "From Schurs to Giants in ABJ(M)," JHEP **1301**, 055 (2013) [arXiv:1210.7705 [hep-th]].